CENTRE FOR BIOLOGICAL ENGINEERING, HEALTHCARE ENGINEERING,
WOLFSON SCHOOL OF MECHANICAL AND MANUFACTURING ENGINEERING,
LOUGHBOROUGH UNIVERSITY

PROCESS MONITORING AND CONTROL USING LIVE CELL IMAGING FOR THE MANUFACTURING OF CELL THERAPIES

by

David Smith

Thesis submitted to Loughborough University for the degree of

Doctor of Philosophy
September 2014

Abstract

Regenerative medicine (RM) represents a promising enabling technology to revolutionize healthcare. This said there are still major gaps between the commercial promise and the reality of the cell therapy sector of regenerative medicine. There is consensus to develop high through-put, automated technologies for the manufacture of RM products. Imaging methods will have the capacity to contribute to this technological gap for cell therapies and are particularly attractive to provide non-destructive monitoring with high spatial and temporal resolution.

This work applied an automated, non-invasive phase contrast imaging platform (Cell-IQ) to measure, analyse and ultimately quantify image derived metrics for human embryonic stem cells (hESCs) and haematopoietic stem cells (HSCs) as part of the colony forming unit (CFU) assay.

This work has shown through thresholding and machine vision identification technology, imaging has the ability to improve the precision of current evaluation methods for cell culture, providing novel information regarding culture state and show image derived metrics to be predictive of future culture state. Building on this, differentiation through the addition of a growth factor cocktail highlighted how in-process monitoring enables protocol optimisation.

After equilibrating the Cell-IQ incubator to a standard incubator, the progress of the CFU assay was monitored and image metrics representative of colony phenotype were analysed. Cell count, distance between cells and cell migration within individual colonies were identified to be informative and provide a degree of colony phenotype separation. Quantitative, novel, image derived metrics were identified that improve reliability through computer automation, cost by removing user verification and time by reducing the assay time from 14 days to 7 days.

Non-invasive imaging provides a fantastic opportunity to create bespoke sampling frequencies to achieve desired precision for manufacturing cell therapies, this work has developed and shown improvement and a level of control to current culture process for ESCs and HSCs.

Acknowledgments

My genuine thanks and appreciation go foremost to my supervisor Dr Rob Thomas who has shown tremendous support, guidance and mentorship whilst maintaining the patience to deal with the lows (and me) through this works lifespan. His advice and helpful criticism alongside Prof. David Williams and Prof. Chris Hewitt have facilitated my development into an independent researcher.

I am grateful for the opportunity that the Engineering and Physical Sciences Research Council (EPSRC) Doctoral Training Centre and the Centre for Biological Engineering at Loughborough University has provided. This includes both the worldclass facilities and financial backing that has allowed for my studies and the outreach of my work.

CM-Technologies, my industrial sponsor, provided both substantial financial aid and expertise in live cell imaging and analysis to assist with this work. In particular I am grateful for the initial guidance from David Bolton, and latterly from Jane Spencer-Fry, John Gray and Elen Bray.

I would also like to acknowledge my colleagues within the Centre for Biological Engineering. It was a pleasure working with you all and thanks for making the CBE entertaining yet rewarding. Academically I am thankful for the life lessons from Juan, Vicki, Katie, Forhad, Rachel, Mark and special thanks go to the CBE cycling team of Thomas, Billy Bowen, Lyness and Chan who offered a welcome escape from the lab and a shoulder to both cry and laugh on, often simultaneously.

They say you cant choose your family, and given the choice I wouldn't require a change of mine. From the support, guidance and love from my parents to the (sanity), competiveness and wisdom of my brother. I am eternally grateful for all your encouragement thoughout this process and the inspiration to aim high.

Finally I must thank Jenn for her support, friendship and love. Her ability to make me laugh during the dull days has kept me going, and the frequent escapes, especially to the beach.

Contents

List of Figures

List of Tables

Abbreviations

ASIA	American Spinal Injury Association
BMP_4	Bone Morphogenetic Factor 4
BSA	Bovine Serum Albumin
BSI	British Standards Institute
BFU-E	Burst Forming Unit – Erythroid
CB	Cord Blood
CFR	Code of Federal Regulations
CFU	Colony Forming Unit
CFU-GM	Colony Forming Unit – Granulocytes/Macrophages
CFU-GEMM	Colony Forming Unit – Granulocytes/Erythrocytes/Macrophages/Megakaryocytes
cGMP	current Good Manufacturing Practice
CLPs	Common Lymphoid Progenitors
CMPs	Common Myeloid Progenitors
CO_2	Carbon Dioxide
CPP	Critical Performance Parameters
CQA	Critical Quality Attributes
CV	Coefficient of Variance
DAPI	4',6-diamidino-2-phenylindole dilactate
DoE	Design of Experiments

EDTA	Ethylenediaminetetraacetic acid
EMT	Epithelial-to-Mesenchymal Transition
EPO	Erythropoietin
FDA	US Food and Drug Administration
FGF	Fibroblast Growth Factor
FMEA	Failure Mode and Effects Analysis
GMPs	Granulocyte/Macrophage Progenitors
HAND1	Heart and Neural Crest Derivatives-expressed protein 1
hESC's	Human Embryonic Stem Cells
HFEA	Human Fertilization and Embryology Authority
HSC's	Haematopoietic Stem cells
HTA	Human Tissue Authority
ICH	International Conference on Harmonisation
IMS	Industrial Methylated Spirit
IOS	International Organization for Standardization
LT-HSCs	Long-Term Hematopoietic Stem Cells
MACS	Magnetic-activated cell sorting
MEPs	Megakaryocyte/Erythroid Progenitors
mESC's	Mouse Embryonic Stem Cells
MNC's	Mono-Nuclear Cells
MPO	Myeloperoxidase

MRI	Magnetic Resonance Imaging
n	Sample Size
PAT	Process Analytical Technology
PBS	Phosphate Buffer Solution
PI	Propidium Iodide
PWB	Perm Wash Buffer
QbD	Quality by Design
R^2	R-Squared (Statistics)
RBCs	Red Blood Cells
Re	Reynolds Number
RM	Regenerative Medicine
ROI	Region Of Interest
RT-PCR	Real Time Polymer Chain Reaction
S	Standard Error of Regression
SCF	Stem Cell Factor
SEM	Standard Error of the Mean
ST-HSCs	Short-Term Hematopoietic Stem Cells
TDL	The Doctor's Laboratory
TNCs	Total Nucleated Cells
UV	Ultraviolet
VEGF	Vascular Endothelial Growth Factor

1. INTRODUCTION

1 Introduction

Regenerative medicine (RM) is used to refer to methods to replace or regenerate human cells, tissues or organs in order to restore or establish normal function. This includes cell therapies, tissue engineering, gene therapy and biomedical engineering techniques, as well as more traditional treatments involving pharmaceuticals, biologics and devices (1). RM has been evolving slowly and gathering pace from translational lab based experimental disciplines into a nascent industry (2,3). This growing industry is expected to move swiftly into the clinic within the next decade, meaning there will be a growing need for a diverse range of RM products many of which will incorporate living cells. This promotes a need for novel yet robust manufacturing processes for cell-based systems that are capable of meeting the stringent regulatory needs imposed on medical product manufacture (2–5).

This requirement to manufacture cell based products poses a brand new challenge to the current industry and prior manufacturing processes which have only utilised cells in order to make a product, in contrast this evolving industry requires cells themselves to be the product rather than using the cells to produce the product, such as monoclonal antibodies and recombinant protein production (6). The challenges revolve around the complexity of a biologically living product where there is sensitivity and responses to the environment. By definition a life is "the condition that distinguishes organisms from inorganic objects and dead organisms, being manifested by growth through metabolism, reproduction, and the power of adaption to environment through changes originating internally" (7). Also defined as "a living organism is an organized unit, which can carry out metabolic reactions, defend itself against injury, respond to stimuli, and has the capacity to be at least a partner in reproduction" (8) These definitions state that a living product is in a constant state of change in response to its environment, highlighting that the manufacturing process requires precise control. Koshland named the seven pillars of life in which one is adaptability, meaning there is an intrinsic feedback response to the environmental

changes within living organisms (8). Importantly there will always be some state of heterogeneity within a cell population due to changes in cell microenvironment which are currently even harder to control than the evolving macro environment (9).

Many of the current solutions and technologies that have been developed within the conventional biologics manufacture cannot be applied to cell therapies (3). This is largely due to the adherent nature of the human cells required for transplantation, whereas traditional biochemical manufacture has used engineered suspension cell lines in large volume bioreactors. New or adapted technologies are also required for the finishing steps of a process where current downstream processing prevents the purification of viable cells as a final product. Living cells do not fall into any of the 'common' medical product categories such as stents, tablets or syringes; which has created a challenge for both regulators and commercial bodies (10). Numerous treatment strategies have been proposed and developed in the field of RM, however there is still a need for fundamental technologies and infrastructure to support this emerging industry and upkeep widespread adoption. The greater sensitivity and difficulty of cell product measurement emphasises the need for better process control and understanding within the field of RM (3,10).

One current aspect of this need for improved process control is being tackled with statistical control. To reduce variability within a process Six Sigma was developed from conventional manufacturing disciplines by the global companies Motorola/Toyota. Prior to Six Sigma, in the 1920's, there had been a history of quality improvement running through statistical control. Following these developments a lean version of Six Sigma was subsequently developed in order to prevent and reduce waste. Mid-way through the 21st century design of experiments (DoE) was adopted to further improve quality within a process. This was later formalised into International Organization for Standardization (ISO's) in the late 1900's. This historical learning has since been built into an industry tailored system that borrows heavily from these historical developments and tools. More recently in 2004, the US Food and Drug Administration (FDA) produced Quality by Design (QbD) initiatives to promote pharmaceutical manufacture and product quality.

1.1 Quality by Design

1.1.1 Introduction

In 2000, the suboptimal drug manufacture process along with FDA's out-dated review process prompted concern for the regulatory industry (11). As far as the pharmaceutical industry was concerned the product quality was satisfactory, however there was a reluctance to embrace new technologies as the adoption by the regulators of such innovation was unknown. There was also concern for the emphasis of drug manufacturing that was placed on final product quality and the manufacturing process itself was disregarded as immaterial. The material shared with the FDA was empirical with little model prediction or forecast for product variability based on upstream variation (11). All this showed an inability to analyse and predict root causes of variation in the final product of drug manufactures. In some cases the reported waste amount was as much as 50% of the manufactured product (11). All of these issues led to higher manufacturing costs which the FDA determined were due to manufacturing inefficiencies and the difficulty regulators made implementing changes to an industrial process. Because of these concerns the FDA implemented more stringent oversight and monitoring of manufacturing processes which had a knock on effect causing delays in development of new drugs, and a large increase in supplementary applications for manufacturing changes. In 2007 alone the FDA received more than 5000 supplements for new drug applications, biological license applications and abbreviated new drug applications (11). The data required for both the supplementary and original applications was largely based on the chemistry with the engineering aspects largely disregarded, along with product development and processing. The FDA continued with further regulatory restrictions and guidance documents in 1996 and 1999 (12,13). By implementing these changes the industry were pressurised with increasing rules and laws to abide by to ensure product quality. These new documents along with new responsibilities for regulators, such as

counterterrorism and pandemic oversight, meant increased review times and put a real burden on the FDA's resources (11).

In 2002, the FDA addressed these issues by releasing a document entitled "*Pharmaceutical cGMP ([current] good manufacturing practice) for the 21st Century – A Risk-Based Approach"* with the goal to 'enhance and modernize the regulation of pharmaceutical manufacturing and product quality – to bring a 21st century focus to this critical FDA responsibility' (14). In-line with this document, the International Conference on Harmonization (ICH) published guidelines stating suggested contents for the Pharmaceutical Development section of a regulatory submission, *Q8 Pharmaceutical Development* (15).

Finally, Quality by Design (QbD) was first introduced into the chemistry, manufacturing and controls review process in 2004 as a result of the Pharmaceutical cGMP for the 21st Century initiative.

1.1.2 Quality by Design Definition

QbD has become an important paradigm in the pharmaceutical industry since its introduction by the FDA in the aforementioned documents (Section 1.1.1). It was the answer for the FDA to move towards a more scientific, risk-based, holistic and proactive approach to pharmaceutical development (11). The global goal of QbD is to embed quality into pharmaceutical products to ultimately protect the health of the public (16), which is the FDA's primary commitment. This notion promotes industries knowledge of both their product and the process used to achieve the said product starting with process development all the way through to the final product. The ICH declares that the desired state for pharmaceutical manufacturing is 'product quality and performance achieved and assured by design of effective and efficient manufacturing processes' (15). This is achieved by incorporating quality by design throughout the lifecycle of a products development with companies defining desired product performance, identifying critical quality attributes (CQAs) and operating within a defined design space (16). With this information in

hand, a company should be able to tailor the product formulation and process to meet these specified product requirements. This leads to the necessary understanding of raw material attributes and process parameters effects on CQAs along with the variability sources. With this as common knowledge a company then has the ability to continually monitor and improve its manufacturing process in order to ensure product quality and ultimately patient safety. This systematic approach draws away from the traditional, empirical approach that was mentioned previously and highlighted below in Table 1. In conclusion the ICH define quality by design as 'a systematic approach to development that begins with predefined objectives and emphasizes product and process understanding and process control, based on sound science and quality risk management' (15).

Table 1. Quality by Design (QbD) approach versus the traditional approach (17,18) This table compares and contrasts how the traditional approaches to manufacturing have been modified to produce a Quality by Design approach to manufacturing that reduces risk by having a science platform to work and learn from.

QBD Approach	Traditional Approach
Knowledge rich approach – showing high levels of product knowledge and process understanding	Data intensive approach – disjoined, uncharacterised information with low process knowledge / understanding
Quality is built into products and process by design, based on scientific understanding of both	Quality is assured by testing and inspection
Specifications based on product performance requirements	Specifications based on batch history
Flexible process within design space, allowing continuous improvement	Fixed process Change / improvement discouraged
Focus on robustness – understanding and controlling variation	Focus on reproducibility – often avoiding or ignoring variation

1.1.3 QbD Implementation

In order to successfully implement QbD into a biotech product, a number of steps must be followed (Figure 1). The process begins with identifying the customer and the need, and ends with process validation and continual monitoring. Throughout the process a number of risk assessment steps are carried out which aid process characterisation. These steps have all been an improvement from the traditional Six Sigma model. Motorola 'invented' the Six Sigma strategy, which is named for a statistical measure of variation (the standard deviation of a normal distribution). Six Sigma was adopted in order to set process tolerance limits to ensure defective products fall to the required low level (19). These process limits are set to include observations within 6 standard deviations of the mean, or Six Sigma. Setting tolerance limits at lower levels of sigma results in higher rates of defects. The Six Sigma design process is shown in Table 2.

Table 2. Six sigma 5 steps for designing a process (20) Six sigma provides a statistical measure of variation, and is carried out through 5 steps, define; measure; analyse; design and verify. Quality by design approaches build on the six sigma base level to further improve manufacturing.

Define	Define the project's goals and customer deliverables (internal and external)
Measure	Measure and determine the customers' needs and specifications
Analyse	Analyse the process to meet the customers' needs
Design	Design the process to meet the customers' needs
Verify	Verify the design performance and ability to meet customers' needs

QbD relates an industry specific adaptation of historic quality principles by introducing further steps to achieve specified product quality. By increasing the 5 core steps of Six Sigma into a flow diagram QbD is better defined by breaking down each step into more defined areas. This is shown in Figure 1.

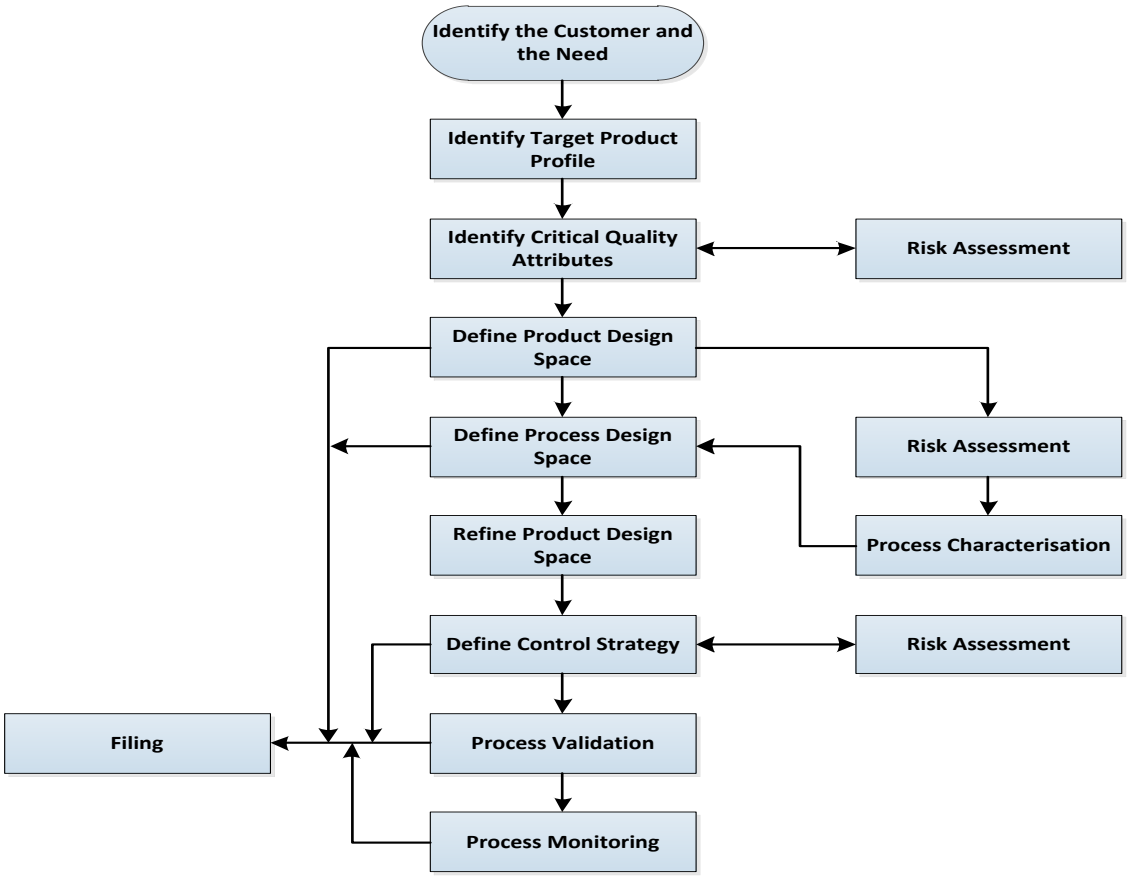

Figure 1. Key steps required to implement the QbD approach for a biotech product (11) In contrast to six sigma, QbD builds on these principles to create a more detailed process map for manufacturing by expanding on each of the 5 six sigma steps.

There currently lies a huge dilemma within the biotech industry, either a company can invest comprehensively in product and process characterisation at an early stage, which QbD strongly suggests, or wait until the market success of the product can be better assessed. The first approach requires a large amount of initial investment but eventually yields a more reproducible, lower risk product. However in order to implement QbD a large upfront work load is required at a time where evidence may not be sufficient to justify the investment, the following sections highlight some of the key required capacity.

1.1.3.1 Identify Critical Quality Attributes (CQA)

Once the need and profile of the product has been recorded, the next step is to express the Critical Quality Attributes (CQAs). These are defined as 'a physical, chemical, biological or microbiological property or characteristic that should be within a range or distribution to ensure

desired product quality is achieved' (15). The CQAs are defined through the use of a risk assessment, previous laboratory knowledge, along with clinical experience and are essential to successfully implement this stage of the QbD process. The CQAs help relate safety to efficacy for the given biotech product, and a completed risk assessment will rank the CQAs in order of importance. Key factors that the risk assessment will highlight include sources of variation, likelihood of deviation from a set range, certainty that the deviation will have an impact on the process or end product, and severity of the change in product quality. CQAs by name are a new concept under the QbD tree, however as part of Six Sigma a key aspect was to analyse why there were 'failures' and prioritise the factors or attributes based on severity, the same as CQA's just not named such under Six Sigma (19,21).

1.1.3.2 Define Product Design Space

After the critical quality attributes have been defined it is possible to set the design space which will determine the probability of achieving the required CQA values. The design space is defined by the ICH as,

'The multidimensional combination and interaction of input variables and process parameters that have been demonstrated to provide assurance of quality. Working within the design space is not considered as a change. Movement out of the design space is considered to be a change and would normally initiate a regulatory post approval change process. Design space is proposed by the applicant and is subject to regulatory assessment and approval.'(15)

Thus by using the CQAs that were previously defined, the design space can be expressed in relation to these stipulating maximum and minimum values. By operating the process within this defined range fluctuations are tolerable and yet the process can still be controlled. Also changes to the process can easily be implemented under the same filing as long as the process remains within the defined design space (22).

In QbD an improved understanding of how the CQAs link with the safety and efficacy of a product is required, and identifies the importance of analytical, non-clinical and animal studies in creating these linkages (23).

1.1.3.3 Define Process Design Space

Using the same definition described previously (Section 1.1.3.2), the design space of the process can be characterised similarly to the product design space approach shown in Figure 2. Firstly a risk assessment will identify the parameters which need to be characterised or optimised within a process. Following this, design of experiments (DoE), can be implemented to help understand the relationship between such factors and therefore design the space which the process must operate within to deliver the defined product quality range. Failure mode and effects analysis (FMEA) can then be utilised to assess the potential degree of risk for every operating parameter. This leads to prioritisation of factors in order to understand the impact they can hold on the performance of a process. The outcome of the FMEA is a risk priority number which identifies the main operating parameters that may require further consideration. By taking the outcomes from these tests there is then often a scale up correlation that is applied to translate operating conditions between different scales or equipment.

Both FMEA and DoE are not novel analysis tools for the biotech industry however their use in linking CQAs to design space within the RM industry is.

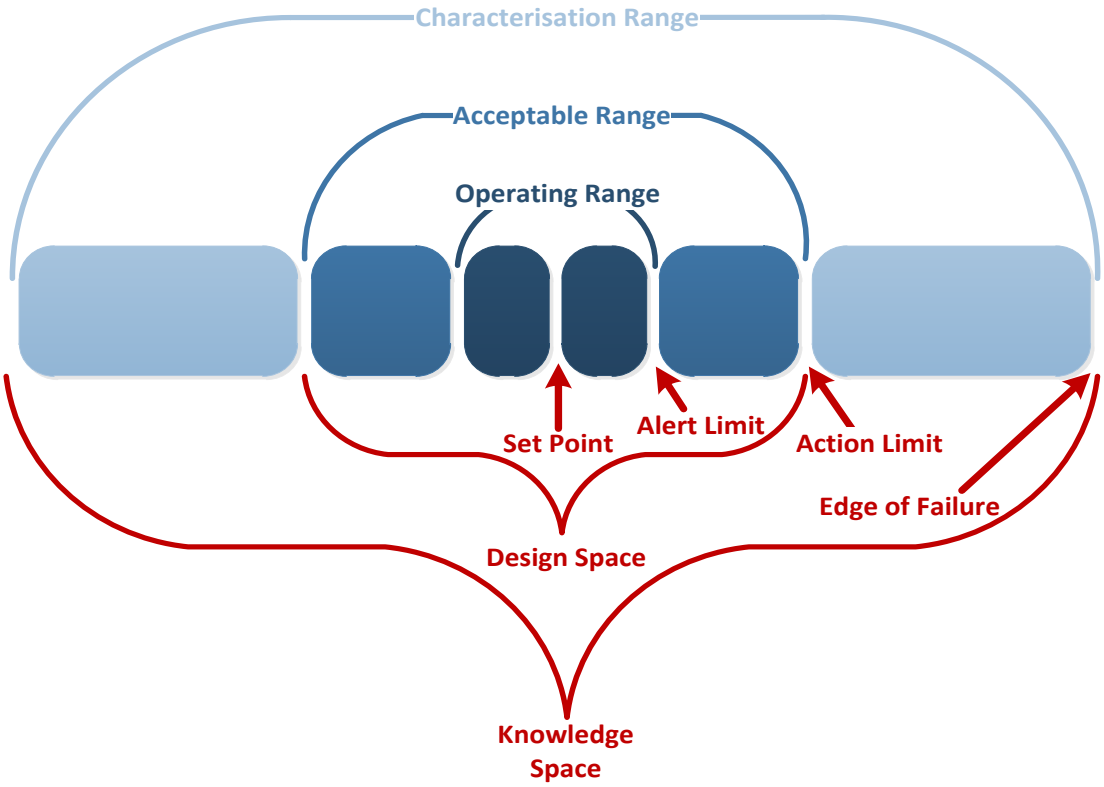

Figure 2. Diagram to define the process design space, which sits within knowledge space. Within QbD a key part is to define the design space in which a process operates. This diagram illustrates the how the knowledge space provides the characterisation. Within the knowledge space will be the design space or the acceptable range for a process to operate. Within the design space sits the operating range, either side of the set-point for a process. By defining the operating, acceptable and characterisation ranges then the alert limits, action limits, and edge of failures are defined.

1.1.3.4 Define Control Strategy

The FDA defines control strategy as 'a planned set of controls, derived from current product and process understanding that assures process performance and product quality'(24). Within the QbD paradigm, the risk assessment will establish the control strategy based on the CQAs and process capability. The control strategy can involve some of the following elements: in-process control, lot release tests, process monitoring and characterisation testing (11). The use of risk assessments to identify the control strategy is a novel concept unique to the QbD notion. By using the DoE approach and the process design space, this allows an assessment of precision and accuracy within which the operating variables need to be controlled, allowing the control strategy to be scientifically designed.

1.1.4 Process Monitoring

After filing, the CQAs are continually monitored to ensure the process is operating within the defined space that was submitted to the regulators. Within the QbD paradigm any process changes that occur within the defined design space are not required to be reviewed or assessed as process changes. This therefore allows process changes without approval submissions, allowing more flexibility whilst maintaining product quality. However in building a QbD system the process has to show robustness towards quality with respect to four key elements (11);

- Process performance/product quality monitoring
- Preventative/corrective action
- Change management
- Management review of process performance and product quality

These steps require optimisation in order to obtain an overall best process; process monitoring. Process analytical technology (PAT) is the name given to such technologies, which are discussed in the following section.

1.2 Process Analytical Technology (PAT)

Biological products are very sensitive to the effects of process perturbations including variations in the raw materials as well as unknown effects of process parameters. These deviations may result in variability, therefore as a consequence the product becomes 'out of specification.' These undesired products can then have an unwanted effect on patients receiving treatment whether it be safety, efficacy or undesired responses. Therefore in order to develop a biological therapy for use in patients, the key objective is to create a controlled process that delivers a consistently high quality product by remaining within the design space and therefore meeting the accepted criteria (18).

The development, qualification and validation of analytical methods are extremely important aspects of reliable safe biological manufacture. Such systems that are used for designing, analysing and controlling manufacturing to make timely measurements or critical quality and performance attributes are known as PAT or Process Analytical Technologies. They are also common practice for validating processes and elucidating the cause and effects of variability seen within a production line (25). Such culture attributes may pose a significant challenge because of their complexities and difficulties, and furthermore analytical tools are expensive but yet a vital aspect for product analysis.

Significant progress has been made recently to develop novel analytical tools for identification, however certain culture attributes are still not well understood (26). Consequently there is still undetected variability within raw materials which may be expressed into a final product. Especially within the RM industry it may never be possible to measure all the required attributes for a comprehensive guarantee of quality, and therefore we only may be able to take a QbD 'spirit' approach. Wrong CQAs can be as bad, if not worse, than no CQAs as they portray a false confidence. It is therefore imperative that the Critical Process Parameters (CPP) which may affect the CQAs within a manufacturing process can be measured. A key point to also acknowledge is that the principle of Process Analytical Technology umbrellas this as a 'mechanism to design, analyse and control…manufacturing processes' (26). The goal of PAT is to define and provide the measurement capability to design and develop processes that consistently ensure a product of required quality, with the ambition to continually improve efficiency through real time or improved product release tests (26). Through PAT there is the ability for continuous quality assurance resulting in improved operational control and compliance, ultimately leading to more reliable product quality (27). Essentially PAT are the tools required to achieve a QbD based process; there are critical attributes that determine process and product success, these attributes need to be measured with well-designed assays, the system as a whole is known as Process Analytical Technologies.

1.3 Benefits of QbD/PAT

One of the primary advantages for incorporating QbD paradigm into current manufacturing processes, whether they are in development or fully functioning is the lower regulatory burdens and greater flexibility in decision making based on science rather than empirical data. This ensures a more efficient, quicker review process, resulting in quicker approval as well as reducing the number of manufacturing supplements required for post-market changes (28).

QbD can also reduce manufacturing costs by reducing waste and improving product quality. For example, by holding a better understanding of both the product or active ingredients and your process, it is possible to fully understand the impact of the process on your active ingredients. This means as well as reducing your waste, there is a possibility to reduce your raw material costs whilst maintaining or even improving your final product quality. This leads directly into an overall lower economic risk due to less probability of patient harm, unforeseen events, failure to manufacture product and therefore failure to deliver the product.

The ultimate goal of PAT is the ability for real time product release, whereby quality is based on a few in-process monitoring tools of process characteristics, and the need for final product release tests are redundant. Due to the QbD framework, right first time quality can also be achieved, rather than the current development that requires constant refining until the optimum can be achieved. The benefits of using PAT under the QbD paradigm are summarised in Figure 3.

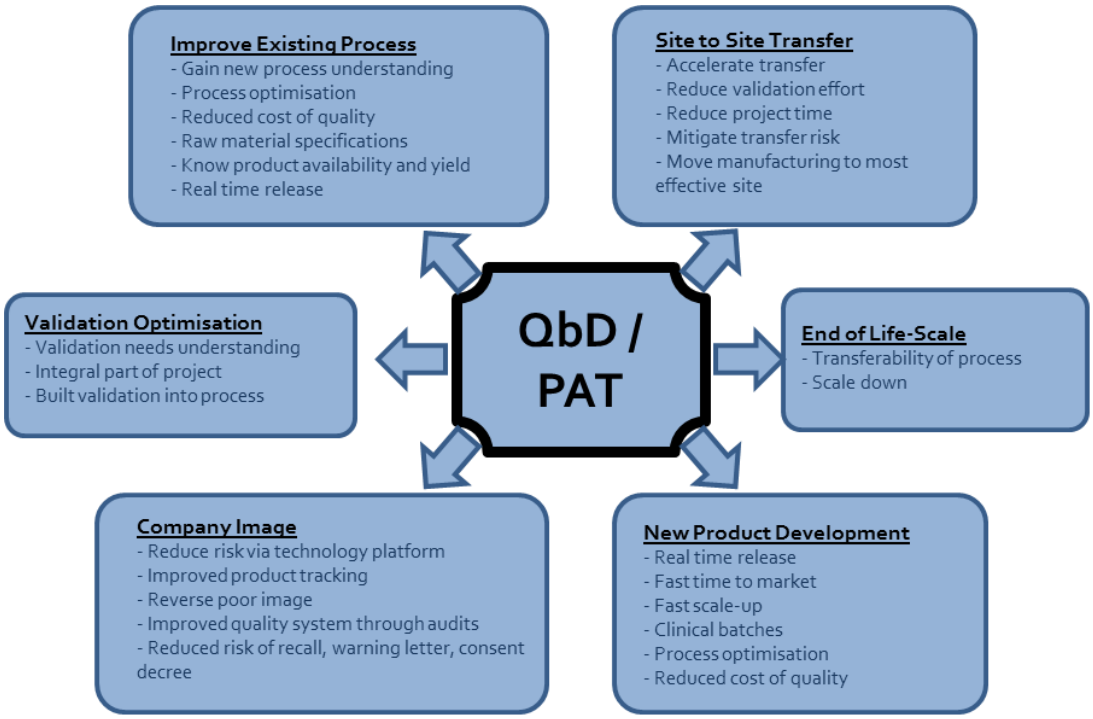

Figure 3. The key business drivers for QbD and PAT (18) There are many benefits to utilising QbD approaches within a process. This diagram highlights some of the key drivers for businesses to adopt QbD grouped into 6 categories ranging from validation benefits to product development and site transfer.

For these goals to become realistic both QbD and PAT need to be embedded within the development of a process as well as the final manufacturing process. Therefore it is important at this stage to begin developing future tools that are capable of allowing QbD to be implemented into the manufacturing process. Although assays are a major part of the analytical toolbox available, to successfully characterise product quality and safety there is a need to discover new tools that can non-invasively produce either similar or improved results.

1.4 A Novel Analytical Tool

Within RM both safety and efficacy requirements must be stringently upheld. This has been possible within conventional chemical-based pharmaceutical drugs through adherence to strict regulations and the ability to monitor processes and complete timely end point assays. However for cell-based material different strategies will be required to evaluate their quality (10,29).

These quality assessment criteria are currently regulated by individual nations and therefore have varying degrees of level and scope when determining quality. Some of the more common referred references are 'Current Good Tissue Practice,' (30) '21 Code of Federal Regulations (CFR) Parts 1270 and 1271 of U.S. Food and Drug Administration (FDA)' (31). These documents attempt to mitigate the risk associated with cellular products mainly in two key areas, cellular contamination and non-cellular contamination. However there are still very few documents that require a control of cell quality and this is often at the discrimination of the manufacturer to advise and provide evidence of conventional cell quality evaluation techniques. These include biomarker tests like RT-PCR or immunostaining; safety assessments in animal implant tests; and chromosomal tests for tumorigenic risk, which all require cell destruction processing such as those associated with fixation reagents or cell-lysis buffers. In order to fulfil quality assessments and provide both examined and non-examined cells to be used for therapy there is a need to develop tools capable of overcoming key problems associated with conventional quality assessments (2,10,28). These problems include invasiveness; lack of exhaustive characterization, time limitations and instability of cell quality markers.

Cells prepared for therapeutic use need to maintain viability and perform as required. The current use of artificial probes, markers and gene transfer for example could all trigger cellular abnormalities (10) and therefore it is advantageous to develop analysis techniques that do not require any invasive mechanism. Another advantage to a non-invasive application is the limited number of cells that are often produced, especially for autologous therapies due to the constraint of the cell source material. This lack of cellular product also means that sampling is undesirable, due to the considerable cost of the product. By removing a sample, there is a reduction in the total product. Compared to conventional chemical compound manufacturing, human cells also exhibit huge variances often unattainable to process control (32). Therefore the variation in the product cannot be controlled through pre-determined fixed process variables (due to sensitivity of product and dimensions of plasticity) and therefore a method of adaptive process control is

required that monitors and responds to product. Sampling therefore does not always assure the total quality of the product and the requirement for constant, large samples further combine to the current lack of cell source material as discussed previously.

Alongside a non-invasive, complete characterisation technique there is also a desire to produce a real-time platform. Current processes often require days or weeks before results are obtained, at which point further processing costs have already been associated, which may even include administration of the cells to a patient. This implies that patients could have cells injected prior to a full analysis being completed. Thus the requirement for a real-time or at least a short term assay is valued. The ability to measure the product immediately before administration currently is not achieved and as is well documented the stability of cells through culture can rapidly change (33). Such stability includes contamination which can take over a culture within hours. This is why end point assays are commonly associated with high error rates as individual cells often differ in their characterisation with respect to differentiation, mobility, size, shape and production activity, to name but a few.

The final point is providing a reproducible characterisation procedure. Many of the characterisation assays commonly used are subjective and user-defined. Process automation has been instrumental in achieving defined, standardised processes in many manufacturing industries (3,5,28). Automation also allows scale-out of processes by increasing the number of units within the production process, with predictable process variation and predictable costs. The afore mentioned systematic process improvement methods such as Six Sigma and QbD have been successfully developed and utilised within electronic and automotive industries within automated processes. Automation is central to using these systematic tools efficiently and effectively by reducing user variation and achieving predictable process variation as mentioned previously (34–36).

Currently there are no automated, non-invasive, real-time technologies used within the RM industry that are capable of accurately and reliably measuring the key critical attributes and

therefore there is no way of relating this to whether a process is operating within specification. This is an important issue currently for cellular therapies where many of the assays are invasive and often include attaching fluorescence probes, which are likely to alter the phenotype of the cells. It is therefore essential to include automation within a novel analytical tool (4,34).

1.5 Current Imaging Techniques

Imaging provides a real-time analysis method for cell therapies. Various imaging modalities are now used within research laboratories, the more common are further discussed in this section highlighting their potential for use in a manufacturing setting for the RM industry.

1.5.1 Raman Spectroscopy

Raman spectroscopy is a technique used to observe vibrational, rotational and other low frequency modes in a system. It relies on an inelastic scattering of monochromatic light. The light source, often a laser, interacts with the molecular vibrations resulting in the energy of the laser being shifted either up or down. This shift in energy provides information related to the vibrational modes of the system. Based on this scattering of photons, their biomolecular composition and structural conformations of macromolecules in living cells can be distinguished (37).

Raman spectroscopy allows functional imaging of live cells non-invasively without labelling or sample preparation however spatial resolution is still a drawback (38,39). Current techniques create a low scattering of light and therefore there is a lack of resolution, this is overcome using ultraviolet (UV) resonance Raman spectroscopy, but this cannot be carried out on live cells due to the UV damage that would be caused (39).

Another drawback of this current technique is acquisition time which is related to the low scattering of light and uncorrelated noise (38). Acquisition times of 2-10 minutes per cell are

commonly reported in literature (37,38,40). This long acquisition time deems Raman spectroscopy currently impractical within a manufacturing setting where large cell numbers require non-invasive analysis, and therefore prevents widespread adoption in both biological research and clinical practice (41).

1.5.2 Magnetic Resonance Imaging (MRI)

Magnetic resonance imaging (MRI) is used primarily in medical settings to produce high quality images *in vivo* (42). The underlying principle is nuclear magnetic resonance; a fundamental property of elementary particles is their nuclear spin or rotation. All particles have a spin and this nuclear spin results in a magnetic moment, but only the atoms with an uneven spin are magnetically susceptible and therefore suitable for MRI (43).

Firstly, to form a magnetic resonance image a strong magnetic field is applied. This causes the spins of all atoms to align with the external magnetic field. Following this, a radio frequency pulse is induced which flips the spins out of alignment. Once the radio frequency is terminated, the spins relax back to their original state, aligning with the external magnetic field. During the relaxation stage, the energy released is recorded and forms an image. In order to build 3D images, magnetic fields are applied in all 3 dimensions with the results collated.

In general the limited sensitivity and high cost of MRI restricts its use for *in vitro* cell imaging applications. Often to increase sensitivity contrast agents are added such as iron oxide nanoparticles (44) or low molecular weight compounds containing lanthanide such as gadolinium (42). Research continues to find toxic free contrast agents such as an engineered transferrin receptor that recently has been used *in vitro* (45), but currently the addition of such contrast agents and the capital cost prevent the use of these cells post manufacturing and therefore deems MRI a non-viable form of non-invasive quality control.

1.5.3 Optical Microscopy - Phase Contrast

The description and classification of cells has, in the past, always derived from visual criteria (46). Therefore, developments were made to improve the visualisation of shape and cellular detail, as early cytochemical tests were used primarily for making cellular detail more distinct (46).

One method that has real promise to help fill this gap in technology is phase contrast microscopy. Imaging is cited as a specific opportunity within the FDA's Critical Path to New Medical Products (47), noting that "new imaging techniques will ultimately contribute important biomarkers and surrogate endpoints, but how soon these new tools will be available for use will depend on the effort invested in developing them specifically for this purpose." Imaging also forms a large subgroup of the current cell characterisation techniques outlined by the British Standards Institution (BSI) in PAS93:2011 (29). Furthermore imaging is a particularly attractive, enabling technology for biomarker development because of its capacity to provide non-destructive monitoring with high spatial and temporal resolution (48). While biomarkers are widely acknowledged as being enabling, it should also be recognized that the continuum from discovery to utility of a biomarker could be quite involved and challenging. Critical elements of that continuum include the validation and qualification of a relevant biomarker (48).

The word microscope comes from the Greek *micros* meaning 'small' and *skopein* meaning 'to look' (49). Using the definition of a microscope as 'an instrument that enables the visualisation of objects or structures that are usually invisible to the naked eye', then microscopes appeared at the end of the sixteenth century (50). The properties of concave and convex lenses were first described around the year 1000, although magnifiers in the form of lens-shaped crystals or glass may have been used much earlier. Spectacles were invented around 1300 and became widely used across Europe (50). There are many different names assigned to the microscope inventor including Zaccharias Janssen, Anthony Leeuwenhoek and Robert Hooke (51,52). The first published work from a microscope appeared in 1665 by Robert Hooke, and therefore it is often Hooke's name that is assigned to the inventor of the microscope. Although small breakthroughs

occurred up to the 18th century is wasn't until 1934 when Dutch physicist Frits Zernike first described phase contrast microscopy (53). Phase contrast is defined as 'a contrast-enhancing optical technique that can be utilized to produce high-contrast images of transparent specimens, such as living cells (usually in culture), microorganisms, thin tissue slices, lithographic patterns, fibres, latex dispersions, glass fragments, and subcellular particles (including nuclei and other organelles)' (54). Frits Zernike later went on to receive the Nobel Prize in Physics for his phase contrast microscope invention.

In effect, the phase contrast technique employs an optical mechanism to translate minute variations in phase into corresponding changes in amplitude, which can be visualized as differences in image contrast (55). This technique exploits interference effects to make transparent objects (such as cells) visible against a transparent background (such as culture media) (54).

Many biological structures can be revealed by using phase contrast that were not visible with a simpler brightfield microscope (29), the simplest microscopy technique that illuminates specimens using bright light, with contrast caused by more dense objects absorbing the light (29,55). One of the major advantages of phase contrast microscopy is that living cells can be examined in their natural state, whereas previously these structures were only seen by killing, fixing, and staining specimens (29). As a result, the dynamics of on-going biological processes can be observed and recorded in high contrast with sharp clarity of minute specimen detail (55). This therefore provides a technique capable of being exploited for the manufacture of living cells within the RM industry and is further deliberated in the following sections.

1.5.3.1 Phase Contrast Microscope Configuration

Presented in Figure 4 is a cut-away diagram of a modern upright phase contrast microscope, including a schematic illustration of the phase contrast optical train. Partially coherent illumination produced by the tungsten-halogen lamp is directed through a collector lens and

focused on a condenser annulus. Wavefronts passing through the annulus illuminate the specimen and either pass through undeviated or are diffracted and retarded in phase by structures and phase gradients present in the specimen (55,56). Undeviated and diffracted light collected by the objective is segregated at the rear focal plane by a phase ring and focused at the intermediate image plane to form the final phase contrast image observed in the eyepieces.

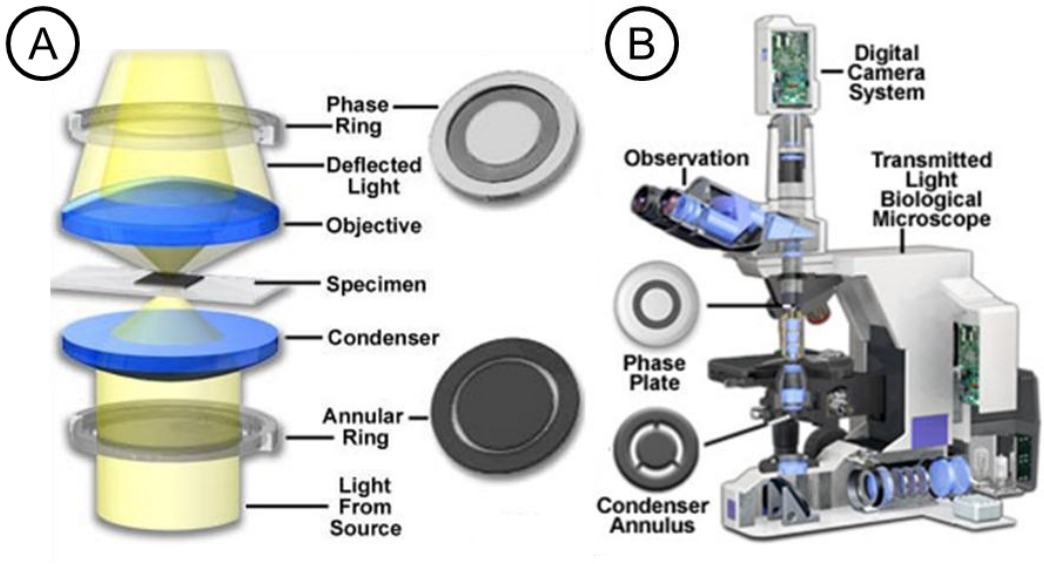

Figure 4. Diagram of a modern upright phase contrast microscope A) Phase Contrast light path(56) and B) Phase Contrast microscope (55). Phase contrast microscopy improves the contrast of cells compared to brightfield imaging. This is completed by the addition of a phase ring that causes the diffracted light to change its amplitude and therefore improve the contrast of the diffracted light when compared to the undiffracted light.

The addition of phase contrast optical accessories to a standard brightfield microscope can be employed as a technique to render a contrast-enhancing effect in transparent specimens that is reminiscent of optical staining (55). The only addition to brightfield microscopes are the annular ring (also known as the condenser annulus) and the phase ring (or phase plate) (29).

1.5.3.2 How Phase Contrast Works

Unstained specimens that do not absorb light are known as 'phase objects' as they alter the phase of the diffracted light by about ¼ wavelength compared to the undeviated light that passes through or around the specimen unaltered. However, our eyes are unable to detect these

phases differences as the eye is only sensitive to colour changes (light frequency) and to differing levels of light intensity (wave brightness).

In phase specimens the light either passes unaffected through the specimen or is diffracted. This diffracted light is not reduced in amplitude (which the eye can acknowledge) but is phase delayed by the specimen due to the specimen's refractive index. The diffracted light, which has now been phase shifted by -90° to the undiffracted or background light, arrives at the image plane out of phase with the undiffracted light but essentially with the same intensity.

In the Zernike phase contrast microscope, the light waves that are diffracted and shifted in phase by the specimen can be transformed by phase contrast into amplitude differences that are observable in the eyepieces. Frits Zernike achieved this transformation of converting essentially a phase shift into an amplitude difference. This is achieved by a further phase shift of -90° of the undiffracted light which as a result the direct and diffracted light arriving at the image level would be able to produce destructive interference. This results in an image appearing darker against a lighter background, known as 'dark' or 'positive contrast'. The opposite of this, phase shifting by +90°, causing the direct and diffracted light to arrive at the image level simultaneously, causes constructive interference. This is where the image appears bright against a darker background, and is known as 'negative' or 'bright contrast'.

The next step is to separate the direct light from the diffracted light. This is completed with the use of an annulus ring, as mentioned in Section 1.5.3.1. As the light passes through the annulus ring, a hollow cone of light is emitted on to the specimen, the direct un-diffracted light passes through the specimen undeviated and therefore arrives at the focal plane in the shape of a ring. The diffracted light is spread over the entire focal plane. With this set-up the diffracted light has roughly the same amplitude and is 90° phase shifted. This would result in little contrast, therefore as stipulated earlier the background light is phase shifted by 90°. This is achieved through the use of a phase ring at the focal plane. The narrow area of the phase ring, where the hollow cone of direct light passes is optically thinner than the rest of the plate and as a result the

undiffracted light is shifted -90° in traversing the glass of the objective than the diffracted light. This causes the direct light to be phase shifted resulting destructive interference providing positive contrast. If the narrow area of the phase ring is thicker than the direct light is shifted -90° and constructive interference occurs. This is shown in Figure 5.

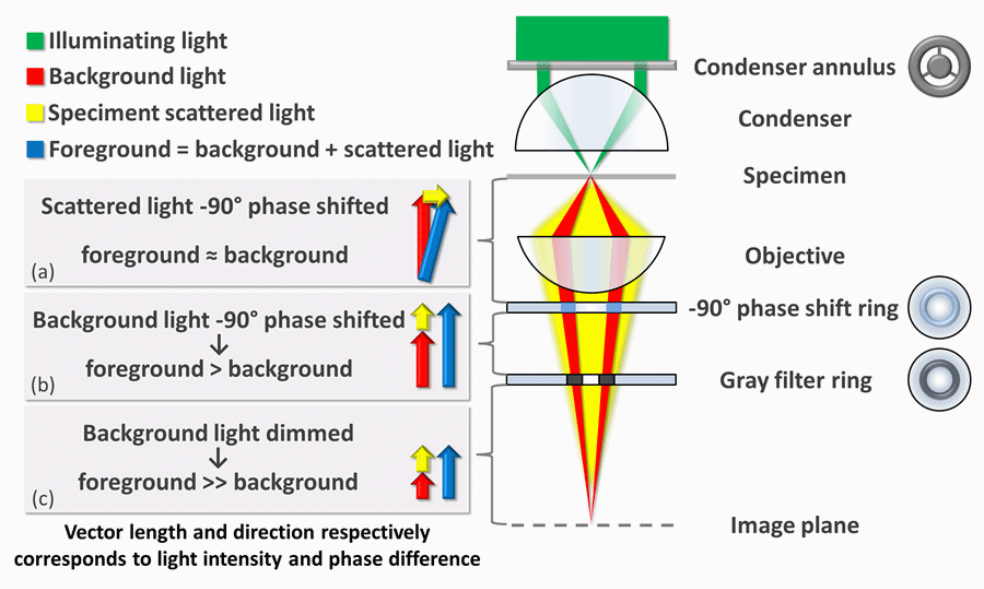

Figure 5. Working principle of phase contrast microscopy. Diagram to show how the condenser annulus and phase rings work in harmony to improve resolution of brightfield microscopy to provide phase contrast microscopy (57).

The performance of modern phase contrast microscopes is so refined that it enables specimens containing very small internal structures, or even just a few protein molecules, to be detected when the technology is coupled to electronic enhancement and post-acquisition image processing (55).

By introducing the ring aperture for illumination and a corresponding phase ring for phase retardation of the undiffracted component of the object wave, a higher lateral resolution and lower noise level are experienced when compared to traditional brightfield microscopy (this can be seen in Figure 6). However, one disadvantage of introducing the phase ring a halo and shade-off effect appear. In a typical Zernike phase contrast microscope the undiffracted component and part of the diffracted component lie on a continuous phase ring in the Fourier plane. When the diffracted component is phase shifted erroneously by the phase ring, the halo, and shade off

effects appear (58). The halo effect can be seen in Figure 6 as a bright boundary around the dark regions of the image, in this case the cells themselves (55). The shade-off effect corresponds to the misleading drop-off of the image intensity in the centre of extended bright areas or the increased intensity in the centre of dark regions (58).

Another effect of using phase contrast microscopy compared to brightfield microscopy is that the use of the phase annulus means the working numerical aperture is limited, this causes a small often negligible effect on resolution of phase contrast images (56).

1.5.3.3 Image Appearance

Presented in Figure 6 is a comparison of living cells in culture imaged in both brightfield and phase contrast illumination. The cells are human glial brain tissue grown in monolayer culture bathed with a nutrient medium containing amino acids, vitamins, mineral salts, and fetal calf serum. In brightfield illumination (Figure 6 (left)), the cells appear semi-transparent with only highly refractive regions, such as the membrane, nucleus, and unattached cells (rounded or spherical) are visible. When observed using phase contrast optical accessories, the same field of view reveals significantly more structural detail (Figure 6 (right)). Cellular attachments become discernable, as does much of the internal structure. In addition, the contrast range of the image taken using phase contrast is dramatically improved.

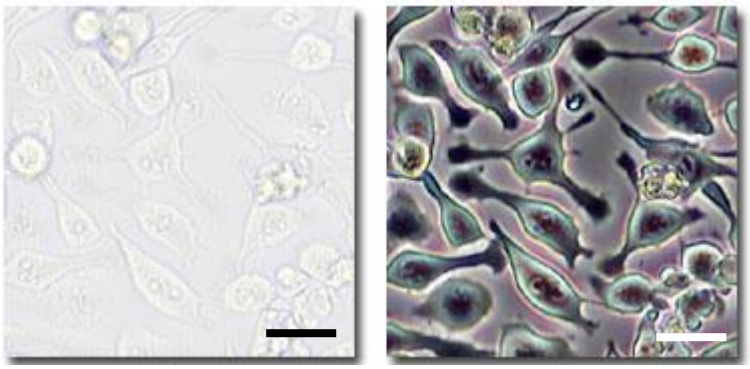

Figure 6. Comparison of Brightfield image and Phase Contrast image (55) Phase contrast microscopy enhances the difference between cells and media. The phase shift that occurs in phase contrast microscopes (right image) provides increased detail that is unattained with brightfield imaging (left image), 10 µm scale bars.

The phase shifts described in Section 1.5.3.2 are dependent on the illuminating lights wavelength, and from this the colours seen in Figure 6 are a result of large phase shifts. Phase contrast is only linear for small changes in phase, and the changes noted here represent much larger changes in phase. This said the comparison of brightfield to phase image in Figure 6 highlights the contrast enhancement using phase contrast microscopy to brightfield. Zernike's development of phase contrast optical theory is an excellent example of how research resulting from a highly specialized field such as optical physics can yield innovative new developments in seemingly unrelated disciplines, such as biology and medicine. During the Second World War, the Zeiss Optical Works in Jena, Germany, was the first manufacturer to incorporate practical phase contrast optics into their microscopes (55). The immediate impact on biological research was significant, and widespread application of the technique continues to the present day. Modern phase contrast objectives, designed and produced by optical manufacturers, are capable of operating in combination with auxiliary contrast-enhancing techniques, such as differential interference contrast, fluorescence, and polarized light (55). These objectives are available with internal phase plates that have varying levels of absorption and phase displacement of the surround (undiffracted) illumination to produce a wide spectrum of specimen contrast and background intensity choices for phase contrast microscopy.

1.6 Automated, Non-invasive Phase Contrast Microscope as a Process Analytical Tool

Phase contrast is an excellent method for enhancing the contrast of thin, transparent specimens with a trivial loss of resolution, and has proven to be a valuable tool in the study of dynamic events in living cells. Prior to the introduction of phase contrast optical systems, cells and other semi-transparent specimens were rendered visible in brightfield microscopy by artificial staining techniques (56). Although these specimens can be observed and recorded with darkfield and oblique illumination, or by defocusing a brightfield microscope, this methodology has proven unreliable in providing critical information about cellular structure and function (55).

The technique of phase contrast is widely applied in biological and medical research, especially throughout the fields of cytology and histology. As such, the methodology is utilized to examine living cells, tissues, and microorganisms that are transparent under brightfield illumination. Phase contrast enables internal cellular components, such as the membrane, nuclei, mitochondria, spindles, mitotic apparatus, chromosomes, Golgi apparatus, and cytoplasmic granules from both plant and animal cells and tissues to be readily visualized (55). In addition, phase contrast microscopy is widely employed in diagnosis of tumour cells and the growth, dynamics, and behaviour of a wide variety of living cells in culture. Specialized long-working distance phase contrast optical systems have been developed for inverted microscopes employed for tissue culture investigations (55).

Industrial and chemical applications for phase contrast include mineralogy, crystallography, and polymer morphology investigations. Colourless microcrystals, powders, particulate solids, and crystalline polymers, have a refractive index that differs only slightly from that of the surrounding immersion liquid, and thus are often easily observed using phase contrast microscopy. In fact, quantitative refractometry is often utilized to obtain refractive index values and for identification

purposes. Other commercial products scrutinized by phase contrast optical techniques include clays, fats, oils, soaps, paints, pigments, foods, drugs, textiles and other fibres (55,56).

Reduction in halo and shading-off artefacts remains a primary concern in phase contrast microscopy. Apodized phase plates are useful for reducing the severity of halo, and specialized variable phase contrast systems can be fine-tuned to control these effects in order to optimize image quality and the fidelity of information obtained by the technique (55). There is also considerable interest in the development of advanced phase contrast systems that provide accurate measurements of phase specimens with large optical path differences, as well as combined observations with other contrast-enhancing techniques. In particular, phase contrast is often utilized by overlapping images with fluorescence imaging to determine the locations of fluorophores, and shows promise for enhancing contrast in scanning optical microscopy with well-understood biological targets.

Already possible are detailed views of how proteins and lipids interact within a cell in order to govern generation, maintenance, and functionality of that cell. This is achieved from biochemical and genetic experiments spanning diverse approaches from reconstructing the cellular processes to atomic resolution imaging (59). However this cellular activity is commonly assessed as only a snap shot, one point in time. Recently it is becoming increasingly possible to view these processes in real time as they happen, with light microscopy adding a vital dimension to the analysis of cellular function (60). One such example was the discovery of kinesin after video light microscopy formed the basis of a motility assay in 1985 (61). Further discoveries of such proteins have transferred our understanding of how mitosis is achieved. In order for live phase contrast imaging to be utilised as a reliable process analytical tool the environment in which the cells are placed in order to capture high quality images is crucial.

1.7 Cell Environment

To successfully image cellular processes in living cells, the cells must be kept in an environment that does not induce stress responses, which can alter the cellular processes of interest (62). Some of the key factors to consider are the type of culture medium and its contents and the temperature of the sample, which must be kept stable at 37°C for mammalian cells. Moreover, the pH of the sample must be maintained at a physiological level and evaporation of the medium must be minimized to avoid changes in osmolarity (63).

1.7.1 Media

Mammalian cells require CO_2 purged bicarbonate-based media to maintain pH levels. Cells grown without this CO_2 environment rapidly enter apoptosis unless there is a suitable buffer replacing the role of CO_2, such as HEPES. HEPES maintains the physiological pH range of ~7.4, and therefore creates an environment for cell proliferation. Carbonate is an essential product for many cellular processes as well as buffering a solution, such ions as Ca^+, Na^+, Cl^- are related to the carbonate solutions and play pivotal roles as exchangers and co-transporters (64). Importantly these buffers have no effect on image quality.

1.7.2 Temperature

Maintaining a constant temperature for the cells is crucial for successful cell culture (65). There are 4 core methods for maintaining temperature whilst also imaging the culture that are relevant if temporal or spatial resolution is required that prevents manual removal from an incubator. Each of these is further discussed regarding their advantages and disadvantages.

1.7.2.1 Microscope Enclosures

The majority of microscope manufacturers now produce large boxes to place around their microscopes to maintain a constant environment, known as microscope enclosures. Compared to

a standard incubator there is still a large fluctuation inherent to these designs, and often stabilization takes a prolonged period of time (65). This is due to the large heat loss to the room, which can itself cause significant room heating. Often these enclosures are similar to a plastic box with windows to allow the user access to the imaging plane, which itself can be cumbersome. However, as these adaptions are suitable for any existing microscope this live cell imaging platform does not require the expenditure of acquiring a new microscope system.

1.7.2.2 Stage-top incubation chamber

A stage top incubation chamber heats only the area where the cells are confined to and is therefore subjective to room temperature fluctuations greater than the enclosures mentioned previously, shown in Figure 7. Stage-top incubation chambers require objective heaters, which can have an effect on focusing as focus drift is a problem with any temperature fluctuations (56). Heated platforms can often restrict some objectives with short working distances, and even affect the light paths if not properly designed. Despite this, access to the incubated vessel is easy and allows for perfusion systems to be implemented, and like the enclosures this can be an addition to most microscopes (66).

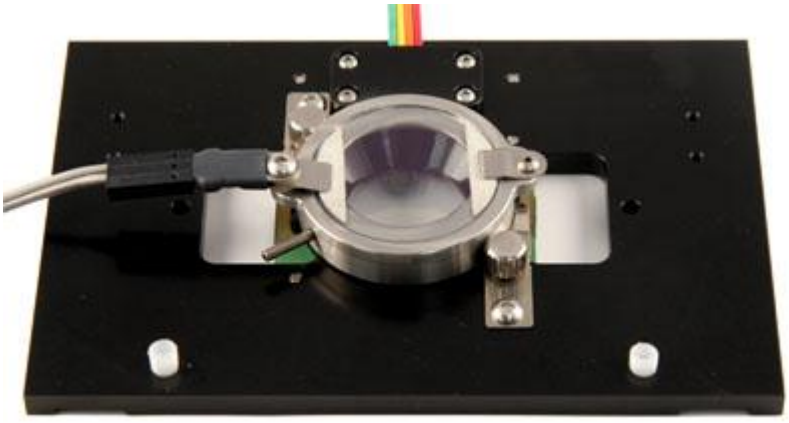

Figure 7. Bioptechs, Inc. Delta T Culture Dish System (67).This is designed to simulate host conditions on the stage of a microscope and provide an optimal optical environment for microscopy. This two-step system allows you to plate your cells and observe them without having to transfer them to another structure

1.7.2.3 Small Microscope designed to fit within a standard incubator

A number of manufacturers currently market systems designed for incubators, such as GE's JuLi (68) and Essen Bioscience's Incucyte (69). These microscopes utilise incubators that are found in all cell culture labs and therefore reduce the microscope cost.

1.7.2.4 Incubator / Microscope combination

Currently on the market are a few versions of combining the microscope and incubator. These are shown in Table 3 below along with commercially available products and their advantages and disadvantages for each method.

Table 3. Advantages and disadvantages of available microscope and incubator combinations. This table highlights some of the common problems associated with commercially available temperature control mechanisms as well as benefits that show which combination is most suitable for individual applications.

Temperature Control Mechanism	Advantages	Disadvantages
Microscope Enclosure	• Cheap • Adaptable to current microscope • Most microscope suppliers now stock	• Poor control (also of gas) • Long stabilization times • Custom modifications • Significant room heating • Cumbersome to work on
Stage-top Incubation Chamber	• Adaptable to current microscope • Perfusion systems possible	• Often single plate holders only • Restricted imaging area • Tricky to implement given short working distances of objectives • Poor temperature maintenance • Poor gas control, if any
Internal Incubator Microscope	• Good temperature and gas control	• Compact microscope • Condensation build-up
Incubator/ Microscope Combination	• Good temperature and gas control	• Expensive • Few commercially available

1.8 Commercially Available Phase Contrast Imaging Platforms

Traditionally, cell cultures are monitored by time consuming microscopy, manual imaging and image processing. Conventional time-lapse recordings have provided new data regarding living cell behaviour and growth. Despite the advantages the technique does have drawbacks, notably user variation, length of follow-up time and non-automation of analysis. This has led to a need in the market for an automated microscope within a culturing system. Such systems incorporate software enabling remote control of image acquisition. This new generation of live-cell imaging microscopes increases throughput and flexibility of examining the dynamic cellular processes (61). There are three vital aspects to live cell imaging platforms, sensitivity of detection, speed of acquisition and viability of the specimen. In this section a range of market available platforms bearing in mind these three crucial points whilst touching on other factors such as light wavelengths, image analysis, and conjunction with fluorescence, which are compared in Table 4.

1.8.1 Cell-IQ™ (Chipman Technologies)

The Cell-IQ™ system (CM-Technologies Ltd, Tampere, Finland) provides the basis for the imaging work in this thesis. Combining long term cell incubation conditions with phase contrast and fluorescence imaging utilising Machine Vision Technology to automatically identify, analyse and quantify cell morphological features (70) the Cell-IQ™ offers the ability to detect and quantitate 'biomarkers' (5,71). While many of these techniques are used independently already in cell biology, Cell-IQ™ is the first system that has combined cell visualisation with Machine Vision Technology for quantitation (70,72).

Figure 8. CM-Technologies live cell imaging platform, Cell-IQ™ (70) This is a fully integrated continuous live cell imaging and analysis platform incorporating phase contrast and brightfield imaging capabilities with its on-board Analyser software package for the quantification of image data. The Cell-IQ offers researchers label free imaging and automated analysis, allowing a multitude of kinetic assays from cell proliferation through to tubule formation to be studied.

The system includes an automated optics module, integrated incubator, 2 incubation gas controllers, precision movement stage all controlled through machine vision based software (35). Cells are maintained in the appropriate environment of temperature, humidity and gas that makes long term observation possible (5,35). Micro-plates, flasks or other culture vessels can be placed in the Cell-IQ™ for sequential analysis (35). The software enables the user to select the location and area to be imaged within each well, specify how long to measure and how often to cycle through the plate or entire plates. This is accomplished automatically by using accurate plate positioning and automatic "all-in-one" focusing that compensates for any variation in the plate structure.

The use of machine vision based training within the Imagen analysis package provides a flexible approach to monitoring proportions with distinct phenotypes within complex systems such as kinetic drug response studies within co-culture.

Although the Cell-IQ™ is one of the more expensive live cell imaging platforms currently on the market, the stand alone kit allows it to be placed anywhere within the lab and comes fully equipped with high specification analysis software. There is no need for other equipment such as incubators or software.

1.8.2 IncuCyte™ (Essen Bioscience)

Figure 9. Essen Bioscience compact microscope, IncuCyte (69) The Incucyte system allows you to place a microscope within an incubator. With configurable trays a wide variety of culture vessels can be used within the system to provide long-term live cell imaging.

The Incucyte™ (Essen Bioscience, Welwyn Garden City, UK) system is a fully automated, fluorescence and brightfield compact microscope that can be incorporated within a standard tissue culture incubator enabling live long term culture imaging (61). The standard Incucyte can hold 6 well plates with custom designed consumables and includes a suite of specific application modules compromising of image analysis algorithms (61). This platform also incorporates a suite of defined analysis algorithms to include cell migration, and apoptosis (61).

A major selling point of this equipment is that it fits into an incubator of which many laboratories already have, and therefore compared to the Cell-IQ system this is much cheaper. Unlike the Cell-IQ however the Incucyte has an automated microscope rather than an automated stage, allowing the system to have a smaller footprint.

1.8.3 Cell Observer (Carl Zeiss)

Figure 10. Carl Zeiss live cell imager, Cell Observer (73) This microscope allows for rapid acquisition of images and can combine up to 5 channels with any number of positions within a single culture vessel. The Cell Observer has an imaging speed of up to 85 images/second and an automatically controlled environmental to acquire dynamic processes in a wide variety of applications

Cell Observer (Carl Zeiss, Germany) allows short time lapse imaging at very high speed as well as long-term experiments lasting several days and involving a number of different fluorescence channels, z-planes and positions (74). This microscope system allows the range from simple observation and documentation to the quantitative analysis of slow and rapid processes. The Perspex container around the microscope allows for a controlled habitat for the cells with both temperature and CO_2 control, however creating a homogeneous environment over a long period of time is difficult with large heat/gas loss and poor heating mechanisms (74).

Although the system has a Perspex chamber to maintain temperature and CO_2 there is poor humidity control with only evaporation from the culture vessel providing humidity. The environmental chamber also has poor environmental regulation with large deviations from a set-point. This is un-surprising as this is a standard microscope that has been adapted for live cell imaging, whereas the other commercial products have all been designed for live cell imaging.

1.8.4 BioStation CT (Nikon)

Increasingly researchers are using live-cell imaging to study cellular functions. The BioStation, a smart fluorescent cell analyser, was developed to easily view and capture images from live-cell experiments (75).

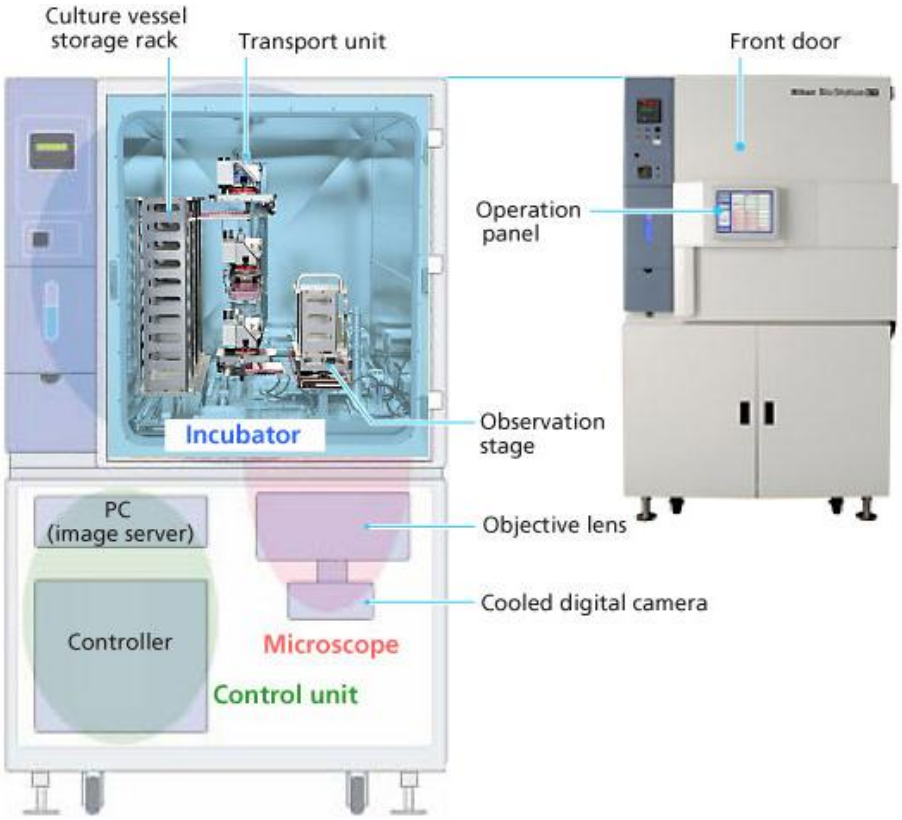

Figure 11. Nikon , cell culture observation system, BioStation (68) The BioStation CT provides a stand-alone incubator and microscope combination able to hold 30 flasks at one time. With phase and fluorescence capabilities the BioStation provides a stable environment for live cell imaging.

The Nikon BioStation CT allows imaging experiments to be conducted without ever removing the cells from the incubator. Consisting of a standard sized tissue culture incubator with an inverted microscope inside, BioStation CT holds 30 vessels ranging from 96 well plates to 75cm^2 flasks, which are moved between the microscope stage and the vessel rack via a robotic device. BioStation CT provides images from 2 x to 40 x phase images with apodized phase contrast optics and fluorescence images with three colour LED illumination. A bird's eye colour

macro view allows the entire vessel to be viewed from above. Complete security is provided: users access only the samples for which they have clearance. Experimental results are reliably traced and can be accessed remotely via an internet connection or local area network. The BioStation is the first commercially available multi-objective fluorescent and phase contrast microscope integrated with automated plate handling robotics all within a cell culture incubator (61). However this comes at a price that is more than double that of the other systems reviewed here. The availability of holding up to 30 flasks means that at capacity the time between imaging each flask is much greater than the other products noted here. This therefore moves the BioStation towards a more manufacturing focus rather than research based, paralleled in its cost. Due to the robotic arm selecting the plate, and placing it on the microscope stage, the time for imaging is much higher than the other platforms, with the advantage of holding more culture vessels. However this comes at a cost to the environment. Due to the large incubator which holds the culture vessels, robotic arm, microscope and stage the BioStation has a large footprint and subsequent environmentally controlled incubator. This incubator exhibits large environmental difference between culture positions and on opening the door takes up to 4 hours to return to humidity set-point. Table 4 gives an overview and some numbers to these observations.

1.8.5 IN Cell Analyzer (GE Healthcare)

GE's IN Cell Analyzer 2200 delivers a widefield cell imaging system with increased acquisition speed to provide high-content imaging workflow (76).

Figure 12. IN Cell Analyzer 2200, GE Healthcare (77) The IN Cell Analyzer allows high content screening and analysis of both fixed and live cells within an environmentally controlled chamber capable of holding a single culture vessel.

The IN Cell Analyser 2200 brings flexibility with each system capable of holding bespoke instruments for individual research needs. It also offers a higher resolution within the fluorescence imaging one of its major selling points. This is completed by using a 2 million pixel camera to capture high resolution images (77). Another aspect is the speed of acquisition, the ability to complete a 96 well plate with 2 channels in less than 2.5 minutes. This does however mean that the stage movement is fast which could disturb live cells.

Table 4. Summary of commercially available imaging platforms

Platform	Company	*Speed of Acquisition (mins)	**Sensitivity of Detection (pixels/µm)	Specimen Viability	Environmental Conditions	Illumination	Image Analysis	Fluorescence Capability
Cell-IQ	CM-Technologies, Finland	***	0.7-0.9 (65)	7 days (28)	37°C 5% CO_2 Humidity from plate evaporation	Green LED	Imagen – protocol building with Machine Vision	Yes
IncuCyte	Essen Bioscience, UK	4 (66)	0.93 (67)	4 days (68)	Placed inside incubator	LED	Pre-loaded protocols	Yes
Cell Observer	Carl Zeiss, Germany	-	-	19 hours (69)	37°C 5% CO_2 Humidity Poor control due to adaptation	User defined LED	AxioVision Modules (optional)	Yes
BioStation CT	Nikon, Japan	40 ***	0.93 (70)	20 days (71)	37°C 5% CO_2 aerosol sprayed humidifier	Red LED	CL-Quant (optional)	Yes
IN Cell	GE Healthcare, UK	<2.5 (63)	~3 (64)	2 days (72)	37°C 5% humidified CO_2	LED	IN Cell Investigator (optional)	Yes

* 96 well plate, 10x objective, 2 channels (Phase and fluorescence channel), 1 image per well

** 20 x objective 1280*960, ***measured on system at Loughborough University 01/04/2014

1.9 The Potential of Automated Phase Contrast Imaging as a Process Analytical Tool

As discussed previously, there is a growing need for a non-invasive, label free measurement system to compliment the Quality by Design paradigm, in order to use systematic process development tools. Phase contrast microscopy shows real promise in filling this current technology gap, and through the use of automating the current user defined analysis using one of the reviewed systems, the cellular therapy industry can benefit through time, cost and regulation.

The Cell-IQ forms the basis of this thesis, which integrates an environmental chamber with a microscope whilst also providing analysis software. This set-up then allows cell culture to be continually imaged to provide information relating to culture state followed by analysis of the images to automate quality assessment. The Cell-IQ provides the best commercial equipment for this compared to the other kit summarised here.

1.10 Thesis Objectives

The work described here will identify how phase contrast image analysis can be utilised to identify and control variable cell culture process in a novel, automated and non-invasive manner. For image-based quality assessment of cells there are five recognised steps for successful implementation. The first being raw image collection, image processing, experimental data collection, data analysis and finally prediction of culture state. This thesis will therefore follow these five steps to develop an enabling tool to measure, define and predict cell culture state in a manner that is useable to improve process control. In order to achieve this exemplars of human Embryonic Stem Cells (hESC's), human Haematopoietic Stem Cells (HSC's) and their respective differentiated states will be assessed. Following the collection of raw images using the Cell-IQ™ there is an identification package of potential attributes that may relate to quality. The analysis of the raw images will

determine image based metrics of features that can be related to quality. Alongside this an understanding of the statistical attributes of the assay will be addressed in order to evaluate the potential for process control and prediction. Following imaging of the cultures common characterisation techniques will also be performed as a comparison and verification of any characterisation changes that are seen within the images.

Whilst imaging and analysing images it is imperative to ensure that the optimum environmental conditions are met. This includes verifying the gas composition, temperature and humidity of the culture system and mimicking that found in a conventional culture system.

Also conducted is a process overview using the image derived metrics to make process decision and therefore prove utility of a non-invasive tool for quantifying quality and controlling a manufacturing process for cell based therapies.

2. MATERIALS AND METHODS

2 Materials and Methods

Much of the work discussed in the following chapters is method development work and therefore is presented in later result chapters. This method section identifies generic methods of cell culture and analysis that have been utilised throughout the work. Firstly embryonic culture is described relating to maintaining pluripotency, measuring pluripotency as well as differentiation protocols. Further work has utilised cord blood from which CD_{34}+ cells are purified before culturing and then the haematopoietic progenitor population was measured using the colony forming unit (CFU) assay. Alongside this flow cytometry is utilised to check for purity and maturity of haematopoietic stem cells.

2.1 Materials

Listed here are tables with all the reagents that have been used within this work.

Table 5. Embryonic Culture materials used in this work. *mTeSR-1 comes in 2 parts, a refrigerated base medium and a frozen supplement.

Embryonic Culture Materials	Supplier	Catalogue No.	Batch/Lot
6-Well Plate	Fisher Scientific	TKT-220-006R	-
T-25 Flask	Fisher Scientific	TKT-130-170F	-
T-75 Flask	NUNC	TKT-130-210T	-
Hg Embryonic Cell Line	WiCell	WA09	-
mTeSR*	StemCell Technologies	05875	12E43890D
			13K51694D
			14C53648D
			12F44304D
			13E50254D
			14A52765D
Cell Scraper	Sigma Aldrich	CLS3010	-
40 µm Cell Sieve	StemCell Technologies	27305	-
Dispase	StemCell Technologies	07923	12M46742
Accutase	Sigma Aldrich	A6964	SLBB0378
mFreSR	StemCell Technologies	05855	12L46780
Phosphate Buffer Solution	SLS	BE17-516F	3MB191
			3MB036
			4MB044
DMEM	Life Technologies	21041-025	1167117
Matrigel	BD Biosciences	354277	2167738
Fetal Bovine Serum	SLS	SH30071.02	AVA60499
Cytofix/Cytoperm	BD Biosciences	51-2090KZ	86916
Bovine Serum Albumin	Sigma Aldrich	A2153-10G	060M1749V
Triton X-100	Sigma Aldrich	X100-100ML	9002-93-1
10% Donkey Serum	Sigma Aldrich	D0536-2ML	056FG651

Table 6. Haematopoietic culture materials used in this work. *Mother had a blood transplant.

Haematopoietic Culture Materials	Supplier	Catalogue No.	Batch/Lot
6-Well Plate	Fisher Scientific	TKT-220-006R	-
T-25 Flask	Fisher Scientific	TKT-130-170F	-
StemSpan	StemCell Technologies	09650	10D34616
Distilled Water	Life Technologies	10977-035	1221782
MethoCult	StemCell Technologies	04034	10B33368
			13K52888
			-
Ficoll Unit	Anthony Nolan	-	G22121104485
Ficoll Unit	Anthony Nolan	-	G22121104487
Ficoll Unit	Anthony Nolan	-	G22121104647
Ficoll Unit	Anthony Nolan	-	G22121206626
Ficoll Unit	Anthony Nolan	-	G22121206507
Cord Blood*	Anthony Nolan	-	G12212311515145
Ficoll Paque	Fisher Scientific	1037-9484	10160575
CD34 Microbeads	Miltenyi	130-046-702	5130419019
Bovine Serum Albumin	Sigma Aldrich	A2153-10G	060M1749V
FGF-basic	Invitrogen	PHG0264	383774A
Activin-A	R&D Systems	338-AC-010	BNV3213012
VEGF	R&D Systems	293-VE-010	II3712112
FGF-basic	R&D Systems	233-FB-025	HKW7412091
BMP-4	R&D Systems	314-BP-010	BEM7212111

Table 7. Flow Cytometry antibodies used in this work (right)

Table 8. Immunostaining antibodies used in this work (left)

Antibody–Flow	Manufacturer	Part Number	Species Raised	Species Reactivity	Conjugated?	Fluorochrome	Antibody Isotype
Nanog	BD Sciences	560589	Mouse	Human	Y	PE	IgG
Oct-3/4	BD Sciences	560589	Mouse	Human	Y	PerCP-Cy5.5	IgG
Sox-2	BD Sciences	560589	Mouse	Human	Y	Alexa Fluor 647	IgG2a
PE Isotype Control	BD Sciences	560589	Mouse	Human	Y	PE	-
PerCP-Cy5.5 Isotype Control	BD Sciences	560589	Mouse	Human	Y	PerCP-Cy5.5	-
Alexa Fluor 647 Isotype Control	BD Sciences	560589	Mouse	Human	Y	Alexa Fluor 647	-
CD34	BD Sciences	555821	Mouse	Human	Y	FITC	IgG
CD45	BD Sciences	555483	Mouse	Human	Y	PE	IgG
CD71	BD Sciences	555536	Mouse	Human	Y	FITC	IgG2a
CD235a	BD Sciences	555570	Mouse	Human	Y	PE	IgG2b

Antibodies	Manufacturer	Part Number	Species Raised	Species Reactivity	Conjugated	Fluorochrome	Antibody Isotype
Sox-2	R&D Systems	967149	Goat	Human	Yes	NL557	IgG
Oct-3/4	R&D Systems	967150	Goat	Human	Yes	NL637	IgG
Nanog	R&D Systems	967151	Goat	Human	Yes	NL493	IgG
Brachury	R&D Systems	967388	Goat	Human	Yes	NL557	IgG
HAND1	R&D Systems	967392	Goat	Human	Yes	NL637	IgG

Table 9. List of equipment used throughout this work.

Equipment	Supplier	Model
Cedex	Roche	Hi Res Analyzer
Countess	Invitrogen	-
Guava	Millipore	EasyCyte 8HT
Cell-IQ	CM-Technologies	MLF Version 2
Safety Cabinet	Thermo Scientific	Herasafe KS Class II
Centrifuge	Eppendorf	5804
Incubator	Thermo Scientific	Heraeus HERA Cell 150

2.2 Embryonic Cell Culture

The human embryonic stem cell (hESC) line H9 was purchased from WiCell, Madison. H9 cells were cultured as colonies on Matrigel (BD Biosciences, Oxford, UK) in the commercially available defined culture medium; mTeSR-1 (StemCell Technologies, Canada). 3 separate batch lots of mTeSR-1 were utilised in this work, each comparable as measured by the manufacturer. mTeSR-1 contains Bovine Serum Albumin, rh bFGF, rh TGFβ, Lithium Chloride, Pipecolic acid and GABA. Cells were cultured in standard cell culture conditions at 37°C, in an environment containing 5% CO_2 in Nunc t-25, Nunc t-75 or Nunc 6-well plates. Unless otherwise stated, cells were fed every 24 hours by aspirating off the spent medium in the well and replacing with an equal volume of fresh, pre-warmed media. The volumes used for culture are shown in Table 10 with the relevant culture vessels.

Table 10. Medium volumes for the culture of H9 cells. This table summarises the volumes of mTeSR-1 that were used during culture of hESC's for various tissue culture vessels.

Culture Vessel	Media Quantity
6-Well Plate	3 mL / well
t-25	7 mL
t-75	20 mL

2.2.1 Matrigel Preparation

hESC-qualified Matrigel (BD Bioscience) was used for coating tissue culture surfaces. As stated from the supplier, this Matrigel has been qualified as compatible with mTeSR-1 by Stem Cell Technologies, thus neglecting any screening for media and surface coating compatible mixtures (78). The purchased stem cell line H9 was also cultured on matrigel with mTeSR-1.

Matrigel was used as per the manufacturer's instructions. Briefly, stock bottles of Matrigel were thawed overnight at 4°C. The bottle was well swirled to ensure a good mix and kept in a chill bucket containing Lab Armor beads (Lab Armor) to maintain a low temperature. All consumables that were in direct contact with Matrigel were pre-chilled to -20°C, including, pipettes, stripettes, cryovials and plates/flasks. The stock solution of matrigel was aliquoted into the manufacturer's lot specific quantities. This varied depending on the protein concentration of the stock but was typically between 290-320 µL for each aliquot. Stock aliquots were stored at -80°C for up to 6 months. Prior to coating, Matrigel aliquots were thawed at 4°C and diluted in 25 mL of cold DMEM (Life Technologies). To coat pre-chilled tissue culture flasks and plates the surface was covered with excess matrigel solution, as shown in Table 11.

Table 11. Matrigel coating volumes for the culture of H9 Cells. This table summarises the quantities of matrigel that were used to coated various culture vessel platforms

Culture Vessel	Matrigel Solution Quantity
6-Well Plate	1 mL / well
t-25	3 mL
t-75	7 mL

Coated vessels were stored at 4°C for up to 2 weeks prior use. Just before use the coated plates were left at room temperature for 45 minutes to ensure polymerisation of the Matrigel had occurred. Excess Matrigel solution was then aspirated prior to hESC plating and replenished with an equal volume of warmed media.

2.2.2 Thawing of Cryopreserved hESCs

After removing a cryovial of frozen cells from storage in liquid nitrogen, the vial was thawed by gently swirling in a water bath set at 37°C. The cryovial was removed from the water bath when only a small ice crystal remained. The cryovial was then soaked in 70% (v/v) industrial methylated spirit (IMS) (Fisher Scientific) and allowed to air dry and sterilise prior to opening. The entire contents of

the vial were gently transferred using a P1000 pipette to a 15 mL centrifuge tube. Pre-warmed mTeSR-1 was added drop wise to the centrifuge tube containing the cells using a 5 mL stripette. An additional 1 mL of media is used to rinse the vial and then transferred to the centrifuge tube.

After mixing the thawed cells and media gently the suspension was then centrifuged at 200 xg for 2 minutes. The supernatant was aspirated and the pellet re-suspended in 4 mL of fresh warmed mTeSR-1. 2 mL of cell suspension was then added to Matrigel coated 6-well tissue culture plates, each already containing 1mL of mTeSR-1 as described in the Matrigel Preparation Section 2.2.1. The plate was then transferred to a standard incubator in which cells were maintained at 37°C in an environment containing 5% CO_2, rocked on x and y axis (to ensure no swirling occurs). Cells were then maintained by feeding every 24 hours as described in Section 2.2.4.

2.2.3 Passaging hESCs

Prior to passage any areas of cell differentiation were identified and removed. This was completed by examining cultures under a 4x objective on a light microscope and marking areas of differentiation with a lens marker which created a small ring around the differentiated area. The spent media was then removed from the plate and the circulated areas of differentiated cells were also aspirated using a 300µL pipette tip on the end of an aspirator.

The remaining undifferentiated cells were washed twice in DMEM (Life Technologies), which involved adding equal volumes of warmed DMEM to each plate, swirling and then aspirating the spent DMEM. This removes excess protein from the culture vessel so that enzymatic digestion occurs more efficiently at the cell attachment surface rather than by digesting protein in solution. Following the final removal of DMEM wash solution, dispase 1 mg/mL (Stem Cell Technologies, Canada) was added to each well and incubated at 37°C for 7-9 minutes. Dispase is a protease which cleaves fibronectin and collagen IV, thus causing cell detachment. After checking that the perimeters of the colonies were beginning to fold back the dispase was carefully aspirated and the

cells washed with DMEM as before. The DMEM wash solution was aspirated and the cells were covered with mTeSR-1. The culture vessel was then tapped to remove the adhered colonies, and if required a Cell Scraper (Corning) was used at this stage to remove any remaining attached cells. Cell scraping involved scraping the entire surface by first following the perimeter of the well and then scraping 3 times in one direction, rotating the plate 90° and scraping 3 more times. The cell suspension was then passed through a 40 µm filter (Millipore, USA) to remove any unwanted single cells and allow collection and purification of the colonies. The filter was then washed using 10 mL of media to ensure all single cells had passed through, inverted over a fresh centrifuge tube and fresh , warmed mTeSR-1 was washed over the upside down filter. Completing a 1:6 split of the initial to final cell density, the cell suspension was distributed over each fresh matrigel coated well using a 5mL stripette making sure the final mL in the stripette is never used, but recycled. The final mL in a stripette is often at a much higher cell density due to drag forces as the media moves faster than the colonies during dispensing. After placing the plates in the incubator the plate was rocked in the x and y axis direction, ensuring the plate was not swirled and then left for the cells to adhere.

2.2.4 Maintenance of hESCs

Cells were fed by a 100% media change every 24 hours (unless stated) and passaging was completed every 5-7 days when approximately 75% confluency was reached. At this stage confluency was assessed under a light microscope, 75% confluency was judged to be complete when colonies began to interact with one another. The daily media change was completed by aspirating the spent media from one corner of a well, adding fresh pre-warmed mTeSR-1 and returning the plate to the incubator. The hESC H9 cell line was routinely characterised with karyotype analysis (Section 2.8) and expression of pluripotent markers (Section 2.5 and 2.6).

2.2.5 Cryopreservation of hESCs

Cryopreservation of hESC cultures was carried out 1-2 days prior to passaging. Colonies were removed as described in Section 02.2.3 Passaging hESCs. Colonies were pooled and were centrifuged at 200 xg for 2 minutes, the supernatant removed and the cell pellet re-suspended in commercially available freeze media; mFreSR (StemCell Technologies) containing dimethyl sulfoxide (DMSO). Colonies were cryopreserved at each 9.6cm^2 by resuspending the cells in 1 mL of freeze media per cryovial, which equated to one well of a 6-well plate per cryovial. Each vial was then thawed as described in Section 2.2.2 prior to use.

2.3 Differentiation of hESCs to the Mesoderm Lineage

hESCs were seeded onto Matrigel coated vessels as described in Section 2.2. After 24 hours of culture in pluripotent media the mTeSR-1 was replace with mesoderm differentiation media. This was mTeSR-1 supplemented with 10 ng/mL BMP-4 (R&D Biosystems), 10 ng/mL FGF (R&D Biosystems), 10 ng/mL VEGF (R&D Biosystems) and 10 ng/mL Activin-A (R&D Biosystems). A complete media change was carried out every 24 hours by removing the spent differentiation media and replacing it with fresh mTeSR-1 containing supplements. The cells were then assessed for early mesoderm markers as described in Section 2.6.

2.4 Cell Count and Viability Measurements

The cell counts and viability measurements were conducted on a number of different automated platforms including the Cedex, the NucleoCounter, the Guava EasyCyte and the Countess.

2.4.1 Cedex Cell Counter

The Cedex (Roche Innovatis) is a fully automated, image based cell analyser providing information about cell concentration, viability, and aggregates. The analyser uses trypan blue exclusion method and a high resolution image scanner to analyse cells and objects (79). Single cell samples of 1 mL were added to the Cedex, which were then mixed with an equal volume of trypan blue automatically. The system was then set to automatically acquire and analyse 30 images to determine the population viability and cell concentration.

2.4.2 NucleoCounter Cell Counter

The NucleoCounter (Chemometec) is a compact image based cell counter utilising the detection of fluorescence from DNA bound fluorescent dye propidium iodide (PI). Briefly the method involves first the lysis of cells to generate free nuclei. To achieve this cells were mixed in equal volumes with Solution A (Chemometec); a lysis buffer. After vortexing this mixture was then supplemented with Solution B (Chemometec); stabilising buffer in the same volume as Solution A. This 3x diluted solution of cells was then loaded onto a disposable cassette which comes prepared with PI stain within, shown in Figure 13.

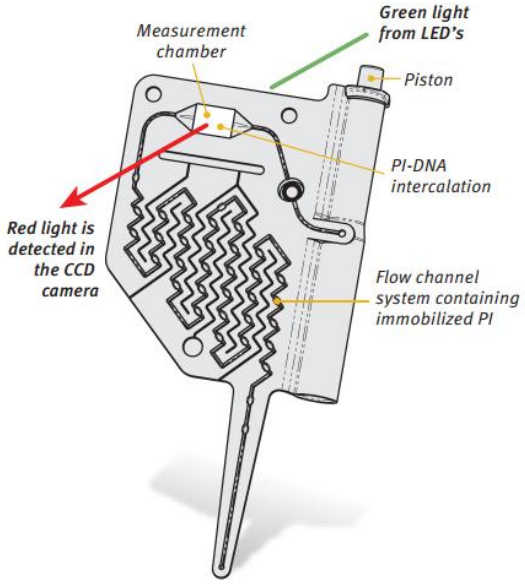

Figure 13. NucleoCounter disposable cassette. This cassette comes pre-loaded with propidium iodide (PI). Cells are sucked up using the cassettes piston and after loading into the NucleoCounter the cells are mixed with the PI solution generating a count (80).

The cassette is then inserted into the NucleoCounter where the lysed cells and PI are mixed. The NucleoCounter then counts the total number of cells. Another cassette is loaded with pure cell solution without the lysis buffer treatment to calculate the dead cells. The percentage of viable cells can then be calculated from the difference between total and dead cells.

Figure 14. Chemometec NucleoCounter NC-100. A compact cell counter using pre-loaded propidium iodide cassettes to determine count and viability of a sample (80).

2.4.3 *Guava Easycyte Cell Counter Application*

The Guava EasyCyte (Millipore) is a microcapillary flow cytometer that has the ability to perform cell counts and viability measurements through its ViaCount assay. This involves mixing the single cell suspension with ViaCount (Millipore). ViaCount is composed of two DNA-binding dyes, one binding to nucleated cells the other to apoptotic cells. This allows the total, dead and viable cells to be calculated.

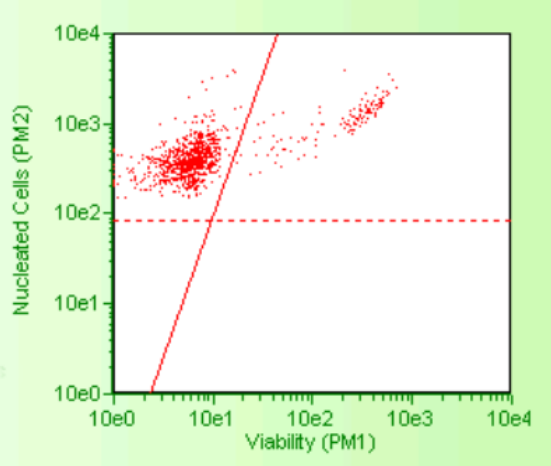

Figure 15. Example figure from Guava EasyCyte counting method Viable cells on the left are separated from dead and apoptotic cells (81).

2.4.4 *Countess Cell Counter*

The Countess (Life Technologies) is an automated cell counter which similar to the Cedex uses trypan blue exclusion along with image analysis to measure viability and cell concentration. Unlike the Cedex, the Countess requires manual mixing of the cell stock and trypan blue prior to pipetting 20 µL of the solution onto a Countess slide. The disposable slide is then inserted into the machine and the results displayed.

Figure 16. Life Technologies Countess, automated cell counter. The Countess uses prepared slides containing cell sample and trypan blue, then uses image analysis to measure viable and non-viable cells (82).

2.5 Flow Cytometry Analysis

Flow cytometry was carried out using the Guava Easycyte 8HT (Millipore) equipped with a 75 mW blue diode (488 nm) laser and a 40 mW red diode (635 nm) laser.

2.5.1 Sample Preparation for Intracellular Markers

Cell cultures were washed twice with room temperature phosphate buffer solution (PBS) prior to enzymatic detachment using Accutase (Sigma). Washing consisted of aspirating the spent media, adding equal volumes of PBS and swirling before aspirating the PBS. Accutase was pre-warmed and added to each culture vessel before incubating in a standard incubator at 37°C for 7-10 minutes. Single cells were then harvested by via pipetting up and down to achieve a single cell suspension, and centrifuged at 300 x g for 5 minutes before being re-suspended in Stain Buffer (BD Bioscience) containing 0.1% (w/v) bovine serum albumin (BSA) (Sigma). A cell count was then completed using the NucleoCounter as described in Section 2.4.2. Cells were then centrifuged at 300 x g and re-suspended in a single step permeabilisation and fixation with Cytofix/Cytoperm Buffer (BD Bioscience) at 10^7 cells /mL for 30 minutes at 4°C. During this incubation, respective antibody

solutions were aliquoted into wells of a deep 96-well plate. After permeabilisation and fixation of the cells, they were washed twice with 1X Perm Wash Buffer (PWB) (BD Bioscience) (centrifuging at 300 xg for 5 minutes) before being resuspended to achieve a cell concentration of 10^7 cells/mL. Then 100 µL aliquots of cell suspension (10^6 cells) were added directly into the relevant wells of the 96-well plate containing prepared antibody solutions. Samples were incubated at room temperature, in the dark for 45 minutes. Cells were washed twice with PWB and resuspended in 1 mL Stain Buffer for analysis. All analysis was completed using GuavaSoft 2.6 software (Millipore). A list of all used antibodies is shown in Table 7.

2.5.2 Controls

All flow cytometry assays were run with comparable controls of a cell only and isotype control (identified in Table 7). The cell only sample was exposed to the same fixation, permeabilisation and wash steps as the stained cells, but was not exposed to any antibodies. These cells were used initially to verify the settings of the flow cytometer so that their signal was recorded within the first log decade.

Isotype controls consisted of samples that were labelled with antibodies that matched the host species and isotype of the target antibodies used. Isotype antibodies are raised against an antigen that is not normally expressed in the target cells and use the same fluorophores as the target antibodies. They are used to measure the level of non-specific background signal caused by primary antibodies. All isotypes were used at the same concentrations as the target antibodies, and their signals were used to set a baseline at 95%, from which any signal above was considered to be specifically labelled with the target antibody.

BD CompBead Plus positive and negative beads (BD Bioscience) were also used as controls to clearly identify positive and negative populations. These beads were either coated with antibodies that are able to bind to utilised antibodies (positive beads) or have no binding capacity (negative

beads). This allows the identification of distinct positive and negative populations for specific antibodies that can then be used for optimizing the photomultiplier tube settings and calculating the fluorescence compensation as discussed in section 2.5.3.

2.5.3 Data Acquisition and Analysis

All samples were acquired using the same gating strategy as outlined below in Figure 17.

Figure 17. Gating Strategy for flow cytometry analysis. Prior to acquiring flow cytometry data the following this protocol is used to initially exclude doublets from the data before gating on just viable cells. This gate is then used to collect 10,000 data points. Following acquisition a gate is applied to each fluorescence channel representing 5% positive on the isotype control. The percentage positive is then recorded on the analysed sample.

Doublets within the sample are often caused by inherent cell adhesion and/or by cross linking of cells by staining reagents. These doublets can lead to artefacts in measurements and therefore are removed first. This is achieved using pulse width analysis, which in practice assesses both the forward scatter width and area to determine doublets. It is then possible to view the forward against side scatter plot to remove any non-viable cells and debris. The gate that contains viable single cells is then used for analysis and 10,000 events are collected.

Alongside all the isotype controls and target samples, BD CompBeads were acquired. During acquisition these beads provide a negative and positive population for the antibodies being used. This therefore allows the photomultiplier tube settings to be optimised prior to acquisition. This was completed for all new antibody lots, and checked for every time there after, although the settings were not altered to allow a comparison to be made between runs.

Once the samples had been acquired the fluorescence compensation was calculated. This initially was completed manually with the matrix of compensations being recorded as a guide. Following this the Guava Incyte software (Millipore) provides an automated compensation on the beads. This was then used to provide a consistent compensation matrix, with each time a comparison to the manually determined matrix to ensure consistency.

Once these populations were analysed percentage positive and median values were recorded based on 5% positive gates placed on the corresponding isotype controls. Mean and median fluorescence intensity values of stained cells were normalised to the mean and median fluorescence intensity values of the isotype controls using the following equations:

$$n\overline{FI} = \frac{\overline{FI}_{sample}}{\overline{FI}_{isotype\ control}}$$

and;

$$nMedFl = \frac{MedFI_{sample}}{MedFI_{isotype\ control}}$$

where: $\overline{FI}$= mean fluorescence intensity and $MedFl$ = median fluorescence intensity.

2.6 Immunocytochemistry

Immunocytochemistry was instrumental in visualising the variation in population based on cellular proteins. All fluorescent images were acquired on a Nikon Eclipse Ti inverted epi-fluorescence microscope (Nikon) and a Coolpix 4500 camera (Nikon). Images were then further analysed with Nikon Elements Ar software (Nikon).

2.6.1 Conjugated Antibodies

6-well tissue culture plates of hESCs were washed in equal volumes of PBS (Lonza) and fixed in PBS containing 4 % paraformaldehyde (Sigma) for 30 minutes at 4°C. Paraformaldehyde was quenched with 100 mM glycine (Sigma Aldrich) for 15 minutes at room temperature. After washing with PBS the cells were blocked and permeabilised with blocking buffer consisting of PBS, 10 % normal donkey serum, 0.3 % Triton X-100 and 1 % BSA for 30 minutes at 4°C. Cells were then incubated for 3 hours at room temperature in the dark with antibodies at the manufacturer's concentration diluted in blocking buffer. Dual and triple staining of cells was completed by pre-mixing the antibodies together after blocking. The cells were then washed 3 times with PBS, and then left in PBS ready for imaging. When required, counterstaining of the samples was completed by incubating the cells with 300 nM 4',6-diamidino-2-phenylindole dilactate (DAPI) in PBS (Life Technologies) for 5 minutes at room temperature in the dark. Cells were then washed twice in PBS before being left in PBS for imaging.

2.6.2 Non-Conjugated Antibodies

6-well tissue culture plates containing hESCs were washed in PBS (SLS, UK) and then fixed in PBS containing 4 % paraformaldehyde (Sigma) for 30 minutes at 4°C. After washing with PBS the cells were then blocked and permeabilised with PBS containing 10 % normal donkey serum, 0.3 % Triton X-100 and 1 % BSA for 30 minutes at 4°C. The blocking buffer was then aspirated and the cells incubated overnight at 4°C with primary monoclonal antibodies diluted in PBS with 1% BSA and 0.3% Triton X-100. After washing with blocking buffer, then PBS, the secondary antibody was added diluted in PBS. After incubating at room temperature for 1 hour, the cells were washed and imaged using a Fluorescence Microscope.

Counterstaining was then completed were necessary as before in section 2.6.1. Control samples were performed by only using the secondary antibody to assess for non-specific binding.

2.7 Phase Contrast Imaging

The Cell-IQ (CM-Technologies) is an automated phase contrast imaging platform. The system comprises of a controlled culture environment, phase contrast microscope (4x, 10x, 20x and 40x objectives) and a camera that is integrated into an automated cell monitoring and analysis system. The imaging system allows continuous monitoring of adherent cells in two plates in a specific plate holder.

Incubation gases are pumped directly into the plate through perfusion holes in the lid. The holes are placed to maximise gas exchange within the plate. The gas is premixed sterile 5% CO_2 gas that is automatically controlled though the software. The default setting uses 30 mL/min flow rate with cyclic perfusion of 5 minutes on and 20 minutes off. This was utilised for all experiments unless stated otherwise as it was manufacturer tested to keep cultures at 5% CO_2 as required.

The Cell-IQ utilises Machine Vision approaches that allow monitoring and analysis of cell cultures. Machine Vision is the term given to duplicating the effect of human vision by electronically perceiving and understanding an image (83). The classification module is based on statistical classifiers, which can be 'taught' to determine morphological changes occurring within the culture down to the single cell level.

Through the use of a grid system, selected positions within the plate are selected, and the automatic stage moves between points at a stated time interval of 30-60 minutes unless stated. The recorded images are then saved as JPEG images in separate folders for analysis.

2.7.1 Phase Contrast Image Analysis

After the successful capture of phase contrast images, each image is then analysed for metrics. There were three overall methods that were used during analysis with more bespoke methods mentioned within the core chapters of this work.

2.7.1.1 Threshold Analysis for Embryonic Colonies

Thresholding is the simplest method of image segmentation. From a greyscale image such as phase contrast, thresholding can be used to segment images into bands of similar pixel intensity. This therefore provides an analysis tool to segment cells from their background.

Initially local contrast was computed to detect regions of high pixel intensity using a threshold value of 20, this highlighted all areas likely to contain cells. Small objects were then removed (value of 40/100), followed by the filling in of any holes using a value of 68/100.

2.7.1.2 Area Finder Analysis for Embryonic Colonies

Area finder analysis is a more in-depth tool. It is formed from two parts, a segmentation phase and a sample library phase, which are run in this order during analysis. Segmentation, similar to the threshold analysis, first identifies interesting objects such as cells in the image. Next these objects are recognised into user defined classes that is created based on information in the sample library. The sample library is built from user defined areas of images that relate to each class of cells. For embryonic colony identification the sample library has examples of periphery core colony, dark colony and edge cell morphologies. An example of the sample library is illustrated in Figure 18.

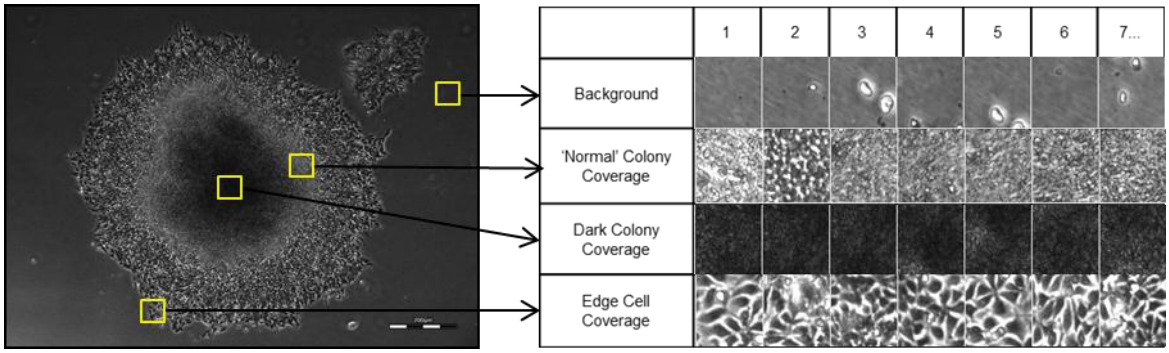

Figure 18. Sample Library built using Area Finder tool. Examples of background, 'normal' colony coverage, dark colony coverage and edge cell coverage are shown. The Area Finder analysis utilises a sample library to categorise all areas of interest such as cells into one of these user defined groups.

2.7.1.3 Count/Classify Analysis for Haematopoietic Progenitors

Count/Classify analysis tool within the Cell-IQ's analyser package uses a similar technique to that mentioned in the Area Finder tool section. First libraries of images are created by selecting individual cells as shown in Figure 19.

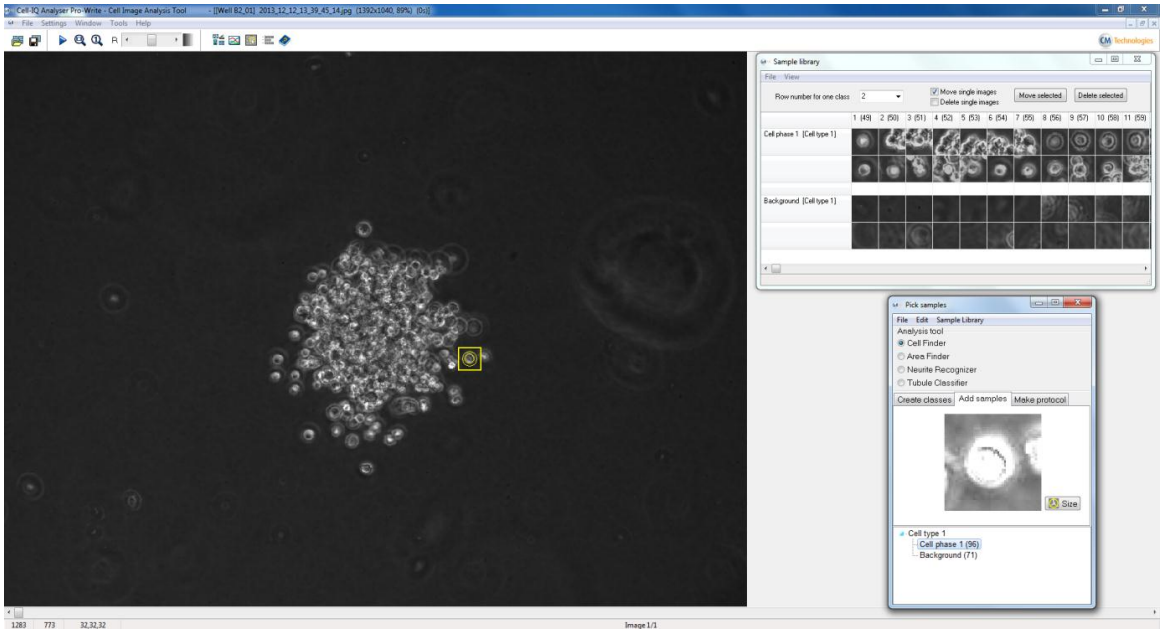

Figure 19. Count/Classify protocol building a library of progenitor images. By selecting individual cells as shown by the yellow boxed circle, the picked sample (shown in the bottom right) is added the library shown in the top right.

Figure 19 shows how a library of images of individual cells is built along with the background to allow identification of cells. Once a library is built this protocol can then be used to identify haematopoietic progenitors in further images.

2.8 Osteoblast Culture

Single cell culture of an attached population was completed using HOST, osteoblast cell line. This was completed in t-25 flasks. A vial of osteoblasts were thawed as described in Section 2.2.2, and cultured in pre-warmed DMEM. A media change was completed every 48 hours by aspirating the spent media and adding fresh, warmed DMEM.

2.9 Karyotype Analysis

Karyotype analysis of hESCs was outside the analytical capabilities of the Centre for Biological Engineering where the majority of this study was based and was therefore outsourced to The Doctor's Laboratory (TDL); a clinical pathology accredited laboratory. For all karyotype analyses live samples were shipped to TDL in T-25 flasks containing 70-80 % confluent cultures. The following protocol is a summary of the procedures carried out by TDL for karyotyping. Live samples were incubated at 37°C and 5 % CO_2 overnight upon receipt. Cells were treated with colcemid, to hold cells in metaphase, for 20 minutes with 20 µL/mL of media. Following this, cells were enzymatically harvested with trypsin/Ethylenediaminetetraacetic acid (EDTA) and left in suspension in a 1:12 solution of FBS in PBS for 25 minutes at 37°C. Cells were then pre-fixed in a 3:1 methanol:glacial acetic acid. Pre-fixed cells were centrifuged and re-fixed in this manner twice, discarding the supernatant before each new fixation step. At this stage, fixed cells were transferred to a wet slide to allow for the suspicion to spread across the surface. Samples were then air dried and aged in an oven at 92°C for 40 minutes or at 63°C overnight. The slides were then treated with a 1:50 solution of trypsin in PBS followed by quenching with serum. Finally, samples were stained with a 3:1 leishman/giemsa solution before being washed in purified water, dried and mounted with coverslips. Sample analysis was performed using conventional bright field microscopy. 10-20 metaphase spreads were examined for each analysis.

2.10 Isolating Mono-Nuclear Cells (MNC's) from Cord Blood

Fresh cord blood was sourced from Anthony Nolan, Nottingham. On arrival a cell count was performed using NucleoCounter (Total nuclear cell (TNC) count). The protocol for the 'Isolation of mononuclear cells from human cord blood by density gradient centrifugation' from Millipore, USA was then followed. Briefly, cord blood (stored at 4°C) was diluted with 3 x volume of MNC buffer containing PBS and 2mM EDTA (stored at 4°C). 35mL of the cord blood suspension was then layered over 15mL Ficoll-Paque (SLS, UK) in a conical tube. This was centrifuged for 35 minutes at 400 x g without the use of a stopping brake; the upper layer (plasma) was aspirated and the second layer (MNC's) transferred to a clean conical tube. The conical tube was filled with buffer and centrifuged at 300 xg for 10 minutes, after aspirating the supernatant the tube was filled with buffer and centrifuged again at 200 xg for 10 minutes. The supernatant was removed leaving the MNC population.

2.11 Isolation of CD34+ Cells from the MNC Population

The MNC's were re-suspended in 300 µL of MNC buffer then 100 µL of FcR blocking reagent (Millipore) was added along with 100µL of CD34 microbeads (Millipore). This was incubated at 4°C for 30 minutes on a rotating platform. The cells were then washed by adding 5-10mL of buffer, centrifuged at 300 x g for 10 minutes and re-suspend in 500µL buffer. The cell suspension was then added to a Magnetic-activated cell sorting (MACS) column in the presence of a magnet to select for CD34+ cells. After the unlabelled cells had passed through, the column is removed from the magnet and using a plunger the labelled CD34+ cells were removed and transferred to a collection tube. Flow cytometry for CD34 was then performed on all isolated cells to test for purity as described in Section 2.5.

2.12 Haematopoietic Cell Culture

CD34+ cells were cultured in upright orientated culture flasks in StemSpan (StemCell Technologies, Canada). A media change was completed every 48 hours by centrifuging the flask contents at 300 x g for 5 minutes, aspirating the spent media and re-suspending in fresh media.

2.13 Colony Forming Unit (CFU) Assay

A cell count was completed on the haematopoietic culture prior to use using the NucleoCounter. 150 cells were removed from the culture and re-suspended in the required volume of 250µL (10% of the CFU Assay Media) to ensure a good plating density of colonies. The cell suspension was then added to 2.5mL of MethoCult (Stem Cell Technologies, Vancouver) and vortexed to ensure the sample was well mixed. This was incubated at room temperature for 5 minutes to allow any bubbles to rise out of solution. Using a blunt-end needle the suspension was removed and plated into a 6-well plate. Spare wells and the surrounding areas were filled with distilled water to help humidification of the plate. This was then placed in an incubator at 37°C in an environment containing 5% CO_2 to allow gelation to occur, and was then either imaged in the Cell-IQ, or left for 14 days in a standard incubator.

After 14 days, the control plate from the incubator and the plate in the Cell-IQ were analysed for colony types using a 4x objective on the inverted Nikon Ti phase contrast microscope. The wells were divided into quarters and each quarter counted to get a total well count.

2.14 Statistics

All the statistical analysis was completed in Minitab 16 for Windows.

3. QUANTITATIVE NON-INVASIVE IMAGE ANALYSIS FOR EMBRYONIC COLONY CULTURE ASSESSMENT

3 Quantitative Non-Invasive Image Analysis for Embryonic Colony Culture Assessment

3.1 Introduction

Embryonic stem cells are derived from the inner cell mass of the blastocyst stage embryo. Their ability to differentiate into any cell within the body deems them pluripotent (84). This characteristic along with the ability of self-renewal makes them a very exciting proposition for the regenerative medicine industry (85). Other stem cells include mesenchymal, haematopoietic and neural stem cells which are multipotent and termed 'adult stem cells' as they are found in a variety of tissues post birth (86).

In 1964 the first embryonic cell was isolated from a teratocarcinoma, a tumour which is generated from a germ cell (87). These isolated cells had the ability to replicate in culture and grew similar to what is now termed a stem cell. Later it was concluded that in fact these isolated cells were embryonic carcinoma cells (88). These embryonic carcinoma cells were extensively studied and used for *in vitro* studies of early mouse development. However embryonic carcinoma cells harbour genetic mutations and abnormal karyotypes which only accumulated throughout development and culture. This work therefore emphasised the importance to be able to isolate embryonic cells from the inner cell mass of embryo development and prevent these genetic mutations arising during development and culture.

17 years after the embryonic carcinoma was isolated Evans and Kaufman from Cambridge University managed to establish successful culture, without karyotype abnormalities, *in vitro* pluripotent cells from the inner mass of mice blastocysts (89). This work was heavily compared to the previous works using embryonic carcinoma cells which at the time was the benchmark. The cells isolated from the embryo of a mouse by Evans and Kaufman were termed 'ES Cells' (embryonic

stem cells) in order to distinguish them from the teratocarcinoma-derived pluripotent embryonal carcinoma cells (90).

It took another 17 years to isolate human embryonic cells, this time involving both ground breaking research along with tackling ethical issues. Thomson et al were the first group to successfully isolate human embryonic stem cells (hESC's). They proposed three main characteristics that were required for cells to be termed hESC's (91):

(i) derivation from the pre- implantation or peri-implantation human embryo,

(ii) prolonged undifferentiated proliferation, and

(iii) stable developmental potential to form derivatives of all three embryonic germ layers even after prolonged culture

These 3 characteristic form the basis for the current definition of hESC's.

3.1.1 Definition of human Embryonic Stem Cell's

As discussed Thomson proposed three characteristics that began to define features required within a human embryonic stem cell (92). As research has advanced, more definitions to determine ESC's have been developed and reported. Various research groups use different analysis methods in order to determine whether they have an embryonic culture. Table 12 summarises some of the foremost techniques and outcomes which are commonly used to define and measure quality of embryonic cultures.

The common analysis techniques shown in Table 12 highlight those found to validate embryonic research in laboratories across the world. The work expressed in this thesis will also utilise some of these techniques to categorise and verify the cultured population.

Table 12. Current characteristics of embryonic stem cells. Table of properties and measurable characteristics for embryonic stem cells. These methods currently make up the core of analysis techniques frequently used to prove or disprove that a population is made up of embryonic stem cells.

Reference	Method	Characteristic	Result
(41)(42)	Optical Imaging	Morphology	Cobblestone
(43)	Fluorescence Imaging	Extracellular Stain	SSEA-3/4$^+$, Tra-1-60$^+$, Tra-1-81$^+$
(44)(45)		Transcription Factors	Nanog$^+$, Sox-2$^+$, Oct-3/4$^+$
(44)(46)(45)	Flow Cytometry	Transcription Factors	Nanog$^+$, Tra-1-81$^+$, Sox-2$^+$, Oct-3/4$^+$
(47)(43)	G-Band Karyotyping	Chromosome number and appearance	Identifies genomic integrity, 23 pairs of chromosomes
(44)	PCR (and derivatives)	m-RNA measurements	DNA quantitation
(42)	Counting	Number of Cells	Cells/mL
(44)(45)(43)	Differentiation	Cell type	Cells from each of the 3 germ layers, endo-, ecto, and meso-derm

3.1.2 Clinical Relevance / Need / Problem

Human embryonic stem cells (hESCs) are pluripotent cells and are therefore capable of differentiation into all 3 germ layers as well as self-renewal (35,93). Along with this differential potential hESCs are also immune privileged, meaning that hESCs possess mechanisms that counteract immune responses, thereby providing protection to hESC-derived allografts whilst allowing the immune system to respond to other foreign antigens (94). These two factors make hESC therapies very attractive for the regenerative medicine industry.

In order for either direct transplantation or differentiation prior to implantation significantly large numbers of embryonic cells are required. The current culture methods practical for development so

far are not proficient at producing these required quantities at an acceptable quality and price for use as a cell therapy (95). In order to successfully improve upon current culture methods there is a growing need for non-invasive process monitoring, a key aspect of this is being able to accurately describe and control the heterogeneity of a culture population.

Heterogeneity describes the mixture of cell populations with functional differences that arise from the self-renewal or differentiation of stem cells (96). Pluripotent cells, such as the H9 human embryonic stem cell presented in this thesis, make lineage fate 'decisions' and descend through a multitude of states before arriving at a fully differentiated cell (97). Therefore within a population of pluripotent stem cells there are numerous sub-populations of cells at varying lineage states. Current methods of identification of pluripotency are limited to key gene networks including Oct-4, Sox-2 and Nanog. Mouse embryonic stem cells (mESC's) closely resemble the inner cell mass of the blastocyst in terms of differentiation capacity and gene expression, although mouse epiblast stem cells show very different characteristics although are still deemed pluripotent (98). This suggests the existence of hierarchy within the pluripotent section.

It is also important to highlight that there are still some major doubts over the *in vivo* use associated specifically with embryonic stem cells. Current *in vivo* injections of embryonic stem cells have shown the ability to form teratomas (99–101). Upon transplantation *in vivo*, undifferentiated hESCs generate large tumours called teratomas. These are (benign) masses of uncontrolled differentiation. When they also encompass a core of malignant undifferentiated cells, these tumours are defined as teratocarcinomas. These malignant undifferentiated cells are termed embryonic carcinoma (EC), and are the malignant counterparts of embryonic stem cells (100), the first embryonic cells cultured in 1964 as previously described. This has caused primary concern for the use of embryonic stem cells for cell therapies, and the potential need for purification of differentiated cells prior to transplantation. The world's first study of a human embryonic stem cell based therapy in man was carried out by Geron which showed safety data where no teratomas formation was found (102). Geron initiated a Phase I multi-centre trial designed to establish the

safety of their embryonic stem cell line, GRNOPC1, in patients with "complete" American Spinal Injury Association (ASIA) grade A sub acute thoracic spinal cord injuries (102). Prior to this Geron submitted evidence of the safety, tolerability and efficacy of GRNOPC1 to the FDA in a 21,000-page IND application that described 24 separate animal studies requiring the production of more than five billion GRNOPC1 cells. Included in the safety package were studies that showed no evidence of teratoma formation 12 months after injection of clinical grade GRNOPC1 into the injured spinal cord of rats and mice (103). Although this trial was stopped, this was due to efficacy and cost rather than safety concerns raised by the study.

Another poignant issue for the use of embryonic stem cells are those associated with ethics. Due to their derivation from early embryos there is a question over their acceptability for use (86). Their ontological status, equivalence to an embryo, is often debated with both sides offering valid arguments. The Human Fertilization and Embryology Act (1990) governed research on human embryos for reproductive health, but recently was extended. In 2008 after public and parliamentary debate this act was modified to accommodate embryonic stem cell research and is now known as Human Fertilization and Embryology Act 2008 (104). Medical researchers can now apply to the Human Fertilization and Embryology Authority (HFEA) for a licence under which embryonic research can take place using 'spare' embryos younger than 14 days (105). However once an embryo is disorganised and cells are grown to create cell lines the Human Tissue Authority (HTA) commences the regulatory authority. Therefore any organisation processing, testing, sorting or distributing embryonic stem cells must do so under the authority of an HTA licence for clinical application (106). To carry out non-clinical research on embryonic stem cell lines the approval is granted from the UK Stem Cell Bank steering committee, with which the work in this thesis is undertaken.

3.2 Chapter Objectives

Embryonic stem cells have been defined according to various measures of quality, discussed in Section 3.1.1. The use of novel image analysis as a quality measurement tool allows for one of 2 separate conclusions. Either the new quantitative metrics derived from image analysis can be directly related to known quality attributes (number, phenotype) to provide a non-invasive correlation for obtaining the same information, or do not directly correlate to the known quality attributes and therefore provide novel information, the significance of which would require further investigation.

In order to evaluate image analysis as a tool for embryonic quality assessment a series of steps will be taken in this chapter. The first stage is to evaluate the precision of image analysis and compare to a conventional technique using statistical evaluation, cell counting will be used due to its common use as a measurement of culture assessment (107). Following this, image derived metrics must be analysed for novel information alongside representation of culture state and correlation to conventional quality assessments. To develop a quality assessment tool these questions must be answered within the chapter:

- What is the precision of a common quality assessment tool?
- What is the precision of image analysis?
- What metrics can be measured from phase contrast images?
- What measured metrics can correlate to common quality assessment tools?
- Do metrics provide novel information on a culture state?
- Can metrics be used to predict culture state?

3.3 Does Invasive Cell Counting Correlate to Non-invasive Cell Coverage?

Cell counting is often utilised as a control measure in order to make process decisions, such as the addition of growth factor at a concentration determined by cell number. However this is an invasive method which requires the sacrifice of cells (107). It therefore would be advantageous to replace this invasive method with a non-invasive technique for representing cell number. For this work being able to show a reliable comparison to cell counting with the ability to achieve it non-invasively would be of great advantage. The first step requires assessing a single cell counting method which is both reliable and precise.

3.3.1 Selecting the Most Precise Invasive Cell Counting Method

Initially the counting method with the lowest noise was determined. Each of 20 independent flasks, with a variety of confluence, were taken and counted by using 3 automated counting methods; Guava (Millipore), Cedex (Roche) and Countess (Invitrogen). Each flask was counted 6 independent times on each counter, allowing a coefficient of variance (CV) to be calculated for each flask. The averaged CV values for all 20 flasks are shown in Figure 20.

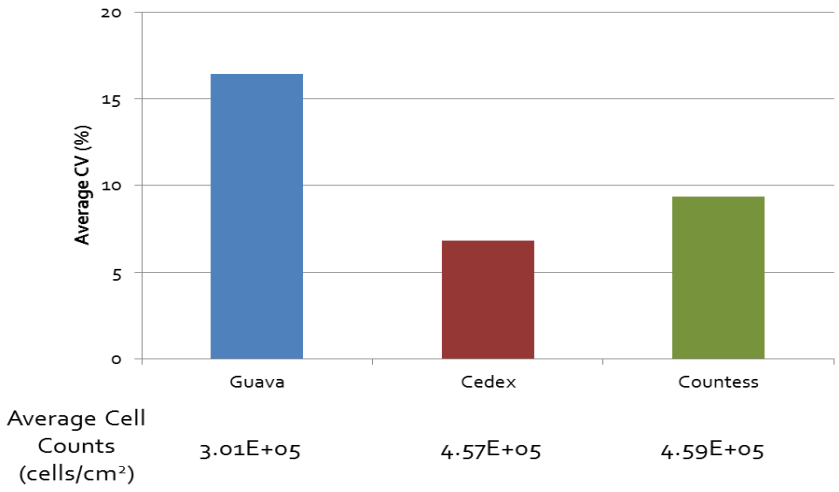

Figure 20. Average coefficient of variance for 3 automated cell counting systems. 20 independent flasks of colonies are dissociated with 6 samples from each flask being counted on each measurement machine (Guava's (ViaCount), Cedex (trypan blue) and Countess (trypan blue). The CV can then be calculated for each flask on each counter and averaged to produce the average CV for each counting method. (n=20, counts repeated 6 times)

Figure 20 shows that the Cedex automated counter provides the most precise counts which are more reproducible then the Guava or Countess, with an average 7% CV. Of these three methods the Cedex uses the largest sample volume (1 mL/count) compared to the other two methods (20 µl/count). This reduction in volume means that a homogeneous stock solution is essential to achieve a precise count. Deviation away from homogeneity could reduce precision, a common trait as cells begin to sediment during sampling. In order to prevent sedimentation the cells can be continually mixed through pipetting, although this can increase the shear stress applied to the cells and in turn cause cell damage. A balance between ensuring a well-mixed homogeneous stock solution whilst maintaining viability is required. Again for this instance an automated mixer is advantageous ensuring consistent mixing is achieved. The mean cell counts are similar for both the Cedex and Countess (460000 cells/cm^2) which use trypan blue to conduct their respective counts, mixing the cell solution with trypan blue before taking images to determine a viable cell count based on membrane permeability. The mixing stage of trypan blue is conducted within the automation of the Cedex whereas the Countess requires a pre-mixed solution to be added to the machine, possibly adding further error from a laboratory user. This added non-automated step, which could account for variation in the samples, is not required in the more automated Cedex counter and therefore it is preferred to the Countess. The Guava counter also requires manual mixing although uses a different mode of action for staining prior to counting which could account for a much lower cell count (300000 cells/cm^2). Instead of trypan blue, ViaCount, an assay that distinguishes viable and non-viable cells based on differential permeability to two DNA-binding dyes, a nuclear stain and a viability stain is utilised. The nuclear stain identifies only nucleated viable cells whereas the viability stain brightly stains dead and dying cells. Consequently viable cells are distinguished to those that are dead or apoptotic. Compared to the Cedex, the Guava includes apoptotic cells into the non-viable count, generating additional information regarding the future of the cell culture; however the lack of precision that is related to the Guava makes the Cedex counter the preferred counting instrument. Due to the difference in counting method a comparison of true

cell counts cannot be made between the instruments, only the variation in count measurement between counters. Having concluded on the Cedex as measuring the most reproducibly it is important to identify if there is a precision deviation dependent on the cell counts themselves. All counting equipment has operating parameters with regard to the concentration of cells, within which they can precisely count. By plotting the mean counts against their respective CV's any bias within the operating parameters can be identified. Figure 21 plots the 20 previous mean counts against their respective CV's.

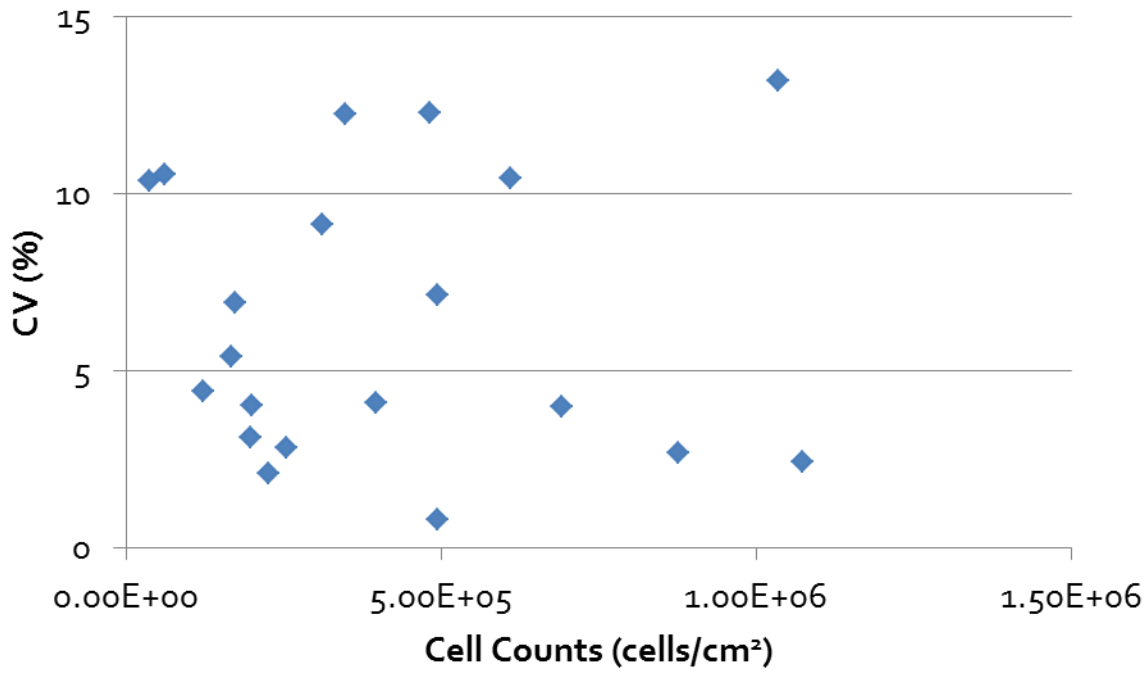

Figure 21. Relationship of coefficient of variance (CV) to Cell Counts The mean cell count, of 6 repeats, from 20 independent flasks, plotted against the respective CV value from the 6 counts taken for the Cedex Counter. This shows that the variation in precision is not biased given the number of cells per sample. (n=20)

No correlation is made between mean cell counts and CV's, proving that there is no bias in precision given the number of cells per sample. Taking Figure 20 and Figure 21 into consideration the Cedex counter out performs the other cell counters in terms of precision whilst also maintaining independence to cell number and therefore will be utilised for counting in this section.

3.3.2 Precision of Non-invasive Coverage Image Analysis

A culture's confluency or coverage is a fundamental measure in the field of biology, the ability to quantify confluency through coverage metrics provides extensive knowledge related to the culture state. Cell behaviour and kinetics are often affected by varying density levels (108), this is often shown by a change in morphology as cultures approach confluency (109). Therefore a method of automating the determination of confluency non-invasively allows culture state to be determined prior to any process actions.

In order to correlate the cell counts discussed previously, an image based method for measuring the coverage of cell colonies in a culture vessel that produces a reproducible, precise value must be developed. Within the Cell-IQ's Analyser software, regions of varying threshold can accurately be segmented. This simplest image segmentation method utilises pixel intensity to separate light to dark regions (110), known as the Threshold Method in Analyser (Figure 22). For a cellular application this allows areas of background to be isolated from areas of cells which are denser and therefore have a higher threshold value. From observation of analysed images it is possible to acknowledge that the threshold method can be used to accurately measure confluency; representative exemplar images are shown in Figure 23.

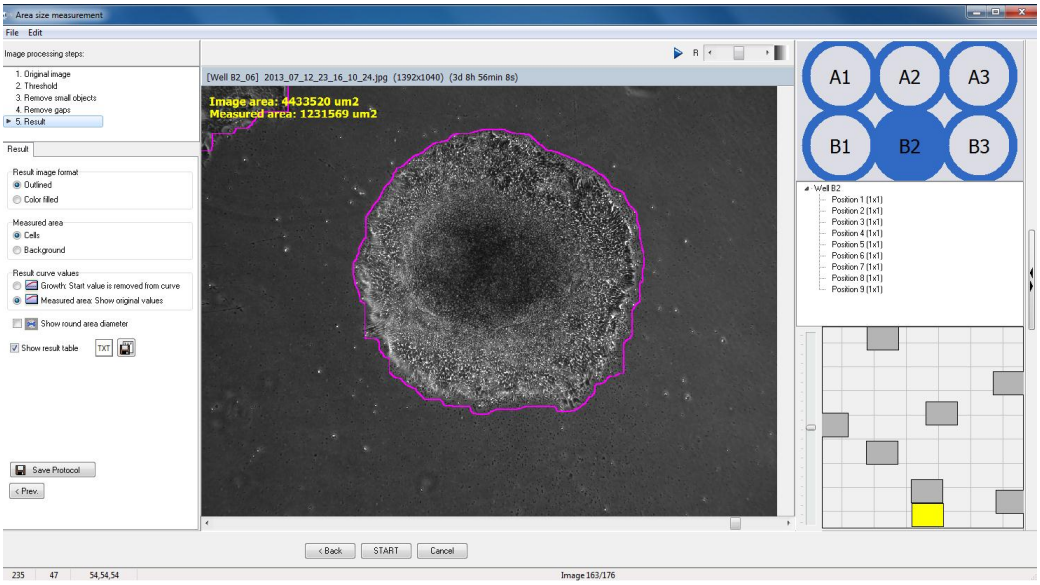

Figure 22. Threshold Method for identifying areas of colony. By optimising the threshold level, areas of colonies can be isolated from the background as shown here encircled within a purple boundary. The area within the boundary can then be measured as shown in the top left of the image.

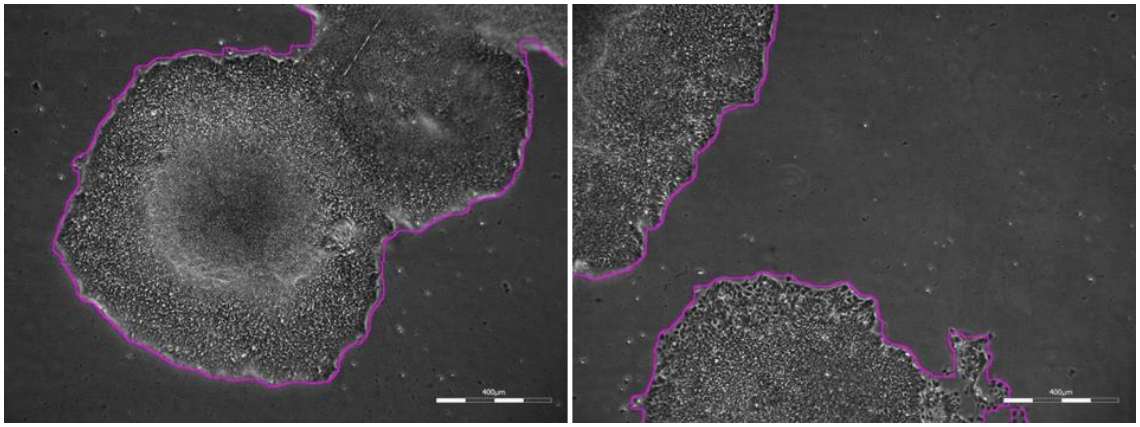

Figure 23. Analysed images of embryonic colonies. Image analysis of embryonic colonies using the Cell-IQ's analyser software to identify areas of higher threshold which relate to the cell colonies, shown enclosed within the purple boundary. These examples show the high accuracy of using the threshold to analyse total colony coverage.

Using this non-invasive image platform it is possible to image the entire surface area of the culture vessel from which the 'true coverage' can be determined along with the standard deviation using the method in Figure 22. Normalising the standard deviation by the mean allows the coefficient of variation (CV) to be calculated. Subsequently it is then possible to determine if the culture vessel coverage influences the CV whilst identifying the coverage that produces the highest variation. This is shown in Figure 24 for 30 flasks of varying coverage.

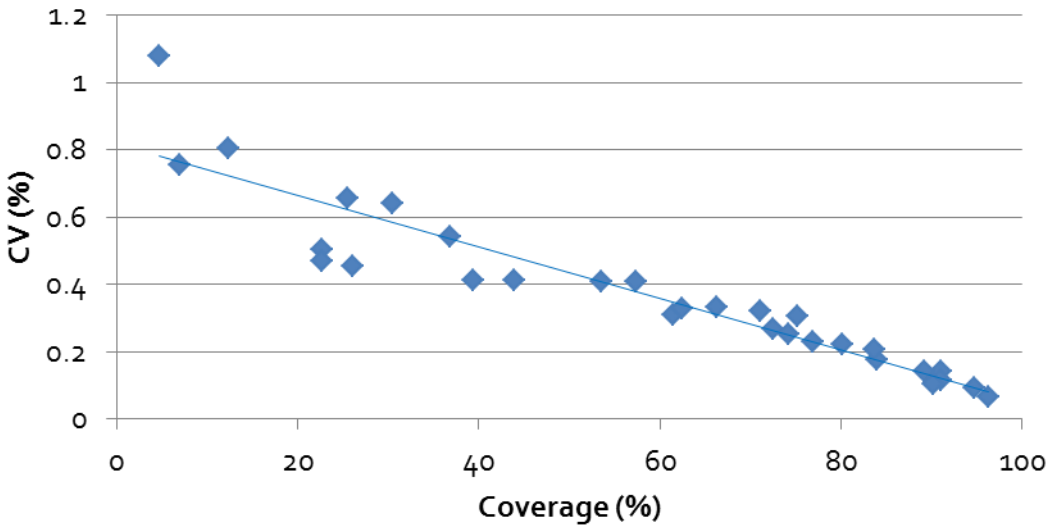

Figure 24. Relationship of CV against cell coverage. The average coverage, from 400 images, against the CV obtained from 400 images for 30 independent flasks. This shows that there is variation in precision based on the coverage within the culture vessel. At a high coverage image analysis is more precise then at low coverage values. (n=30)

Increasing the coverage reduces the CV signifying that the measurement system is more precise at higher coverage values. During analysis it is possible to measure all coverage values between 0 and 100%; this provides the range of coverage represented in the images. At low cell coverage there will be images with no cells in giving a value of 0%, and also images that fall directly onto a colony giving 100% coverage. At high cell coverage there is less chance of imaging an area of 0%, and therefore the range of measurements is the same but the probability of the lower coverage's are reduced, giving an overall reduced CV.

It is important to note that a low coverage produces the largest variation in a population, although it is unlikely that process decisions will be utilised for low coverage. However in building a tool it is imperative to know the limits of operation. Highlighting that at low coverage the tool is least precise allows a bottom limit to be provided with known error.

This CV calculation is based on imaging 400 areas of the culture flask; however for a real time assessment taking a smaller sample would speed up both the acquisition and analysis. By taking the standard deviation which occurs within the entire population the standard error of the mean (SEM) can be calculated using the below equation.

$$SEM = \frac{\text{s.d.}}{\sqrt{\text{n}}}$$

Where:

SEM = standard error of the mean
s.d. = standard deviation
n = sample number

For culture vessels of varying coverage the standard deviation is calculated, and thus by changing the sample size the relative SEM can be deduced. Figure 25 shows the SEM reducing as sample size is increased as expected for various coverage values.

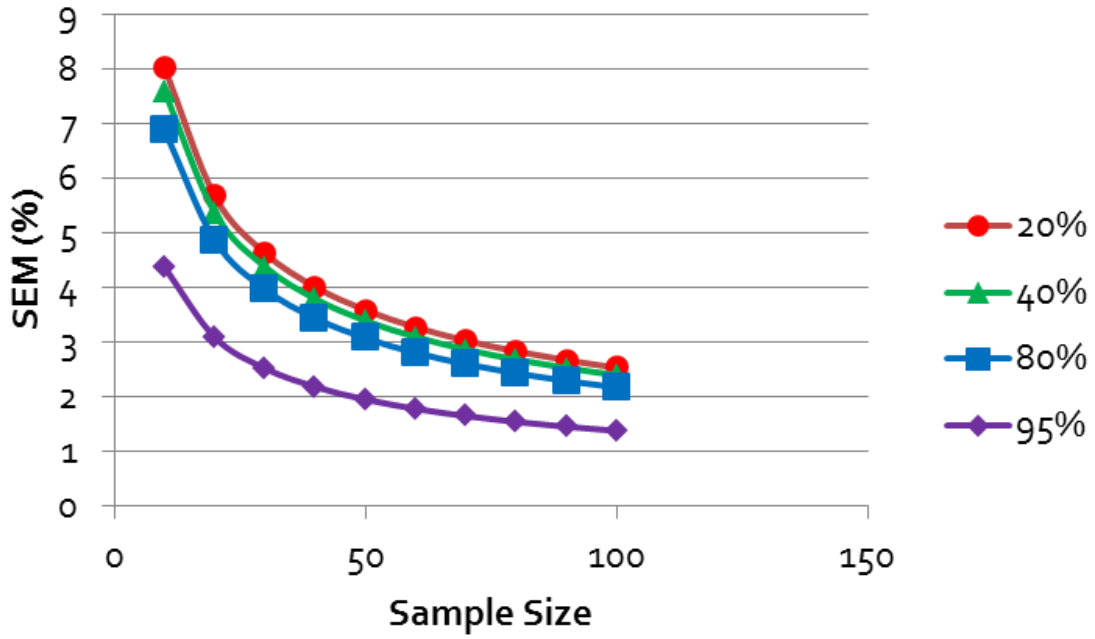

Figure 25. Relative standard error of the mean (SEM) against sample size for 4 flasks of varying coverage values. This shows that the low coverage values have a higher standard error of the mean due to a larger standard deviation when compared to higher confluence values.

Figure 25 shows that the highest SEM values are shown for the lowest coverage, as shown by the red circles representing a coverage of 20%. This agrees with Figure 24 that showed the lowest coverage had the largest CV's, demonstrating that low coverage provides the least precision. The purple diamonds identify the highest accuracy at 95% coverage. As explained previously at the higher coverage there is a near complete layer of cells covering the culture vessel, and therefore taking just a single image provides a close prediction to the true mean.

Statistical theory determines that the SEM decreases as the sample size increases. So the larger the sample sizes the more accurate the measurement will be. However it is important to choose a sample size where the SEM is less than the accepted error, whilst adjudging factors such as time to acquire and analyse the data.

By setting the SEM, the sample size (n) can then be deduced for a given standard deviation. This allows a sample to be imaged rather than the entire flask, which is time consuming both in acquisition and analysis. Selecting an error of less than 5% improves on the 7% error measured from the Cedex cell counter (seen in Figure 20). The Cedex counter is taken as having a standard error rate for cell analysis, to which image analysis might be able to improve on. The next step is to determine a sample size where all coverage's have an error under 5%. Thus from Figure 25 a sample size of 50 has been chosen to be of sufficient precision to represent the entire population. Previous work has shown that coverage determination through visual inspection is subjective and prone to high inter-individual variability (108). Jaccard et al. conducted a survey from 14 experienced cell culture researchers which yielded a combined variability of 11.7% (111). Using embryonic stem cells in gel coated 6-well plates images were taken using an inverted phase contrast microscope. 20 random images were captured per well and utilised for this experiment. Taking 7 separate sets over a range from 10% to 90% coverage the 14 researchers each had over one year experience of conducting coverage assessments highlighting the high variability of confluence estimations made by human operators. By selecting an error of less than 5% improves on this reported manual assessment of confluency.

Having selected a satisfactory sample size the next step is to validate the sampling method. There are 3 methods of acquiring the images; cluster sampling, systematic sampling and random sampling. Due to hardware constraints the use of random sampling is not possible. A visual assessment of colonies in flasks suggested that systematic sampling was better than cluster sampling due to the macro distribution of colonies within the flask. Most notably the edges of the flask are not sampled during cluster sampling (Figure 26).

The extrapolation of SEM from a complete scan, as discussed previously, can be utilised for a reduced sample. This method carries no bias as the sampling method is a random sub selection of the full scan. This provides a sampling method and image number which can be used for flasks knowing that less than 5% error will be recorded. To verify this cluster and systematic sampling were compared to an entire flask with systematic sampling also carried out with the reduced sample size of 50; this is shown in Figure 26.

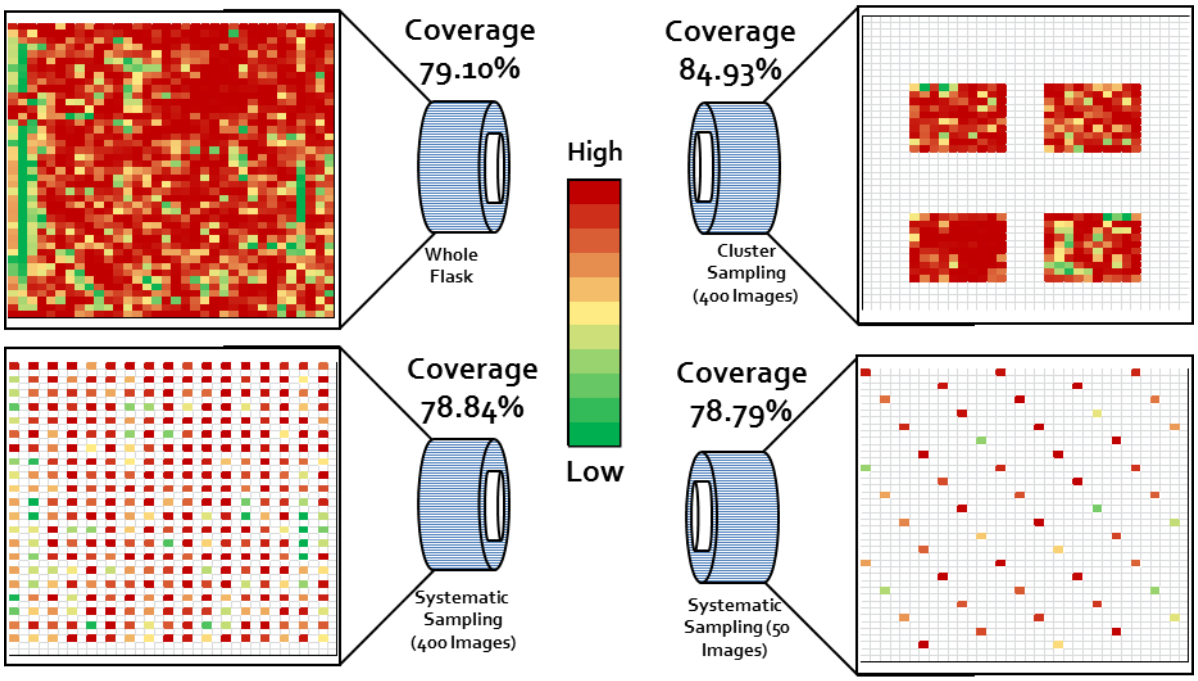

Figure 26. Example flask comparing entire flask coverage to possible sampling techniques Cluster and systematic sampling methods for estimating colony coverage compared to the entire population with heat maps identifying coverage values for each image. This shows that systematic sampling provides a better estimate of the true value comapred to cluster sampling. Taking this a step furtherusing a sample size of 50 as estimated from previous data, maintains the estimate wihtin 10% error as previously calculated.

Figure 26 shows the true coverage given as 79.10%, which is calculated by imaging the entire flask region where cells are capable of growing. The sample pattern forms another important parameter that can affect the coverage estimate. From Figure 26 it is possible to see that the cluster imaging oversights the low coverage edge (green area on Figure 26) that is seen within the entire imaged flask as predicted. Therefore cluster sampling is only accurate when there is a reproducible pattern which falls within each cluster. Due to the variable colony size and seeding, cluster sampling provides an inaccurate estimation of coverage for the macro colony distribution. Systematic

sampling eradicates the need for a reproducible pattern as a snapshot from the entire surface is taken into account. This therefore means that for this selection systematic sampling is more representative of the population then cluster sampling. By using a sample size of 50 with systematic sampling the standard error of the mean is less than 5%. This allows the measured coverage values to be compared to the corresponding cell counts which have a variation >5%, as shown from Figure 20.

It is important to note that this sample size of 50 can be used for all culture vessel sizes although the data here was collected on t-75 culture flasks. The image size of 50 accurately represents the variation from the macro distribution of cell colonies, so unless this macro distribution changes significantly then a sample size of 50 can be used for all culture vessels for a standard error of less than 5% across all coverage values from 20%.

3.3.3 Correlating Invasive Cell Counts to Non-invasive Coverage

Having measured the statistical resolution of cell counts, and found an improved imaging platform precision, it is then possible to correlate the two metrics to one another. To carry this out systematic sample imaging with 50 images was completed on 30 t-75 culture flasks of varying confluence, followed by a sacrificial cell count. These are then plotted against one another to determine if there is a correlation as shown in Figure 27. Also included is the point 0,0 as at 0 coverage there will be no cells. This was verified through imaging a flask with solely media in, to check that image analysis correctly analysed this at zero coverage. This was successful, although the images are not shown here. The regression however is not forced through this origin point to ensure the best correlation can be made with the data rather than skewing the data.

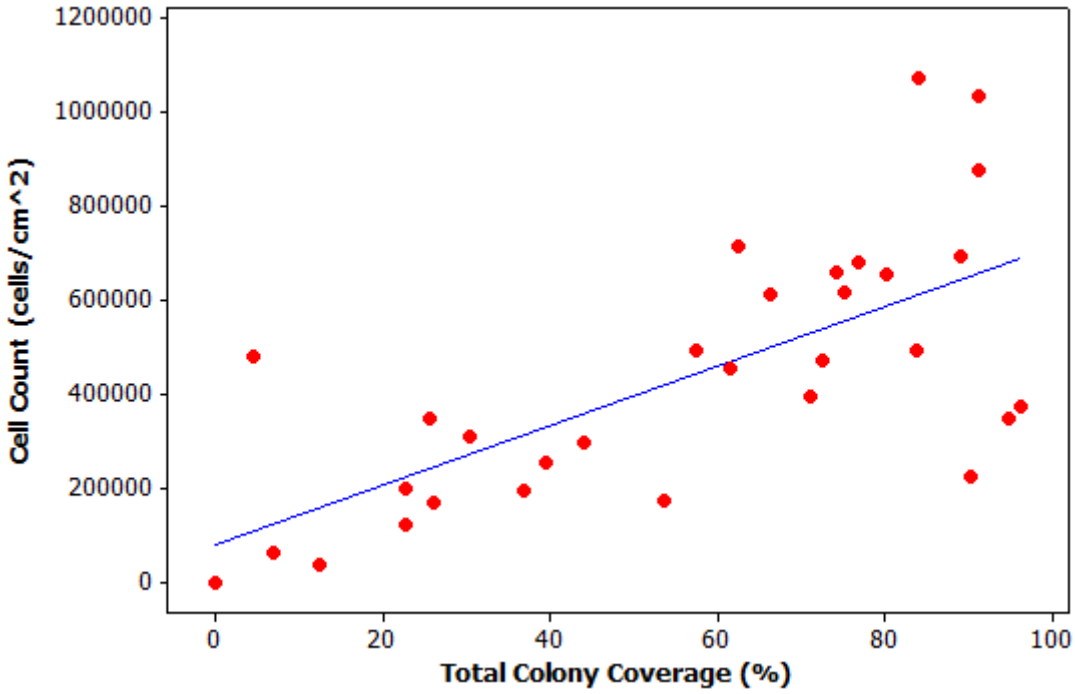

Figure 27. Relationship of Cell count against Coverage with plotted linear regression. Linear regression performed on total colony coverage against cell counts for 30 independent flasks (and 0,0 as an extra point). Using 50 images acquired with systematic sampling, and cell counts from the Cedex counter using 6 repeated measures only the cell counts from Cedex automated counter. The predicted model assumes a linear relationship of equation y = 81289x + 6317. (n=30)

Coverage is loosely correlated to cell number, shown by an R-squared value of 47.4% assuming a linear relationship as shown in Figure 27. There is significant noise, or confounding factors in the relationship reducing the accuracy of the correlation. Figure 27 shows that in order to replace invasive cell counting with an image derived metric, coverage, the correlation needs further improvement. The first step to an improvement is to ensure that the correct model is used to correlate to the data. This is achieved by assessing the biology that the mathematics is predicting. Taking the first example with total colony coverage against counts the equation which linear regression is trying to fit takes the order of:

$$y = C_o x + C_1$$

Where:
y = Cell Count

C = Constants

x = Coverage

Differentiating this will give the expected gradient or shape of the line of best fit.

$$\frac{dy}{dx} = C_o$$

This suggests that there is a constant gradient of change of coverage with cell density. By applying simple linear regression models to our data for low densities the following assumptions are made:

- Mean response varies linearly with predictor
- Unexplained variation in the data is normally distributed
- Unexplained variation is independently distributed with constant variance

To test these assumptions Figure 28 shows statistical plots relating to the regression shown in Figure 27.

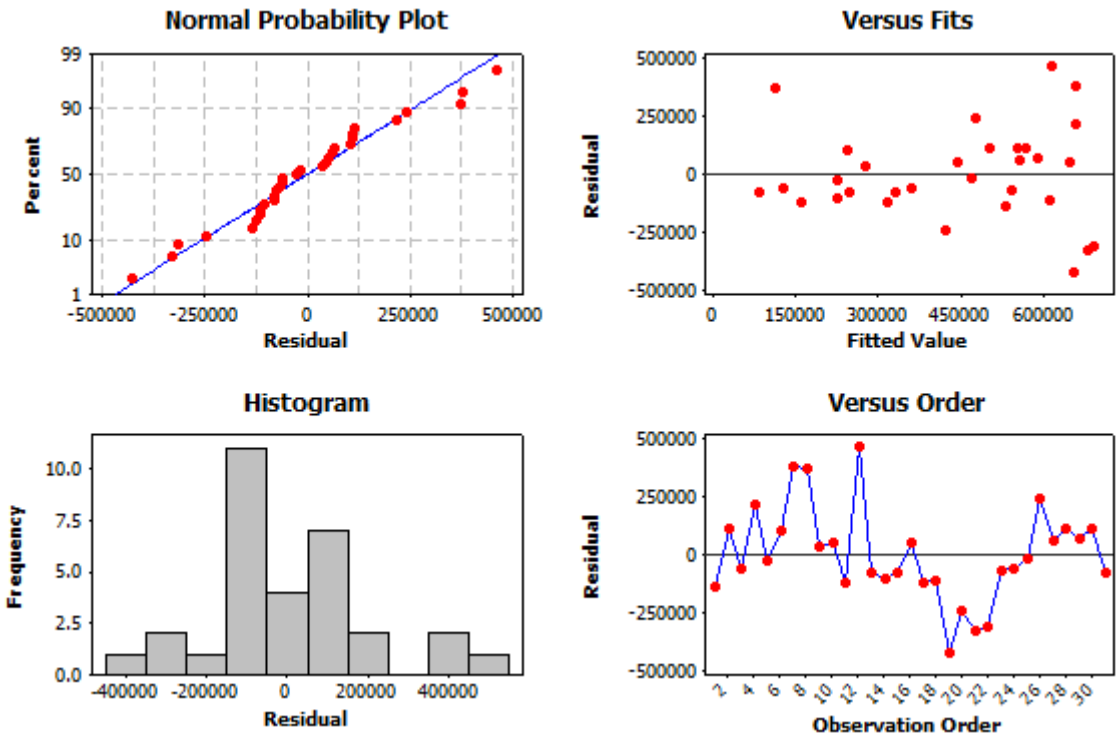

Figure 28. Plots of statistical measures from count against coverage graph seen in Figure 27.. These graphs show measures of normality, linearity and variation across the data set. By plotting the residuals on a normal probability plot an estimation of normality can be deduced. The points all lie close to the centre line suggesting that the data follows a normal distribution. By comparing the residuals against the fitted value an estimate for whether the data represents a linear or nonlinear fit can be seen. The slight spreading seen on the right suggests that this may not fit a linear model as the higher values lie further from the regression fit. (n=30)

Figure 28 shows a linear relationship for the residuals and therefore regression is a suitable method as the error is normally distributed in the Normal Probability Plot. To justify the aforementioned assumptions the Versus Fits plot shows the residuals against the fitted values. This plot should show a horizontal band of roughly equal width to prove a linear relationship. However Figure 28 shows the width of the band increasing as the data moves from left to right, this suggests that the variance is also increasing. Therefore there is not a constant variance across the data set suggesting a non-linear relationship between coverage and cell counts. There is also a weak 'U' shape to the data suggesting that the linear regression is not a representative model and actually the data may better be predicted with a non-linear relationship.

Figure 28 has cast doubt over the use of simple linear regression to explain how cell density varies with coverage. Linear regression holds true for low coverage, and low cell densities where the colonies are in logarithmic growth without inhibition of space. As proliferation increases this surface area becomes limiting, potentially forcing the cells to grow into denser regions and hence there are more cells per given area. This is witnessed through darker regions of colony in response to limiting area by production of morphologically different cells. This therefore suggests that at a low starting cell number there is a linear relationship between coverage and cell density, as cell count increases the relationship becomes non-linear. So a constant gradient over the entire range is unlikely; therefore suggesting the linear hypothesis is an inaccurate model.

It is also true that from a biological view point a non-linear model is more logical as at higher cell density dark patches appear within the centre of a colony where an increase in cell number per area occurs. Therefore if a quadratic relationship is expected this would take the form of:

$$y = C_o x^2 + C_1 x + C_2$$

y = Cell Count
C = Constants
x = Coverage

With the differential:

$$\frac{dy}{dx} = 2C_0x + C_1$$

This quadratic relationship provides a gradient which would change dependent upon the cell number. This is more likely to occur due to the aforementioned reasons, and by fitting a suitable quadratic the following graphs can be produced showing the fitted line, normality and residuals plots. The non-linear model is based on an exponential curve increasing with increased coverage.

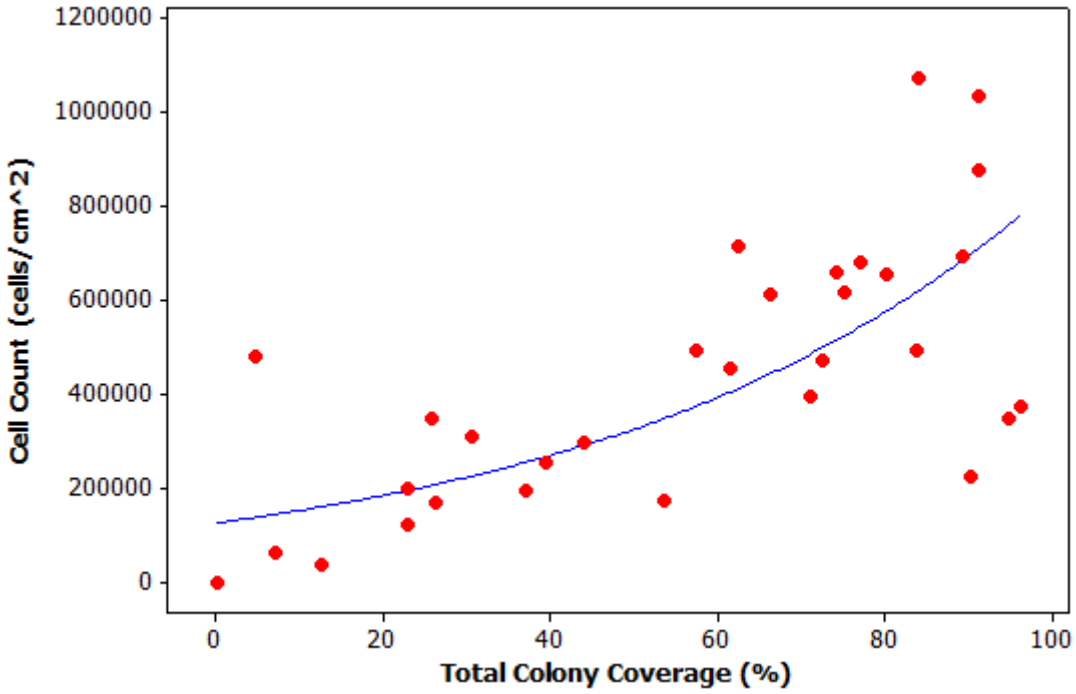

Figure 29. Non Linear exponential regression of cell counts against coverage. Scatter plot of counts against coverage using a non-linear exponential regression model. As with the linear regression, 30 coverage vessels are included with 0,0 point, using average of 6 counts performed on Cedex. A comparison of linear against non-linear is hard to judge which is the better predictor, in this state the error is too large to be useful for process control. (n=30)

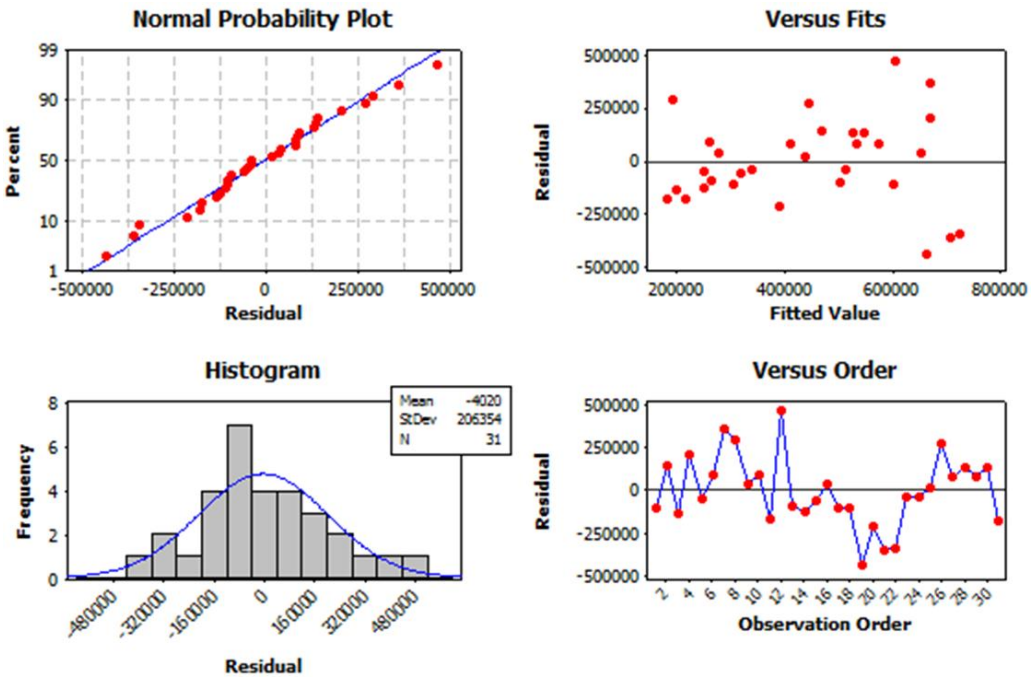

Figure 30. Plots of statistical measures from non-linear count against coverage graph seen in Figure 29. These graphs show measures of normality, linearity and variation across the data set. By plotting the residuals on a normal probability plot an estimation of normality can be deduced. The points all lie close to the centre line suggesting that the data follows a normal distribution. By comparing the residuals against the fitted value an estimate for whether the data represents a linear or nonlinear fit can be seen. The slight spreading seen on the right suggests that this may not fit a linear model as the higher values lie further from the regression fit. (n=30)

Due to the weak correlation it is hard to judge by eye whether a linear or non-linear model fits best. Often the r-squared (R^2) term is used to compare best fits. The R^2 or coefficient of determination indicates how well data points fit a statistical model. Similar to the R^2 term, the standard error of regression is another measure of fit often depicted as 'S'. Unlike r-squared however this error is measured in the units of the response (in this case cell count) and represents the standard distance data values fall from the regression line; therefore the smaller the value of S the better the fit. Using this S value the linear model achieves an error of 207544 with the non-linear model calculating the error as 210820. Therefore from a mechanistic point of view and an analysis perspective the linear model fits better, however there is still an unexplained residual error, likely due to biological response with the differences noted being far too small to select one over another.

So neither Figure 27 nor Figure 29 are fit for purpose as a direct correlation to determine cell number from coverage with accuracy, in which the imprecision of prediction of cell density from coverage outweighs any non-invasive benefit from image analysis over sacrificial cell counts.

The lack of correlation comes from neither an error in the cell counting nor the image analyses ability to identify total colony coverage as shown in Figure 20 and Figure 25. We know intuitively that if all cells were the same size and not overlapping they would correlate. Therefore this must not be the case. There is a requirement to identify ways to measure this lack of coverage homogeneity to improve the correlation. The ability to measure coverage precisely allows us to use these images for further analysis and provide novel information on cell culture relative to a count. There are changes in contrast that we hypothesise represent changes in density/quality, average colony size, shape, circularity etc. These measurable traits potentially have the ability to improve the relationship of coverage to cell counts by addressing a change in cells/area relationship.

3.4 Identifying Further Non-invasive Image Derived Metrics that Relate to Cell Quality

Observation of the pluripotent cultures shows that there are colony areas that have a different morphology and density. Therefore the logical position that the cell/area is variable within a colony is supported. oFigure 31 shows where these thoughts have developed from, highlighting 4 separate colony regions that can be distinguished where the cell number per area is predicted to vary, along with a schematic of these areas.

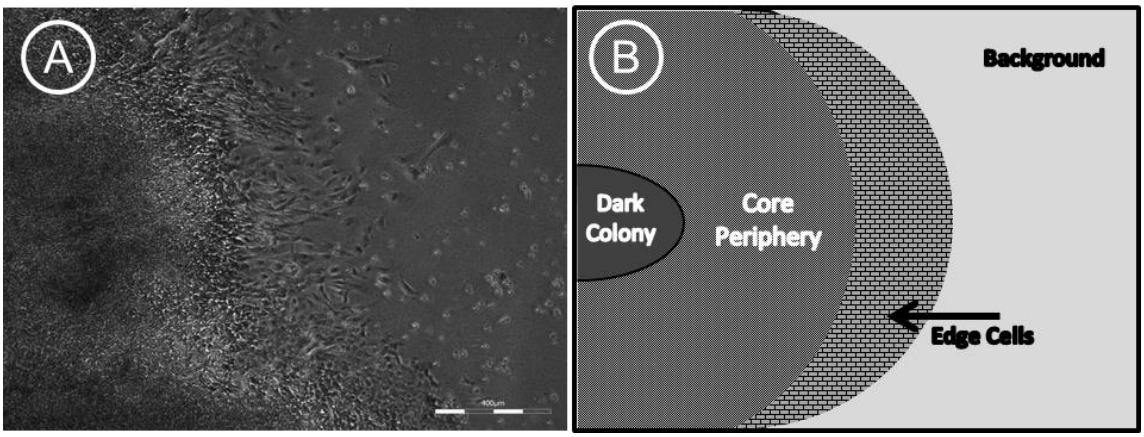

Figure 31. Acquired Image and schematic showing further metrics for analysis A) Image of a colony showing a dark centre within the colony, and single cells on the periphery, showing the heterogeneous morphology within a single colony. B) A schematic of the 4 different regions that can be identified in a phase contrast image of a colony; background, edge cell, core periphery and dark colony.

As seen in Section 3.3.2 the total colony coverage can be precisely measured using the Threshold Method, this successfully separates the background from all cells. From oFigure 31 it is possible to appreciate that the total colony area can be further segmented into 3 areas representing varying degree of cells per area. The 'dark colony' areas represent dark, dense areas where the cell number per area is increased either due to different cell morphology or due to multi-layering of cells. Another area is the monolayer of cells around the periphery of the colony. These cells, hereafter called 'edge cells,' are much larger in surface coverage than the compacted cells making up the core of the colony. The third and final area to be identified is the remaining colony. This represents the morphology that is most abundant in pluripotent culture, coined 'core periphery' as it makes up the periphery of the dark colony area. The morphological variations seen from images provide a list of observable metrics from images that may provide further information on culture state (Table 13).

Table 13. List of measurable characteristics from image analysis. Possible measurable metrics which could be useful for predicting colony quality, along with evidence for their usefulness and ability to determine quality.

Characteristics	Metric		Evidence/Usefulness
Entire cell population	Total Colony Coverage	TC	Confluency is often used as a process decision gate
Pluripotent Colony	Core Periphery	NC	This is total colony minus the dark and edge cells. This therefore represents an area deemed to be pluripotent.
Cell Density / Phentotype	Dark Colony	DC	The dark areas represent a higher density of cells or regarded as differentiated cells (36,37)
Differentiation / Phenotype	Edge Cells	EC	These cells have different cell morphology to the rest of the colony, either have a different role, or maybe differentiating cells
	Rate of change of total colony coverage	dTC/dt	This gives the growth rate of the entire colony
	Rate of change of core periphery coverage	dNC/dt	This gives the growth rate of the core periphery area
	Rate of change of dark colony coverage	dDC/dt	This could determine either differentiation rate or show when cells become more dense, maybe space limiting indicator
	Rate of change of edge cell coverage	dEC/dt	May give an early differentiation indicator

Each of these traits is initially tested to ensure they can be identified using the analysis software. Following this the metrics can be assessed for their ability to be predictive of cell quality and potentially correlate image derived metrics to cell counts. Further analysis will allow the behaviour of all these metrics over time providing their rate of change which may provide further novel information regarding culture state. It is further hypothesised that continual monitoring of the metrics may provide predictive evidence of culture state, which would be extremely powerful for online process control.

3.4.1 Coverage of total colony

Total colony coverage has already successfully analysed images previously using the threshold method to identify the total coverage of culture surface which is inhabited by cells. This includes dark areas and edge cells but successfully removes the background and debris within the culture system as shown in Figure 32.

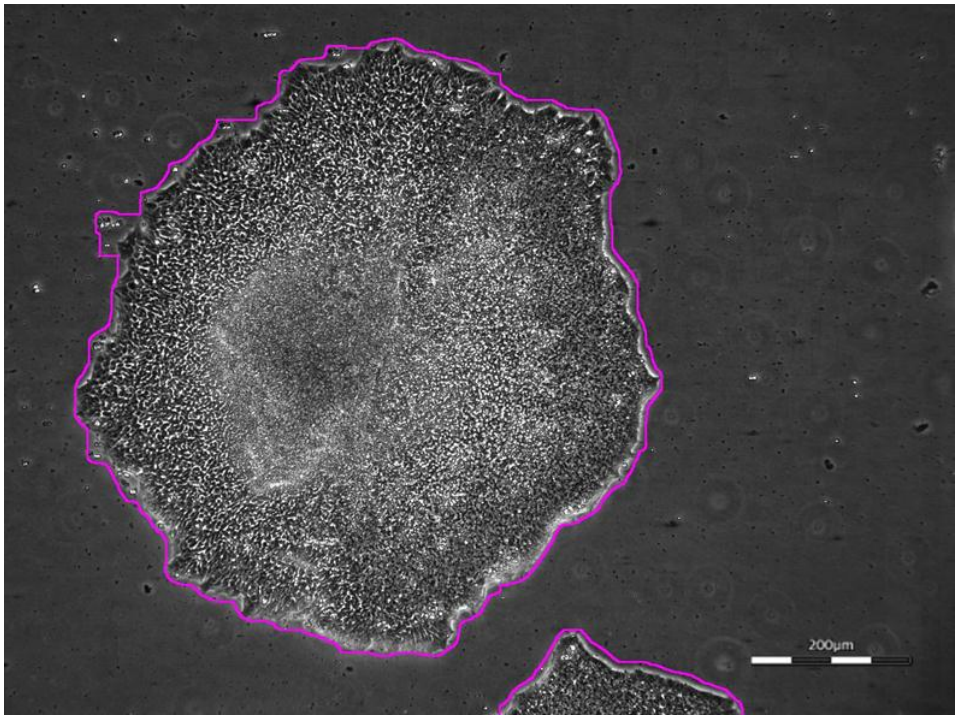

Figure 32. Analysed image for total colony coverage. Image analysis of total colony coverage using the Cell-IQ analyser software's Threshold Method to calculate the area covered by cells. The purple boundary represents where the colony ends and the background begins, this successfully measures the total colony coverage.

3.4.2 Dark Coverage

The dark coverage will detect areas of colonies that are denser and therefore have a higher threshold value. This increase in density is likely to appear due to a modification of biological properties; a change in phenotype relating to a denser cell, a change in morphology causing tighter packed cells, the formation of cells on top of each other thus appearing denser or any combination of these factors. All of these attributes would lead to a change in cells per surface area.

Numerous scientific reports suggest varied opinions and observations with regard to the dark central areas. Lijun Ji et al. reported in 2012 that embryonic stem cells grown on silica colloidal crystal microspheres form central pits that appear dark under white light illumination (112). Further growth of the colonies caused these cavities to increase in size for colonies with a depth of greater than 80 µm measured by scanning electron microscopy. These central pits appear to have a defined edge unlike the continuum seen in the phase contrast image of oFigure 31. Therefore it is likely that these central pits are an artefact of the surface substrate used and do not appear in the cultures reported in this work. Another report publicised in 'Human Embryonic Stem Cell Protocols' (113) has reported that within the core of colonies neural rosettes are capable of developing, thus changing phenotype. Figure 33 identifies these dense regions within a human embryonic colony on a brightfield image reproduced from Turksen et al (113) and a phase contrast image taken with the Cell-IQ.

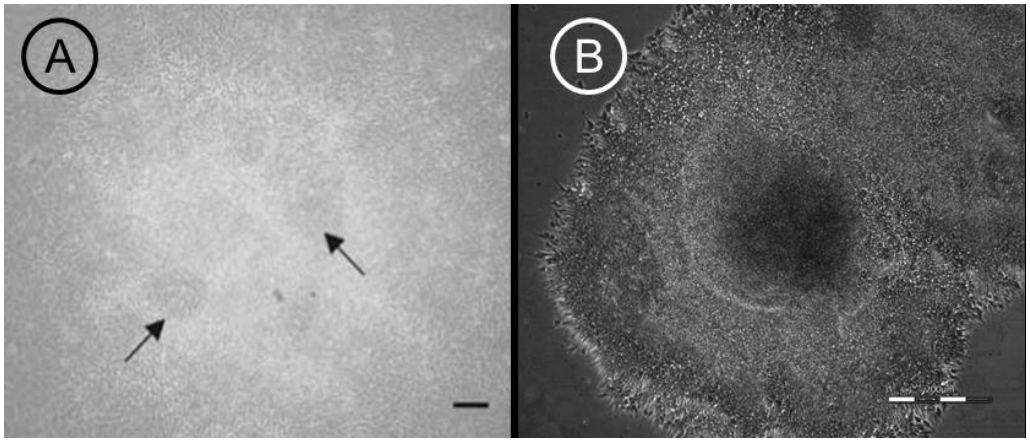

Figure 33. Comparing dense areas of colony from brightfield and phase contrast. A) shows developing neural rosettes (arrows) within an embryonic stem cell aggregates with in the colony centre. Re-produced with permission from Humana Press. Bar =50 μm (113). B) shows H9 embryonic colony with similar dense area taken on the Cell-IQ as a phase contrast image.

In comparison the dense areas seen from the Cell-IQ has an increased contrast due to the use of phase contrast to capture the images. But a similar morphology can be noted. Reubinoff et al (114) also report seeing high density areas in colonies undergoing neural differentiation. Therefore in conjunction with these studies and the appearance of user defined neurones in culture (shown in Figure 34) it is concluded that the dense areas within the centre of a colony identify a population that is differentiating, and therefore could provide a direct link to cell population quality.

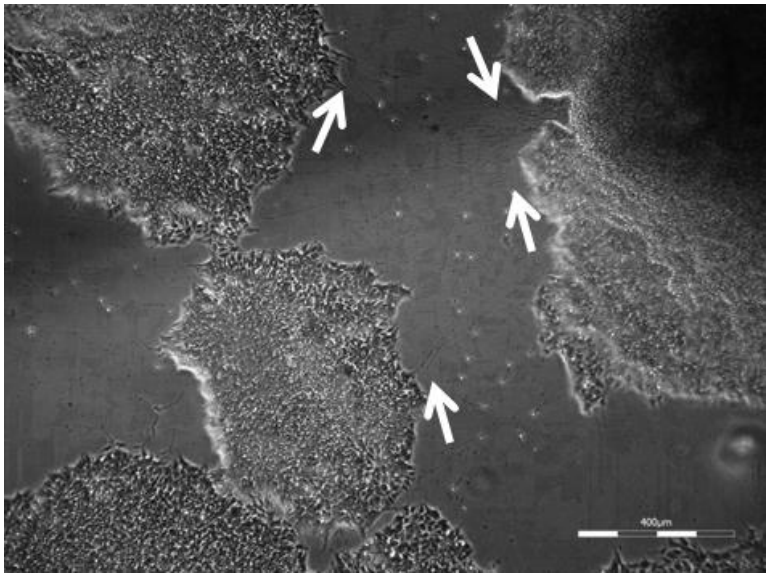

Figure 34. Identification of neuronal growth from dark centred colonies. The dark centres of colonies are often debated to what they represent, either compact pluripotent centres, or differentiating cells. This image shows neuronal outgrowth growth from the colony with a dark centre (arrows), with the surrounding colonies remaining with the pluripotent morphology. This suggests that these dark centres are indeed neuronal rosettes as described by Turksen et al. (115).

By measuring these dark areas the cell density to coverage correlation might also be improved, but more importantly the dark areas may provide a measure of pluripotent status. There are two image analysis methods that have the ability to identify dark areas of colony; the Threshold Method (used to measure total colony coverage) and Area Finder, each are discussed in the following sections.

3.4.2.1 The Threshold Method

The ability to identify total colony coverage utilised the Threshold Method by choosing a threshold value that was able to distinguish the background from the denser cells. The same method with a higher threshold value can be used here to differentiate the dark areas of colony to the light areas of colony. By increasing the threshold level only the darkest areas are identified, therefore selecting the dense dark colony coverage. Representative images of using the higher threshold value are shown in Figure 35.

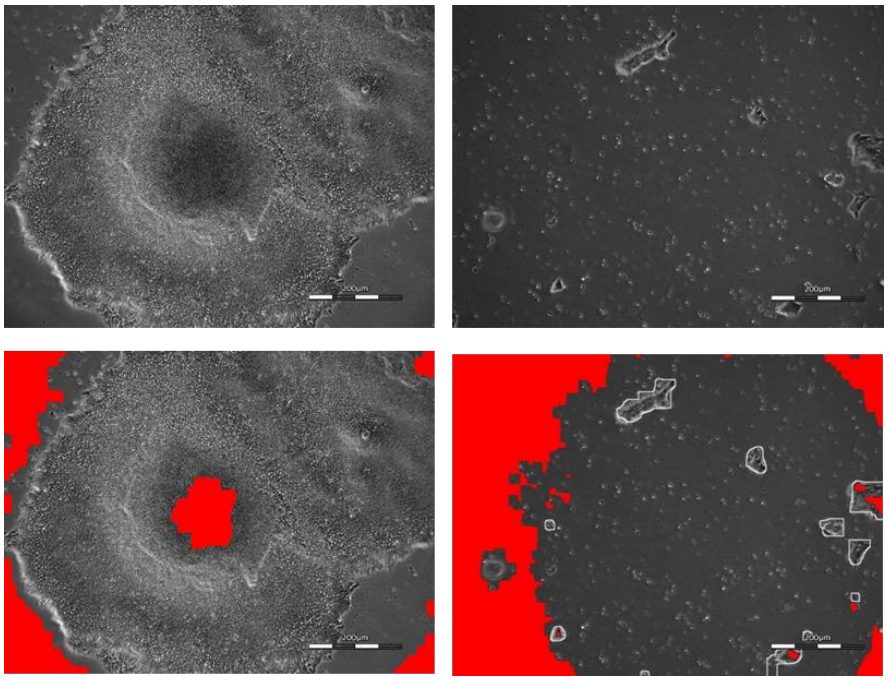

Figure 35. Threshold Method identifying edges and dark background Due to the variation across an image as the illumination of the centre of an image is brighter than the edges means that increasing the threshold value to identify dark areas of colony also includes the dark edges. This method therefore wrongly identifies the dark colony.

The threshold method built to isolate dark regions within a colony also distinguishes dark areas of background. The edges of the images are darker due to the circular illumination of light as it passes through filters to create a cone of light. This basic principle within light microscopy often means that the outer edges of an image are darker, often unobservable to the eye, but the more powerful resolution of image analysis detects this change in pixel intensity. This therefore creates a high level of noise in the output, where the edges are deemed part of the dark colony. The Threshold Method analysis therefore is not useful for identifying dark areas due to the lack of precision in identifying only the dark areas, another method must be developed.

3.4.2.2 Area Finder Method

Area finder uses both threshold and pattern recognition to identify areas. By 'teaching' the software a pixel pattern the software then has the ability to detect further areas of similar pixel patterning in future images. Rather than shades of grey that is seen on the screen, pixel recognition uses numbers. Each pixel is given a value representative of its colour as shown below in Figure 36.

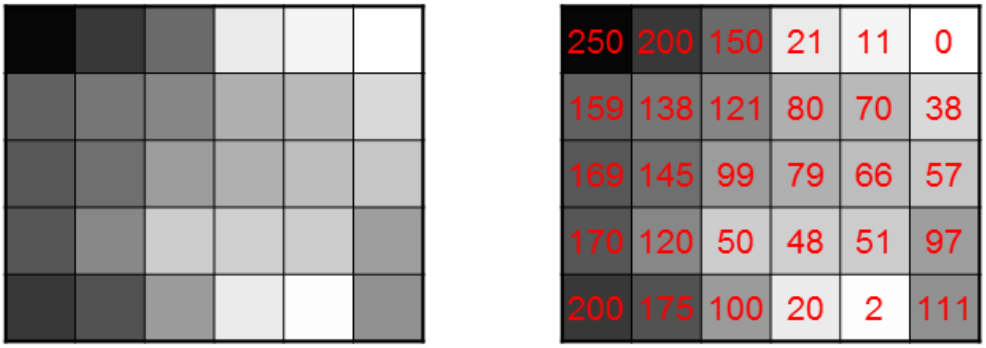

Figure 36. Area finder method utilises pixel patterning. Instead of using shades of grey the analyser uses the raw data of numbers, each which are represented by a shade of grey as a phase contrast image. After teaching a pattern of pixels to the software this can then be used to search for similar patterns.

By teaching the software groups of similar pixels a library of images is created which the Area Finder tool then compares to batch images in order to identify similar areas. This technique is shown in Figure 37 where a 3x3 grid of pixels has been taught, therefore allowing identification of

this pattern elsewhere in the grid. The output then is to highlight this area red. This can been seen on a phase contrast image of a colony in Figure 38 where dark areas have been taught previously and then recognised in this image.

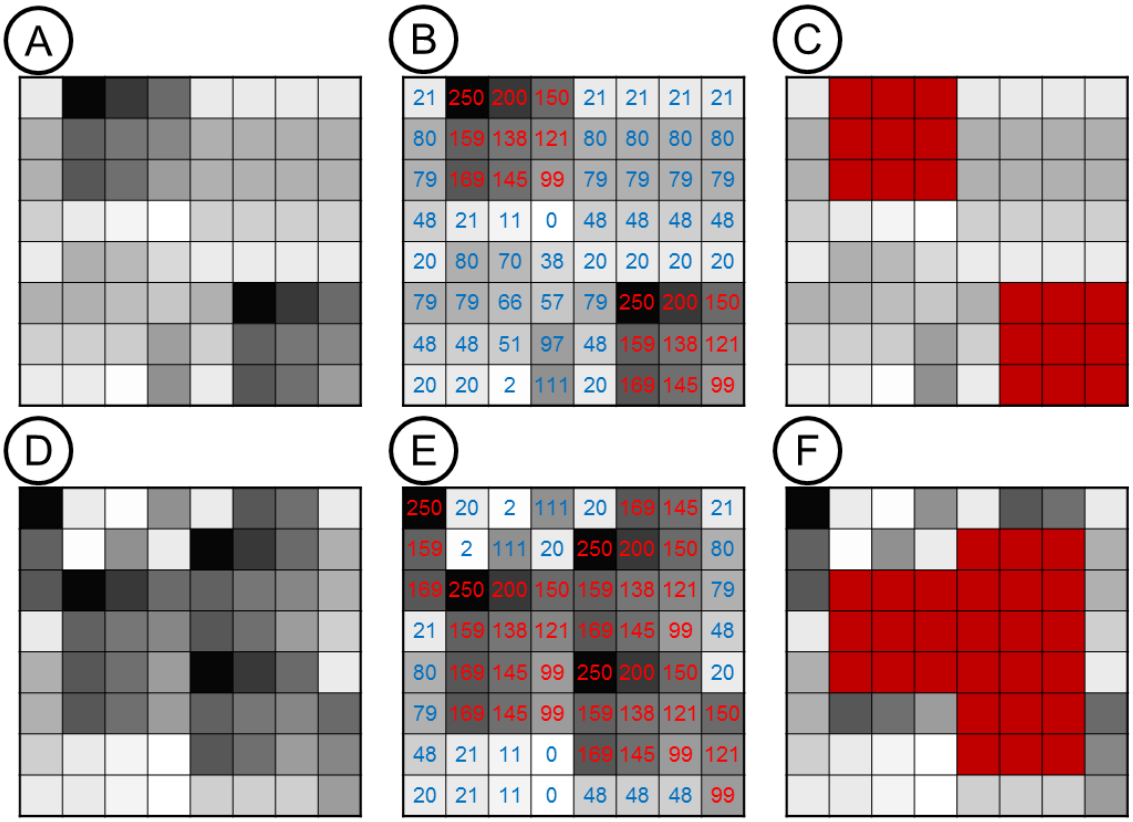

Figure 37. Using Area Finder's pixel pattern recognition to highlight common areas. By assessing groups of pixels the software can be 'taught' similar area shown with red numbers in B) and therefore identify these area and colour them separately C). This protocol can then be applied to future images such as D) where the same pattern of pixels can be identified E) and coloured in the analysed image F).

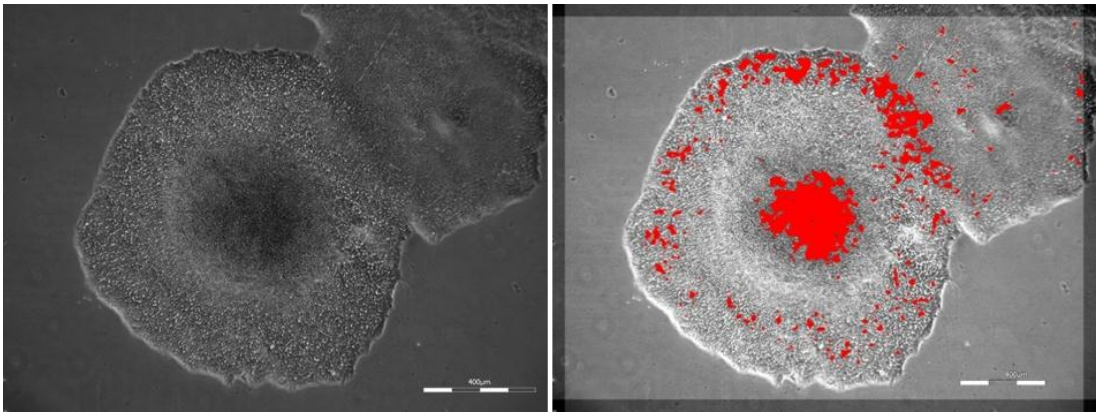

Figure 38. Acquired image and analysed image with area finder method. Comparison of the stock image and the analysed image using the Area finder tool identifying the dark regions of a colony

within a single image, the dark area is coloured red. This method better assess the dark area in the centre of the colony without measuring the edge factor as previously described due to the illumination.

The area finder successfully detects the pixel pattern of dark colony in the centre core of a colony compared to background and remainder of the colony (Figure 38). Further 'teaching' and refinement of this method would enable the darker areas around the periphery core not to be detected. Visual evaluation of both methods concludes that Area Finder provides a more accurate assessment of dark colony coverage than the Threshold Method.

3.4.2.3 Evaluating the Accuracy of Area Finder

It is important to assess the accuracy of Area Finder as a method of image analysis. Previously work was carried out to assess the threshold method for accuracy, see Section 3.3.2. Area Finder utilises known images of cell morphology to 'teach' patterns of recognition in order to evaluate 'new' images for each of these metrics. In order to use this method, image libraries must be made with independent pixel patterns and thresholds. This is created as the depiction shown in Figure 39. By selecting representative areas of dark colony as identified previously, and areas of background, a library of each pattern is built.

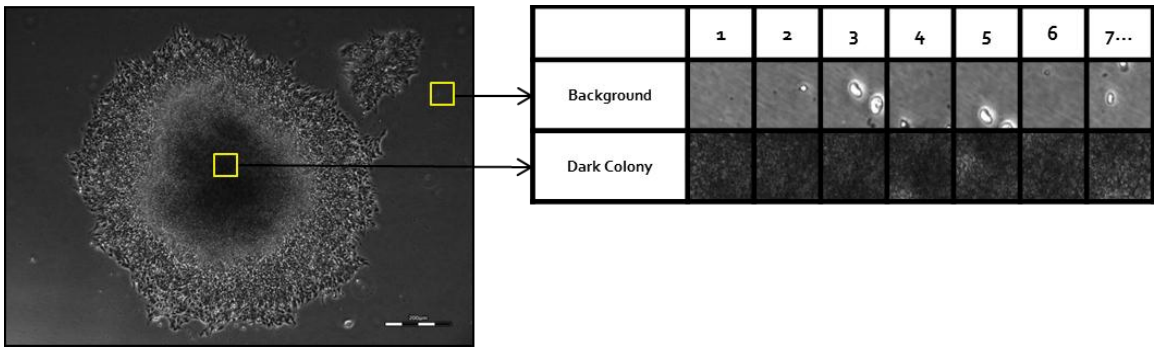

Figure 39. Sample of 2 libraries identifying dark colony and background. Depiction of creating an image library which can then be used with Machine Vision technology to further identify similar regions to those identified in the image library. Shown here are examples from background and dark colony coverage.

After creating the library of images the analysis can be run on multiple images to assess the images for similar areas. If the library has been built with a wide range of pixel patterns and threshold values then the accuracy is reduced. Therefore it is imperative for an accurate analysis to ensure the library

is formed of representative images showing the pattern and threshold to which is being identified. The library must be of sufficient quality to accurately identify regions; however this quality is not a metric that can be measured.

Taking the example of dark areas, it is hard to determine accuracy due to the spectrum of levels and the non-discrete data set. Instead the Area Finder tool was used to identify single cells, which in turn could be user identified and consequently the accuracy measured. This was completed using osteoblast cells that were identified as adhered cells, proliferating cells that have come off the surface, or background. These 3 libraries are shown in Figure 40.

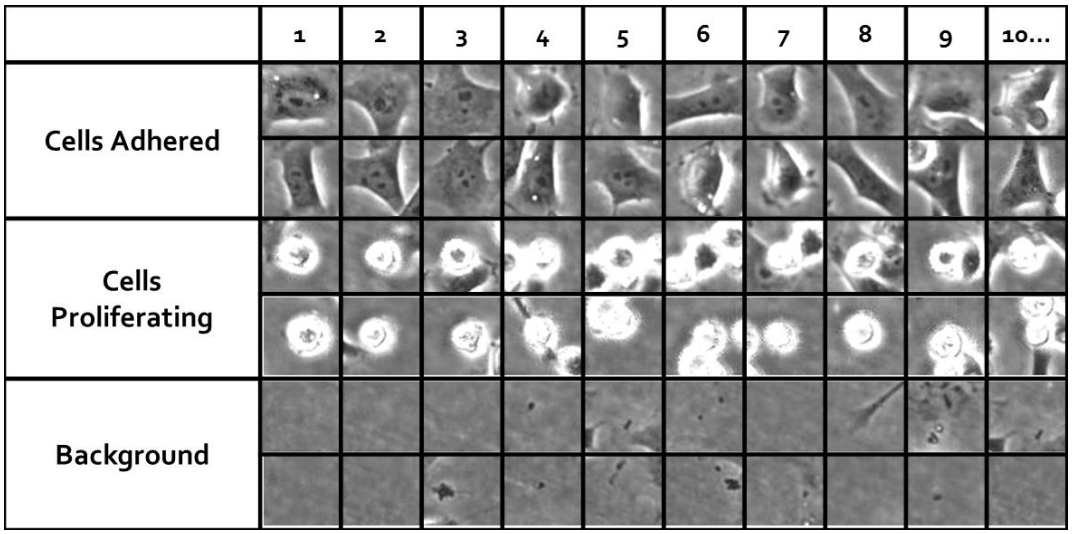

Figure 40. Snapshot of 3 libraries representing 3 morphologies from Osteoblast culture. A selection of images that make up the libraries used to identify osteoblast populations, taking the adhered cells, proliferating cells and background.

Using these libraries it is possible to analyse further images, and then user define the accuracy of this binary classification test. It is hypothesised that a larger library size of representative images will improve the overall accuracy of identifying these 3 populations. Accuracy is defined by two measures; sensitivity and specificity. Sensitivity relates to the tests ability to identify correctly, and is defined as:

$$Sensitivity = \frac{number\ of\ true\ positives}{number\ of\ true\ positives + number\ of\ false\ negatives}$$

In other words the number of correctly labelled red dots, over the same number plus wrongly identified red dots in Figure 41.

Specificity relates to the tests ability to exclude a condition correctly. It can be defined as:

$$Specificity = \frac{number\ of\ true\ negatives}{number\ of\ true\ negatives + number\ of\ false\ positives}$$

In other words the number of correctly labelled green and blue dots, over the same number plus wrongly identified green and blue dots in Figure 41.

The sensitivity and specificity of the libraries can consequently be determined by user verification, an example is shown in Figure 41 using library sizes of 100 and 1000 images where the purple circles determined increase in sensitivity, and the orange circles identify an increase in specificity with increased library size.

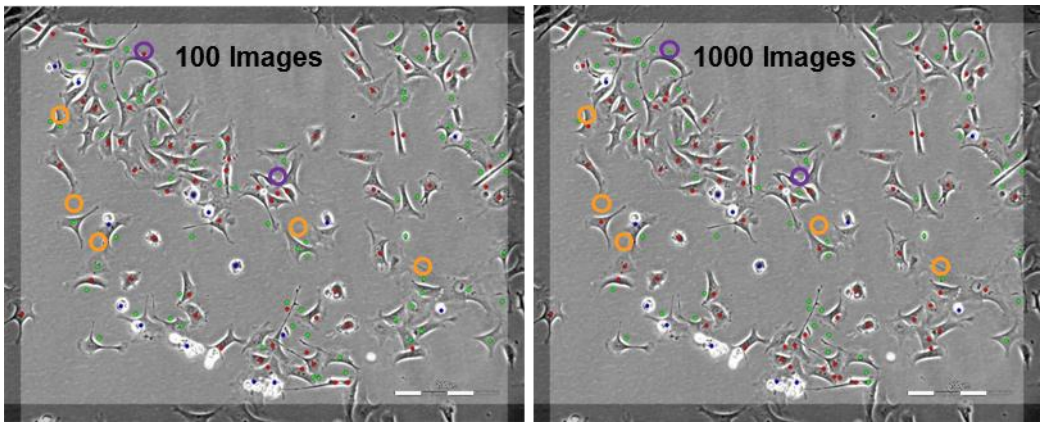

Figure 41. Analysed images using 100 and 1000 library size. Machine vision accuracy is determined by the library size. Osteoblast cells are identified here using a library size of 100 or 1000 images. The red dots represent where the software has measured a cell, the green dots represent background and the blue dots show a cell proliferating. The purple circled dots show where the 100 image library is less sensitive than the 1000 image library, the orange circled areas show where the 100 image library is specific than the 1000 image library.

Figure 41 highlights the improved sensitivity achieved by using a larger library size. The errors are detected by visually assessing a number of images, and marked with purple and orange circles to show where using a library of 100 is less sensitive and specific respectively. This highlights the sensitivity of Area Finder to measure the proportion of actual positives. Specificity of the analysis is based on the percentage of negatives which are correctly identified, for this example the green and

blue dots. The algorithm initially identifies pixel areas based on threshold and following this assigns each detected area to one of the three possible categories from the libraries. Therefore in each of the images shown in Figure 41 the number of dots are equal, the difference is to which category they are assigned. By analysing both of these accuracy metrics it is possible to determine the required image library size.

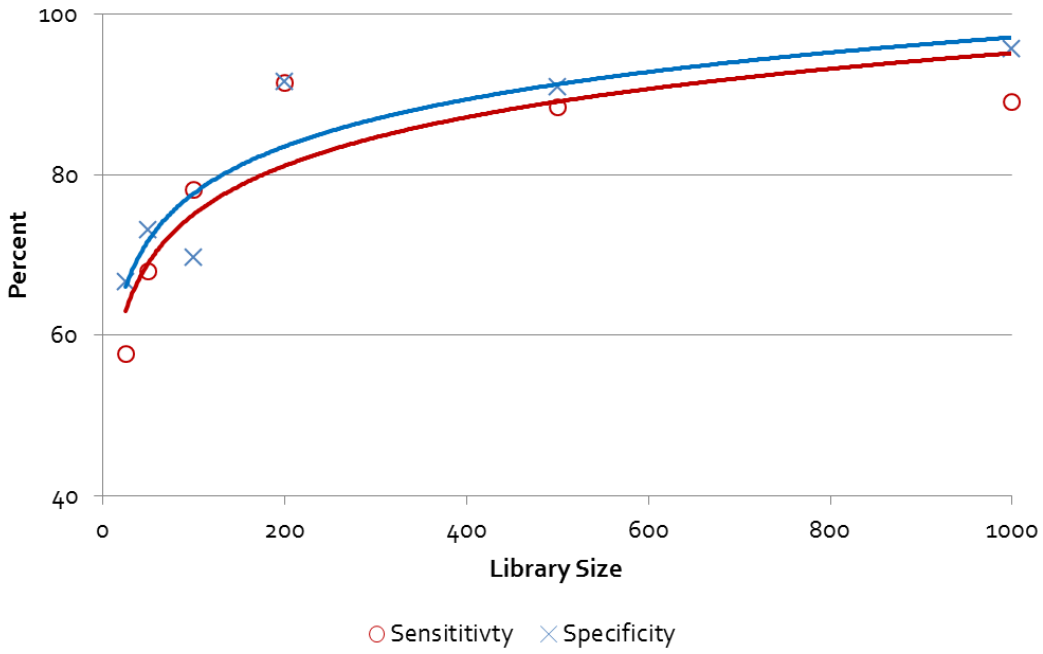

Figure 42. Graph of sensitivity and specificity for various library sizes. The sensitivity, shown by red circles is increased from less than 60% to 90% by increasing the library size from 25 to 1000 images. A similar result is seen with specificity shown with blue crosses.

As hypothesised, increasing the image library increases the overall accuracy in terms of both sensitivity and specificity. Figure 42 allows the smallest library size to be chosen above which the accuracy returns for increased library size are trivial, this is with 200 images.

Another important aspect of this analysis is the computational time to evaluate the images. For real time analysis it is important to determine an outcome as quickly as possible allowing timely process decisions. Using a stop watch the analysis time was measured for library sizes of 25 up to 1000 images. It was found that all the library sizes produced the same analysis time (data not shown). This is due to how the algorithm is built, by taking the entire library and creating a rule with which

to work. Therefore it is the algorithm building that is time dependent on library size rather than the analysis itself. As the algorithm only needs to be built once then utilised, the library size has no effect on time for analysis. Therefore within a manufacturing setting a very large library size could be utilised to maximise accuracy with little disadvantage.

Using the different library sizes it is then possible to plot a growth curve of cells measured by image analysis. Figure 43 shows the accuracy of using various library image sizes over a time period for cell growth. The growth curve demonstrates the software's ability to identify cell numbers, where 1000 images is the most accurate, as determined from Figure 42, shown in orange and 100 images the least accurate shown in blue.

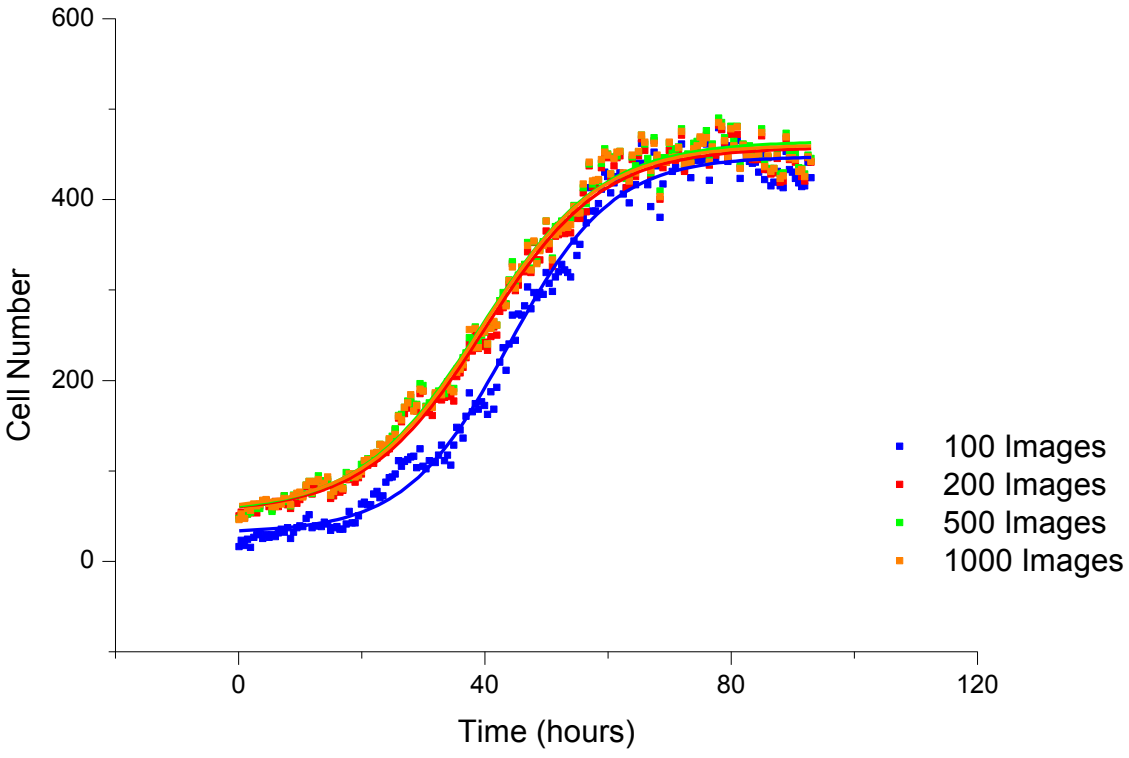

Figure 43. Comparison of using a larger library size to increase accuracy Growth curve of cells using machine vision technology to identify cells with varying 'taught' image library sizes ranging from 100 images in the library to 1000. This shows that a library size greater than 200 images provides very little improvement in detection of cell type.

Figure 43 confirms plateauing of accuracy seen in Figure 42 as once 200 images are used there is very little difference in identified cells. Interestingly this accuracy difference between library sizes is less noticeable at a high cell number. On reflection of the captured images this is due to the

complete monolayer and resulting lack of resolution in the identification of individual cells. Therefore evident from this data set is that the accuracy is reduced due to the overcrowding of cells. It is important to note that this is not seen when dealing with colonies due to the larger area they occupy, so the resolution between pixels can be reduced.

3.4.3 Edge cells

From the images of embryonic colony development there are 3 distinct cell morphologies present. So far total colony coverage along with dark colony coverage have been identified which describe different cell states. This third morphological population of cells, edge cells, appear at the edge of specific colonies and individual cells are larger than those found within colony cores allowing individual cell identification. In order to assume a linear relationship it was stated that '*size of cells must be a constant,*' this is therefore contrary to this statement. These edge cells are more frequently seen during poor quality cultures and are often referred to as differentiating cells (116). In many methods these edge cells are removed by aspirating away the so-called differentiated cells prior to passaging (78). Within differentiation protocols this periphery banding has been noted, specifically Das et al see that an 'area of morphologically differentiated cells, characterized by a cobblestone appearance, becomes visible at the periphery of the colony and progresses inward' (117). However further papers quantify them as pluripotent due to their transcription factor expression (118). These morphologically different cells are seen in Figure 44 around the periphery of colonies.

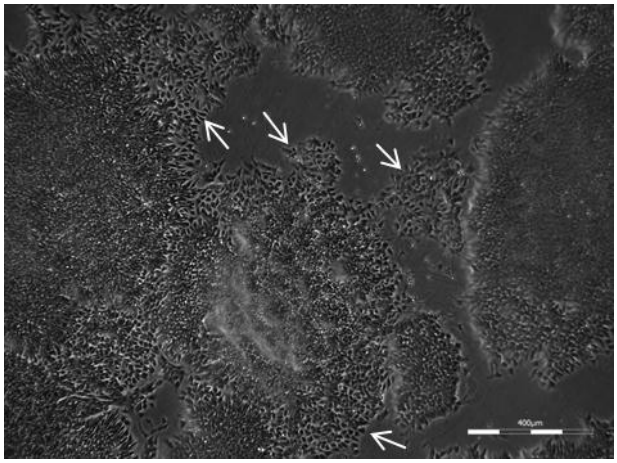

Figure 44. Embryonic colony surrounded by edge cells. This raw image shows tightly packed colonies with single cells surrounding the colonies, identified by white arrows; these cells are hereafter called 'edge cells.' These edge cells have a different number to surface area ratio compared to the tightly packed colonies. Therefore these cells could cause the cell count to coverage correlation to be poorly represented if lots of these edge cells are present.

The centre of colonies show tightly packed cells, where it is not possible to distinguish one cell from another. Around the periphery of the colony lie individual cells which can be singularly identified. These cells clearly have a different number to area ratio when compared to the colonies. Therefore this could affect the coverage to count approximation either way dependent on whether there were many or few of these edge cells.

These edge cells vary in contrast and cannot be successfully detected using the threshold method. As they have a very different morphology from the cells within the colony, Area Finder provides the best analysis to identify these. The same method as described previously in Section 3.4.2.2, with a new library being created for these edge cells. An example of a raw image and analysed image is shown in Figure 45.

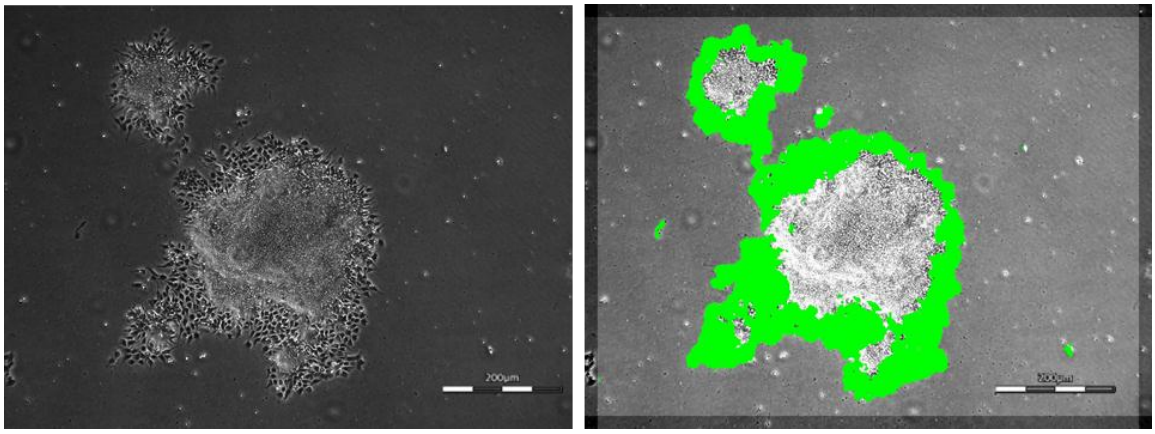

Figure 45. Raw image and Area Finder analysed image. This image shows the identification of edge cells as highlighted in green on the right image. This population represents a different count to surface area ratio, and therefore by assessing and quantifying edge cells an improved correlation of coverage to cell count might be made. The identification also has an impact on cell quality as these edge cells represent a differentiating population. Therefore it is possible to put a numerical value on pluripotent status non-invasively.

Area Finder provides an accurate image analysis technique to identify these edge cells and quantify their coverage. As previously mentioned these cells may have an impact on both embryonic culture qualities, as they are reported to refer to early differentiating cells (78,116,117), as well as correlation to cell counts as they have an increased area to number ratio.

3.4.4 Core Periphery Coverage

Successful identification of the edge cells and dark colony allows the core periphery coverage to be calculated as the remaining area of total colony coverage. This also refers to the pluripotent region of a colony, and therefore by comparing the values of 'Core Periphery' to 'Edge' and 'Dark' a measure of pluripotency can be resolved. Prior to this analysis the new metrics are first correlated to cell counts to see if there is any improvement by using the 3 newly developed metrics.

3.4.5 Correlating All Metrics to Counts

Having assessed colonies for 3 metrics independently it is possible to combine the analysis into one single protocol. An example of all three metrics being measured at once in the same image is shown in Figure 46.

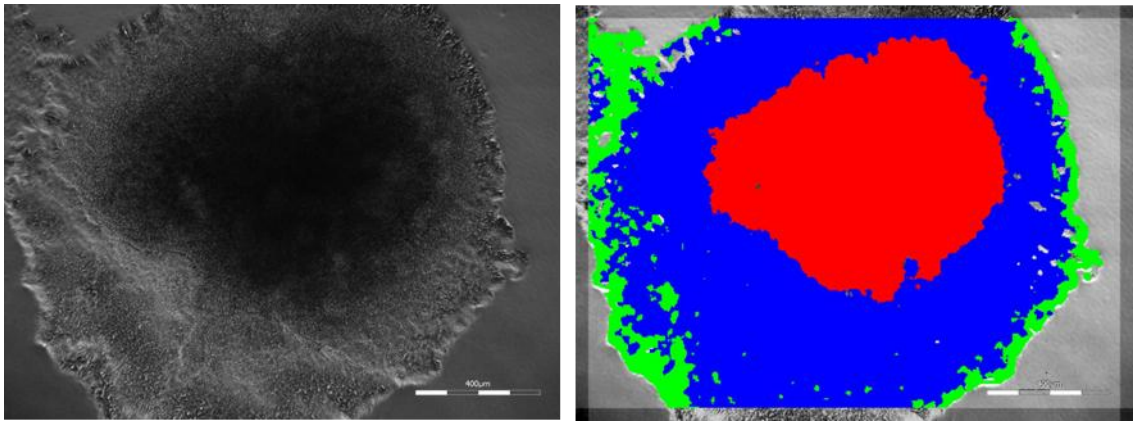

Figure 46. Raw image and Area Finder analysed image. This image shows the identification of 3 populations of colony of dark colony (red), edge cell (green), remained of colony (blue). These three populations all represent different count to surface area ratios, and therefore by assessing all three together an improved correlation of coverage to cell count might be made.

Area Finder provides a good measurement of these three areas, and it is hypothesised that these 3 metrics all represent areas of a colony that have a different cell/area value. Therefore by completing regression on all three metrics to cell counts an improved correlation is expected. This is completed in the following sections.

3.4.5.1 Statistical Resolution

As previously mentioned, r-squared is an indicator of how well the data fits the model, however R-Squared adjusted provides a better predictor as it is adjusted to account for the small number of data sets that are available. Here the data is taken from a sample of 30 flasks, with 400 images taken within each flask. Although it is calculated the same way as r-squared it is then adjusted using the degrees of freedom accounting for small sample sets. R-squared predicted is also calculated. This predicts the response for new observations, therefore providing a numerical output for how well new observations will fit rather than how well the current data fits, shown by r-squared. The final recorded statistical measure is S, standard error of the regression. As previously mentioned S is expressed in the units of the regression, providing a useful measurement of error for comparison.

Table 14 summarises the correlation fit through statistical fit analysis values for each of the three metrics individually and then also a combination to identify any potential improvement. The total

colony coverage is a summation of the three metrics and therefore cannot be used in conjunction with any of the other metrics. For completeness it is included in the table below to show the correlation previously acquired.

Table 14. Statistical measures of variance for metrics. The metrics can be used singularly or in combination to determine the most informative metrics that relate to count. As expected by individually assessing the metrics there is a poor correlation. By using metrics as doublets the correlation can be improved, but by using all three metrics (Core Periphery, Dark and Edge cell coverage) the best correlation can be made shown with the largest R^2 value and smallest standard error of the regression (S).

Method	R-Squared	R-Squared (Adjusted)	R-Squared (Predicted)	Standard error of the regression (S)
Total Colony Coverage	47.4	45.5	32.3	204589
Dark Colony Coverage	44.2	42.3	38.4	210571
Edge Cell Coverage	6.0	2.8	-1.0	273355
Core Periphery Coverage	35.5	33.2	22.9	226516
Core Periphery and Dark Colony Coverage	74.7	72.8	67.7	144484
Core Periphery and Edge Cell Coverage	48.7	45.0	38.7	205537
Core Periphery, Dark and Edge Cell Coverage	75.8	73.1	67.6	143693

Table 14 shows that the best correlation can be made between cell coverage and cell counts by combining the three metrics compared to using only a single or double metric, showed by the lowest S value 143693. This was hypothesised as these three metrics all represent different cells/area and therefore all contribute separately to the overall cell count. By measuring the core periphery, dark and edge cell coverage and correlating all three metrics back to the cell count then an R-squared value of 75.8% can be achieved. This regression calculates the following relationship of all three metrics to counts:

$$Count/cm^2 = 227404 + 9456\ Core\ Periphery + 10403\ Dark - 3137\ Edge$$

In order to use a linear model it is assumed that there are three stages of cell density that occur within the image. The dark areas represent the most dense area, the edge the least dense and core periphery in-between. Therefore the regressions of all three metrics are hypothesised to follow this concept, so that the dark colonies have the largest influence on cell count with the edge cells having the least. This is shown by the constant in front of each metric in the above equation being larger for the more dense area. It is also worth noting that the dark/ core periphery coverage combination is nearly as good as all three metrics. This is not surprising as the edge cells have relatively low cell number per area and therefore have little effect on the total cell count in the pluripotent conditions utilised here. However in cultures with more edge cells this value would start to make more of an impact. As discussed however edge cell coverage may provide a measurement of cell quality, so although less useful in this example of correlating to cell count, it may be a powerful metric. This is discussed later in the Chapter.

The equation generated from the triple regression can be used to show the calculated values using least squares regression, and is shown in Figure 47.

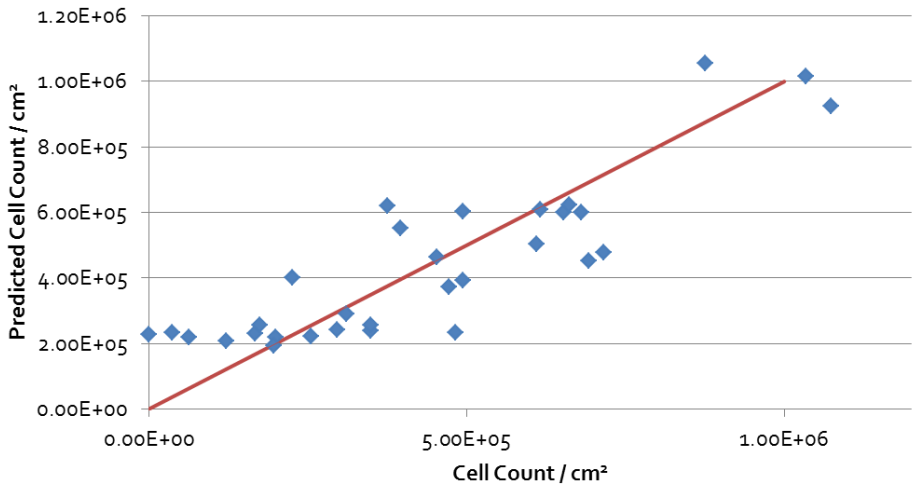

Figure 47. Linear regression of 3 metrics against cell counts By performing a triple regression over the 3 metrics (total, dark and edge cell coverage) these values are then plotted against the measured cell counts from Cedex. The plotted red lines shows where predicted is equal to the actual cell counts. This shows the over estimation of the model at low cell numbers. (n=30)

Figure 47 shows that at low cell numbers the model over predicts the cell count, however generally the model provides a good fit to the actual cell counts. This model has been fit assuming a linear relationship of count to coverage. By identifying each metric within the regression it is possible to highlight if this is a fair assumption.

The edge cells are defined and each cell can easily be identified. There is little variation in the size of these cells during a culture period. Therefore there is a rationale for a direct linear relationship between cell counts and coverage of edge cells. This relationship is also true for the core periphery assuming that there is no change in density. The final metric of dark colony is used to account for this change in darkness and presumed density. As the colonies increase in size a dark centre appears, likely to represent a change in cell state. The change in threshold of this area implies an area of higher density then the surrounding colony. As this surface area of darkness increases then so too will the cell number within the area. This would only be true and linear if there was only one level of darkness. In reality the darkness threshold level is variable that is to say within the identified dark region there are varying amounts of darkness. However the image analysis is given only one contrast value, therefore once this level has been detected any further darkening will not be detected. This suggests that this image analysis method can become saturated. Further work could introduce a range of dark level thresholds, however this would only be justified if further control was required. The current method of assessment first needs to be explored for process control utility before investing in further coverage classification.

A further verification of the linear relationship utilised can be made by assessing the residuals of the regression to depict the error between observed and regression model values. This is shown in Figure 48 along with a normal probability plot, and histogram of residuals.

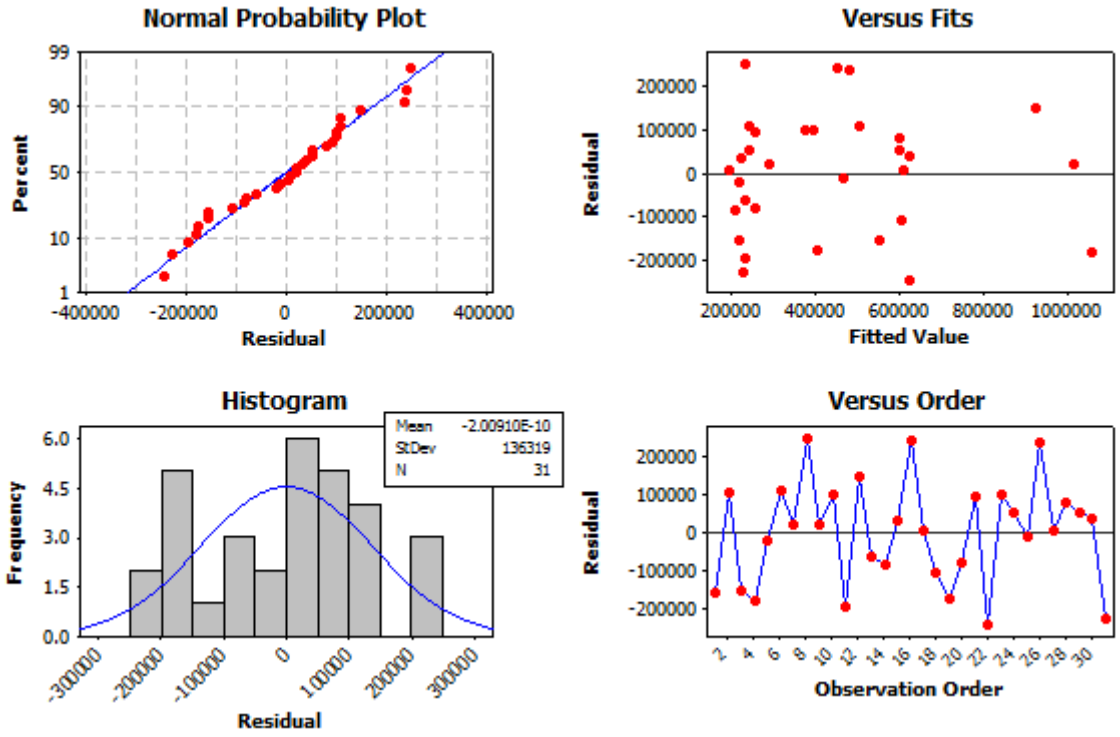

Figure 48. Residual plots of triple regression. Taking the residuals from the triple regression allows a check for normality, linearity and bias. The Normal Probability Plot shows that all the residuals fir along the line of best fit suggesting normal statistics are valid. This is further demonstrated in the Histogram with a typically normal bell shaped curve. The Versus Fits graph provides a measure of linearity. The spread in residuals is fairly similar as the fitted values increase suggesting that the data is linear, although more data points at the high end would be needed to strengthen this statement. (n=30)

The normal probability plot shows that the model error is normally distributed. The histogram plot allows the confidence interval to be determined. Using the mean and standard deviation as shown in Figure 48 (mean = -2.00E-10 and standard deviation = 136319), it is possible to state that 95% of the time the data will deviate less than 150 thousand cells from the true value. This also agrees with the S value recorded of 143693 from Table 14 previously.

The 'Versus Fits' graph shows that the absolute error size is independent of the cell count value. At low cell density the percentage error is larger than at high cell counts. Therefore the error is dependent on when the imaging will be used as a decision tool. For high cell densities such as passaging the percentage error will be small as the coverage will be high. By assessing the Versus Order it is possible to see that there is no bias in the order of the data.

3.4.5.2 Correlating 3 Metrics of Coverage against Count

Having shown improved statistical resolution it is possible to see if using 3 image derived metrics can improve the correlation to cell counting seen in Section 3.3.3. In Figure 49 the initial correlation with one image derived metric is shown along with the new model utilising 3 metrics.

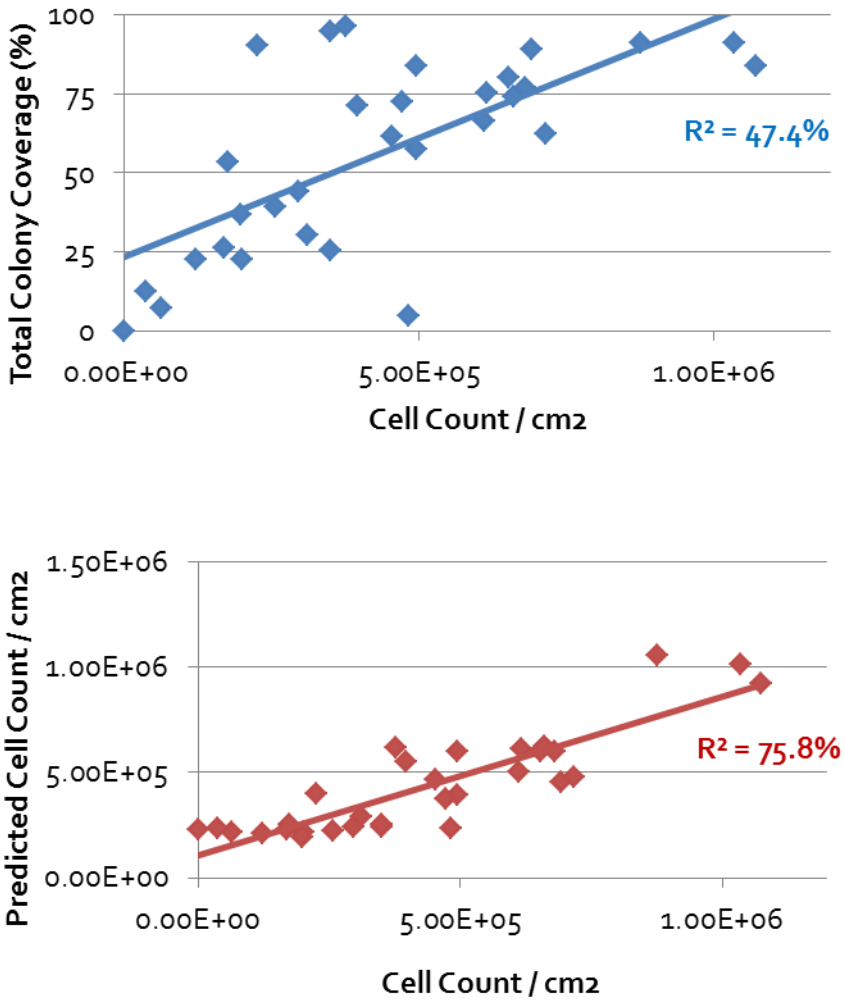

Figure 49. Comparison of single to triple image derived metric correlation to count. This figure highlights the improvement made by using 3 metrics of core periphery, dark and edge cell coverage against the single metric of total colony coverage. (n=30)

This data has shown the ability to improve the correlation by using more metrics to predict the cell count. This now allows image analysis to be used within a process to assess the number of cells to ±150,000, 95% of the time. However of note is that the dark and edge cell coverage that can now accurately be assessed maybe direct measures of culture quality. These metrics are hypothesised to

measure the amount of differentiation within a culture and therefore provide a direct measure of quality. In order to assess this colony phenotype must be measured, this is completed with immunostaining.

3.5 Embryonic Colony Culture State with Regard to Quality

The ability to identify further image derived metrics has improved the correlation of coverage to cell counts. However as noted previously in Section 3.4, the ability to precisely measure these new attributes could also provide a measure of culture quality. The first stage is to understand the correlation of the recorded metrics to cell quality. Numerous techniques, as discussed in Section 3.1.1, can be used to assess the quality of embryonic cultures. One of the most prominent and widely used techniques is the evaluation with regard to cell markers, specifically Oct-3/4 and Sox-2. This can be achieved by flow cytometry; however this only provides a population assessment. It is therefore advantageous to be able to identify these markers within individual colonies, which can then be correlated back to captured phase contrast images. This is achieved with immunocytochemistry, this allows the colony to be continually assessed through phase contrast imaging before end point marker identification through fluorescence microscopy. An example is shown in Figure 50 with pluripotent colonies imaged over time before analysed for Oct-3/4 expression.

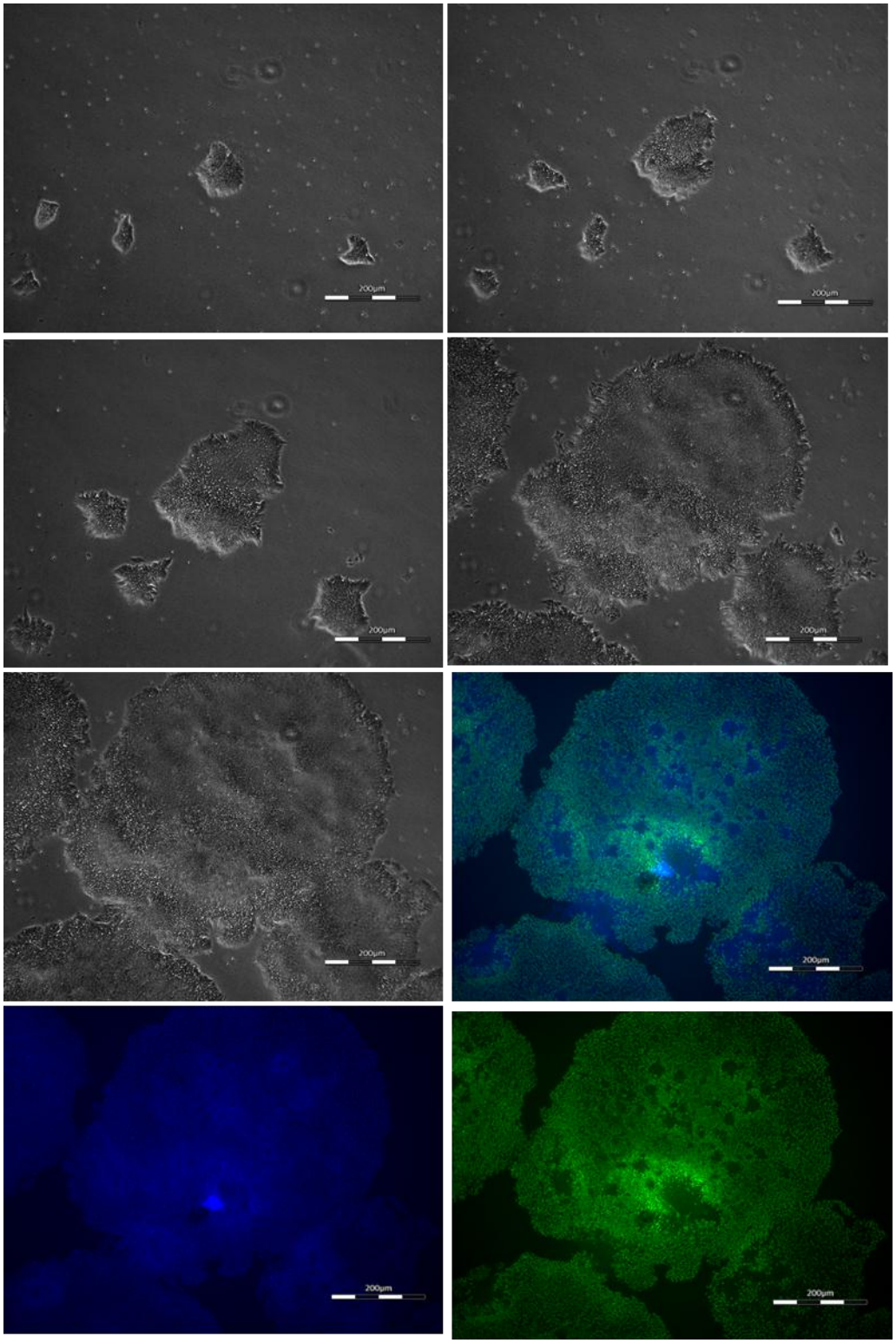

Figure 50. Pluripotent colony phase images with immunocytochemistry markers. Phase images are taken on Cell-IQ during culture and then imaging the same area after staining using the fluorescence on the Cell-IQ showing pluripotent marker Oct-3/4 as an end point analysis by immunocytochemistry. The blue shows Syto16, a nuclear staining for all cells.

Figure 50 shows that Oct-4 stains a colony maintained in pluripotent medium. It is worth noting the heterogeneity found across a colony as shown from the Oct-4 variation in expression. This is unsurprising as many articles claim a 'phenomenon of metastability within the pluripotent compartment' (96). That is to say ESCs fluctuate their expression of pluripotent markers as they transit between naive and a lineage primed states; with a certain plasticity (119), this is represented in Figure 51.

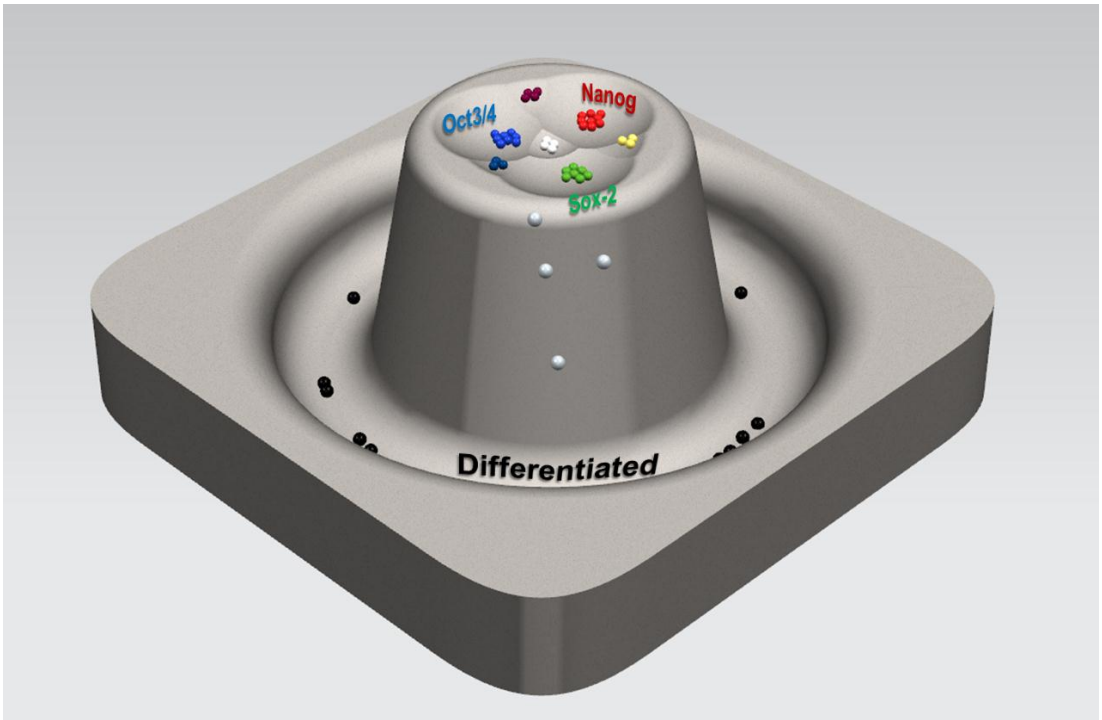

Figure 51. Pluripotent marker metastability. Diagram showing the transient states those cells can fall between, with each colour representing a different population with regard to marker expression. In the centre, white cells represent those positive for Nanog, Oct3/4 and Sox-2. We then have each marker of Nanog (red), Sox-2 (green) and Oct3/4 (blue) as solo markers, followed by their intermediates represented as yellow (mix of red and green, so Nanog and Sox2 positive), magenta (mix of red and blue, Nanog and Oct3/4 positive) and cyan (mix of green and blue, Sox-2 and Oct3/4 positive) Cells have the ability to move between these states, as they approach the edge (grey cells) they beginning differentiation, with black cells in the gutter as fully differentiated cells.

Within an embryonic colony there is a heterogeneous population with regard to pluripotent markers that have the ability to move between states of expression. However once the cells have moved from the 'top level' and begun to fall through differentiation there is no possibility to reverse into a pluripotent state without methods similar to those utilised in the production of induced pluripotent stem cells.

Once the embryonic colonies have begun to differentiate it is hypothesised that their morphology changes, seen with the production of edge cells and dark areas identified earlier in Section 3.4. This change in morphology can be precisely measured using image analysis it is therefore important to verify that this change in morphology relates to a change in culture state. Figure 52 shows some examples of where the loss of pluripotent markers is related to the change in morphology.

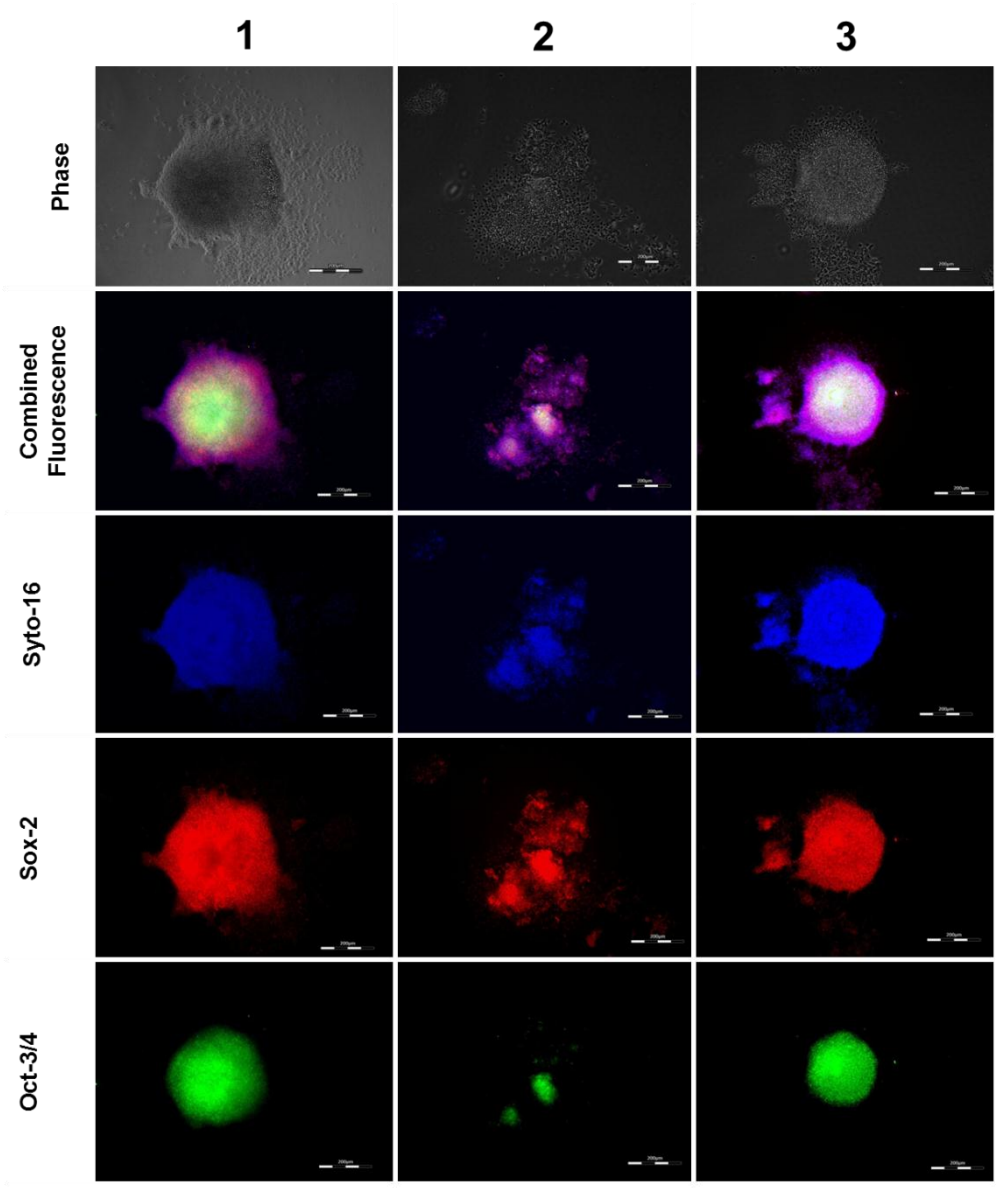

Figure 52. Examples of pluripotent H9 embryonic stem cell colonies. Phase images were captured using the Cell-IQ, then the same colonies were immune-stained and fluorescently imaged. Syto-16, Sox-2 and Oct-3/4 are shown both combined and individually. Syto-16 stains the nucleus of all cells and is used to identify the entire population. Sox-2 stains all cells, but Oct-3/4 is more specific to the colony core. This identifies that specific areas such as the centre of the colonies are phenotypically distinct for key markers and measuring these provides a relevant element of quality assessment.

Three examples of embryonic colonies maintained in pluripotent media are shown in Figure 52. The immunostaining identifies that there are discrete micro-environmental areas within the colonies expressing these key pluripotency related factors. All cells within the population stain positive for Sox-2. However, the Oct-3/4 staining identifies a colony core that is phenotypically discrete, being relatively high expressing compared to the edge cells of the colony. This separation in phenotype suggests a mechanistic rationale for sub-division of the colony by morphology and investigating the value of monitoring of the different areas for a process analytical technology. A further example of this immunostaining in conjunction with the raw phase contrast image and analysed image using Area Finder is shown in Figure 53.

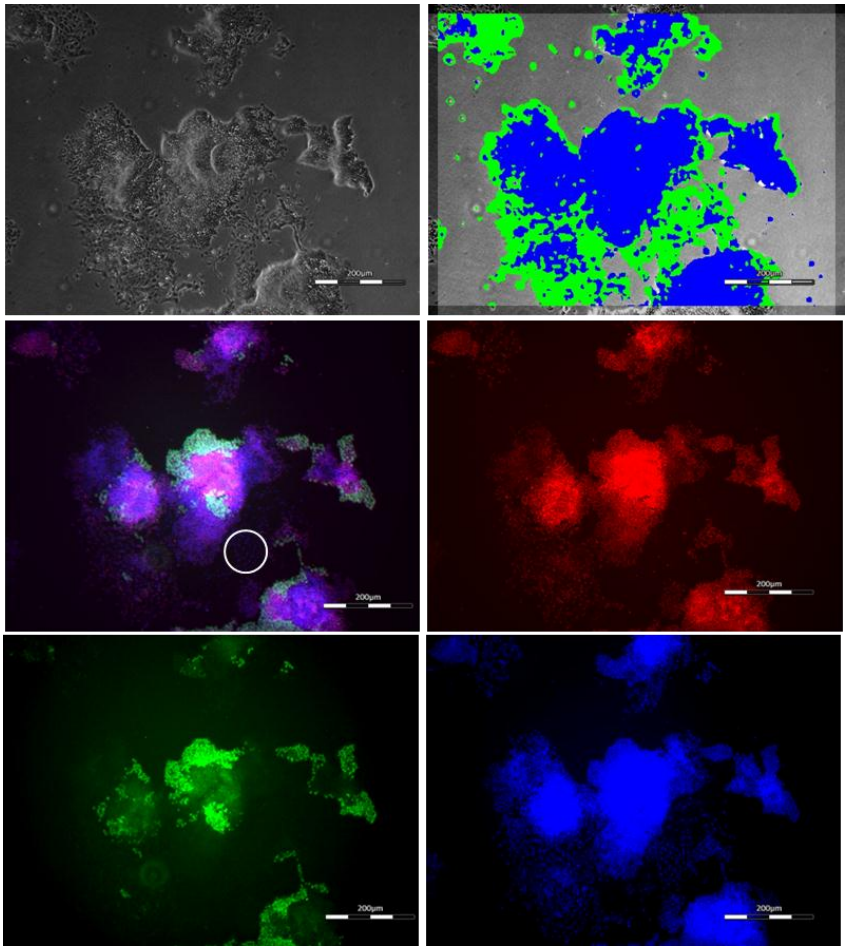

Figure 53. Immunocytochemistry staining of differentiating colony. Red Sox2, Green Oct4, Blue Syto16. This shows that the pluripotency markers are lost at different stages of differentiation. Oct-3/4 is lost first showing only the core of colonies still positive, whereas Sox-2 stains for more of the colony with only the far periphery negative. Syto-16 is used to stain the nuclei of all cells.

Figure 53 shows that it is possible to mark colonies at different stages of differentiation. Syto-16 is used to as a nuclear stain to highlight all cells. Sox-2 is positive for the majority of cells except those highlighted on the merged fluorescence image with a white circle. These have lost all pluripotent expression and therefore are deemed differentiated. The next level of pluripotency is shown through the expression of Oct4, a much smaller population then those positive for Sox-2. These images provide evidence that there is a hierarchal level of pluripotency markers with Oct4 expression lost first, followed by Sox-2 later into differentiation. This data shows that the change in morphology is related to the expression of colony pluripotency, which can be assessed using phase contrast image analysis.

By introducing a cocktail of growth factors (FGF, VEGF, Activin-A and BMP-4) differentiation can be forced. Further staining for the differentiation marker heart and neural-crest derivative expressed protein-1 (HAND1) shows that the colony periphery is positive for the early mesoderm marker (Figure 54).

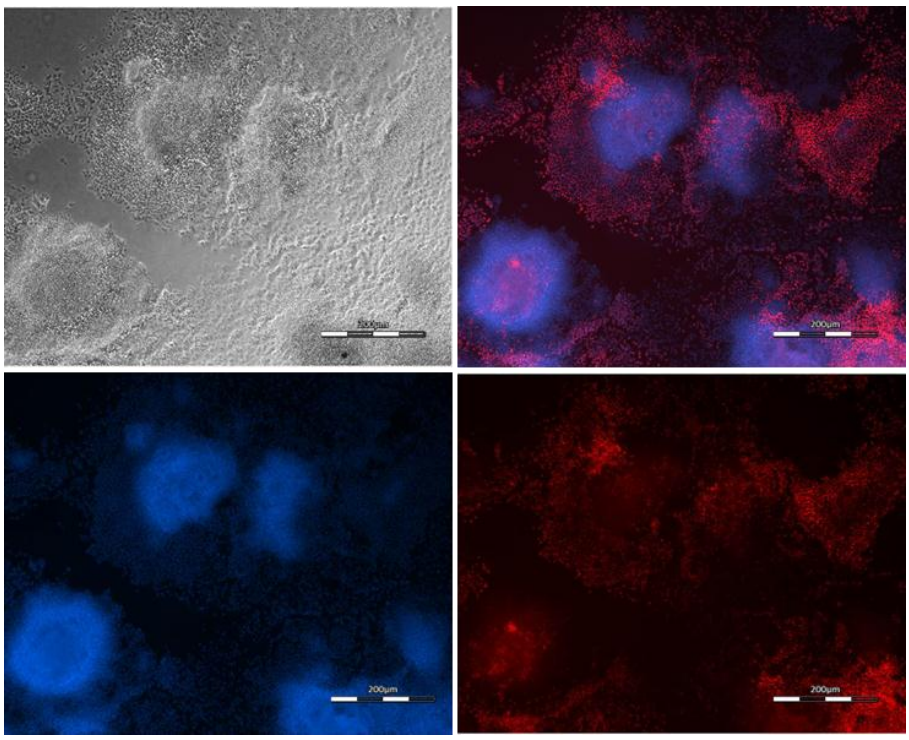

Figure 54. Immunocytochemistry for early mesoderm marker HAND1. Colonies exposed to mesoderm differentiation media for 48 hours then stained for HAND1 expression and subsequent DAPI staining for nuclei. This shows once again that the periphery of the colonies differentiate, leaving a core of pluripotency.

The expression of HAND1 in Figure 54 represents differentiated cells into the early mesoderm lineage from embryonic colonies. The edge cells from the colonies all express the differentiation marker with the centre of colonies being less positive for HAND1, suggesting a core of pluripotency remains as differentiation occurs from the periphery inwards, described previously by Das et al. (117).

The data presented here in Figure 54 provides evidence that the edge cell morphology represent a population that is undergoing differentiation from embryonic stem cell colony. This therefore allows edge cell coverage to be a powerful metric to quantify the pluripotent status of a population. It is also possible to follow the metrics behaviour over time, rather than the spot analysis shown here, which may provide further information regarding the culture quality, and even deliver a predictive assay.

3.6 Behaviour of Metrics over the Culture Process

The previous sections have assessed metrics based on spot analysis, one point in time. This provides useful information at a single time point but it is also possible to assess these attributes (total colony coverage, core periphery coverage, dark colony coverage and edge cell coverage) with respect to time. This allows the change in these attributes to be measured and therefore any variation over a culture a period is measurable. The advantage of doing this is to potentially identify rates of change of coverage type that may be either more sensitive or provide more information of culture quality than spot analysis. It therefore allows a prediction of culture state allowing a feed-forward approach to maintain a pre-determined culture state through process actions.

3.6.1 Total Colony Coverage

During culture in pluripotent media embryonic colonies grow, increasing the number of viable cells, thus increasing the coverage overtime. This follows a standard growth curve represented by a sigmoidal function as described by the mathematical Monod equation (120). Figure 55 shows a selection of colonies growth curves inferred from total colony coverage.

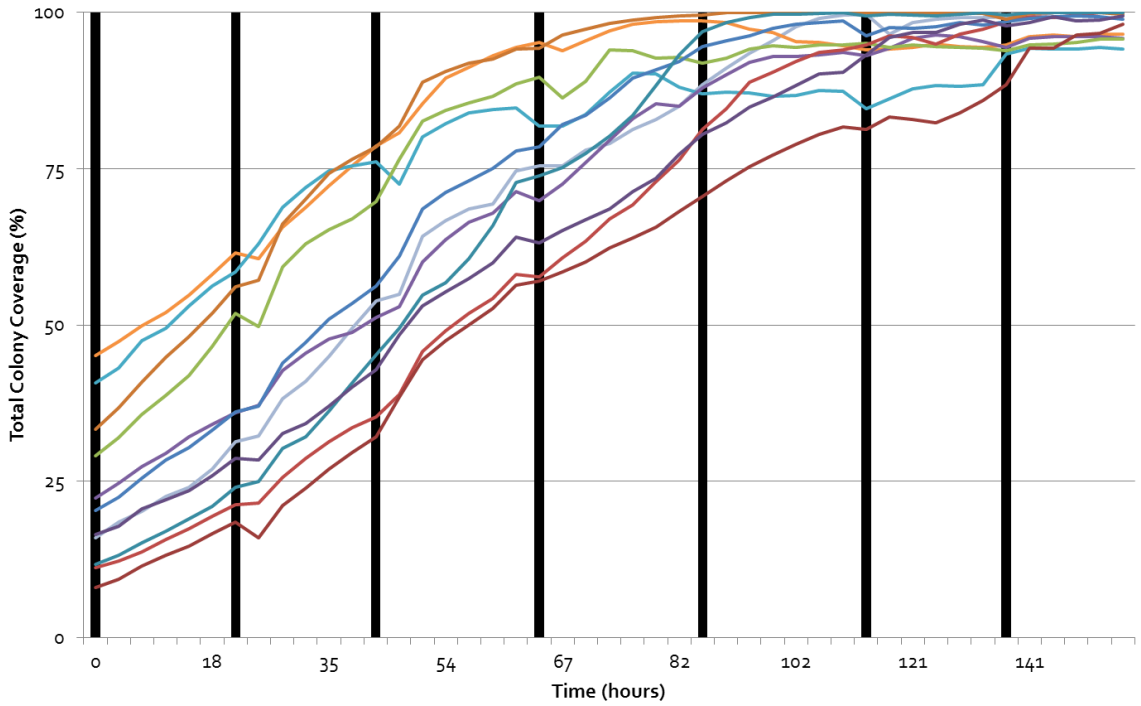

Figure 55. Total colony growth measured from colony coverage. Graph showing total colony coverage change over time with feed times (vertical black bars) for multiple colonies imaged in the same culture vessel. (n=11)

From this graph it is apparent that the colony coverage increases over time as expected. However as the colony grows there are cyclic growth drops where the colony coverage decreases. After these growth dips represented by a sudden gradient decrease, the following data points show a slow recovery back to the original growth gradient. The dips occur immediately after each media change represented by a black bar in Figure 55. This highlights the effect that a media change may have on these cells. However by completing a media change the nutrients are replenished, waste removed but also there are physical effects derived from removing the culture plate from the environmental chamber including change in temperature, pH and CO_2 concentration. These two effects either

nutritional, deemed chemical cues, or from environmental changes deemed physical cues both have the ability to cause the dips in growth seen. In order to assess the cause of the fluctuations, the process action of feeding on cell culture is discussed further in Section 3.7. These fluctuations can be further enhanced by plotting the change in total colony coverage over time, this is shown in Figure 56.

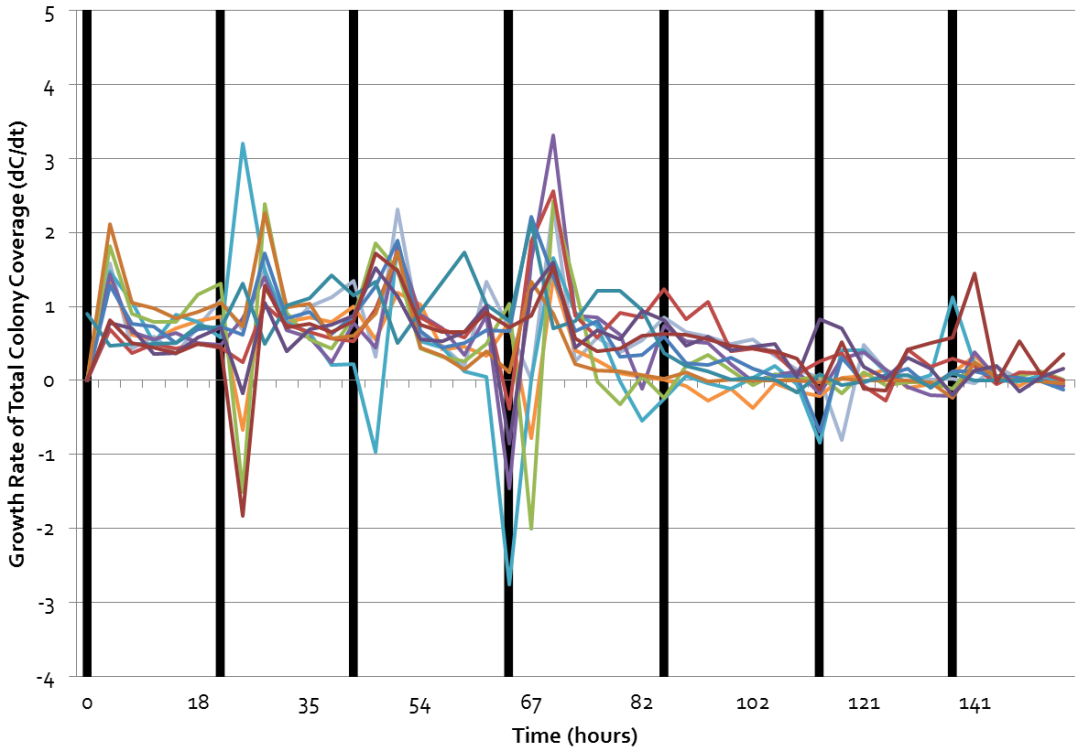

Figure 56. Gradients of total colony growth. The gradients from Figure 55 show the growth rate (dC/dT) between each image, against time. With spikes and dips throughout culture representing increased and decreased growth, although overall these balance out. Further understanding of these dips is required. (n=11)

By assessing the growth rates it is clear that immediately surrounding a feed there is a sudden dip of growth from the colonies as described previously. Figure 56 also highlights spikes in growth just after the initial dips suggesting that the colony shrinks immediately after feeding and then expands before settling back to the original size. These dips however seem to have very little effect on the overall growth curve, suggesting a contraction of colonies is then reversed as the colonies are exposed back to the incubators environment/protein concentrations. This effect is further discussed in section 3.7.

After ~80 hours the growth according to coverage plateaus, this however ties in with the colonies reaching 100% coverage and therefore the image analysis is unable to identify further growth without taking a larger image area. At these higher coverage values the peaks and troughs of growth are again not seen, an effect due to the boundaries of the colonies not being present within the image.

From user identification of the captured images it is interesting to highlight the colonies have a cyclic smooth to rough transition at the colony periphery. Either there is a tight boundary shown with a slight halo common for phase contrast images, or on the contrary there is a rough boundary with individual cell protrusions noticeable. The difference between these two states is shown in Figure 57.

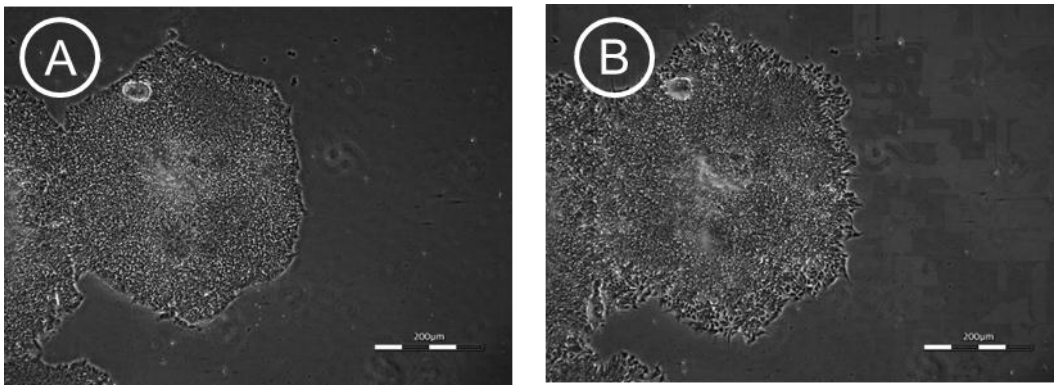

Figure 57. Smooth v Rough colony edge. A) Image of colony with the periphery as Smooth versus B) the colony hours later that now has a rough edge. The rough edge often is regarded as a differentiating colony, although live cell imaging has shown that colonies fluctuate between the two states. This therefore shows the importance of continual monitoring over single time point analysis, which could give false outcomes.

Similar to previous work assessing the growth rate declines in conjunction with feed points the rough and smooth can be user defined by individually assessing images. This is shown in Figure 58 with total colony growth shown measured by coverage, feed points and smooth and rough transitions.

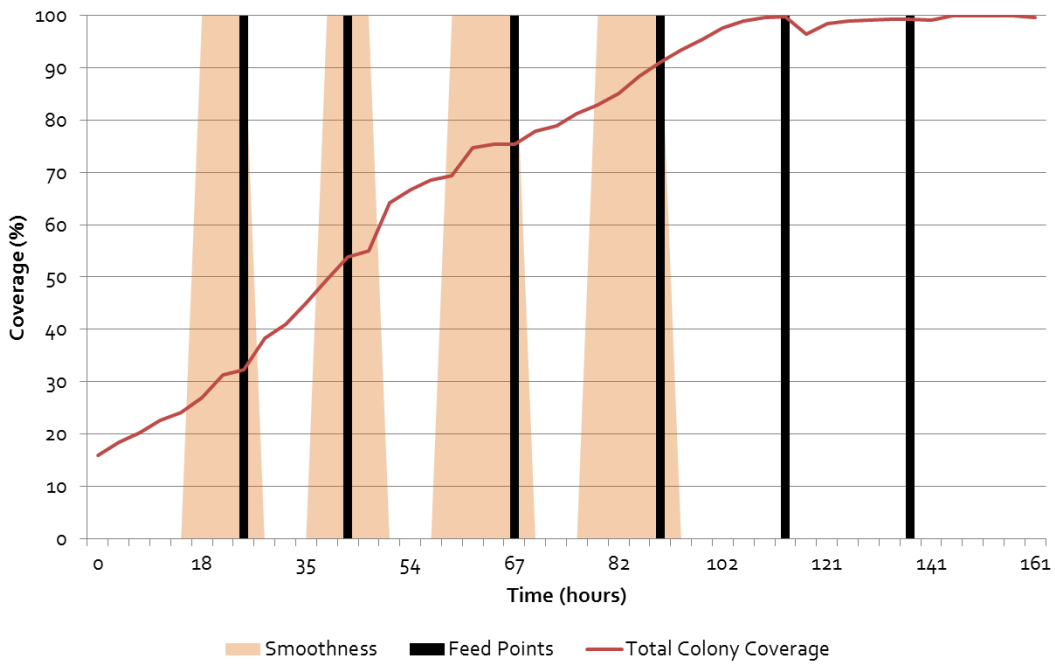

Figure 58. Example of colony growth with smooth/rough. Measurement of attributes over time (total colony coverage and dark colony coverage) including feed points and the transition of smooth to rough. This graph shows that there is constantly a conversion between smooth edges and rough edges which cycle around feed points, suggesting feeding may be effecting this transition.

This cyclic effect shows the importance of feeds on cell behaviour and also shows that the time point when any analysis (one time image), including manual verification using a microscope, is taken can have an effect on the morphological assessment. This is especially significant as the smooth edged colony is subjectively assessed by many users as undifferentiated embryonic colony (121), whereas the spikey, rough, indistinct colony border is regarded as inferior quality in many populations, often deemed differentiating (121–123). This provides significant evidence that a spot analysis is not sufficient for measuring culture state; rather a continual imaging portfolio is required. Having identified the traits of total colony coverage it is then possible to follow each of the defined metrics over time to assess the behaviour compared to the overall growth of the colony.

3.6.2 Core Periphery Colony Coverage

The core periphery is regarded as the pluripotent morphological region, and therefore during this pluripotent maintained culture the core periphery is expected to follow very closely to total colony coverage discussed previously.

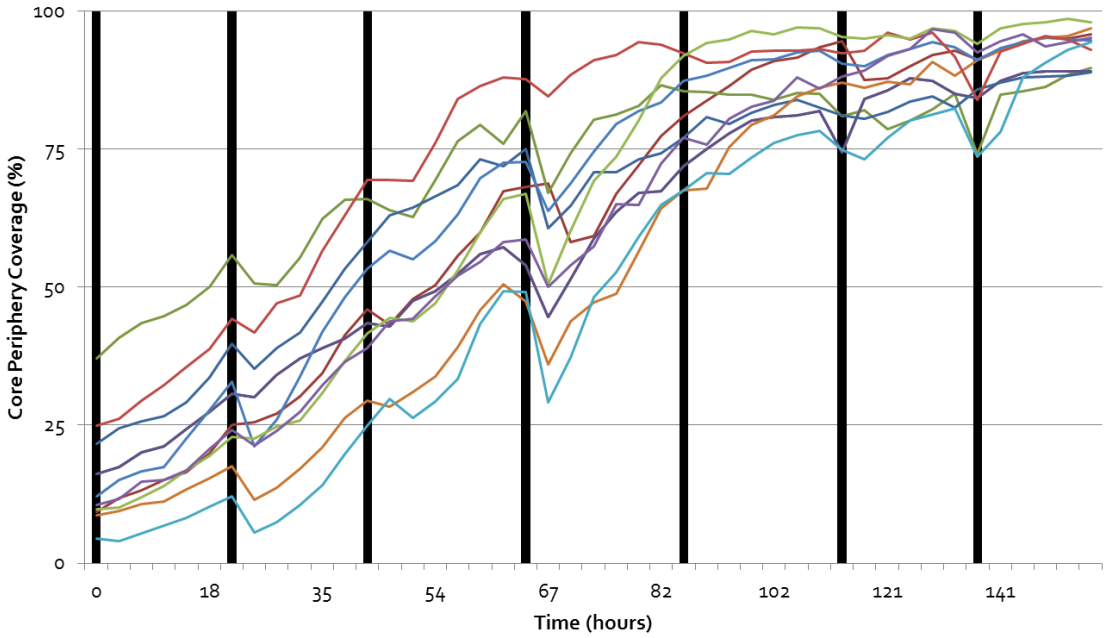

Figure 59. Core periphery coverage growth. Graph of core periphery colony coverage growth for various colonies identified within the same flask and imaged over a 150 hour period. The continual growth of core periphery colony areas is due to the proliferation of pluripotent cells in the colony core. (n=11)

As expected the core periphery colony growth follows a similar path to total colony coverage. This is due to very little edge and dark in pluripotent populations, which combine with core periphery to make up the total cell area. The slight difference with total colony coverage noted in Figure 59 is that they do not reach 100%, again due to the other metrics being present as a small percentage of coverage. The dips seen previously are also shown here in core periphery coverage.

3.6.3 Dark Colony Coverage

The next factor to assess is the dark area quantification with regard to growth. This is shown in Figure 60, and follows a similar, although noisier, pattern to the total colony coverage.

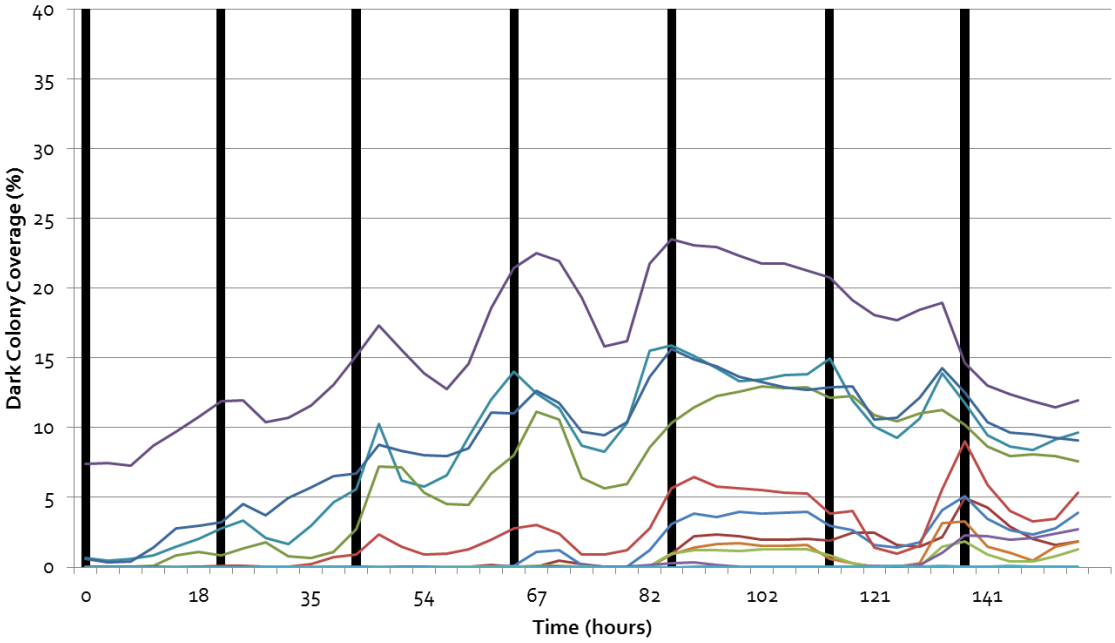

Figure 60. Dark Colony coverage growth. Graph of dark colony coverage growth for various colonies identified within the same flask and imaged over a 150 hour period. The continual growth of dark areas is due to the differentiating cells making up the dark area both proliferating and secreting factors promoting further differentiation in the surrounding population. (n=11)

As with the linear increase in the total colony size, the dark colony coverage behaves in the same manner. As discussed previously in section 3.4.2, this denser area of cells is attributed to a differentiating population. Therefore an increase in this population is predictive of an increase in differentiated cells. Unlike total colony growth this dark region does not take a logarithmic growth curve which would be expected if the differentiated cells will both proliferate and release factors causing further differentiating in the surrounding population. Therefore there must be another effect occurring which is likely that the embryonic population is spontaneously differentiating, this is a common response seen as spontaneous differentiation in adhered embryonic cultures (124) and embryoid bodies (125).

The data presented in Figure 60 shows large non-systematic fluctuations. Unlike for total colony assessment the image quality including contrast and focus are important in the identification of the dark area using the Area Finder protocol as pattern recognition is utilised. However for the work described here the current identification of dark colony coverage is sufficient to compare populations, and identify a difference in culture state. As before it is possible to plot the gradient changes with time to identify any common growth rate variations within the identified colonies, this is shown in Figure 61.

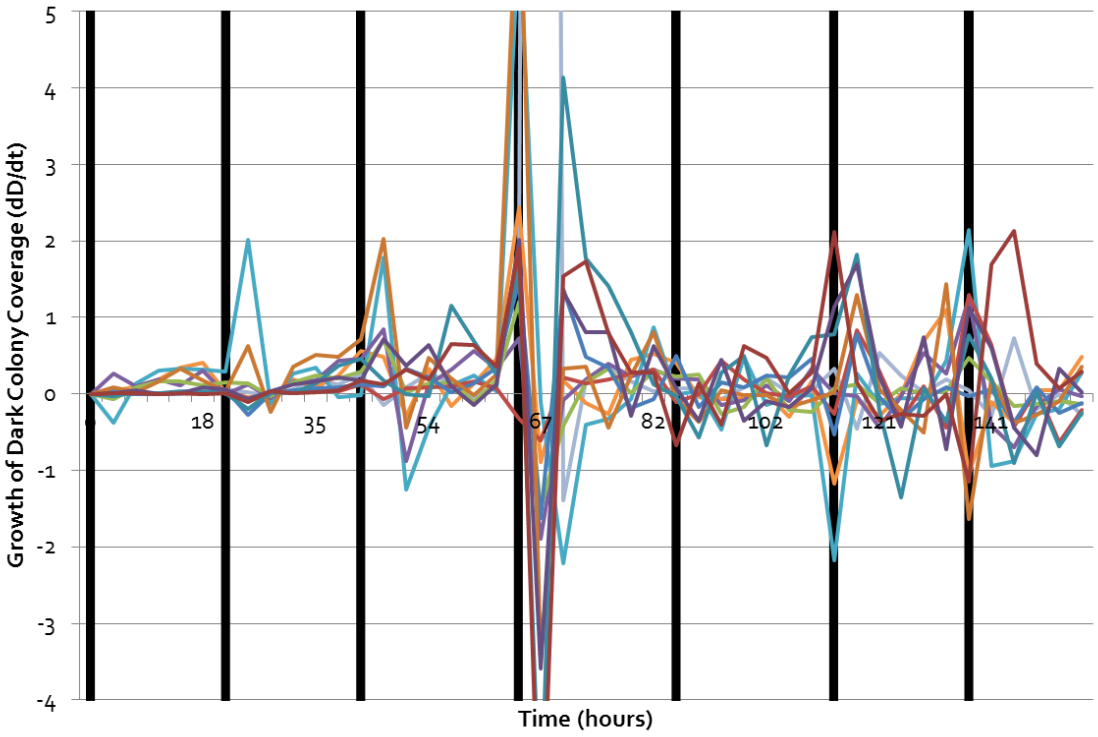

Figure 61. Gradients from Figure 55 which show the growth rate between images By assessing the growth rates of dark colony coverage it is possible to see that the spikes and dips seen previously in total colony coverage are also present here. Additionally this cyclic growth continues past 80 hours, where total colony coverage could not be seen due to confluency. As dark coverage only takes a proportion of the colony it continues to be monitored and provides valuable data. (n=11)

As with the total colony there is a change of growth rate following the feed points, a factor further investigated in Section 3.7 to determine whether this is an artefact due to feed and/or environmental changes.

It is worth noting that these spikes and dips continue past 80 hours, where the total colony coverage metric was unable to accurately measure coverage due to the colony covering a greater

area then the image. As the dark coverage only takes a proportion of the image, commonly found in the centre of a colony, this metric can further measure the growth of a colony past image confluency. It may therefore be possible to use dark coverage as a metric for predicting colony growth at confluent conditions. An example can be seen in Figure 62, where an increase in total colony growth is limited but could be correlated from the increase in dark area. It is important to note that this would only be possible if the dark area growth was representative of total colony growth, and that a separate growth rate exists for this dark area.

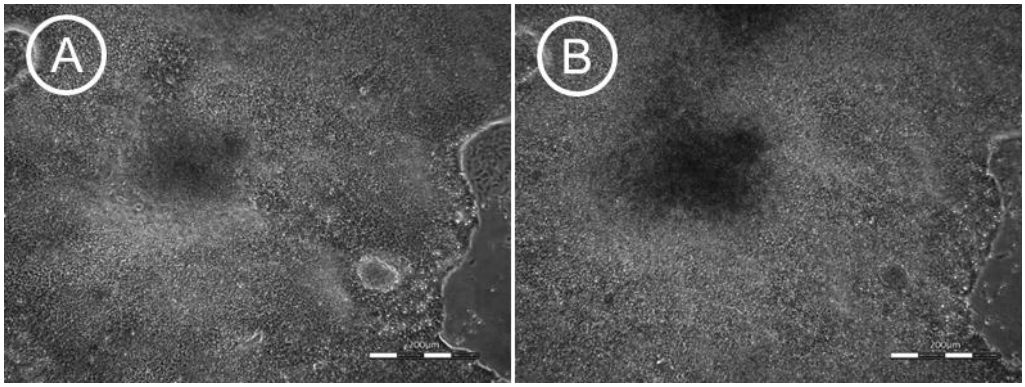

Figure 62. Colony with a dark centre showing continual growth past image confluency. By continuing to monitor dark colony coverage further growth can be identified independent on total colony growth due to the colony being too large to fit within a single image. A) shows all dark area but colony larger than the image size. B) Increased dark area, although total colony coverage remains constant, dark area has increased allowing further analysis of growth.

3.6.4 Edge Cell Coverage

The cells on the periphery of a colony exhibit different cell morphology to those held within the bulk of the colony. These edge cells are deemed to represent a different state to the core colony cells, often associated with early phases of differentiation, with uncertainty regarding their capability to return to a pluripotent state. Many operators would therefore try to avoid the emergence of excess peripheral cells which therefore allow culture quality to be assessed based on the quantity of these cells. However in Figure 57 it was shown that colonies continually move between a smooth to rough edge morphology, and therefore the timing of the assessment can be an important factor. The behaviour of edge cell coverage is shown in Figure 63.

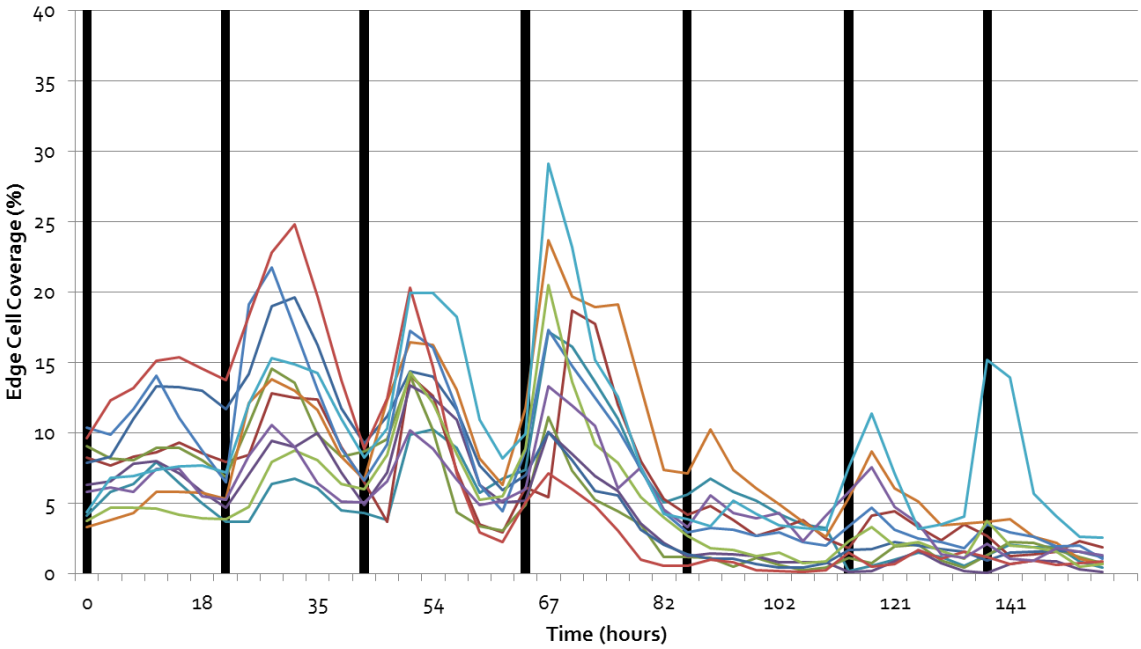

Figure 63. Edge Cell coverage over time. Graph of edge cell colony coverage for various colonies identified within the same flask and imaged over a 150 hour period. The graph shows very little growth of an edge cell population, as would be expected as edge cells are a differentiating population. The edge cell coverage declines overtime as the colony grows larger than the image area, therefore little edge is detected. (n=11)

Figure 63 shows that the identification of edge cells in a pluripotent population is very little, and declines as the colony grows larger than the imaged area with the periphery lost. As with all the metrics there is a lot of noise surrounding the feeding points shown as black vertical bars. Further analysis will investigate the effect of feeding on all metrics. Figure 64 highlights the loss of colony periphery during growth as the colony area succeeds the imaged area, and hence the decline in edge cell coverage over time.

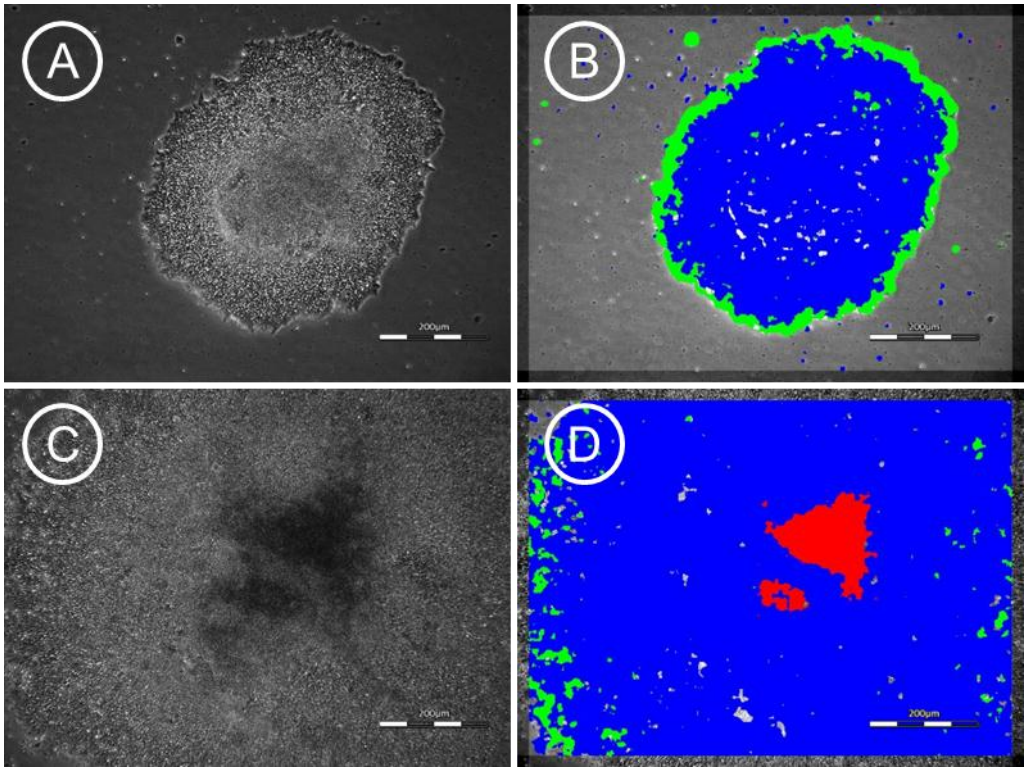

Figure 64. Image of a colony with analysed metrics. A) Initially the entire colony is in the field of view, however over time as the colony grows unless the imaged area is also increased the colony grows outside the field of view, C). This therefore prevents the detection of cells migrating away from the periphery as shown in D) compared to C).

The emergence of identified metrics over time has shown the power of being able to record the effects of external factors on each metric. Specifically the effect of feeding has had a noticeable consequence on all the metrics. The next section will analyse the metrics after a process action.

3.7 Analysing Process Actions Effect on Cell Culture

In order to assess how process actions can affect the culture procedure, it is possible to vary the nutrient renewal period and in turn the effect of removing the vessel from the incubator. As has been seen throughout section 3.6 the feed points create large disturbances within the quantified metrics. It is therefore important to see if these are a true deviation, or external noise from the system. The first experiment was set-up with feeding points at 12 hours, 24 hours and 48 hours. The resultant data from each metric, of selected colonies, are analysed in the following sections.

3.7.1 Total Colony Coverage

By assessing the total colony coverage for cultures with different feed regimes it is possible to conclude the effect of feeding on the overall growth of embryonic colonies. Figure 65 shows the effect on colony growth with 12, 24 and 48 hour feeding patterns with the removal of the cells from incubation every 12 hours. This therefore caused a cooling of the cells along with a reduction in CO_2 % and humidity. Form this data it is possible to conclude whether the variations in growth rates seen previously in Section 3.6, are due to environmental cues or media supplementation.

By following the change in coverage over time where the cells are fed every 48 hours, but removed from the incubator every 12 hours it is possible to state that the observed dips in coverage are governed by environmental cues (Figure 65 C). All 3 conditions shown here were conducted on the same plate, therefore exposing the cells to the same external conditions independent of their feeding regime. Even when there is not a media change (only orange bars) there is still this dip proving that they are governed by environmental cues rather than any metabolic cues from feeding. This dip is only visible at some of the removal points, potentially when the flask was removed for a longer period of time than the others. The environmental chamber is temperature (37°C), CO_2 (5%) and humidity (95%) controlled, on removal from the incubator all of these conditions can change, although it is most likely that temperature has the greatest short term effect due to the contraction of the cell cytoskeleton, a response discussed in depth by Almeida (126).

Interestingly the dips in coverage are most notable in the 24 and 48 hour feed patterns rather than the 12 hour feed patterns. Although these dips are unrelated to whether the well has had a media change the dips are more noticeable at higher coverage's. At 48 hours there is a large dip for all colonies in both the 24 hour and 48 hour feeding patterns, however at 72 hours when only the 24 hour feeding pattern plate had a media change both still have significant drops in coverage. This said the overall growth curve is unaffected by these dips with the colony growth continuing on the same trajectory if these dips were ignored.

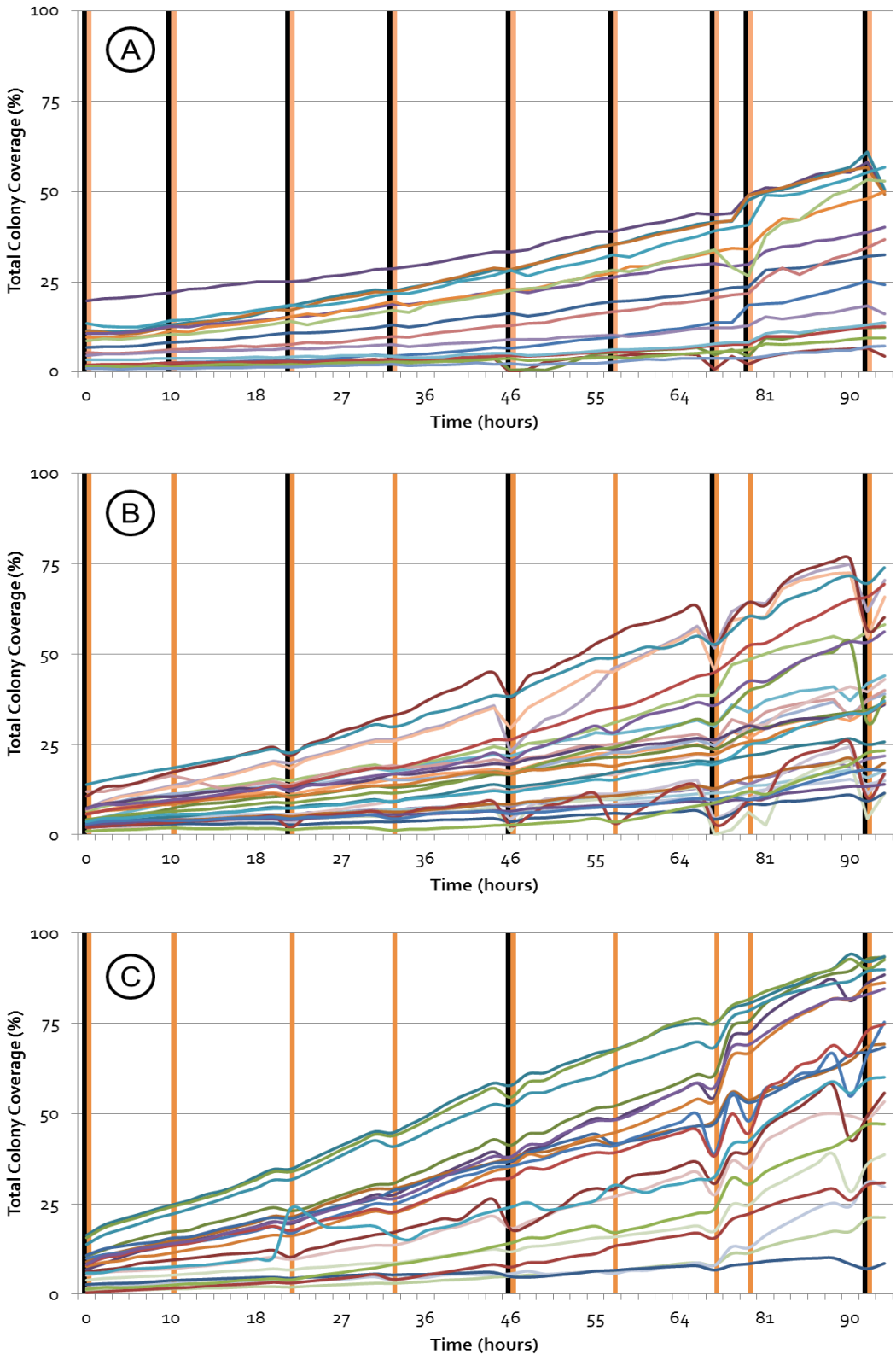

Figure 65. Total Colony Coverage measured over time with different feed regimes. By assessing the coverage values with different feed regimes it is possible to identify the cause of coverage dips. This diagram shows 12, 24 and 48 hour feed regimes in graphs A), B) and C) respectively. The orange bars represent when the culture vessel is removed from the incubator, with the black lines showing when the cells were fed. From this data it is possible to see that dips occur even when there is not a feed, suggesting environmental cues rather than metabolic cues cause the dips. (n=20).

All the colonies begin with a coverage range of 0-20%, independent on the feeding pattern. However after 90 hours the 12, 24 and 48 hour feeding patterns have coverage ranges from 0-55, 0-70 and 0-90% respectively. Although there are larger fluctuations due to environmental cues in the less frequently fed plates, the average growth rate is increased. This suggests that less frequent feeding has a positive influence in the growth of hESC colonies.

This data has proved that rather than a chemical cue, the fluctuations in coverage are due to environmental factors. By assessing the individual metrics of a single image it is possible to identify the cause of these dips, Figure 66. As the total colony coverage changed very little, but the core periphery coverage had large dips, potentially the colony is being wrongly identified after a feed. To further investigate this, a single colony was chosen, with the 4 metrics all plotted together in Figure 66.

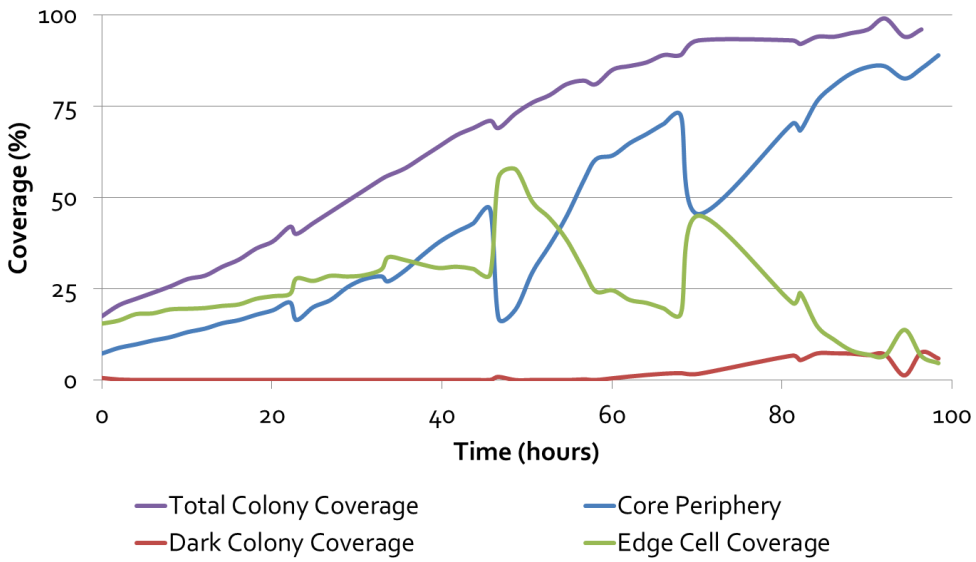

Figure 66. Coverage values for a single colony. By assessing single colony all the 4 metrics can be plotted together. This shows that there is little deviation in the total colony growth, but the core periphery coverage and edge cell coverage are opposites with regard to peaks and dips. This suggests that surrounding the incubator removal points the image analysis is wrongly identifying core periphery as edge and vice versa. Overtime this wrong identification returns to the original growth curve for each metric.

Apparent from Figure 66 is that the dip in core periphery (blue) is offset by a spike in edge cell coverage (green). As the total colony coverage changed very little, but the core periphery and edge cell coverage have large dips, potentially the colony is being wrongly identified following a feed. To

further investigate both raw and analysed images surrounding an incubator removal point were further examined, an example of such a filmstrip is shown in Figure 67.

By assessing the images for those with the most noticeable dips in growth it is possible to see that often the first image following the culture vessel removal has an increase in edge cell identification replacing core periphery coverage identification. By assessing the raw images it is possible to see that the images directly after the vessel is placed back into the incubator and imaged is slightly out of focus. These out of focus images causes a poor identification of colony coverage, and appear to classify out of focus colony as edge cell coverage. This further highlights the importance of capturing high quality images for analysis with Area Finder.

It was previously noted that these dips were more prominent in plates that were fed less often. Now it has been proven that these dips are due to incorrect identification it is possible to identify that those fed more often also grow slower. Therefore for image analysis the larger the colony the more of the colony is wrongly identified, causing a more prominent dip around the plate removal points. A number of solutions could be used to overcome this. Either a manual re-focussing of each position could be completed, although this would be time consuming and prone to human error. The better solution would be for the software to complete an auto focus of each position. This has been set-up within the software to allow a 50 µm scan to determine the optimum focus prior to imaging on all positions. All future work will utilise this auto focus feature of the software.

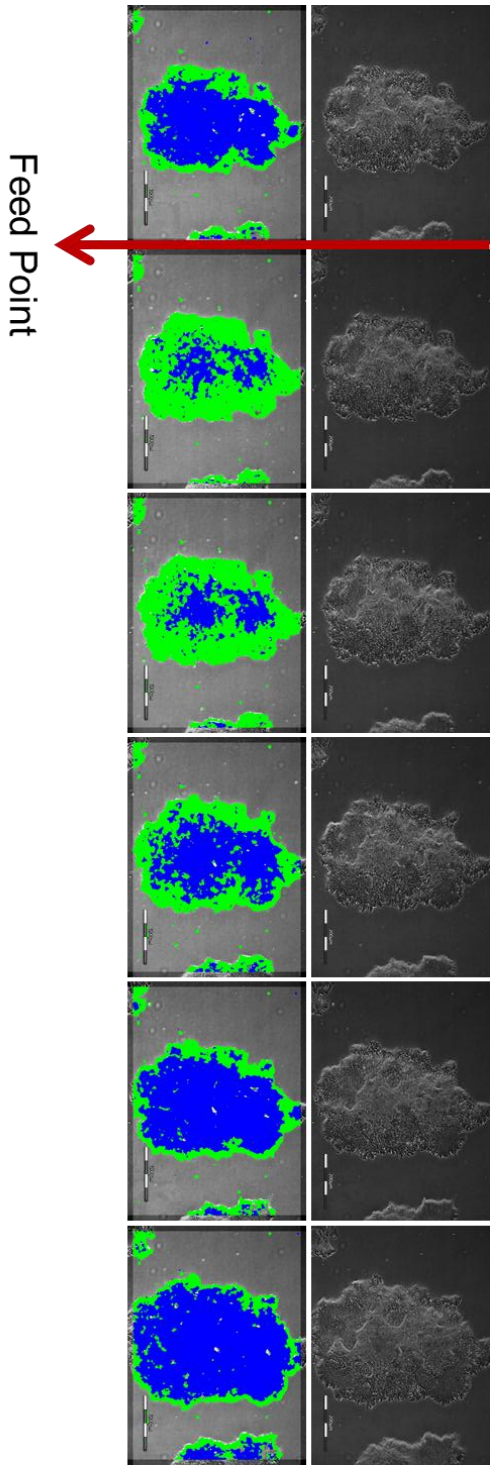

Figure 67. Filmstrip of colony growth around a feed point. By viewing the analysed colony overtime it is possible to identify that immediately after feeding the area of core periphery coverage (blue) is wrongly identified as edge cell coverage (green). By comparing to the raw images it is possible to identify that the images after feeding are out of focus, and only as they become in focus is the analysis improved.

3.8 Karyotype Assessment

Following culture and analysis representative samples of H9 embryonic stem cells were sent away for karyotype analysis. The results are shown in Figure 68.

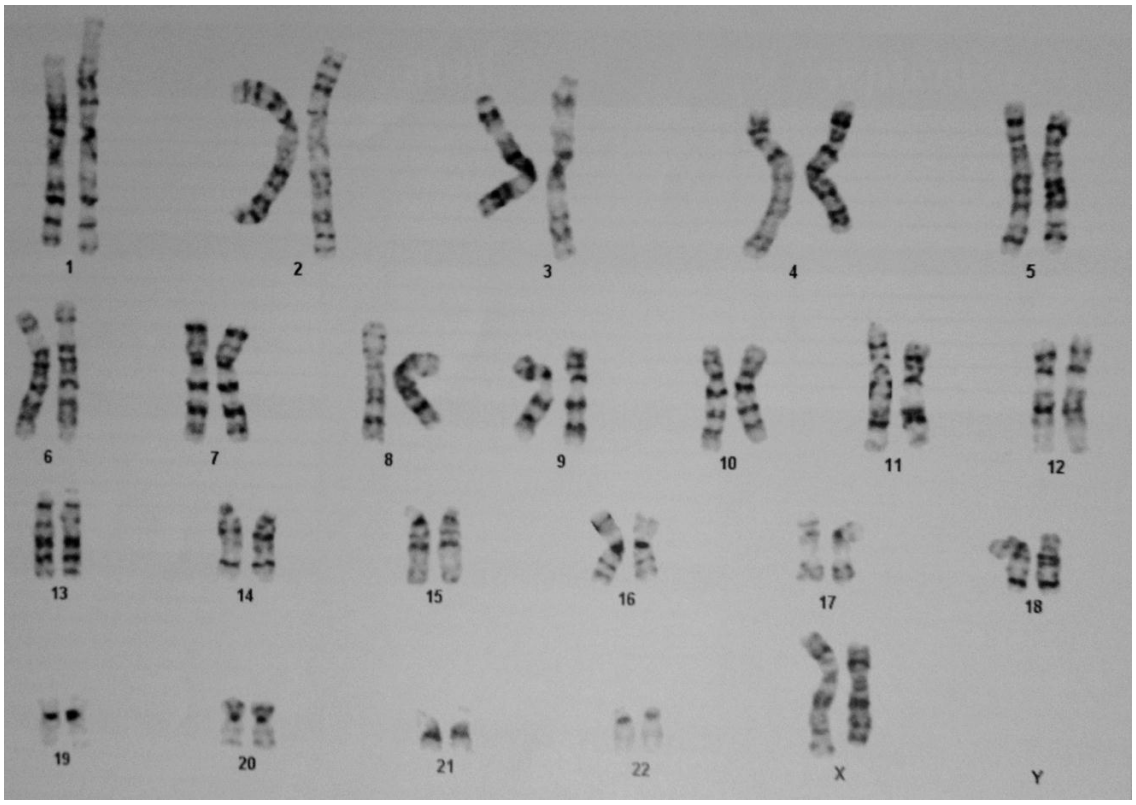

Figure 68. Karyotype analysis of representative hESC populations. This image identifies a normal female karyotype with no chromosome abnormalities reported.

Figure 68 highlights a normal karyotype analysis for female embryonic stem cells. There are no signs of chromosome defects reported in this report.

3.9 Conclusions

This chapter has shown the potential of measuring image derived metrics from phase contrast images. Initially image analysis has been shown to be more precise then traditional cell counting, with 4 novel metrics derived. Total cell coverage was initially used to correlate image analysis to cell

counts, but it was shown that unless all cells occupy the same area that further metrics are required. Following this dark colony areas, edge cell morphology and the remaining colony were determined as further image derived metrics. These metrics helped to account for the heterogeneity within an embryonic stem cell population, and therefore provided a better correlation to cell counts. However , during analysis it was seen that these metrics were directly linked to quality, and capable of quantifying the population state. Further development of how these metrics behave over the culture period allows them to be used as a tool for process control. The next stage will be to assess the utility of these image derived metrics to provide a quantitative output to inform a process action.

4. DEMONSTRATION OF USE IN PROCESS CONTROL AND DEVELOPMENT

4 Demonstration of Use in Process Control and Development

A hurdle currently preventing the development and commercialization of many therapeutic products is the current cost of manufacturing (4). There remains a vast technological challenge to translate processes which originate largely as laboratory-based, into clinically appropriate larger scale production techniques that are reproducible, safe, clinically effective and economically acceptable. Failure in this area has been the root cause of many commercial problems of early companies in this field (127). Developing and using scalable automated systems that consistently generate a product with predetermined acceptable variations and at increasing production volumes offers the path to affordable production (4).

Kino-Oka (128) accurately describes the current situation with regard to automated mammalian cell culture:

'The term "automation" has been used to describe some bioreactor systems developed so far. Because of the fluctuating nature of the tissue culture process, "automated operation" implies manipulation directed by operator decision or pre-set schedules without numerical warrant, in other words a passive or rigid system. Whereas an intelligent bioreactor system, one incorporating sophisticated tools not only to determine fluctuating culture properties but also to predict growth profiles, is required to realise fully automated operations.'

Because the characterization of human cells is especially challenging, the automated analysis of material throughout bioprocessing will be critical (28). The only reported use of online process monitoring was from Balis et al. within their bioartifical liver development, and then this was 'the minimum entry level for process control' (129). As discussed previously, there is a growing need for a routine, high-throughput, in-process monitoring and evaluation platform to make informed process decisions and therefore direct quality control (130).

In order to prove utility for the metrics developed previously the non-invasive imaging must be applied within a process which in turn can provide information for process control. A key aspect of embryonic culture is maintaining pluripotency across the population before directing differentiation through the use of chemical cues. It is therefore important to be able to initially measure a difference between a pluripotent colony and a differentiating colony. This can be achieved either as a population response (sampling multiple images) or individual colony units within the culture. The former analysis will be the most useful process tool to apply process control as it does not require a separate step of target identification. The latter will be more informative in determining target colony characteristics across the population in order to develop and optimise differentiation response. Therefore two separate sampling techniques can be applied to gather population or individual colony behaviour.

In order to prove utility of the image derived metrics a number of in process monitoring steps can be evaluated in the chapter. The first procedure to compare current process monitoring to the newly identified image based system is to evaluate cell counts. Initially a sacrificial, invasive technique is compared to using the image metrics in order to better predict cell number within a culture vessel. Following on from this both pluripotency and differentiation will be evaluated using invasive imaging and flow cytometry techniques whilst evaluating the non-invasive image derived metrics as a predictor of culture state. The final section investigates the effect of size on differentiation yield. This allows for real-time analysis to continually monitor the size of the colonies and determine an optimum size to make a process action in the form of differentiation stimuli. These varied culture processes allow the utility of novel metrics to be analysed and determine if they can be successfully integrated into cell therapy manufacture through the following key areas.

- Using image derived Metrics to Predict Cell Counts
- Using image derived Metrics to Predict Culture Quality
- Using Image Derived Metrics to Measure Differentiation
- Using the Metrics to Improve Differentiation Yield
- Real-Time Analysis for Process Prediction and Improvement

4.1 Using Image Derived Metrics to Predict Cell Counts

As discussed previously in Section 3.3, count is one route to measurement of process state and potentially control, however unlike single passaged cells, colony culture requires sacrificial vessels rather than sampling. This is due to the colonies macro distribution and the requirement to break the colonies down into single cells prior to count, image analysis therefore removes the need for sacrificial counting. Also due to colony culture there are many microenvironments that are not represented by count, compared to monolayer cultures where a single microenvironment is represented fairly well by count. The variation from cell counts can be seen in Figure 69 by taking 12 vessels that have been equally seeded with colonies and cultured for 4 days prior to sacrificial counting.

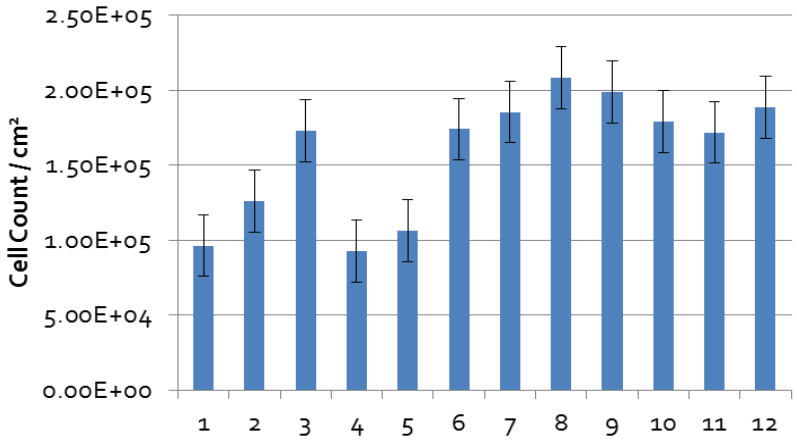

Figure 69. Variability in cell counting of embryonic colonies. By measuring the cell counts of 12 wells, this work has demonstrated that there is a large variation, therefore taking just a single count and assume the other wells contain the same number produces a large variable within a process (Error bars standard deviation of the population, n=12).

Figure 69 shows 12 samples that were seeded with the same volume of a well-mixed suspension of embryonic colonies, grown for 4 days followed by a sacrificial count on each culture vessel. This demonstrates the variation that occurs within colony culture. Comparing sample 4 and 8, the extremities, there is more than 100% difference in these two samples, with the entire population giving a standard deviation of 40,000 cells/cm^2, shown by the error bars in Figure 69. This variation may come from a number of sources including; poor mixing, variation in growth characteristics, size distribution and the counting method itself. It is common practice, as used by many collaborators, to sacrifice one flask and assume that count to the other flasks that were seeded at the same density. This data highlights how using a single sample to predict the count of an entire population can provide a large error.

Therefore another method would be to use the image derived metrics developed previously to estimate the cell counts. This allows every culture vessel to be imaged non-invasively, followed by analyse of the images to make a prediction of count as shown in Section 3.3.3. This was completed using both the original method of analysing the total colony coverage, deemed single metric, and also using the combination of three metrics 'core periphery', 'dark' and 'edge' coverage, deemed triple metric. 50 images from each culture vessel were taken, as previously mentioned one of the key advantages to non-invasive imaging is the ability to tailor the error in measurement by taking a set number of images. 50 images were chosen due to the statistical resolution shown in Section 3.3.2. Producing an estimation of count using coverage allows a non-invasive application of the same control algorithms currently used for count but using coverage. The correlation of single and triple metrics data to predict count and the actual counts are shown below in Figure 70.

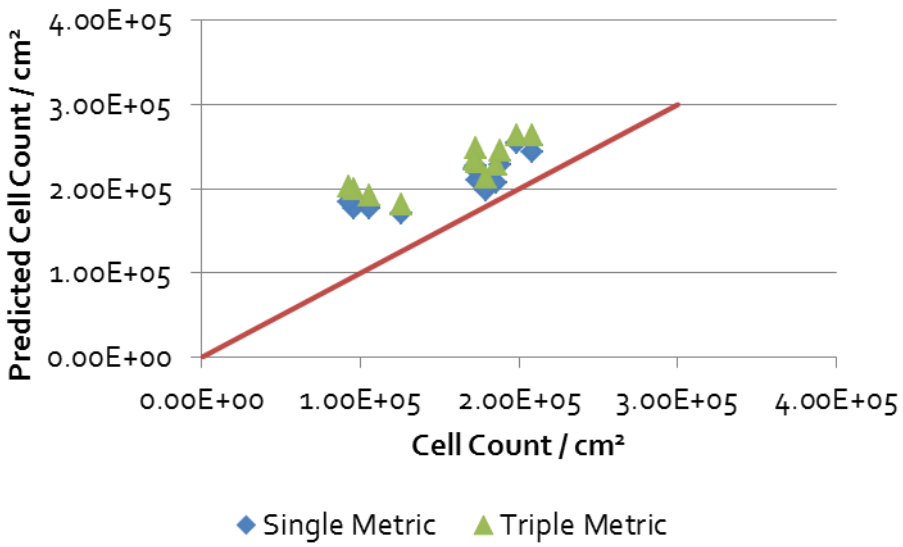

Figure 70. Correlating cell counts to image metrics using pre-defined relationships. Taking the same cell counts as previously shown in Figure 69, these can be correlated to a non-invasive predicted cell count. This is achieved by taking the percentage coverage derived in 3.3.2 to produce a predicted cell count based on one metric, or by taking the regression equation from section 3.4.5. This therefore allows every vessel to have its own cell count, reducing unknown variation within a process. A linear correlation is shown with an R^2 value of 0.753. The red line highlights where prediction would equal the true value. (n=12)

Figure 70 shows that using either the single or triple metrics produce very similar predictions of count. This is due to the variation seen over the data set where these equations were developed from. All of the culture vessels analysed here were of a low cell number after the 4 days culture experiment. From 3.4.5, it is clear that at low cell numbers the image metrics over-estimate the count, a feat shown here by all the predictors lying above the red true fit line. It was also noted previously that at low cell coverage's the metrics are less precise then at higher cell densities, so this experiment operates at the reduced precision range for the image derived metrics.

Having calculated the predicted cell counts from triple metric image analysis it is then possible to compare these to a typical process where a count is performed on one culture vessel, and extrapolated for the remaining vessels. Using this example it is possible to randomly select one vessels count and assume this to the remaining 11. Using a random number generator $1.85x10^5$ cells/cm (vessel 7) was chosen to represent the other vessels. Following this the error between true and predicted count that arises by using the single count is calculated. This single vessel error can

then be compared to the error sustained by using imaging to predict the count in each vessel. The errors are shown in Figure 71, where there is an error to the single vessel predicted count in blue, or an error to the image analysis predicted count in red.

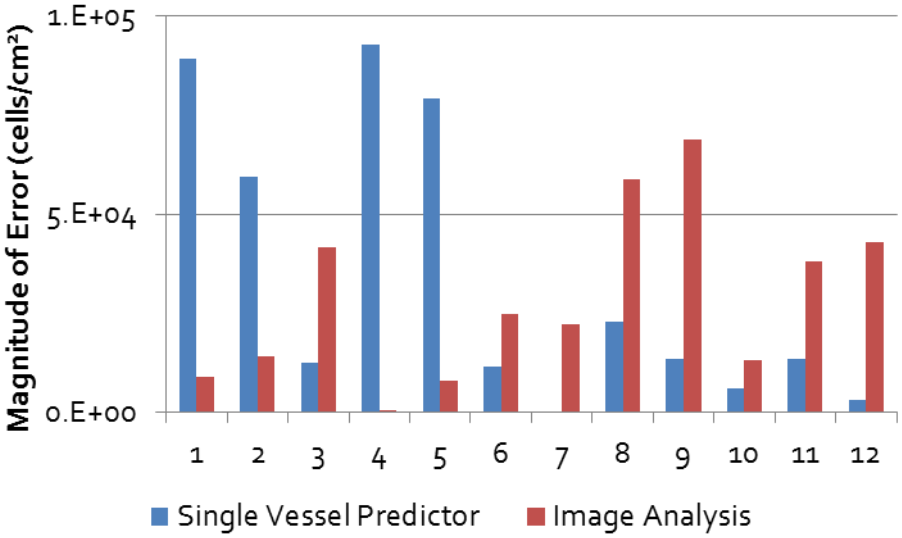

Figure 71. Error of single vessel predictor with error of using image analysis. The blue bars represent the error in the real cell count to using a single count, whereas the red bars represent the image analysis error to the true cell count. (n=12)

Figure 71 shows that there are errors greater than 50,000 cells/cm^2 in both the single vessel predictor and image analysis. The largest errors occur in the single vessel predicted analysis, however it is possible to average the errors for each predictor which highlights that the single vessel predictor has an average error of 3.36×10^4 cells/cm^2, whereas the image analysis has an average error of 2.85×10^4 cells/cm^2. This suggests that image analysis is a more accurate predictor of cell count than using the current single vessel predictor method. It is important to note that this is using only 12 culture vessels; a larger study would be required to test the validity of using image analysis over a predictive single vessel count. This would also need to be tested over a range of cell counts, although this was completed at low cell numbers where coverage was shown to be least precise, suggesting improvement with higher coverage. Also there is a probability that one of the culture vessels from the extremities would be selected and therefore produce a large error in predicting the counts of the other vessels.

This data has shown that using the image derived metrics in their least precise range, an improvement on the current practise is noted. It was seen in Figure 47 that under 300,000 cells/cm^2 the model is a poor predictor, especially noted in the regression equation on page 109 which has a constant of *227404*. This highlights that the model is only valid of cell numbers above 300,000 cells/cm^2 and becomes more powerful the larger the cell number. This is due to the effect that edge cell and dark colony metrics begin to have a more prominent effect at higher cell densities. By operating at a higher cell number and ultimately higher cell coverage range the image analysis is predicted to be further enhanced and the magnitude of error further reduced compared to the single vessel predictor.

4.1.1 Conclusions

As stated, colony culture counts are not representative of the microenvironment in which they habituate which suggests counting is a poor measurement for colony quality. This chapter has shown the variability in counts from vessels seeded with the same volume of a well-mixed solution of cells. Following on from this variation image analysis has been used to predict the cells counts, although an over-estimate is made, the error in image analysis compared to the current method is reduced in this example. The images also provide further information regarding the culture state than cell counts alone. By developing image derived metrics this novel measurement technique is also more informing about colony culture and therefore a promising method for process control.

4.2 Using Image Derived Metrics to Predict Culture Quality

An important aspect of optimised cell culture is feeding regime. In order to improve cell production and quality the feeding regime and media development are crucial factors to optimise (131,132). For embryonic cells, as per manufacturer's instructions, cultures should be fed with pluripotent media, mTeSR-1, every 24 hours in order to prevent differentiation (78). This feeding regime is also

designed to maintain concentrations of growth factors, nutrients and buffer reagents to maximise homogeneous quality growth (78). Alongside this the replenishment of media daily removes waste products to maintain these levels within an optimum range, specifically ammonia and lactate (132).

It is therefore hypothesised that by decreasing the feeding frequency the quality of the culture deteriorates with regard to its pluripotency status and growth. Using the image derived metrics developed previously the culture can be assessed and correlated back to traditional end point analysis using flow cytometry pluripotent markers Nanog, Oct3/4 and Sox-2. Cultures are fed every 12 hour, 24 hours or 48 hours with pluripotent media. A less frequent feeding regime is expected to decrease the pluripotency measured as a drop in pluripotency markers and an increase in the differentiation metrics of edge cell coverage and dark colony coverage.

4.2.1 Image Analysis Pluripotency Verification

By using the 4 metrics developed previously it is possible to see if culture state can be identified and monitored through phase contrast image analysis. Figure 72 shows graphs for all 4 metrics of total, core periphery, dark and edge cell coverage that have been averaged for the population expressed to each feeding regime. For this experiment imaging was restricted to user defined areas where colonies were visible. This equated to 19 images per well with 2 wells of each feeding regime in a 6-well plate, giving a population of 38 samples per condition. The data shown here is all normalised for colony size to remove any artefacts that size may provide on the behaviour of the metrics.

It is possible to see that feeding less frequently has increased the total colony coverage, shown by the red line above that of the green and blue in Figure 72 A). This was expected as research suggests a 100% media change may remove autocrine factors that are potentially 'instructive for cell proliferation' (132). Dividing the total coverage into the 3 categories of Core periphery, Dark and Edge cell coverage shows that the 48 hour feeding also has a higher core periphery B) and edge cell coverage D). The dark cell coverage C) is low for all feed regimes and therefore a poor predictor of

culture state in this experiment. Identifying total colony coverage 12 and 24 hour feeding regimes show little difference, with 48 hour growing faster, assumed due to the reduced removal of autocrine factors. Core periphery coverage is slightly separated following the same pattern of 48 hour feed regime having the most and 12 hour the least.

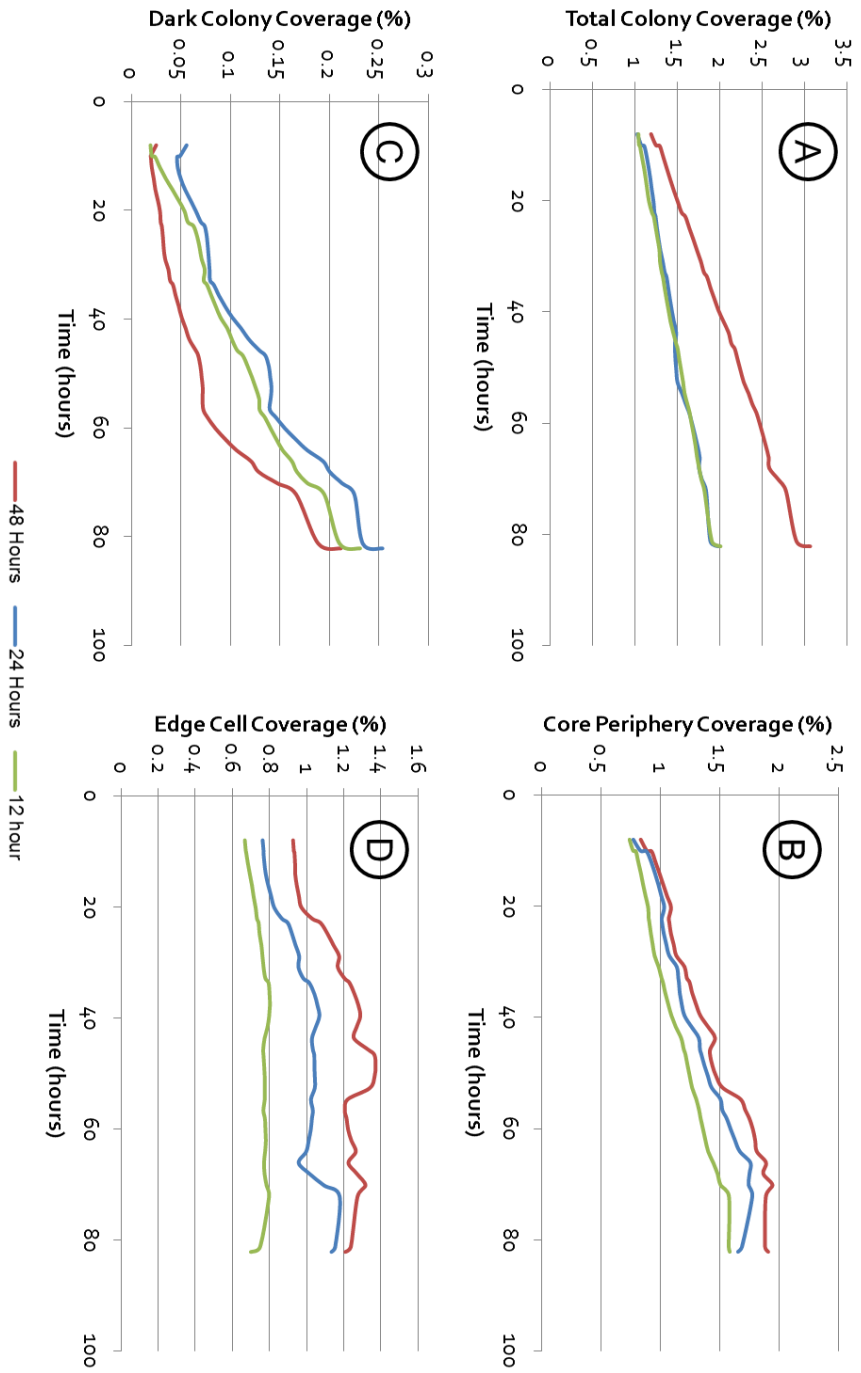

Figure 72. Behaviour of 4 metrics with feeding regimes normalised for colony size. It is possible to compare 48, 24 and 12 hour feeding regimes (red, blue and green respectively) with respect to the 4 identified metrics; A) Total colony coverage, B) Core periphery coverage C) Dark colony coverage and D) Edge cell coverage. The total colony coverage increases greatest for the less frequently fed cultures, suggesting there may be an effect of removing autocrine factors in the more frequently fed cultures reducing their growth rate. The core periphery colony coverage follows a similar relationship to that seen for total colony coverage. The dark area remains a very small percentage of the total colony coverage (<5%), and therefore is hard to comment on the relationship. Edge cell coverage again is highest for the 48 hour feed regime, suggesting increased differentiation, however it started higher than the other feed regimes which may cause a bias on the results. This said comparing the gradients of the 3 feed regimes, 12 hour is much flatter than 48 hour suggesting a slower growth of edge cell coverage. (n=38)

Due to the low values for dark coverage this metric is not further analysed, however edge cell coverage appears to show a greater amount for those fed less often. The edge cell metric which is a measure of differentiation is clearly separated between the 3 feed regimes. Although all this data has been normalised for size, the increased growth of 48 hour could be artificially providing larger edge cell coverage due to the analysis. The larger the colony, the larger its circumference and therefore more absolute edge cell coverage will be detected using the analysis protocol. To remove this bias it is possible to take colonies of the same size in each regime and analyse them, therefore removing the effect of both time and size on the cultures. In order to accomplish this 3 diameters were chosen at 879, 971 and 1158 µm then the edge cell coverage was recorded for each condition when the average colony distribution reached this diameter. This is shown in Figure 73.

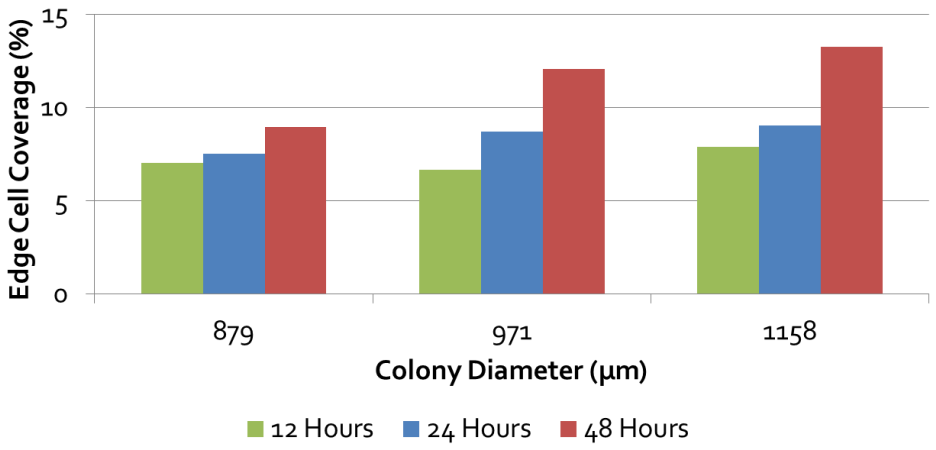

Figure 73. Edge Cell Coverage for 3 colony sizes in each feed regime. This shows that for a given colony size, those fed least often will have the greatest amount of edge cell differentiation. n=38

From Figure 73 it is possible to see that the edge cell coverage is greater for the less frequently fed even when all the colonies are the same size. This further suggests that the different feed regimes effect the growth of edge cell coverage within the population. There is also an increase in the percentage of edge cell for larger colonies. This would be expected if the thickness of edge cell depth remain unchanged, as the circumference would be greater. As has been mentioned before the reasons behind this response require further work especially around media development which sits outside of this works scope.

To ensure that the starting size is not biasing the analysis, this experiment was repeated. This time 38 images were taken from each well in a systematic sampling pattern as identified in Section 3.3.2. The average values from 2 wells composed of 76 images in total are shown in Figure 74.

Figure 74 confirms that feeding less regularly increases the edge cell coverage of the population. The previous results seen in Figure 72 were compiled from only imaging in areas where colonies were present. This time systematic sampling was used, taking 38 images within each well of a 6-well plate. Each condition had 2 wells, so a total of 76 images per condition were captured and analysed.

Immediately it is possible to see that the coverage percentages are much lower in this experiment compared to the previous, due to some images containing little or no colonies. However the relationship of edge cell coverage remains the same with 48 hour feeding producing more edge cell coverage then both 12 and 24 hour feeding. Also worth noting in this experiment is that unlike previously the 48 hour feeding regime did not start with the largest colonies. In fact the 12 hour feeding regime started with the most edge cell coverage, and ended with the least. This provides further encouraging results that edge cell coverage can be used as a metric to determine culture state. To determine if this change in edge is predictive of pluripotency state end point flow cytometry was conducted in the next section.

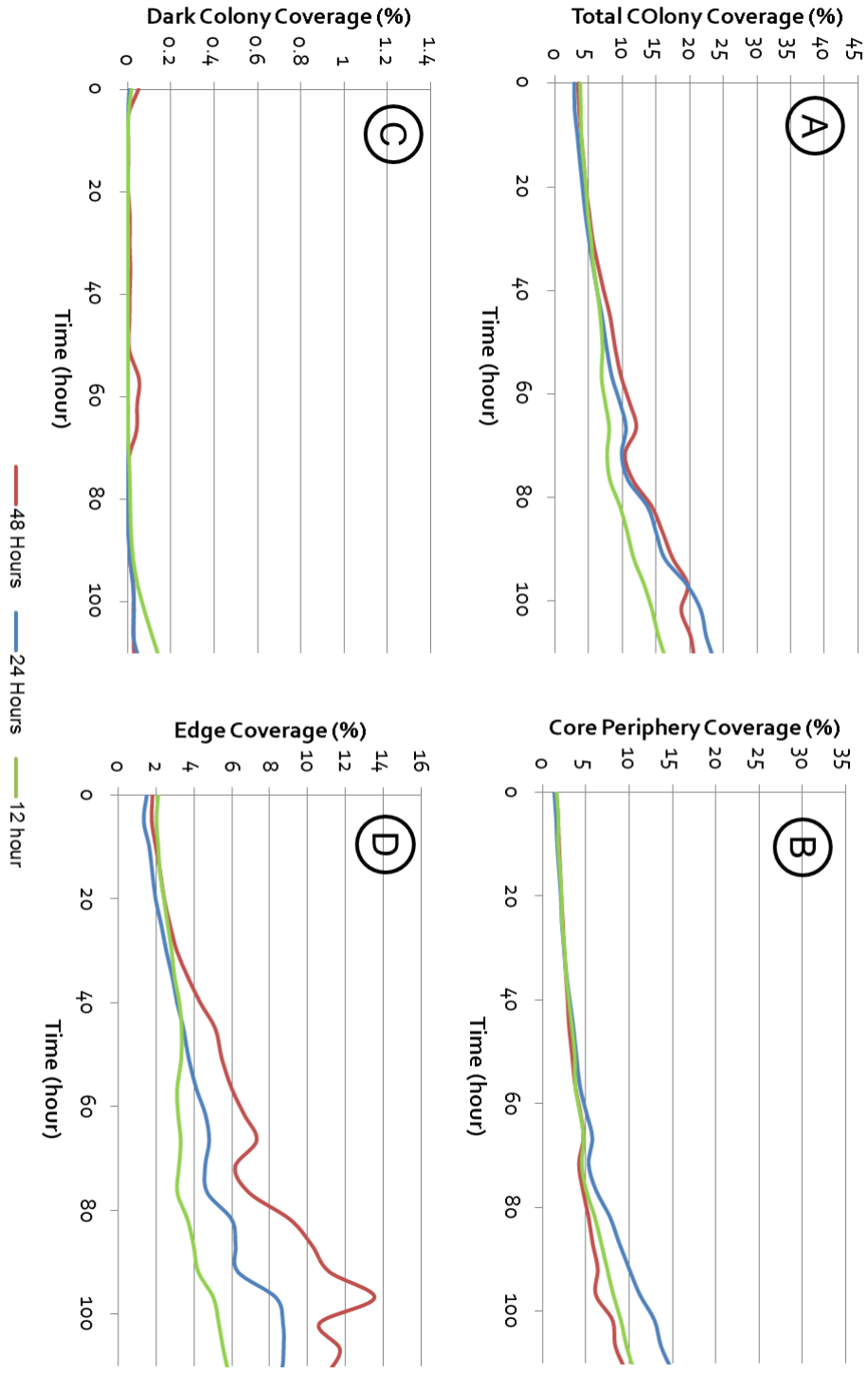

Figure 74. Repeat of colony coverage growth with different feed regimes. This figure confirms that feeding less regularly shown by the 48 hour feeding red line, that edge cell coverage increases. This shows that edge cell coverage can be used as a quality metric for embryonic cultures. (n=2)

4.2.2 End-Point Traditional Pluripotency Verification

After the culture process was finished analysis by flow cytometry was conducted to assess if there was a change in 3 pluripotent markers, Nanog, Oct-3/4 and Sox-2. Example flow cytometry data is shown in Figure 75.

As shown with immunostaining previously in Section 3.5, Sox-2 remains the most positive throughout the culture as a proportion of the expressing population. Both Nanog and Oct-4 are lost earlier during differentiation, and represent a smaller positive population. By comparing the feed regimes, it can be seen that the positive peak decreases on all the markers shown here with less frequent feeding, shown by a decrease in the y-axis. As well as the peak decreasing showing a decrease in positive cells, there is also a drop in the median fluorescence. This is seen by the positive peak shifting in the x-axis. The median fluorescence intensity can be used to accurately describe a population of cells in culture. It has been reported that the median can provide a more accurate representation of a population as it is not governed by a negative control such as the positive cells percentage (133). Also deviations in median measurements can be important indications of subtle changes within the population, with progression of differentiation or down regulation of marker expression changing the median value prior to being noted in the positive cell fraction (133). For both experiments the medians have been normalised based on the 24 hour feed regime and are shown in Figure 76.

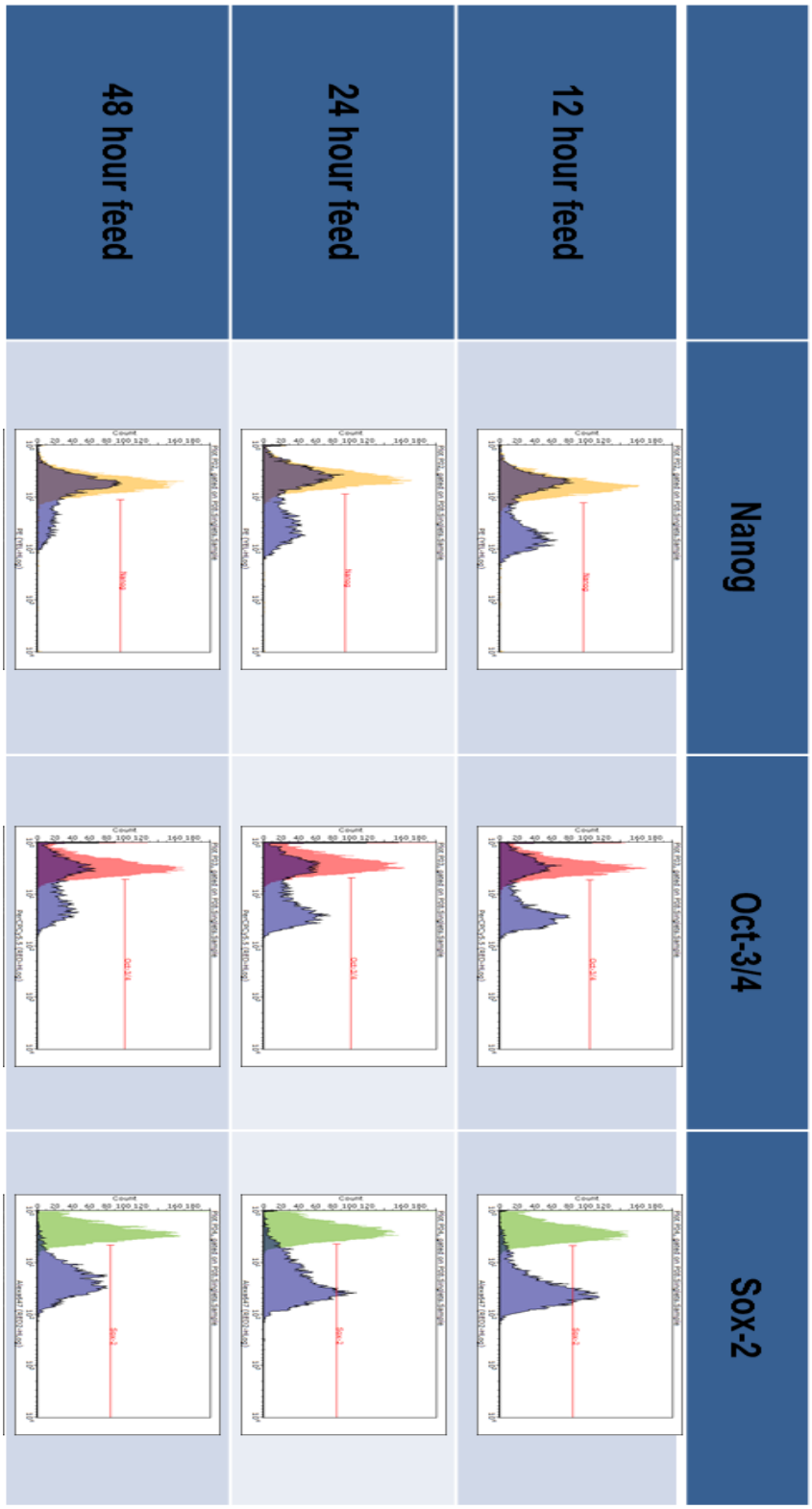

Figure 75. Flow cytometry data based on feeding regimes Showing the histograms of Nanog, Oct-3/4 and Sox-2 with varying feeding regimes of 12, 24 and 48 hour feeds. (n=2)

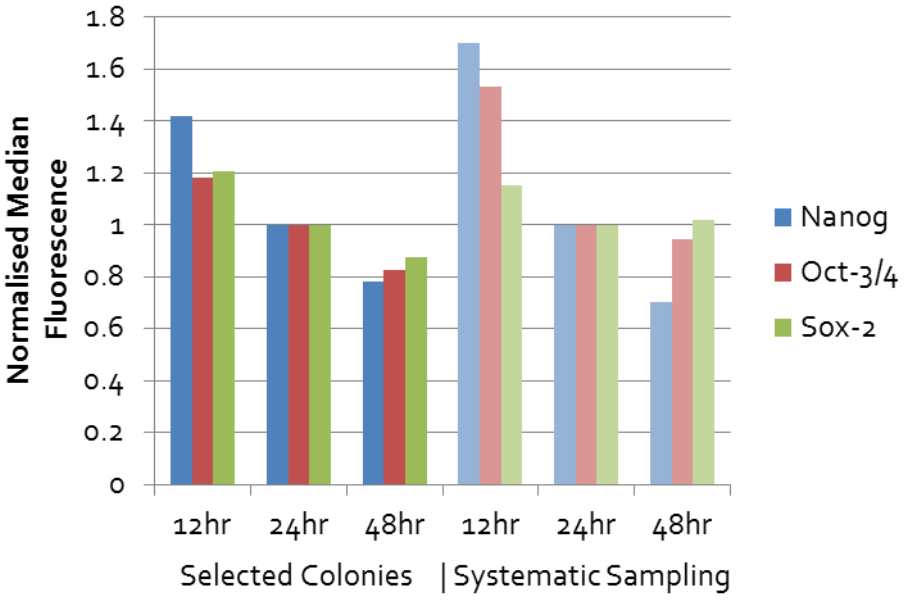

Figure 76. Flow cytometry data of normalised median value of positive cells from various feeding patterns on pluripotency markers Nanog, Oct-3/4 and Sox-2. The left 3 columns show data from Figure 72 where invidiual colonies were selected and image. The right 3 columns show the data from Figure 74 where systematic sampling was conducted in each condition. (n=2)

The median values are suitable here as the flow distribution is normalised without outliers as shown in Figure 75. Figure 76 highlights the decrease in median fluorescence across all the pluripotent markers that occurs with less frequent feeding. This suggests that pluripotency is better maintained by feeding every 12 hours compared to 24 or 48. The greatest change is seen in Nanog, again this is unsurprising as this is one of the first markers to be lost during differentiation, with Sox-2 remaining the longest during differentiation, and showing the least change over the feed regimes.

The decrease in pluripotency with decreasing feeding frequency correlates to the effect seen through phase contrast imaging, an increase in edge cell coverage. This increases confidence in the ability to use these two metrics to identify the pluripotent state of a population.

4.2.3 Conclusions

By varying the feeding regimes, image analysis has been able to monitor a change in metrics which have then been correlated back to conventional flow cytometry pluripotent markers. This highlights the merit of using non-invasive imaging to continually monitor the pluripotent state of cultures and quantitate an output of pluripotency state. This work has highlighted that the resolution of the Cell-IQ system is able to accurately identify a change in culture state using image derived metrics. The next process to evaluate is the suitability of measuring a directed differentiation with a chemical cue within the Cell-IQ system.

4.3 Using Image Derived Metrics to Measure Differentiation

Embryonic differentiation can be directed down each of the germ layers by introducing known growth factors (134), however 'differentiation *in vitro* is consistently disorganised and frequently variable' between colonies (135). When colonies are removed from adhered surfaces and placed in suspension they form embryoid bodies which spontaneously differentiate into multicellular aggregates (135). This uncontrolled differentiation method produces inconsistent results due to the variable micro- environment surrounding the embryoid bodies. Therefore by keeping the colonies adhered and introducing known growth factors, it is hypothesised that the 3 metrics described previously (core periphery, dark colony coverage and edge cell coverage) will predict a response to a differentiation stimulus and correlate to the extent of that differentiation. This allows the Cell-IQ to be useful to continuously monitor, predict and provide a measure of culture state in order to make informed process decisions to improve differentiation efficiency.

For this example of in-process monitoring the epithelial-to-mesenchymal transition (EMT) is studied. The complex nature of the EMT causes a change in tissue architecture, cell morphology, adhesion and migration capacity (136) and plays a pivotal role in the germ layer formations (137).

This morphological change is a key process through which it is anticipated that the Cell-IQ can be utilised to monitor and quantify metrics related to such changes in morphology.

H9 human embryonic stem cells were cultured for 24 hours in mTeSR-1 culture media. Following this a daily media change of mTeSR-1 with 10 ng/mL of BMP-4, FGF, Activin A and VEGF is carried out. These growth factors have previously been shown to induce mesoderm differentiation (134,137–139). This daily replenishment is continued for 4 days with continual imaging using the Cell-IQ imaging platform. By day 4 the colonies morphology have dramatically changed creating a ring of single cells on the colony periphery. The difference between a colony maintained in pluripotent media and differentiation inducing media is shown in Figure 77.

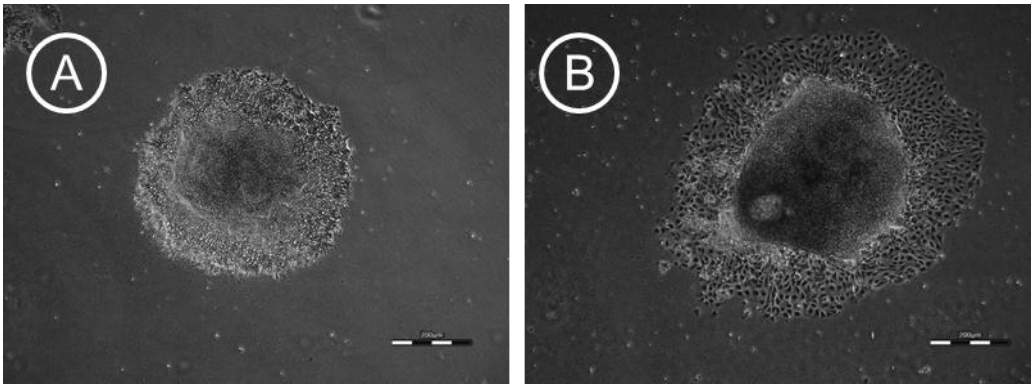

Figure 77. Embryonic colony with and without differentiation stimuli Image A) remains in pluripotent media (mTeSR-1-1, StemCell Technologies), maintaining a tight boundary edge with a similar morphology throughout the colony. The colony in image B) however has been exposed to 10 ng/mL of BMP-4 FGF, VEGF and Activin A for 3 days prior to imaging. This colony has a ring of edge cell morphology as the differentiated cells migrate away from the colony.

Following the 4 day culture period the captured images were analysed for the 3 metrics developed previously in Chapter 3.4. The metrics were then plotted over time to identify the colony response. This is shown by taking two representative colonies, one in Figure 78 A) where no differentiation stimulus was added and Figure 78 B) where a differentiation stimulus was added.

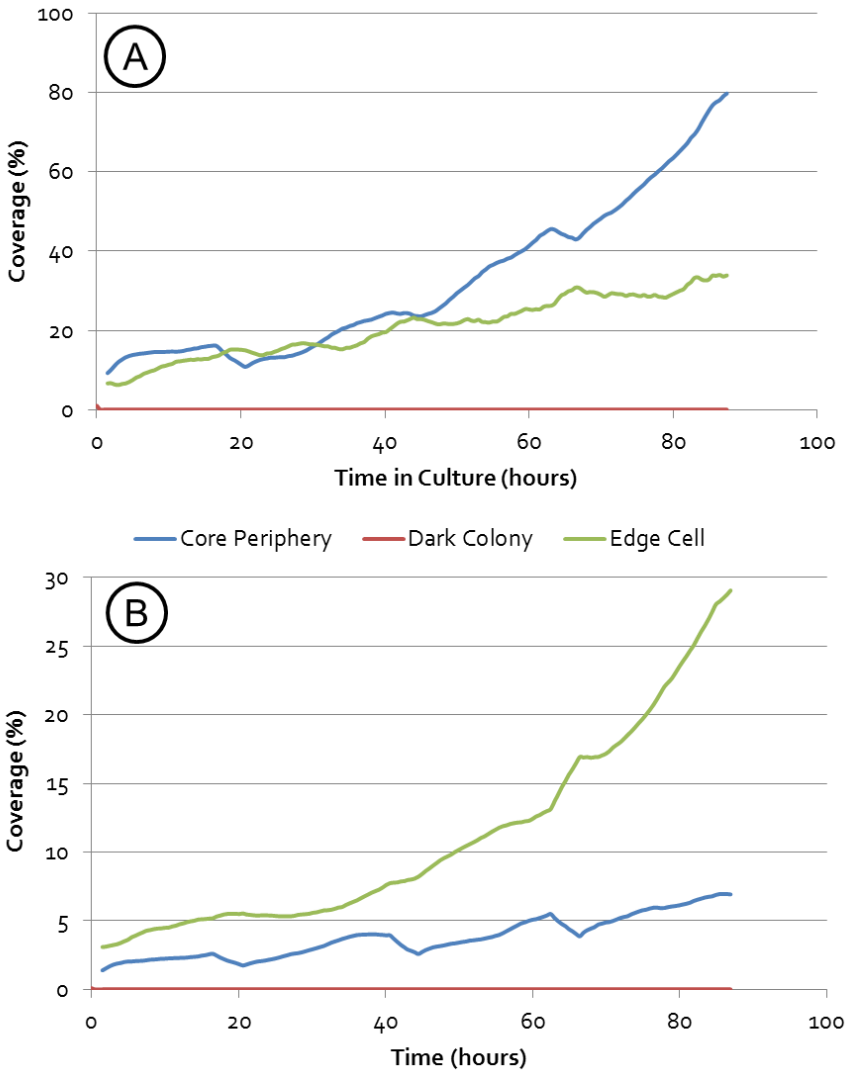

Figure 78. Trio of metrics measured for pluripotent and differentiating colony. A) Dark colony coverage, Edge cell coverage and Core periphery coverage of embryonic colonies cultured in pluripotent media. There is continual increase in core periphery and edge cell morphology as the colony increases in size, roughly doubling in coverage every 24 hours. Dark colony coverage tends to be seen later in culture as the colony continues to proliferate prior to passaging. B) Dark colony coverage, Edge cell coverage and core periphery colony coverage of embryonic colonies cultured in mTeSR-1 for 24 hours before including BMP-4, FGF, VEGF and Activin A in the daily feeds. It can be seen there is a 24 hour delay before any effects of the addition of BMP-4 are seen. At 48 hours the edge cell coverage dramatically increases exponentially, whereas the other metrics remain stable.

Figure 78 A) shows the behaviour of an embryonic colony that is maintained in pluripotent media, whereas Figure 78 B) shows the effect of adding bone morphogenetic factor 4 (BMP-4), Activin A, fibroblast growth factor (FGF) and vascular endothelial growth factor (VEGF). This stimulates a morphological change that can be measured using the Cell-IQ. For a colony maintained in its pluripotent state the core periphery coverage grows faster than the edge cell coverage, represented as the blue line outperforming the green line in Figure 78 A). This suggests that the core periphery

coverage is indicative of pluripotent morphology whereas In the presence of a differentiation stimulus there is a delayed increase in edge cell morphology. 24 hours after the addition of the differentiation stimulus the green line exponentially increases, the overall effect of more edge cell morphology being present then core periphery. The difference in morphology can be seen in Figure 79 shown with analysis of the 3 image derived metrics successfully identified.

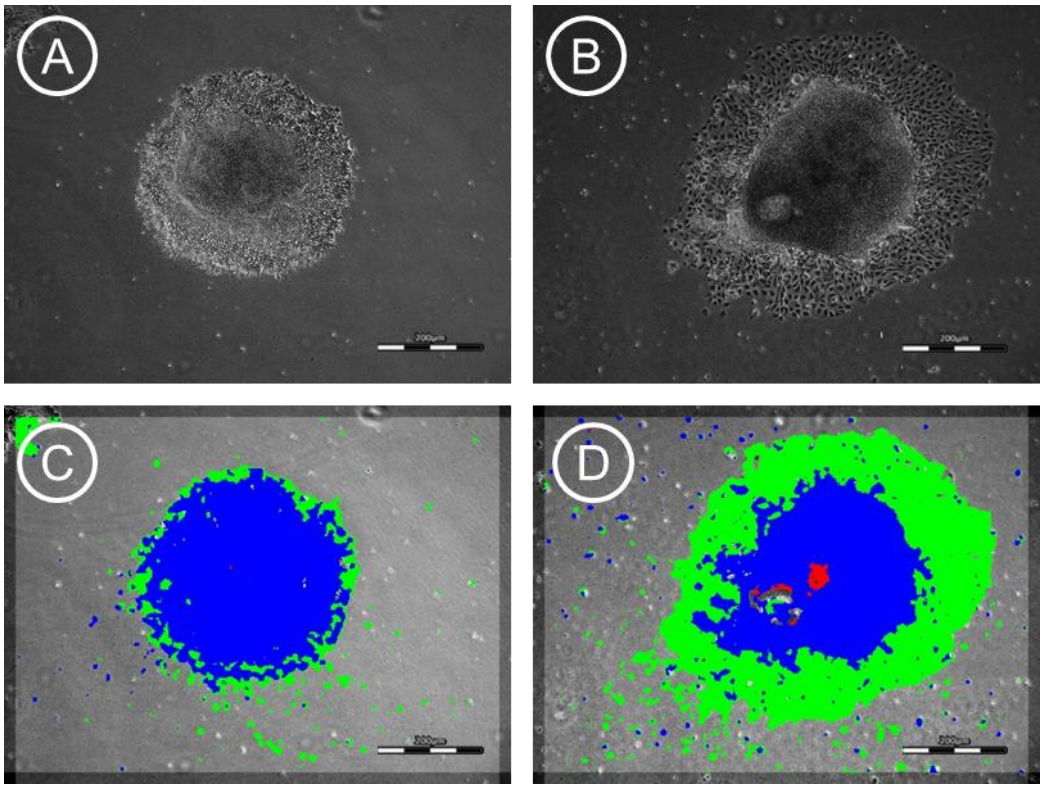

Figure 79. Raw image and analysed image of pluripotent and differentiating colony. Colony morphology difference between A) control (maintained in pluripotent media) and B) differentiating colony (induced with BMP-4, Activin-A, FGF and VEGF). There is a clear band of monolayer edge cells in the differentiating stimuli conditions, this is represented in the analysed images as a band of green (D), this is not seen in image C where the colony is maintained in pluripotent conditions.

Figure 79 shows the accuracy of analysed images in detecting the 3 metrics. Following this analysis it is possible to identify the edge cell population with immunostaining. The cocktail of growth factors were used to induce mesoderm differentiation, and therefore early mesoderm markers were used to identify the population. Heart and neural crest derivatives-expressed protein 1 (HAND1) was found to be positive in the edge cells as shown in Figure 80, with 4',6-diamidino-2-phenylindole (DAPI) counterstaining.

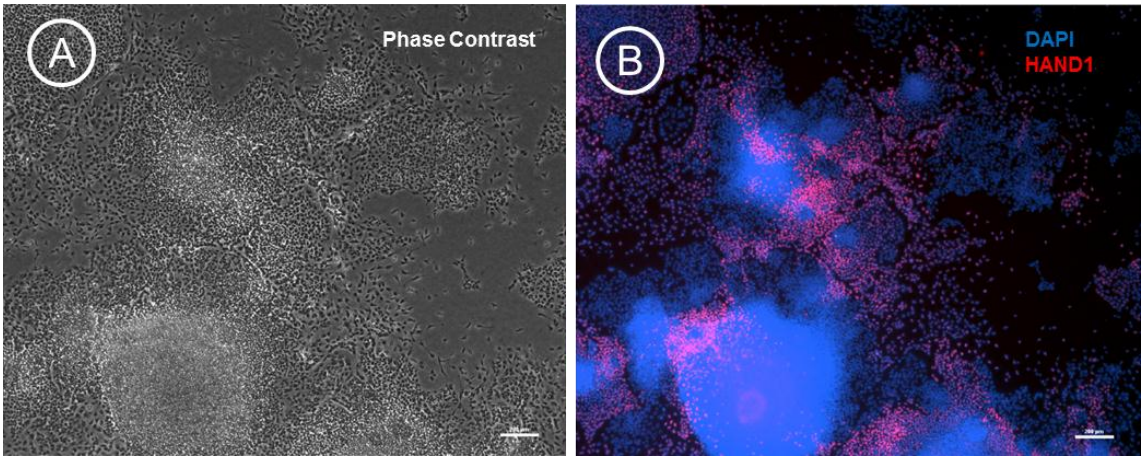

Figure 80. Phase and fluorescence image of embryonic colonies post differentiation. After 2 days of being exposed to differentiation media. DAPI is shown in blue with HAND1 shown in red. The core of the colonies is negative for HAND1 whilst the periphery cells are positive. This therefore agrees with the morphological analysis where the edge cells are in a different culture state to the colony core.

The immunostaining shows that around the periphery of the colonies there is positive staining of the edge cells for HAND1, whereas the central core of the colonies are predominantly blue, showing DAPI staining. This shows that our cocktail of growth factors induces mesoderm differentiation, with the image analysis correctly depicting this differentiation in measuring edge cell growth.

The data in Figure 78 is taken from only 2 colonies exposed to different conditions; however it is possible to average the data from all the colonies to see the overall effect of edge cell coverage and core periphery coverage. The average data is taken from 3 wells of each condition capturing 9 images per well, giving a total of 27 images per condition. This is shown in Figure 81 as a growth curve of edge cell coverage over time.

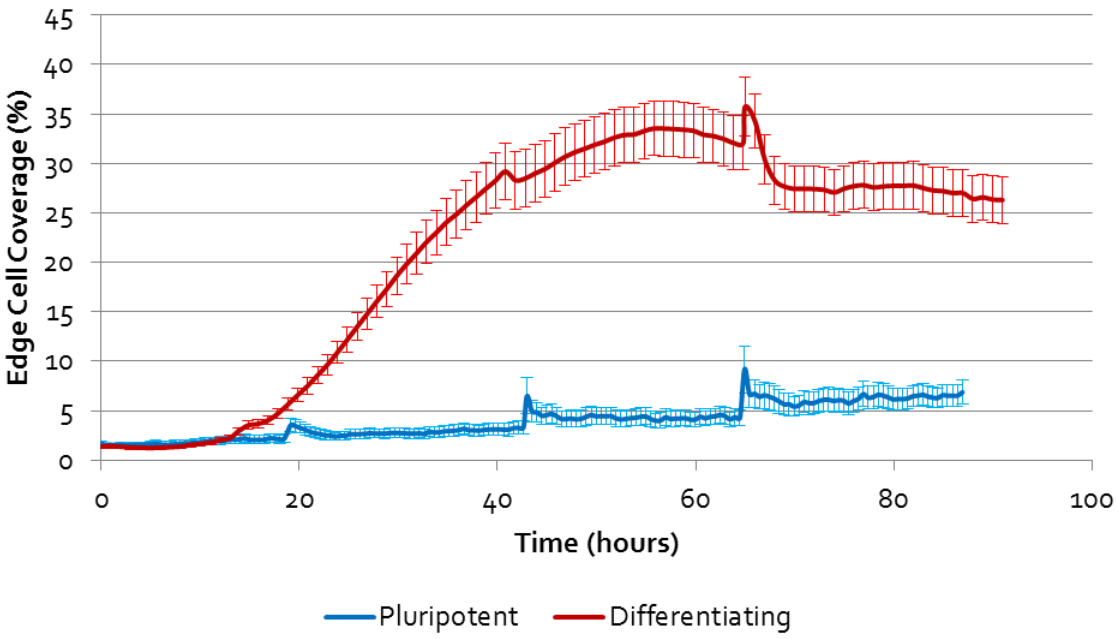

Figure 81. Averaged edge cell coverage for pluripotent and differentiating colonies. This graph visualises the mean difference between colonies kept in a state of pluripotency; where the edge cell coverage increases at a much slower rate than that of colonies exposed to differentiation media (mTeSR-1 with growth factor addition). The fluctuations show the feed points roughly every 24 hours during culture. (The error bars represent the standard error of the mean, n=27).

Colonies are passaged and left for 24 hours to attach before any treatment is started. Zero hours represents the time that imaging begins which is 24 hours after passaging and the same time as a differentiation stimulus is introduced to half of the cultures, pluripotent colonies remain in pluripotent media.

There is a 12 hour delay before any effects are seen with the differentiating colonies, after 12 hours there is an exponential growth in edge cell coverage, this is in stark contrast to the pluripotent maintained colonies that remain with edge cell coverage of less than 5%.

From ~20 hours there is a marked difference in the edge cell growth rate which allows a distinct discrimination between the differentiating population and the population not exposed to a differentiation stimulus. It is important to draw a quantitative value from the data that predicts this morphological difference at the earliest time point with the highest resolution. At 20 hours the 2 lines including error bars separate from each other. This is the earliest time point where the resolution is sufficient to quantitate a difference in the two populations. A key aspect of this

separation is the error bars. This is conducted with a sample of 27 selected colonies, to be useful for process control the sample size can be tailored for a given error, and therefore resolution can be tailored to the process requirements.

The spikes seen at ~40 hours and ~65 hours are due to the auto focussing that occurs when the plate is removed from the incubator, the media is replenished and the plate is returned. As discussed previously the first image was given a 50 µm Z-stack to focus the first image. This is suitable when only a small deviation from the focal point is made, a much larger Z-stack to find the focal point is required though should the culture vessel be placed back into the Cell-IQ further than 50 µm from the original placement. From the spikes it is possible to see when 50 µm was not adequate, producing variable time periods of erratic data. For this data set these spikes do no interfere with the overall trend, and such is the resolution they do not disturb the result. However further hardware improvements could address this issue by better autofocussing following the plate removal.

4.3.1 Conclusions

By using growth factors to initiate differentiation in a pluripotent population it is then possible to monitor differentiation thorough the change in morphology detected predominantly with the edge cell coverage metric. After the addition of a differentiation stimulus the morphology begins to rapidly change after a 24 hour lag period. This is detected as an increase in edge cell morphology which can be used to calculate a percentage of differentiation. This provides a tool to monitor and measure the rate of differentiation. With this information it is possible to use image derived metrics to improve differentiation processes, an example of this is shown in the next section.

4.4 Using Image Derived Metrics to Improve Differentiation Yield

It has previously been reported the importance of embryonic colony size on differentiation induction (140,141). This work aims to provide an optimum colony size for differentiation as measured by complete differentiation to a homogenous morphological state.

4.4.1 Colony Size Distribution

The first stage is to identify the size distribution that follows from a passage. Due to the macro growth and distribution of colony size it is hypothesised that colony sizes are very variable, and are affected by many factors including, previous growth rates, pluripotent status and pipetting technique. A typical distribution from passaging H9 colonies as disclosed in the methods section 2.2.3 is shown by Figure 82.

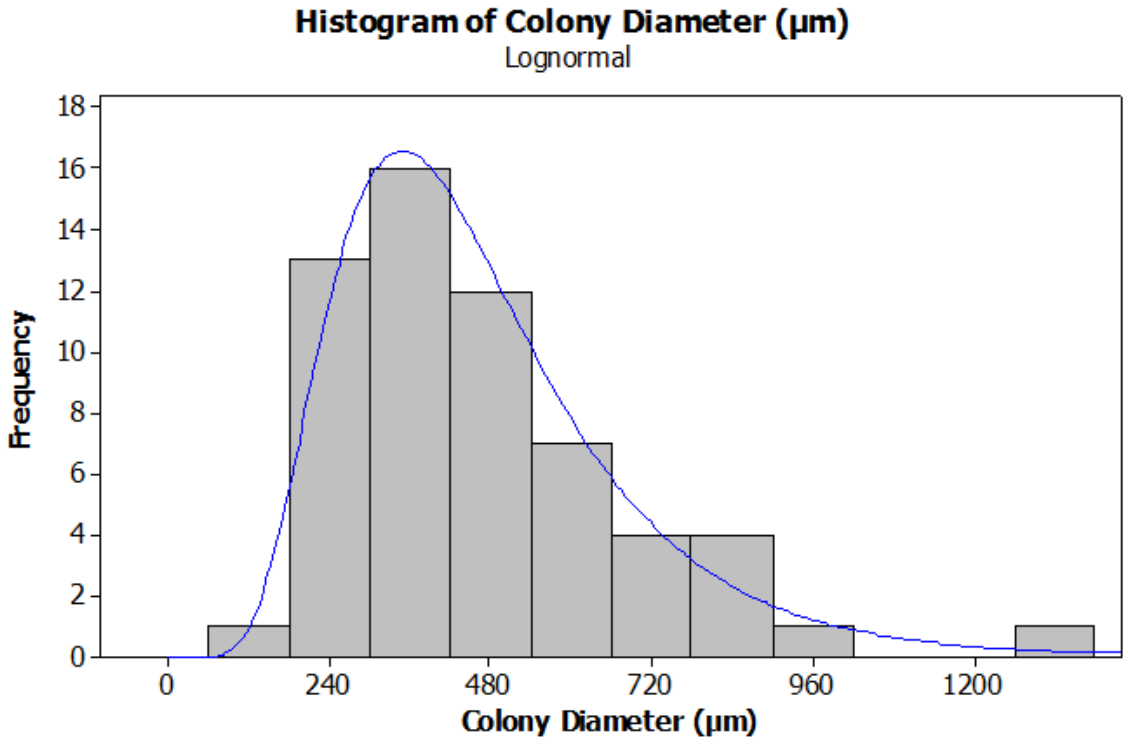

Figure 82. Colony size distribution following a passage. This shows a lognormal distribution, as measured from image analysis, centred around a peak colony diameter of ~350 µm for 58 identified colonies 24 hours after passaging. This allowed colonies to adhere to the surface prior to imaging, n=58

A lognormal distribution centred around a peak colony diameter of ~350 µm is recorded from a sample of 58 colonies analysed 24 hours after a passage. The 24 hour delay allows for colonies to adhere to the plastic surface prior to imaging and analysis. This data shows that as predicted there is a large variation of colony sizes that are produced following passage. This provides one variable which may affect the differentiation efficiency, and therefore is further analysed.

The initial diameter of a colony can be plotted against its diameter of a later time point. This therefore shows if all colonies grow at the same rate independent of size, or if there non-linear growth with respect to diameter. Figure 83 shows colonies at 24 and 36 hours in both pluripotent media and differentiating media. The differentiation media is added at 24 hours, therefore taking a 36 hour time point neglects any morphological response.

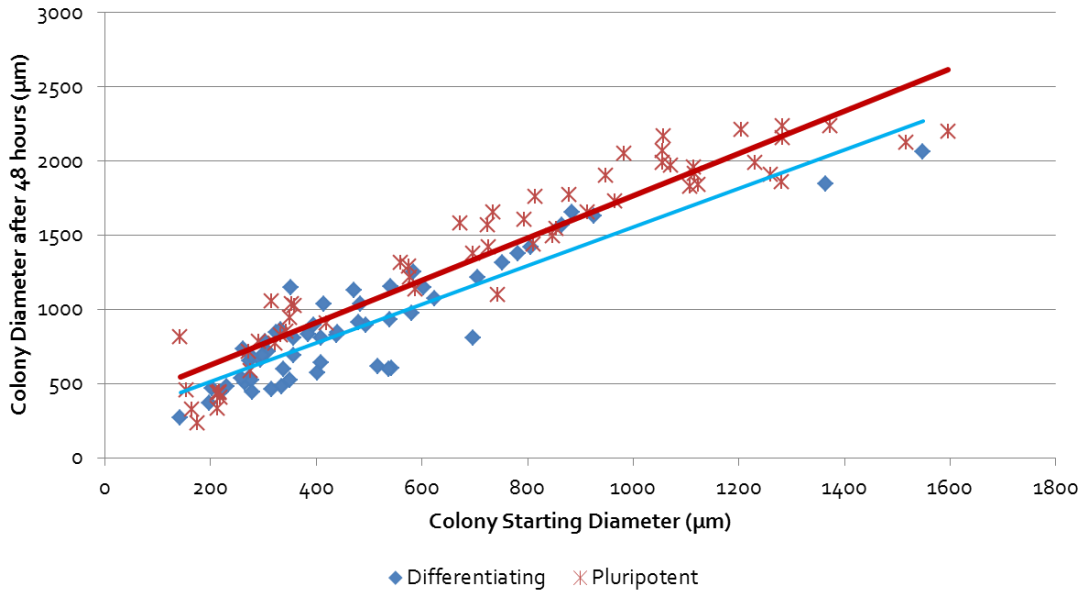

Figure 83. Diameter of colony at 24 hours against 36 hours By comparing the first 36 hours of data for differentiating colonies (BMP-4, Activin-A, FGF and VEGF addition) and pluripotent conditions the same trend is seen. The growth rate overall of each colony therefore remains the same initially, the difference in gradient of the two best fit lines shows differentiation colonies grow slower. (n=58)

Figure 83 shows a linear relationship between initial and colony diameter after 36 hours during culture in both pluripotent and differentiation conditions. It is important to note here that diameter is used as a predictor of growth, which is an area. The relationship between diameter and area is squared. This data therefore suggests growth is slowed in larger colonies, although due to the

tailing off at large diameters, is can be assumed that this effect is negligible and within the error of calculation when used within the range of 200 µm to 1200 µm. It is clear from this that the line of best fit for differentiating colonies falls below that of pluripotent conditions, suggesting that differentiating colonies grow slower. However this slow in growth rate could be due to a change in culture state that is not morphologically measureable until later in the culture. Now that the growth of colonies has been shown not to be influenced on size it is possible to evaluate the colonies differentiability.

4.4.2 Effect of Colony Size on Differentiation Efficiency

It has been highly documented that extensive dissociation of hESC colonies into single cells during serial passage severely compromises the survival and propagation of these cells in vitro (114). ROCK inhibitor is used to prevent differentiation of embryonic single cells (142), but routinely for established embryonic culture protocols cells are passaged as clumps rather than single cells (91,114). This work has suggested that the size of the hESC colonies is an important factor in maintaining their viability and pluripotent status, although to date there are no reports of being able to monitor or control the size. Mechanical dissociation used to be the only dissociation method to control colony size with varied estimates of clump sizes of 100 cells being optimum (114). Recently tools have been developed to help control colony size during passage which include the STEMPRO EZPassage from Life Technologies (143) and ReLeSR from StemCell Technologies (144). Although these are reported to help control colony size EZPassage tool is not suitable for scale-up or for use in culture flasks and on testing ReLeSR it has no effect on the removal of embryonic stem cells from matrigel. This work aims to test the importance of colony size whilst producing a method of quantitative analysis of colony sizes, whilst maintaining mechanical dissociation.

In order to evaluate if size affects the ability of colonies to differentiate, colonies are initially measured and then after differentiating can be assessed for edge cell colony. This provides a

measurement system for evaluating the differentiation capabilities of colonies of varying size, and to identify if control of size is an important factor. The results of 58 colonies are shown in Figure 84.

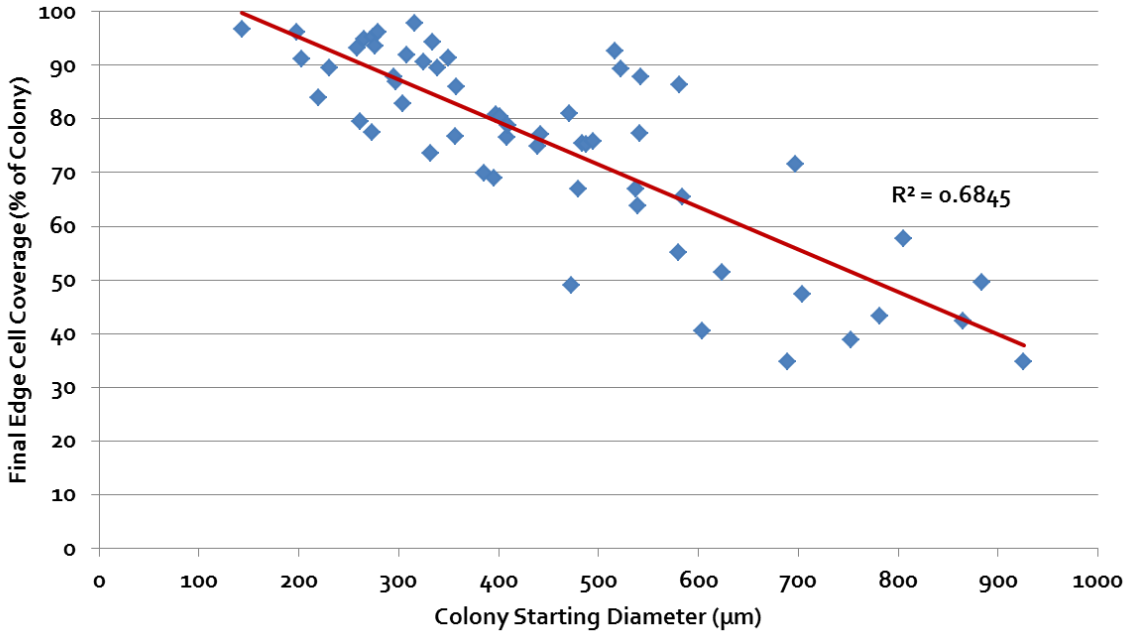

Figure 84. Relationship of colony starting diameter to final edge cell coverage. Colonies diameters are measured prior to the addition of a differentiation stimulus, then after 3 days of being exposed to differentiation media the edge cell coverage is recorded as a percentage of the total colony coverage. The relationship shows that as colonies increase in size they are poorer at complete differentiation. This is shown by a decreasing percentage of final edge cell coverage as the diameter increases. This data suggests that smaller colonies are required for homogeneous differentiation. (n=58)

Figure 84 shows a range of colony diameters from 150 µm to 900 µm, measured prior to adding differentiation stimuli in the form of a cocktail of growth factors (BMP-4, FGF, VEGF and Activin-A). After 4 days of culture the edge cell coverage is measured as a representation of differentiation. There is a decline in the percentage of edge cell coverage with increasing colony diameter. For this experiment edge cell coverage is expressed as a percentage of the total colony, previously it was reported as a percentage of the total image. This data therefore suggests that the larger colonies maintain a morphologically pluripotent area, whereas the smaller colonies completely differentiate. This is validated by assessing the images, the small colonies differentiate causing single cells to migrate from the colony periphery causing the pluripotent colony to shrink and eventually

disappear. The larger colonies follow this as well but due their size a core of pluripotent morphological colony remains as shown in Figure 85.

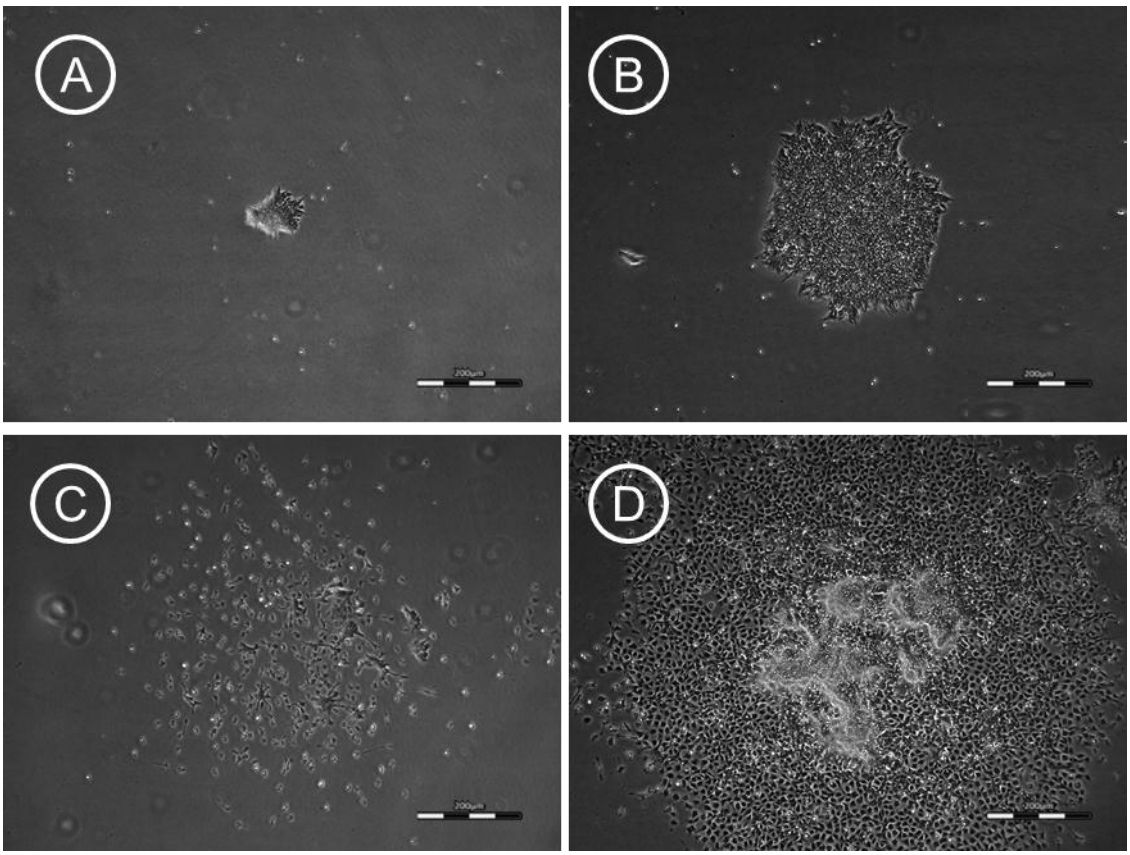

Figure 85. Comparing the effect of small and large colonies differentiating. The small colony in image A) appears to completely disintegrate into single cell morphology in image C), whilst larger colonies, such as the one in image B), remain with a core of colony morphology with just the periphery showing signs of differentiating in image D).

The difference in disintegration of small colonies and a remaining core in larger colonies is size dependent and can be correlated back to their starting diameters prior to the addition of differentiation stimuli. There is a clear divide between colony size in Figure 85 A) and Figure 85 B), 200 µm and 900 µm respectively. Then after differentiating Figure 85 C) shows a colony that has disintegrated into a homogeneous morphology whereas Figure 85 D) maintains a central core of pluripotent morphology as well as edge cell coverage around the periphery. This therefore provides evidence that there is critical colony diameter where complete differentiation of a colony occurs based on morphology. The data in Figure 84 suggests that this decline in homogeneity is immediate with increasing diameter. This experiment was completed over 3 days, by increasing the time it

would be hypothesised that there would be a decrease in the line of best fits gradient as less central core remains. However it is important to consider that the longer the period of time during differentiation may cause further phenotypic changes, and a further lack of homogeneity. Therefore a trade-off between time, number of cells and homogeneity exists. This difference in reaction to differentiation stimuli is important for controlling homogeneity, where clearly the larger colonies have at least 2 cell morphologies, whereas the smaller colonies only have a single morphology present. The effect of size on differentiation potential has been noted previously by many groups that have had trouble culturing and passaging single embryonic stem cells. Peerani et al. showed that 'endogenous signalling and pluripotent gene expression change with colony size' (141). Furthermore Watanabe et al. reported that a critical colony size was required to antagonize pSmad1 activity which in turn prevented differentiation (142). The data also suggested that ROCK inhibitor, which is often utilised to permit single ESC growth (92,145,146), may have similar function in pSmad1 regulation (142). Heng et al. studied the effect of split ratios during passaging on the differentiation capacity of hESCs, they found that higher split ratios increased differentiation ability (124). However this study did not look at colony size although their images suggest that the higher split ratios produced smaller colonies, likely to be due to mechanical dissociation.

4.4.3 Conclusion

In conclusion this section has shown that the smaller colonies have a greater tendency to differentiate, whilst the larger colonies are able to prevent differentiation within a central core. This is likely to be governed by microenvironments (140,141,147), with larger colonies producing more factors into the surrounding media to maintain pluripotency. However in order to fully understand this further analysis needs to be conducted, especially assessing media components in the microenvironment. This could be particularly useful for complete differentiation where the cells are to be used within therapy where pluripotent cells are undesirable due to side effects such as teratomas production which have been seen after injected into mice (101,114,148,149).

One hypothesis that contradicts the homogeneity statement above would be that this core of pluripotency is critical for certain lineage development, and therefore is required. This method therefore allows a measure of pluripotency core; either stimulating differentiation in large colonies to retain a pluripotent core or differentiating small colonies to retrieve a more homogeneous population.

Here a tool to quantitate the level of differentiation within a colony has been utilised to show how image analysis can be used to improve the homogeneity and/or yield for stem cell differentiation.

4.5 Real Time Analysis for Prediction and Process Improvement

The post image analysis of data provides useful information to link responses to causalities. For the manufacture of cell therapies an online version of this tool would provide an improved mode of operation to make informed process decisions. After consultation CM-Technologies, the company that developed the Cell-IQ, built an online analysis tool that provides real-time data, Real-Time Analyser. Using the Cell-IQ Real-Time analyser, captured images can be immediately analysed rather than post image analysis. This allows for real time measurements to be made in order to make informed process decisions. In order to test the reliability and suitability of the new software colonies were continually assessed for their diameter based on the threshold method discussed in Section 2.7.1.1.

This allowed for colonies to grow to a given diameter before a differentiation stimulus was added to the media in the form of growth factors, as used previously. It was seen previously that the small colonies differentiate to a single population whereas with larger colonies a core of pluripotent morphology remains. To further test this colonies were plated and then a differentiation stimulus was added to colonies that reached 300 μm or 750 μm. The results are shown in Figure 86 from averaged colony data.

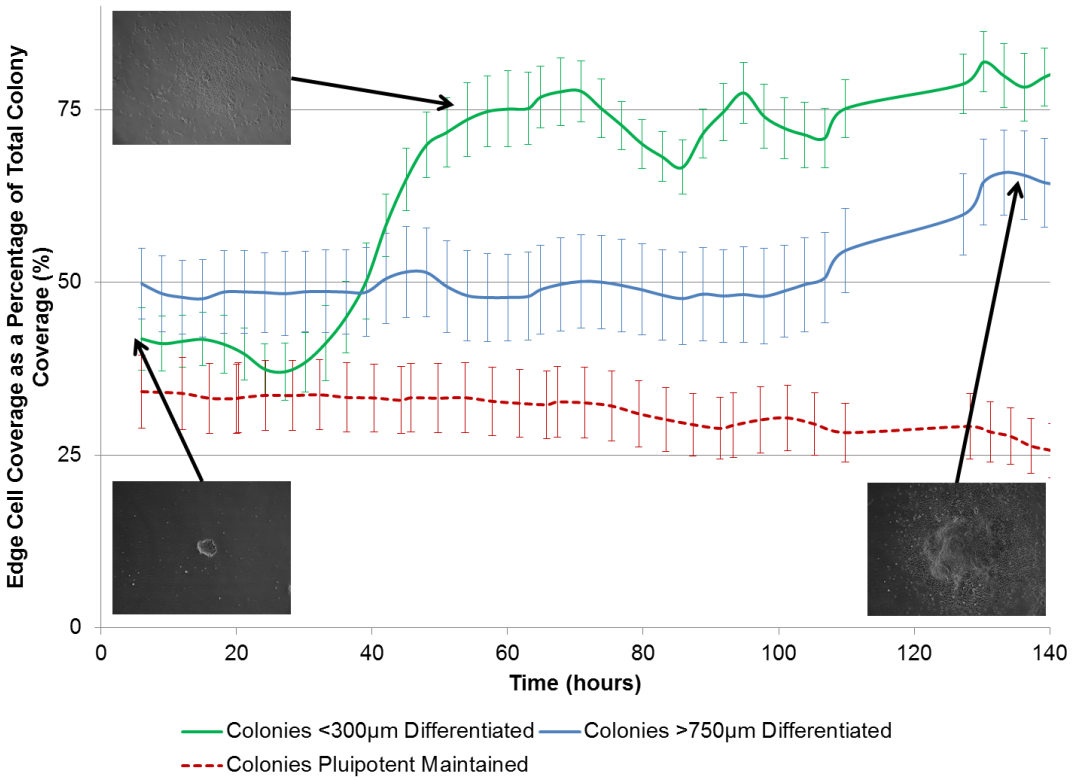

Figure 86. Edge cell coverage of colonies exposed to differentiation stimulus at different sizes, along with undifferentiated colonies. This graph highlights the effect of providing a differentiation stimulus when the colony is small (<300 µm) in comparison to larger colonies (>750 µm). A control of average colonies maintained in pluripotent media is also shown as dotted line. This highlights the core of pluripotency that remains in the larger colony as the peripheral edge differentiates, whereas the smaller colony has complete differentiation shown by the rapid increase in edge cell coverage and remaining core periphery detection. This data is taken form an average of 16 colonies of each type spread over 2 wells in a 6-well plate. Insets show examples of colony morphology at specific places. The data is then smoothed using average of 3 time points. (n=20)

Figure 86 shows that by using real time imaging colonies can be continually monitored and a process action can be taken when a certain criteria is reached. In this experiment the real time analysis provided size data of the colonies. Once the average colony diameter in a well reached 300 µm a differentiation stimuli was introduced. The response can be seen as an increase in edge cell coverage 24 hours after the stimuli. Further colonies remained in pluripotent conditions until the average was 800 µm. After the addition of differentiation media an increase in edge cell coverage is also seen at 110 hours. However the difference in percentage of edge cell coverage can be seen by comparing the spike of edge cell growth. The smaller colonies reach ~80% edge cell coverage whereas the larger colonies reach ~60%. This difference is due to the remaining central core of

pluripotent morphology within the larger colonies, whereas the smaller colonies completely separate into single differentiated cells.

These colony sizes were chosen to represent two different outcomes as identified in Section 4.4.2, Figure 84. As can be seen the smaller colony differentiates with only a small amount of core periphery detected, which is actually due to larger colonies identified on the edge of the image as seen in Figure 87.

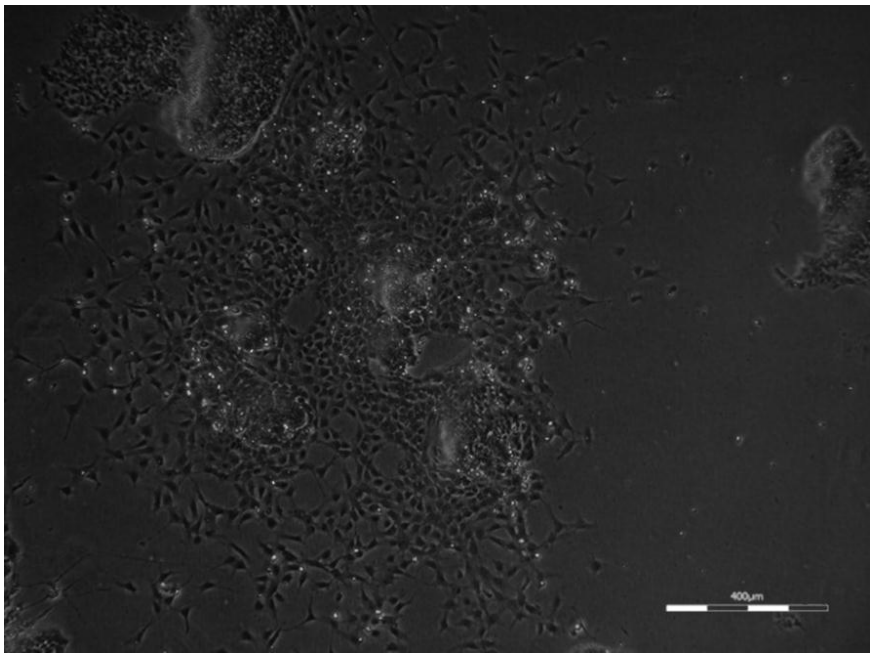

Figure 87. Image of small differentiated colony with larger colonies on the image periphery which will be identified in the analysis and therefore skew the data.

The larger colony keeps this central core of pluripotency shown by the continual increase of core periphery coverage. The edge cell coverage drops off onwards of 150 hours due to the overcrowding of edge cells which begin to form a more core periphery like appearance. Importantly this data also correlates back to the previous experiment which identified edge cell coverage after 3 days of differentiation in a range of diameters in Figure 84. Taking the diameters of 300 µm and 800 µm it can be seen that the edge cell coverage was ~80 and ~60% respectively in Figure 84. This repeat therefore emphasises the effect size has on differentiation capacity.

4.6 Conclusions

This chapter has highlighted the utility of using image derived metrics to analyse the culture state of a pluripotent and differentiating population. By following the behaviour of these metrics overtime it is possible to evaluate the response to different stimuli. The ability to measure colony size non-invasively has allowed feedback correlation to the differentiation ability of the colonies. This has provided evidence to highlight the importance of colony size on differentiation ability and therefore provides a measure of control. The final example in this chapter has shown how measuring one metric such as colony diameter can be used to improve differentiation yield, also measured non-invasively. By continually monitoring the size, the time point where colonies are at a suitable size can be used to improve differentiation yields. This chapter has highlighted the ability to do this initially with work providing evidence of the effect of size, and then consequently developing online monitoring software to allow such control. This therefore highlights the benefits of using image derived metrics to make process decisions and gather further data regarding the culture state of a population.

5. QUANTITATIVE NON-INVASIVE IMAGE ANALYSIS FOR COLONY FORMING UNIT ASSAY FOR FUNCTIONAL EVALUATION OF HAEMATOPOIETIC PROGENITOR CELLS

5 Quantitative Non-Invasive Image Analysis for Colony Forming Unit Assay for Functional Evaluation of Haematopoietic Progenitor Cells

5.1 Introduction

Hematopoietic stem cells (HSCs) are derived from ventral mesoderm, and the sequential sites of haematopoiesis during development include the yolk sac, fetal liver, placenta, and within adult mammals, the bone marrow (150). The properties of HSCs produced in each tissue differ, presumably reflecting diverse niches that support HSC expansion and/or differentiation (151). The primary function for primitive haematopoiesis is production of red blood cells (RBCs) that facilitate tissue oxygenation as the embryo undergoes rapid growth (152,153). The hemangioblast of the yolk sac is proposed to give rise to both blood and endothelial cells. Subsequent definitive haematopoiesis involves the colonization of the fetal liver, thymus, spleen, and ultimately the bone marrow. In definitive haematopoiesis, long-term HSCs (LT-HSCs) give rise to short-term HSCs (ST-HSCs). ST-HSCs produce common myeloid progenitors (CMPs) and common lymphoid progenitors (CLPs). CLPs are the source of committed precursors of B and T lymphocytes, whereas CMPs give rise to megakaryocyte/erythroid progenitors (MEPs) and granulocyte/macrophage progenitors (GMPs). GMPs give rise to the committed precursors of mast cells, eosinophils, neutrophils, and macrophages (154–156), this is shown in Figure 88.

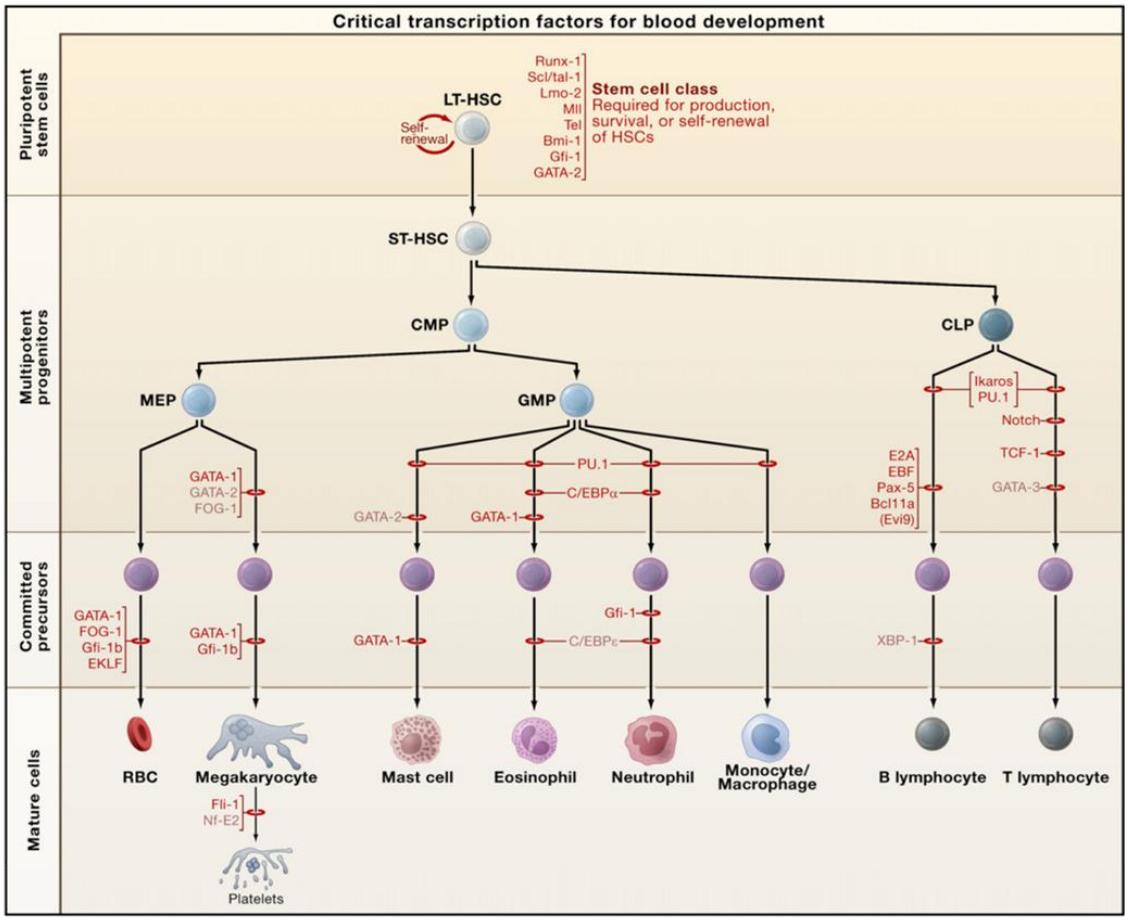

Figure 88. Lineage tree for haematopoiesis. This shows the lineage pathway from haematopoietic stem cell through to fully differentiated cell types for blood development along with critical transcription factors. Abbreviations: LT-HSC, long-term hematopoietic stem cell; ST-HSC, short-term hematopoietic stem cell; CMP, common myeloid progenitor; CLP, common lymphoid progenitor; MEP, megakaryocyte/erythroid progenitor; GMP, granulocyte/macrophage progenitor; RBCs, red blood cells (150).

5.1.1 Definition of human Hematopoietic Stem Cells

As discussed previously blood cells are responsible for the maintenance and immune protection of every cell type in the body. The stem cells that form blood and immune cells are known as hematopoietic stem cells (HSCs). They are responsible for the continual production of billions of blood cells every day. Hematopoietic stem cells have been studied for more than 50 years (157), however there still remains challenges in their production, maintenance and detection *in vitro*. This therefore has a knock-on effect that if they could be produced rapidly, reliably and truly identified then research would progress on characterisation (157).

5.1.2 Haematopoiesis

Mature blood cells are short lived and therefore there is a need for constant renewal throughout a lifetime. This is achieved by haematopoietic stem cells (HSCs) continual replenishment of multilineage progenitors and the precursors committed to individual haematopoietic lineages (150). HSC are defined by their operational capacity to reconstitute the entire blood system, with billions of red blood cells produced each day. HSCs therefore serve as a constant reservoir for the regeneration of haematopoietic lineages.

Umbilical cord blood (CB) derived HSCs, have been shown to promote stronger immune recovery and show fewer instances of immune rejection (158). However, CBs have fewer stem cells and progenitors per unit, making a single unit insufficient for complete repopulation in an adult patient and limiting CB use mainly to paediatric cases. Various techniques have been proposed to boost the HSC potential of CB, including incubations with biological modulators or small molecule compounds as well as a novel fed-batch approach to cell culture. Several of these are in clinical trials now, and could show significant improvements in the HSC levels derived from CB allowing the technique to be used for adult transplants (158).

5.1.3 Clinical Relevance / Need

Stem and progenitor cells can be collected from the bone marrow, mobilised peripheral blood or cord blood and used to restore hematopoietic activity in patients who have undergone chemotherapy or irradiation, destroying their bone marrow. Worldwide there are over 60,000 HSC transplants annually (159), currently total nucleated cells (TNC's) and the colony forming unit (CFU) assay are used as predictors of engraftment. However TNC's are becoming less popular as further studies prove their lack of correlation to engraftment, suggesting that only CFU assay is a true predictor of hematopoietic quality *in vitro* (160–162). The CFU assay provides both a count and functional assessment of hematopoietic progenitors.

Another aspect where the CFU assay is utilised is in the manufacture of blood cells (163–166). More than 80 million units of whole blood are collected from donors worldwide every year (167). Supply constraints and uncertain screening for infectious diseases are of particular concern in developing and transitional nations. In wealthy nations the other side of the coin is the occurrence of multiple immunisations to RBC antigens in 0.1% to 0.5% of transfused patients, leading first to difficulty in finding compatible RBC concentrates and very high costs, and eventually to full transfusion blockade (168). In response to these concerns, ex vivo manufacture of RBC from stem cells makes sense to enable safe and quantitatively sufficient transfusion. This is the concept of cultured RBC produced ex vivo from hematopoietic stem cells originating from bone marrow, peripheral blood, cord blood or pluripotent stem cells. Research is already focused on the feasibility of this approach at the industrial level US Defence Advanced Research Programs Agency (USDARPA)'s 'Blood Pharming' program (169). Further work looks to build on this background with the identification of an unlimited source of RBC's allowing the production of cultured RBC from the constraints of the supply of hematopoietic stem cells (168,170).

5.1.4 Current Identification Methods

The analysis of haematopoietic progenitors is complex and needs to be fit for purpose. Two types of assays can be used to identify haematopoietic progenitor cells, either phenotypic assays that measure a biological marker or functional assays which measure the cell's capability.

5.1.4.1 Phenotypic Assays

Phenotypic assays measure physical properties, such as expression of cell surface antigen marker CD34, or expression of the intracellular marker of stemness such as the enzyme aldehyde dehydrogenase. These individual markers associated with specific cell types can be retained after functional properties are lost, and therefore an over estimate of the number of stem or progenitor cells is possible. So if cells that have already begun apoptosis are not excluded from the assay they

can over estimate the number of progenitors in a population, especially if the cells have undergone a freeze thaw cycle.

Clonogenic cells are a minority of a routinely identified phenotypic subpopulation. Within the CD34+ population only 10-20 % have the potential to form a colony, a functional cell with the ability to proliferate and differentiate. Therefore using CD34+ cells as a measure of functional cells would also provide an over estimate. It has previously been identified that the population of CD34+ cells are heterogeneous containing a variety of maturation levels (171), and a variety of marker expressions including CD13, myeloperoxidase (MPO) and CD33 (172). This is further examined by Page et al. who conclude that CD34+ count is only weakly correlate to engraftment and function and that colony forming unit assay is a much better predictor although more time consuming with currently a 14 day wait time for results (161).

A list of cell-surface markers of undifferentiated hematopoietic stem cells proposed in 1992 by Baum et al. are shown in Table 15, however these markers are still disputed today (157) with CD34 being the most widely used marker for HSC's.

Table 15. Cell-surface markers of undifferentiated hematopoietic stem cells. A list of positive and negative surface markers to define haematopoietic stem cells as proposed by Baum et al. (173)

$CD34^{+}$
$CD59^{+}$
$Thy1^{+}$
$CD38^{-/low}$
$C\text{-}Kit^{-/low}$
Lin^{-}

5.1.4.2 Functional Assays

Functional assays directly measure biological properties such as engagement with the niche, cell proliferation, differentiation or response to a stimulus. As the assay occurs over a period of time only viable stem and progenitor cells are detected, as the cells have to be alive and healthy over the entire assay period. Functional assays can either be *in vivo* or *in vitro*. An *in vivo* assay is the best method for identifying the most primitive with long term repopulating ability and often involve a transplantation (174). By irradiating a mouse of its HSC population, a population of cells can then be injected. If then there is a detection of lymphoid, myeloid and erythroid progeny within the host the population is deemed to have contained long term HSC's (173). This typically is at least 5 weeks after transplantation, is very expensive, cannot be conducted on humans and is impractical for routine use in lab procedures found in cord blood banks or transplant labs. Therefore in-vitro assays are more commonly found in laboratories that use either liquid or semi-solid systems. *In vitro* culture assays are used to detect the proliferation and differentiation ability of haemopoetic progenitor cells. The ability of these progenitors to produce colonies is the basis for the colony-forming unit (CFU) assay.

5.1.4.2.1 Colony-Forming Unit (CFU) Assay

Currently the gold standard to assess the frequency and number of hematopoietic stem and progenitor cells is the colony-forming cell (CFC) or colony forming unit (CFU) assay (175). This in vitro assay requires a small sample of cells to be placed into a semisolid culture medium containing a suitable cocktail of growth factors (176) and incubated for 14-16 days. The gel results in limited dispersion of replicating cells allowing locally dense populations to be visualised where cells are highly proliferative. The gel effects migration of the cells which is dependent on the cell character. The morphology is the key characteristic along with colour that is currently used to identify the starting cell population. Progenitors in different stages of maturation produce colonies differing in size, morphology and composition. This assay directly measures the number of viable progenitor

cells, with 1 colony being formed from 1 CFU. Examples of colonies produced are shown in Figure 89.

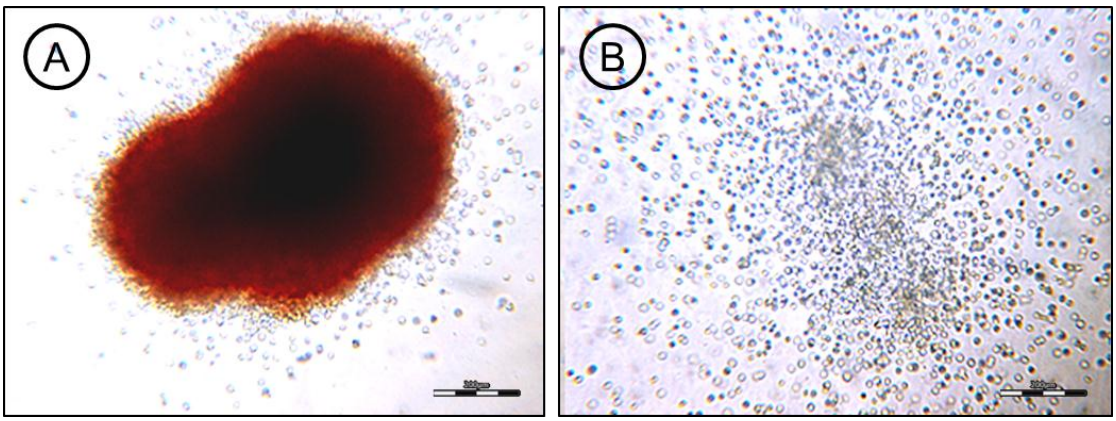

Figure 89. Haematopoietic progenitor colonies. Example of BFU-E (A) and GM (B) colonies cultured for 14 days in MethoCult, followed by taking brightfield images. These images highlight the difference in morphology and colour which currently is user defined. Reproduced from (177)

The CFU assay has been shown to be the single best predictor of successful engraftment following a cord blood transplantation by a number of research groups (161,164,178). Prasad et al. showed that the number of CFUs infused is the best measurement and the only technique that correlates to the overall survival (178). Total nucleated cells (TNC) and CD34+ cell counts were seen to be less predictive then the CFU results, the same outcome was acknowledged by Page et al. (161).

The CFU assay remains the gold standard tool for haematopoietic stem cell research *in vitro*, and provides the best measure of cord blood unit engraftment potential (179). There are several international standards that recognize the importance of the CFU assay including the *FDA Guidance for Industry: Potency Tests for Cellular and Gene Therapy Products (2011)*, *FACT: Draft 5th Edition of the NetCord-FACT International Standards for Cord Blood Collection, Banking and Release for Administration (2012)* and *AABB: Draft 6th Edition of the Standards for Cellular Therapy Products (2012)* which states that 'the colony-forming unit or equivalent functional assay shall be performed before distribution' when discussing cord blood transplants (180–182).

The CFU assay is abundantly used within research alongside numerous steps within cord blood banking and transplantation, as shown in Figure 90.

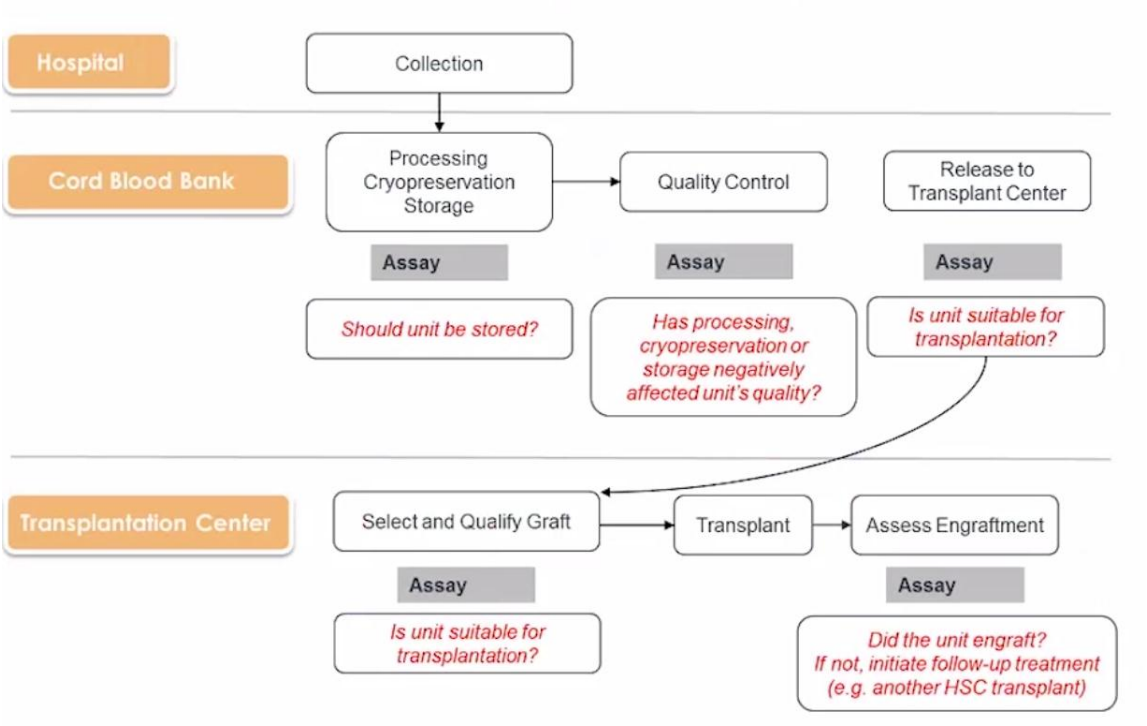

Figure 90. Time points in processing where CFU assay is commonly utilised. Within the cord blood banking and transplantation procedures there are many points where CFU assay is often used to verify cell number and quality (179). In this figure five CFU assay points are identified from collection through to patient delivery.

After the cord blood is collected and processed for storage, the assay is first used to determine whether the cord blood should be stored, if there are sufficient progenitor cells to warrant storage, which is determined from a minimum threshold. Cord blood can then be routinely thawed to check that the cryopreservation procedure has not had any adverse effects on the number of progenitors within the cord unit, and therefore be used as quality control test. A CFU assay is also required by regulatory bodies before a cord blood can be released to a transplant centre.

The transplant centre itself may elect to confirm the results from the cord blood bank prior to transplantation, and then sometime after the transplant a sample of blood is taken from a patient to perform another assay to confirm unit engraftment.

However even with the CFU assay playing a dominant role in measuring the quality of cord blood units there are many associated problems which include time for the analysis outcome, standardisation with measuring the colonies and variability connected with colony defining.

The Cell-IQ has shown previously (Section 3.6) that it has the capability to continually monitor and analyse cell cultures. By using 'machine vision' the colony types can be automatically identified and therefore the variability associated with user-definitions of colony populations is addressed. This also standardises the counting ability as well through the use of automation. The last concern is the current 14 day period that is required before the results are known.

Continual monitoring allows rates of change to be assessed such as those in Section 3.6. By assessing changes greater differentiation between heterogeneous progenitor populations may be distinguished. Potentially this permits the detection of sub-populations of colony forming cells based on growth attributes. This also could allow for colonies to be reproducibly identified prior to the current 14 days.

As discussed by Pamphilon (183) in his review paper of current techniques across 105 researchers there are three commonly categorised colony species. These being burst forming unit-erythroid (BFU-E), colony forming unit – granulocytes, macrophages (CFU-GM), and colony forming unit - granulocytes, erythrocytes, macrophages and megakaryocytes (CFU-GEMM). It is therefore important that any automated system has the ability to detect these colonies to improve on current user defined categorisation.

This chapter aims to:

- Correlate the growth characteristics seen in a standard incubator to the Cell-IQ imaging platform.
- Define quantitative, novel, image derived metrics to automate colony classification.
- Measure metrics over time to correlate observed metrics to colony phenotype.
- Identify sub-populations within each classification based on image derived metrics.

5.2 CD34+ Cell Separation from Fresh Cord Blood

The first stage of developing the CFU assay was to isolate CD34+ cells from fresh cord blood. This was completed using the Ficoll-Paque method (Section 2.10) followed by magnetic-activated cell separation (MACS) as described in Section 2.11. Cell counts were conducted throughout the protocol as recorded in Table 16.

Table 16.NucleoCounter counts from CD34 separation procedure. Taking cell counts as the CD34 positive population is separated from fresh cord blood. This shows as expected that about 1% of the starting population is positive for CD34.

Counts conducted on…	Average Cell Count
Fresh Cord (Trypan blue method)	$4.88x10^8$
MNC's after Ficoll Paque	$1.17x10^8$
CD34+ Population	$1.08x10^6$

Following the Ficoll-Paque method nearly 80% of the cells are removed. These are the erythrocytes which are abundant in the fresh cord blood, and the main use of Ficoll-Paque is to remove these surplus enucleated cells. The CD34+ population represented about 1 % of the mono-nuclear cell (MNC) population after Ficoll-Paque, this agrees with numerous papers that document similar percentages (184–187). Flow cytometry was completed after MACS to determine the population purities; representative data is shown in Figure 91.

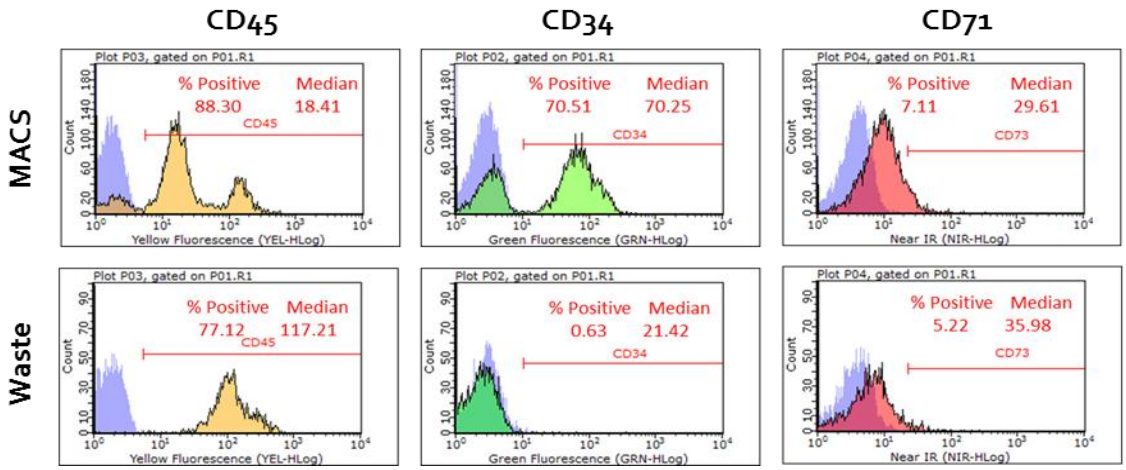

Figure 91. Flow cytometry data from the MACS CD34 purified sample and waste stream. Staining for CD34, CD45 and CD71 it is possible to compare the selected cells to the unselected cells from cord blood. The CD34 selected cells show 70% purity for CD34 in contrast to 0.63% positive in the waste stream. Both CD45 and CD71 are similar in both the selected MACS stream and the waste stream. Gating is based on 1% of the isotype control shown in blue.

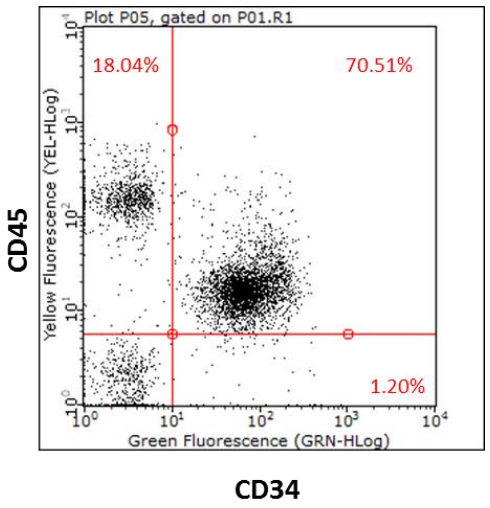

Figure 92. Example dot plot of CD34 and CD45. This plot shows that there are 3 distinctive populations, CD45-CD34-, CD34+CD45+, CD34-CD45+The cd34 positive cells are nearly all CD45 positive as well.

The purified $CD34^+$ population is 70% pure, which is the expected purification performance stated from literature (188,189). This purity could be increased further by passing the cells through another MACS column if required to receive purities closer to 98% (190). The increased purity is a balance between how pure the population required is and how much could potentially be lost through increasing the number of steps during purification. For this study 70% purity was deemed sufficient to analyse colony production. The CD45 positive population shows a double peak; the first peak shows the $CD45^+CD34^+$ whereas the second much smaller peak is the $CD45^+CD34^-$ population. This

is more noticeable in the dot plot shown in Figure 92. Following purification the $CD34^+$ population was frozen into 250,000 cell aliquots. When required cells were thawed and cultured in suspension with samples taken and placed into MethoCult (Stem Cell Technologies) for the CFU assay.

5.3 Equilibrating the Cell-IQ System to a Standard Incubator

The environment in which cells are cultured is critical for development and can be used to change the pathway a cell is directed down. Haematopoietic stem cells are no different and the stem cell niche or microenvironment plays a crucial role in the phenotype characteristics. It has been shown that factors including O_2 tension, O_2 gradients, pH gradients, cytokine gradients, perfusion rates, flow-induced shear forces and biomechanical forces can all effect the decision of progenitor cell fates (191). It is therefore important to maintain a tight control on any assay that is used to functionally characterise these cells.

To ensure the environment within the Cell-IQ is equal to a standard incubator the first experiment placed progenitor cells within MethoCult into both environments. After less than 4 days in the Cell-IQ, the viscous gel is seen to have dried out preventing the formation and growth of colonies, as shown in Figure 93. This drying is not seen in a standard incubator and therefore there must be an environmental difference between a standard incubator and the Cell-IQ culture conditions.

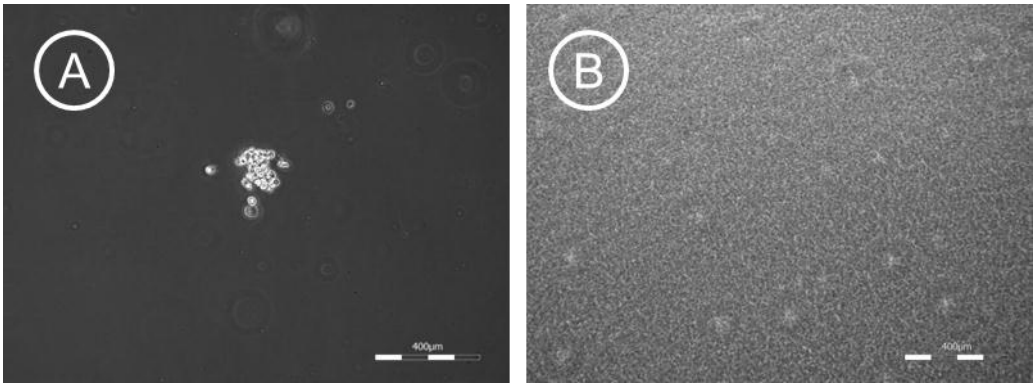

Figure 93. Colony forming unit assay before and after drying. Images showing cells in methylcellulose in a standard incubator and in comparison to that in the Cell-IQ. The Cell-IQ causes the methylcellulose to dry out and appears bright under phase contrast microscopy.

The Cell-IQ causes the methylcellulose to dry out; this is seen as a solid gel rather than the liquid gel that is seen within a standard incubator. Under phase contrast imaging the drying out causes the gel to become more translucent and therefore appear lighter in colour. Also the drying of the gel causes crystal formation shown by the speckled appearance seen in Figure 93. There is a requirement therefore to measure this difference in environment in order to maintain consistency between incubators.

5.3.1 Comparing Environmental Conditions in the Cell-IQ to that of a Standard Incubator

Temperature and humidity sensors allow process monitoring overtime, by comparing sensors in a standard incubator to that of the Cell-IQ any discrepancy can be seen. This was achieved by adapting a 6-well plate to hold the sensor by removing the walls of the centre wells as shown in Figure 94.

Figure 94. Adapted 6-well plate with humidity and temperature sensor MSR 145. By removing the central walls if wells A2 and B2 on a 6-well plate the sensor can fit in the centre whilst wells A1, B1 and A3, B3 can still be used for culture.

By removing the walls from the centre wells on a six well plate a MSR 145 data logger can be placed within the culture vessel (Figure 94). This set-up retains four useable wells that can contain either

water or gel to study the evaporation rates. This set-up was used in both the Cell-IQ and a standard incubator to measure the humidity which is shown in Figure 95.

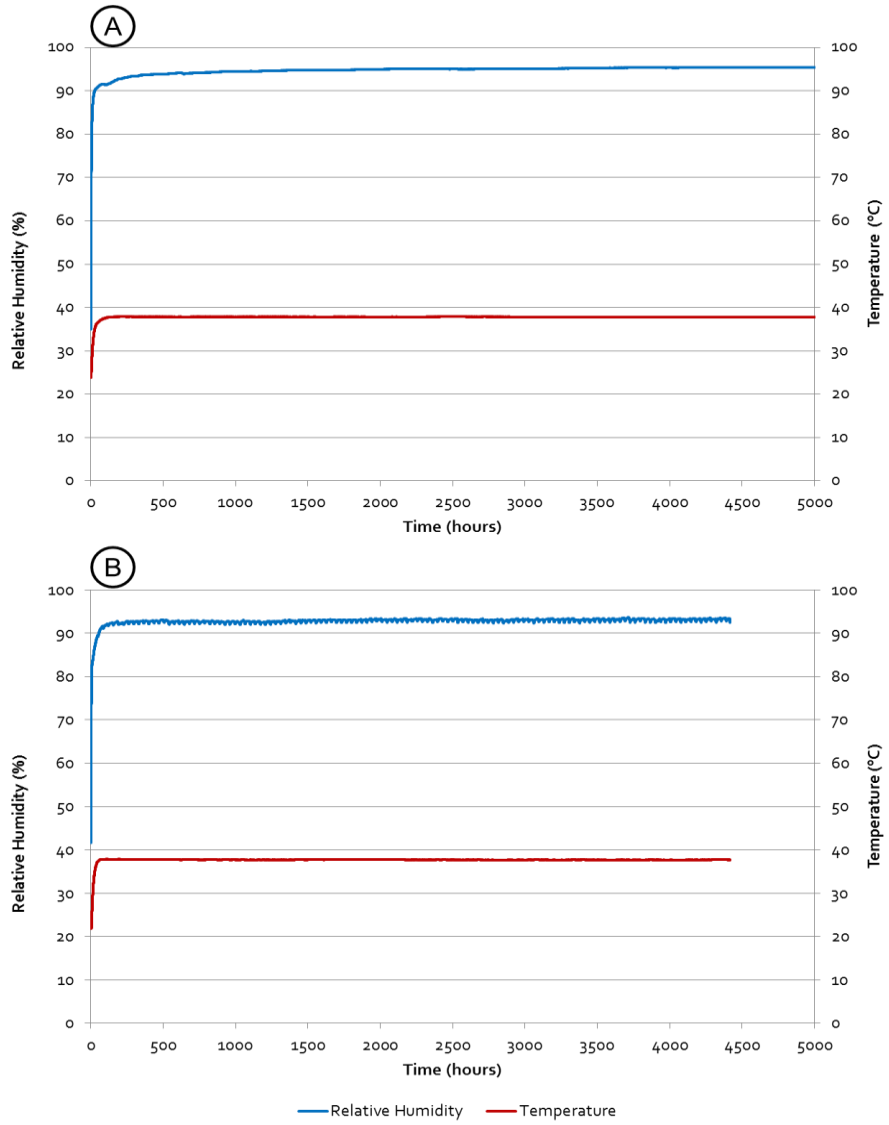

Figure 95. Graph of humidity and temperature variation in a standard incubator (A) and Cell-IQ (B). After placing a temperature and humidity sensor into a standard incubator the true value is quickly approached. There is then very little deviation from the set point. Within the Cell-IQ the sensor quickly reaches the true value, however once reached there appears to be fluctuation within the humidity over time. The gas was on for 5 minutes, off for 20 minutes cyclically during the period recorded here.

Figure 95 shows that the culture vessel in which the probes were inserted quickly rise from room temperature and humidity to ~95% humidity and ~37°C, culture conditions in both the standard incubator (A) and the Cell-IQ (B). The data from the Cell-IQ, Figure 95 (B), shows a 'wavy top' for the humidity, this shows that humidity levels drop but are quickly restored with a negligible effect on

the overall humidity condition. However this 'wavy top' is an important feature of the Cell-IQ conditions. A smaller time period from the humidity graph is shown in Figure 96, which further details the fluctuations.

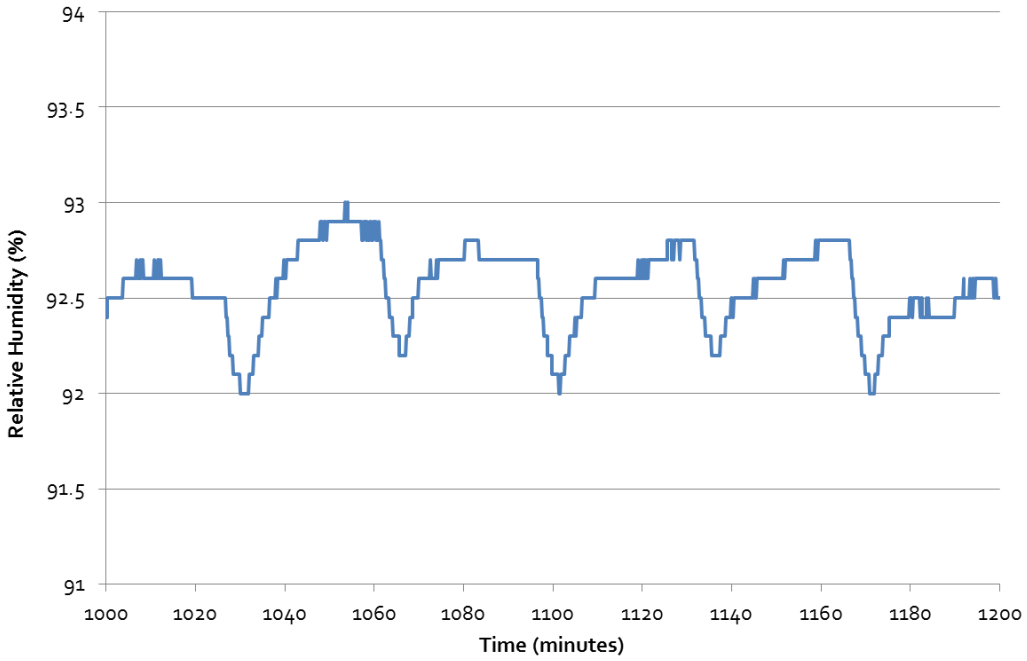

Figure 96. Re-scaled section of graph from Figure 95 showing Cell-IQ humidity. Enlargement of humidity graph for hours 5 to 10 to highlight the 'wavy top' effect seen by turning the gas on and off on the humidity. This shows that when the gas is turned on for 5 minutes the culture vessel loose about 1% humidity, this is then regained as the gas is turned off for 20 minutes. The re-humidifying of the vessel gas must come from the gel as there is no other water present in the system.

This 'wavy top' can be seen as a decrease in humidity for 5 minutes before rising and plateauing over 20 minutes. This coincides with the gas being turned on and off within the Cell-IQ. Unlike a conventional incubator the Cell-IQ passes gas directly into the plate, and therefore every 25 minutes there is a 5 minute period of adding in dry air. This 'wavy top' highlights that during the 5 minutes of gassing the humidity drops as dry air enters. The humidity is then restored during the 20 minutes whilst there is no gas flow. This re-humidification must arrive from evaporation from within the culture vessel. This explains why the gels dry out rapidly in the Cell-IQ when compared to a standard incubator. In-between the culture wells water is added to try to prevent the gel drying, but

there must also be evaporation from the gel itself to humidify the dry air. The relative effect is predictable as the gel surface area is larger than the surrounding water.

Figure 96 shows that the relative humidity within the culture plate fluctuates around 93%. However dry gas that is pumped directly into the culture vessel and therefore this humidity must arise from the MethoCult gel and surrounding water reservoirs. To confirm this, the humidity within the culture vessel with no media or water was measured to assess the inlet gas humidity; this is shown in Figure 97.

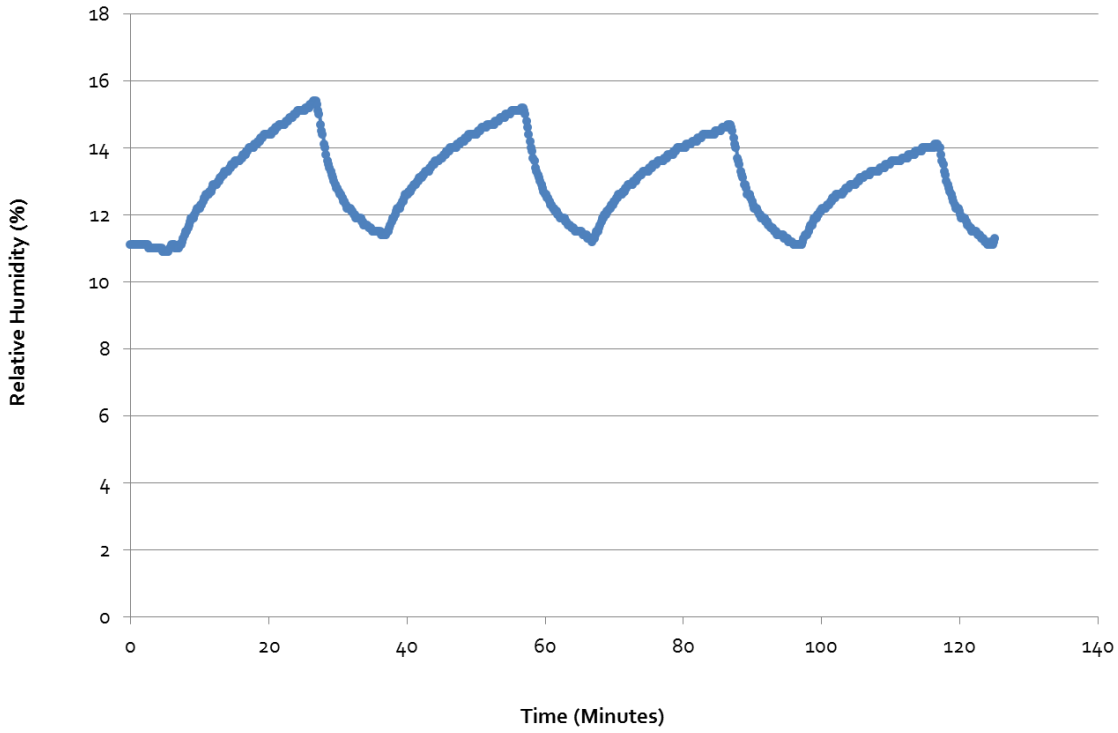

Figure 97. Humidity of the gas entering the culture vessel The humidity of the gas straight from the gas cylinder is about 16%.Therefore as this is pumped directly into the culture vessel the humidity will drop causing the drying of the gel as the gas is humidified.

Figure 97 shows that the humidity increases over the 20 minute period when the gas is turned off, and then drops as the dry gas enters. This shows that that the inlet gas has a very low humidity, with the culture vessel increasing humidity from the environment when the gas is turn off. Therefore the humidity values of above 90% highlight that water is continually evaporated from the culture medium. It is important to note that this would also have been the case for embryonic

culture in Chapter 3, however with a medium replenishment every 24 hours, and excess media used the evaporation rate was not seen to affect the culture.

Within the Cell-IQ the temperature is controlled at 37°C. At this temperature using the vapour saturation pressure from thermodynamic tables the mass of water to humidifier the dry air can be calculated.

Knowing that the relative humidity is the ratio of actual partial pressure to saturated vapour pressure, this can be assumed to be 0.9 or 90%. Then taking the saturated vapour pressure at 37°C as 6369 Pa (calculated from Appendix 8.1) the number of moles can be calculated from the ideal gas law. By multiplying the number of moles by the molar mass the mass of water within a humidified volume of air can be calculated. So within 150 mL of air 5.94 mg of water is held at 90% humidity at 37°C (calculation shown in Appendix 8.2). During the culture period of 14 days, this equates to 6.70 mL of water evaporating (Appendix 8.2) using the assumptions stated in Appendix 8.2. This calculation highlights the importance of being able to minimise evaporation to prevent the gel drying and keep the conditions stable for controlled colony growth. To combat these evaporation problems there are 3 methods which are possible:

1) Reducing the gas flow
2) Addition of liquid to the top of culture gel
3) Humidify the gas inlet

5.3.2 Reducing the gas flow rate

Reducing the gas flow results in less dry air entering the culture plate and therefore there is less capacity for the air to strip moisture, so overall there is a reduction in evaporation. A reduction in the air flow will have a knock on effect for the culture conditions. The controlled 5% CO_2 gas acts as a buffer to ensure the culture system remains at the correct pH. By reducing the flow rate the culture medium can become acidic and loose its gelation properties. This therefore changes the

culture conditions significantly and affects the assay measurement system. Although a reduction in gas flow rate will increase the time until the gel dries out it will lead to uncontrollable variation in colony growth over the 14 day period, and therefore is undesirable as an approach to reducing evaporation.

5.3.3 Addition of Liquid to the top of the culture gel

The drying gel occurs primarily at the surface as moisture evaporates into the surrounding gas, consequently adding water to the surface of the gel will help prevent the gel drying. The added water will then evaporate rather than the liquid from the gel itself. However similar to the previous method, over time this addition of liquid will mix with the gel and change the gelation properties. Specifically the viscous properties will vary overtime along with the growth factor concentrations within the gel. This again would cause uncontrollable variation during the culture period, and therefore is not a suitable method to prevent drying.

5.3.4 Humidifying the Gas Inlet

As previously noted the culture system within the Cell-IQ directly pumps conditioned air into the culture vessel. The gas is a pre-mixed 5% carbon dioxide / air medical dry gas mixture with a relative humidity of 0% as stated from the manufacturer. As the gas passes into the culture vessel it is humidified by stripping liquid from the gel and surrounding water reservoirs. By pre-humidifying the gas inlet the evaporation rate will decline rapidly with increasing humidity. This is most successfully achieved by passing the dry gas through warmed water. Within industrial applications this can be achieved with membrane technology or atomisers by bubbling through a column of water. In this set-up it is possible to place the gas inlet into a water reservoir leaving a 1mm end pipe submerged, and using the humidified headspace gas to enter the culture vessel. The then humid air entering the culture plate has less capacity for evaporation then dry air (192). Although humidifying the dry air prior to going through the culture plate is a technical issue this should provide the best conditions

for reducing evaporation. Figure 98 provides a schematic of the proposed humidification set-up that can be used within the Cell-IQ.

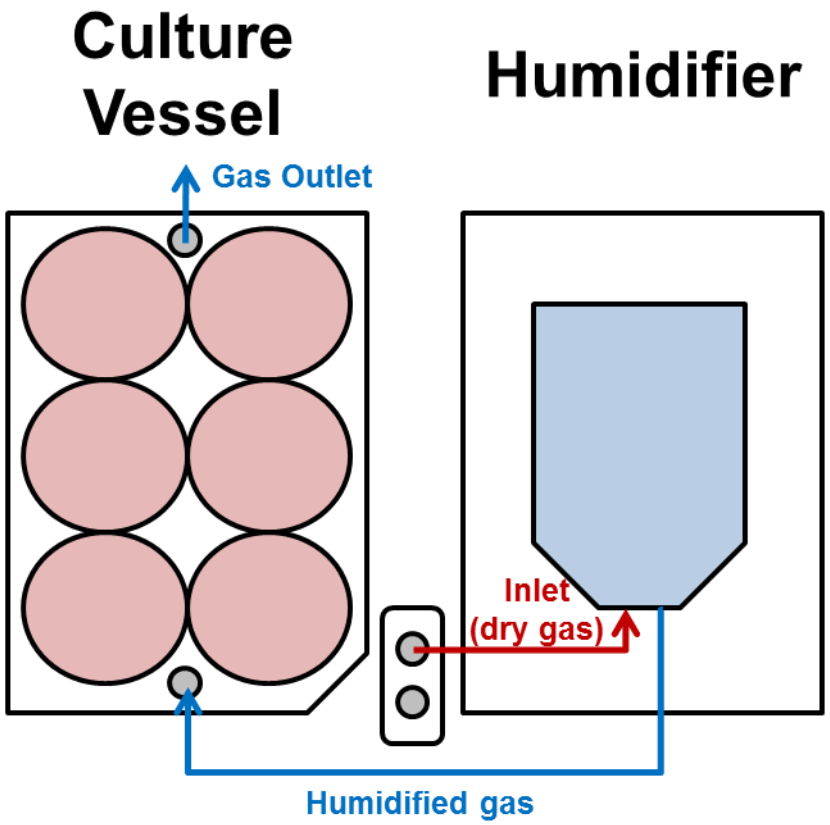

Figure 98. Diagram of humidifying loop in the Cell-IQ. By passing the inlet gas through a flask of water, the gas is humidified before entering the culture vessel. This therefore should help prevent the gel drying out.

This humidifier takes the dry inlet gas and passes it through a reservoir of water held at the same temperature as the culture vessel. It is important to maintain this temperature equilibrium to prohibit condensation or further evaporation. The inlet then bubbles up through a column of water held in a t-25 flask, striping moisture and remains in the headspace of the t-25. As further gas is pumped in, humidified gas in the head space then travels into the culture vessel. The gas outlet on the culture vessel has a filter on the end to prevent any non-sterile air from the surrounding environment entering, and allows excess gas to pass out preventing pressure build-up within the culture vessel. This set-up was then tested by placing the empty 6-well plate with a humidity sensor

in to measure the relative humidity that is created by passing the dry air through the humidifying set-up; this is shown in Figure 99.

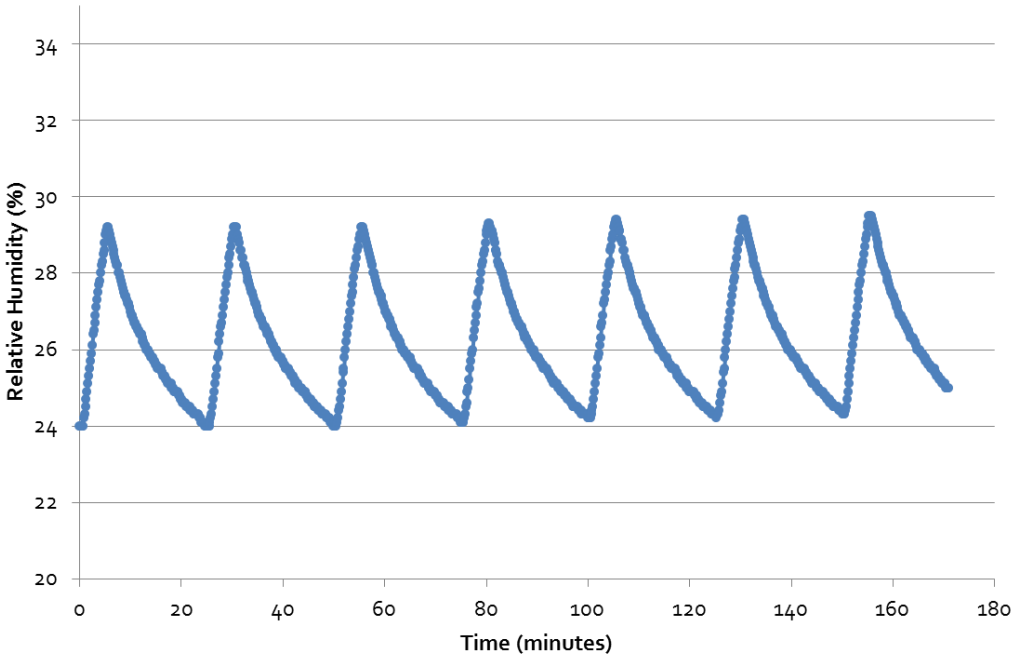

Figure 99. Humidity of the Cell-IQ culture plate using the humidifier. Using the set-up in 0 the dry gas is passed through a flask of water before entering the empty culture vessel at a rate of 30 mL/min on for 5 minutes, off for 20 minutes. This has increased the humidity from 16 to 26 %, but compared to 90% humidity from a standard incubator this is still low.

These results show that the 5 minutes of passing the gas into the plate increases the humidity, but then by turning the gas off the humidity drops until the gas is turned back on. This is likely due to the outlet controlled by a filter; this therefore permits constant losses, returning the relative humidity to equilibrium with the room humidity. This demonstrates that in order for the culture plate to remain humid a constant gassing is required. So by using a constant gas flow rate of 30 mL/min the humidity can be further increased as in Figure 100. The data is fitted using a Pearl-Reed logistic fit, which provides an estimation of the asymptote as required.

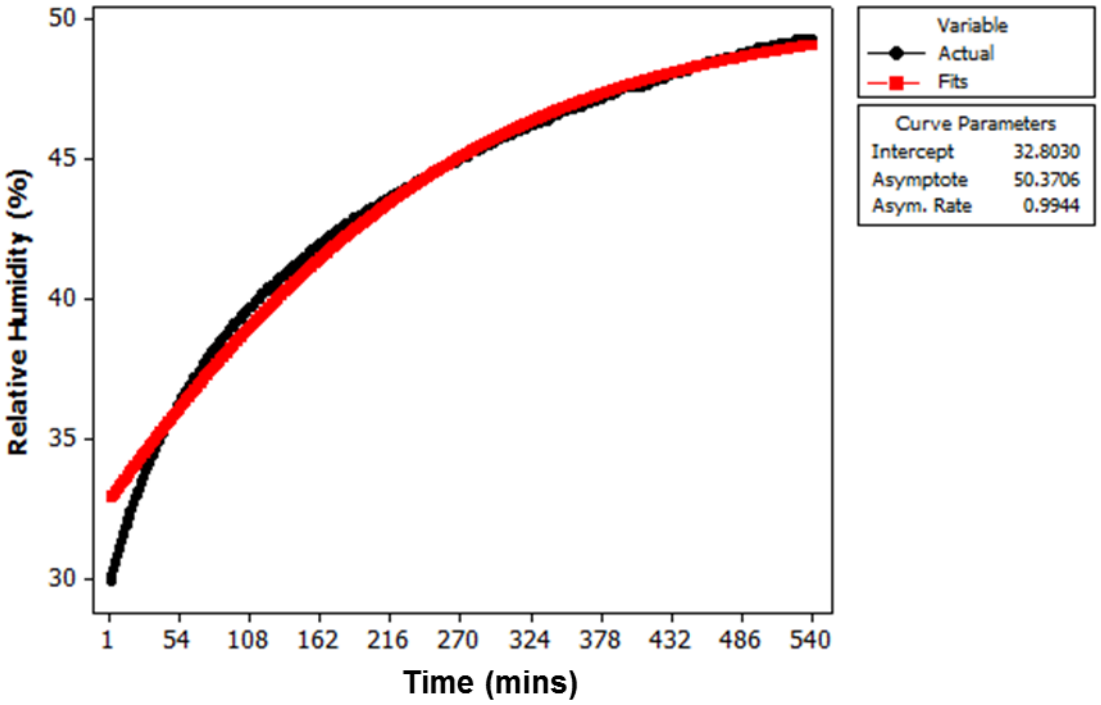

Figure 100. Constant gassing at 30 mL/min with humidifier. Previous data has shown that using a cyclic on/off control of gas prevents a high humidity being reached. Here using a constant flow, a humidity of 50% is being reached, an improvement on 26% previously seen with cyclic gas flow.

By supplying a constant gas flow rate though the humidifier the relative humidity asymptotically reaches 50%. This is about twice that seen by turning the gas on and off as seen in Figure 99. However compared to a standard incubator which operates at 95% humidity further optimisation of the system is required.

As the system is not reaching 100% humidity, the inlet gas therefore is not stripping enough moisture before it enters the culture plate. There are three possible factors that affect the rate of moisture gain to dry assuming a constant temperature; gas flow rate, size of gas bubble and residence time relating to both contact time of gas with liquid, and headspace within the humidifier.

The first factor to investigate was flow rate. By reducing the flow rate there is a knock on effect by increasing the residence time for the humidified gas in the head space of the humidifier. It is therefore hypothesized that by reducing the flow rate the residence time increases, increasing the relative humidity of the gas. Figure 101 shows the effect on humidity of reducing the gas flow rate to 6 mL/min.

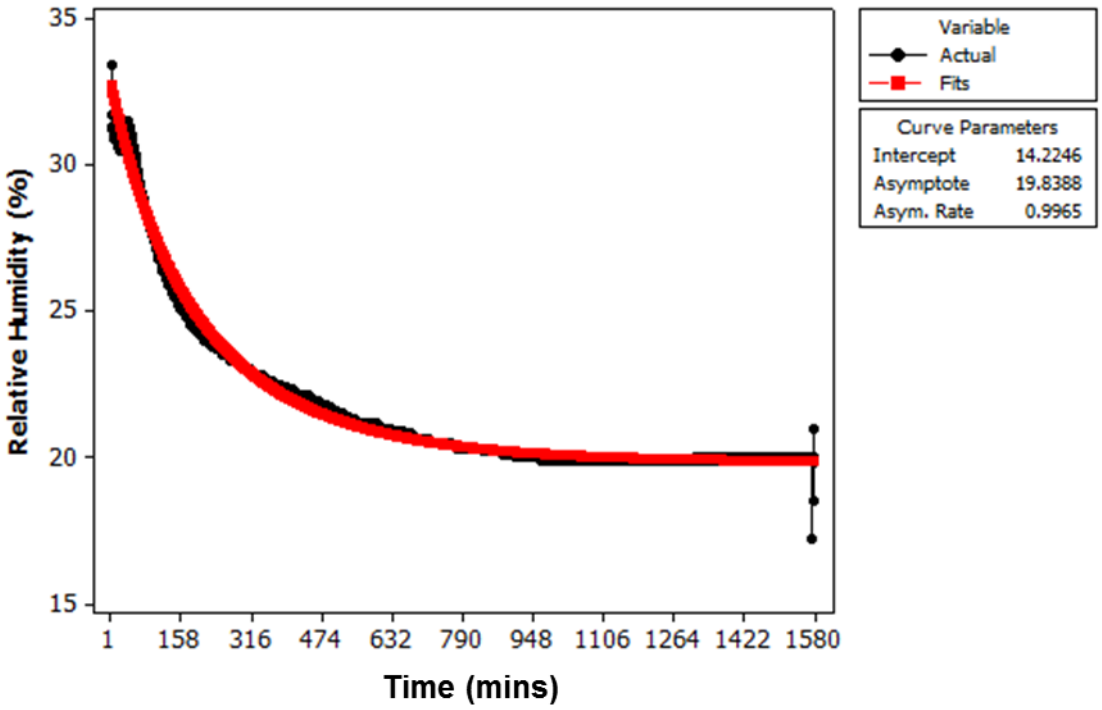

Figure 101. Constant gassing at 6 mL/min with humidifier. In order to try and improve humidification of the dry air a slower gas flow rate is used to give the gas more time within the humidifying chamber to pick-up water. Using 30 mL/min 50% humidity was seen, but by lowering the flow rate a decrease in humidity is seen, only 20% humidity.

Figure 101 shows that the culture plate approaches room humidity (~20%), and therefore by reducing the gas to 6 mL/min actually has a negative impact on increasing the humidity. It is hypothesised that this is either due to the losses experienced earlier, or 6 mL/min is outside of the measuring accuracy of the flow meter, with the potential of no air entering the culture vessel. Either way using a flow rate this low is not sufficient to humidify the system, therefore a variation of flow rates were tested and are shown in Figure 102.

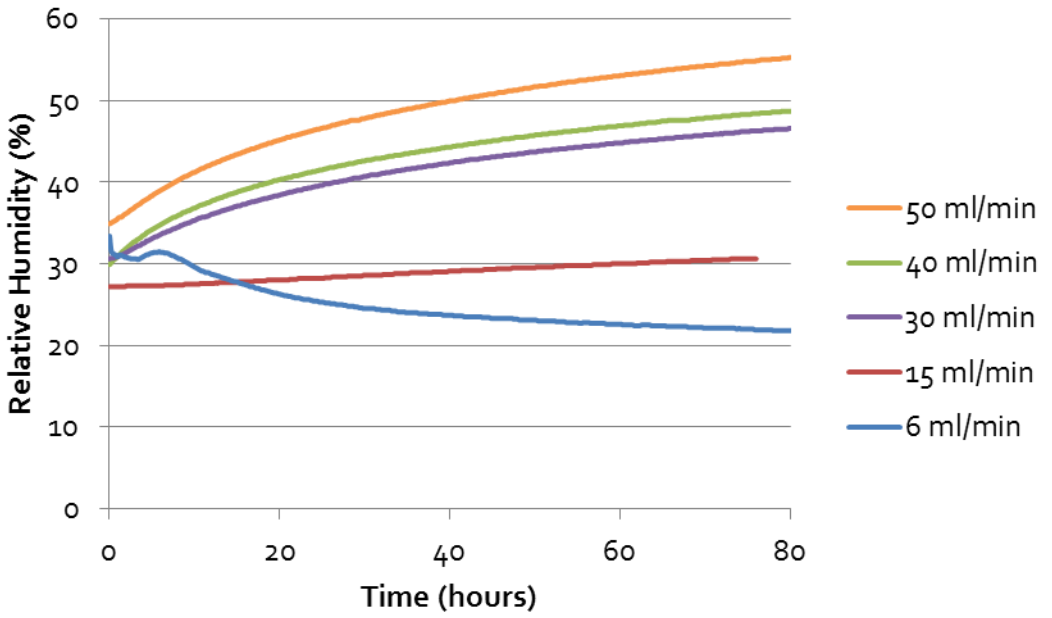

Figure 102. Effect of flow rate on humidity in the Cell-IQ culture plate. Comparison of 5 different flow rates of dry gas into the humidifier with the respective humidity profiles measured in the empty culture chamber. The highest humidity is produced with the highest flow rate of 50 mL/min.

Figure 102 shows that as the flow rate is increased the humidity increases, the opposite to what was hypothesised. This therefore demonstrates that the residence time in the headspace is not the limiting factor for reaching a high relative humidity. Therefore the moisture must be acquired as the bubbles of gas pass up through the liquid rather than in the headspace of the t-25 flask. The higher flow rate is likely to cause a more turbulent flow regime, creating smaller gas bubbles.

The increase in humidity related to an increase in flow rate has been attributed to an increase in turbulence. The Reynolds number (Re) provides a measure of flow regime characterisation. By comparing inertial forces to viscous forces the Reynolds number provides a dimensionless measurement of flow turbulence. The Reynolds number (Re) is defined as:

$$Re = \frac{\rho v D}{\mu}$$

Where taking the following values, the Reynolds number can be calculated for the various flow rates:

- ρ, density of air at 37°C = 1.1384 kg/m^3 (Appendix 8.1)

- v, velocity of fluid = 30 mL/min = 0.1592 m/s (Appendix 8.1)
- D, diameter of pipe = 1 mm = $1x10^{-3}$ m
- μ, dynamic viscosity of air at 37°C = $1.9795x10^{-5}$ kg/ms (Appendix 8.1)

$$Re = \frac{\rho v D}{\mu} = \frac{1.146 \cdot 0.15923 \cdot 1 \times 10^{-3}}{1.9795 \times 10^{-5}} = 9.22$$

By doubling the gas flow rate from 30 mL/min to 60mL/min (0.1592 m/s to 0.3185 m/s):

$$Re = \frac{\rho v D}{\mu} = \frac{1.146 \cdot 0.3185 \cdot 1 \times 10^{-3}}{1.9795 \times 10^{-5}} = 18.44$$

This shows that although both provide very low Reynolds number, suggesting laminar flow, there is a considerable difference as the flow rate is doubled from 30 mL/min to 60 mL/min. This increase in flow rate provides an increase in the turbulence instigating improved humidification. Although humidification does not happen in the tube itself, this increase in Reynolds number due to increases flow rate will have a similar effect as the gas passes from the end of the tube.

Given the relationship seen in Figure 102 the flow rate could further be increased, however it is important to note that the higher the flow rate the greater volume of gas passes over the gel surface. If this gas is not at 100% humidity then there will still be a loss of liquid from the surface. The greater volume of gas the more liquid will evaporate. Therefore it is more advantageous to increase the humidity of the inlet gas rather than increase the flow rate.

This increase in turbulence is attributed with the bubble size and therefore leads directly into identifying the bubble size effect on humidity. In order to obtain a high rate of humidification the area contact between the gas and water needs to be as large as possible (193). Rather than just increasing the flow rate to increase turbulence, a more controlled method of decreasing bubble size is to pass the gas through a sparger or atomizer. These are designed to break up the gas and create smaller bubbles of air. So far a 1mm pipe end has been submerged. This pipe can be fitted with a bioreactor sparger used for fermentation reactors as shown in Figure 103.

Figure 103. 20 µm fermentation sparger. Adapted from a fermentation bioreactor sparger, this Sartorius sintered metal sparger can be sterilised and used to increase the surface area of gas bubbles in contact with liquid, therefore improving humidification.

The sparger is sintered metal creating pore sizes of 20 µm. This therefore creates uniform small gas bubbles to increase the contact area of gas to liquid. Shown in Figure 105 is the effect of using bubbles that come directly from the end of a 1mm diameter pipe end or by passing the same flow rate of gas through a sparger device with a pore size of 20 µm, termed humidifier versions 1 and 2 respectively.

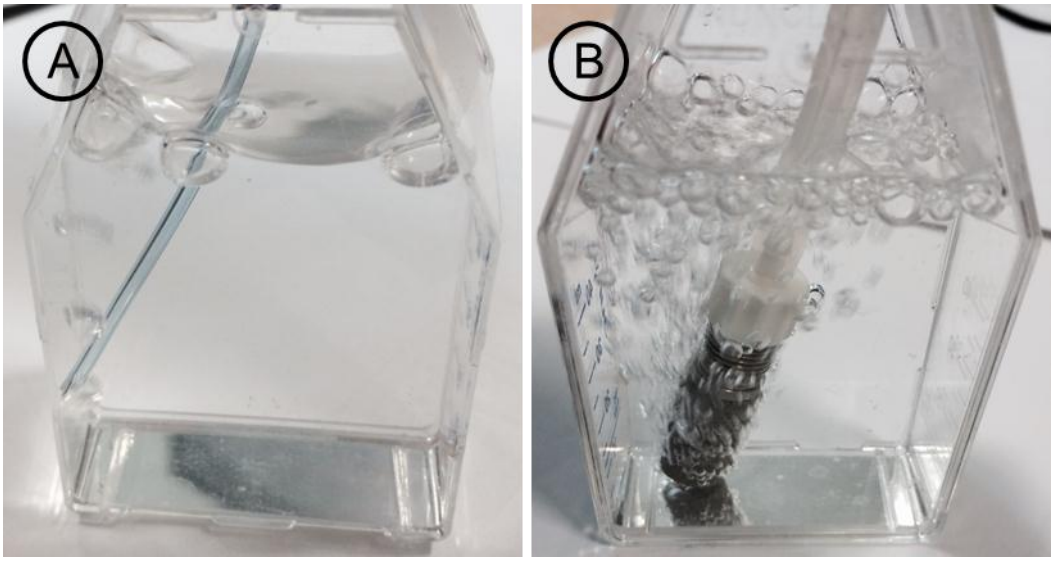

Figure 104. Images of gas bubbles from a submerged 1mm open bore pipe. The bubbles that come from an open bore 1mm diameter pipe shown in A) are much larger than those that come from the sparger in B). This decrease in bubble size increases the surface area for air to water contact, which improves humidification.

Using the same flow rate it is possible to see from Figure 104 that by using the sparger much smaller bubbles are formed compared to the 1 mm open bore pipe. This increase in surface area and therefore contact area of air to water means that there is a greater ability to strip moisture as the bubbles rise. This in turn relates to a higher humidity by using the sparger device. A comparison of the two humidifier types is shown in Figure 105.

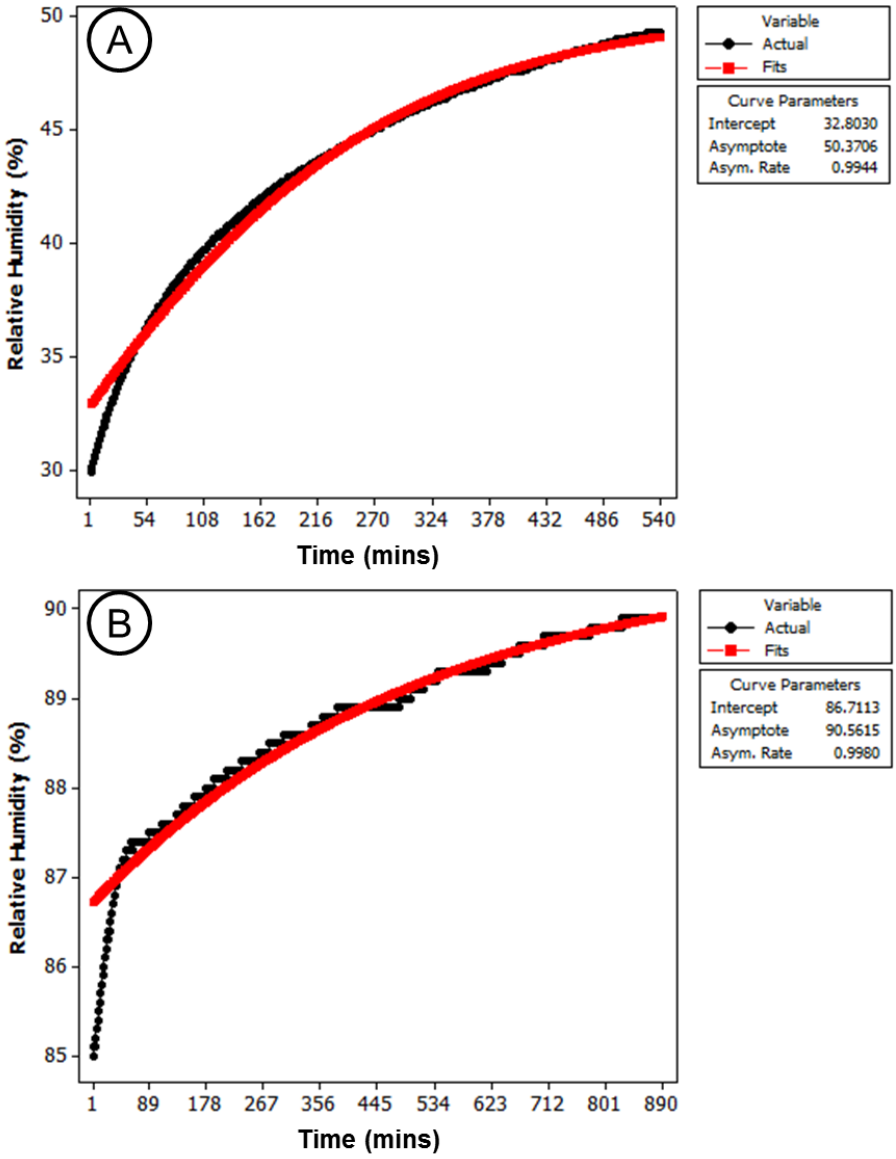

Figure 105. Comparing of achieved humidity using a single bore pipe (A) and a sparger (B). (A) Measuring the humidity in the culture vessel using a 1mm bored pipe to pass dry gas through in the humidifying chamber produces a humidity of 50%, as shown previously. By replacing the 1mm bore pipe with a sparger (B) with many 20 µm pores the humidity can be increased to 90%, that found in a standard incubator.

As can be seen from Figure 105 graph (B) by using the sparger a far higher humidity is reached than graph (A) with the 1mm pipe end. This has allowed a direct comparison between humidifier version 1, an open pipe and version 2, the sparger. By decreasing the bubble size the humidity value can be nearly doubled. This also shows that the residence time or head space has less effect on humidifying rates compared to bubble size.

The final effect to assess is the liquid depth. By increasing the depth of liquid that the gas passes through, the time that the bubbles can interact and strip moisture is also increased. This therefore may increase the humidity within the culture vessel. The effect of increasing the liquid depth is shown in Figure 106 along with humidifier version 1 and 2 for comparison.

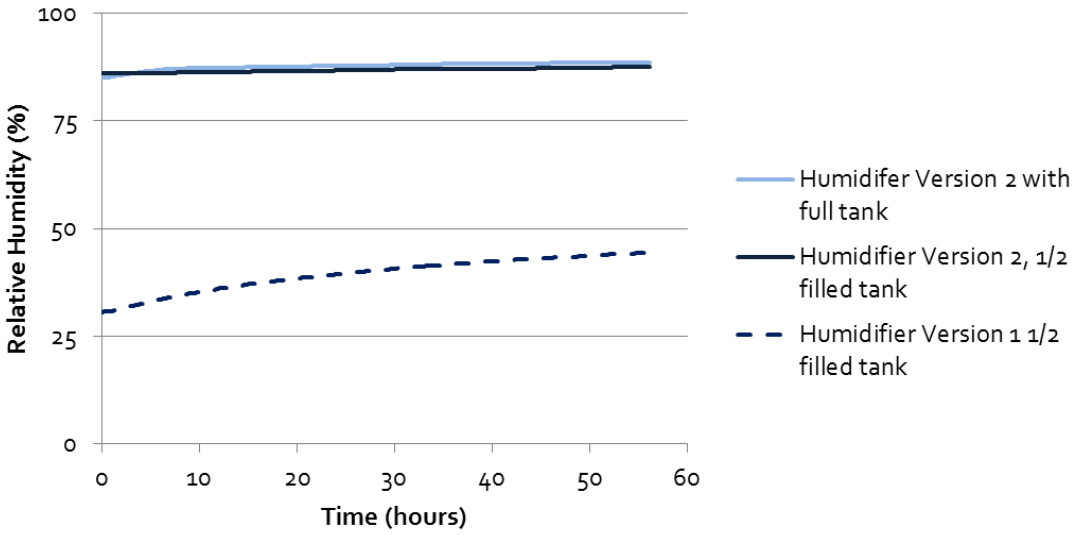

Figure 106. Effect of sparger and height of water column on humidity rates. All conditions used 30 mL/min gas flow rate. By varying the water volume in the humidifier the head space is reduced, therefore it is possible to determine if the gas is humidified by bubbling through water, or in the head space. Comparing the dotted line with the filled in lines it is possible to conclude that there is little difference in humidity with a half or full filled chamber of water.

By atomising the gas, the relative humidity can be doubled from ~45% to ~90%, a result seen previously in Figure 105, and noted again here in Figure 106 by comparing the dotted line to the solid lines. The increase in liquid depth also increases the humidity; however this effect is less proficient, comparing the two solid lines. This again shows that bubble size has a more significant effect then residence time in this system on humidifying the inlet gas.

By using a sparger and a full tank of water it is possible to humidify the dry inlet gas to ~90% humidity. This has all been achieved using a constant flow rate of 30 mL/min. However it was noted previously in Figure 102 that the flow rate has a big impact on the humidifying rate. Therefore the flow rate can be varied to determine which flow rate is best suited for reaching high humidity levels with humidifier version 2; this is shown in Figure 107.

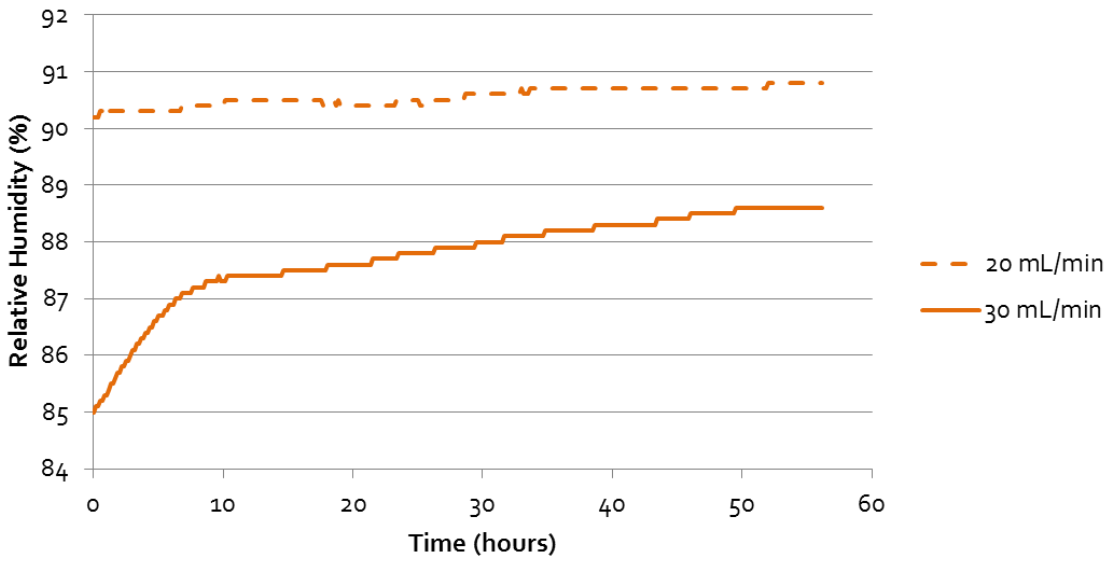

Figure 107. Flow rate effects when using sparger. Using a full tank of liquid and the sparger the flow rate is varied showing that a higher humidity can be reached with a lower flow rate when using humidifier version 2.

Previously it was seen in Figure 102 that by increasing the flow rate the humidity was increased, this was hypothesized that the higher flow rate was more turbulent with smaller bubble sizes and stripped more moisture. However, now the gas is passed through a sparger constant bubble size independent of flow rate is achieved. Figure 107 shows that a reduced flow rate is required for a higher humidity. This therefore shows that with equal bubble size from the sparger, the residence time is having a more prominent effect then previously seen. The lower the flow rate the greater the residence time, however the manufacturer suggest a flow rate of at least 20 mL/min to overcome losses in the culture vessel, and also to run within the specification of the flow rate controller. Therefore 20 mL/min is used to provide the improved conditions to the default 30 mL/min.

This work has successfully shown that it is possible to increase the humidity of the inlet gas by passing a continuous flow rate of dry gas through a 20 µm sparger at a liquid depth of 4 cm. So far all the experiments have been conducted under static conditions, that is to say the imaging platform within the Cell-IQ has not been moving. In order to conduct the CFU-assay this platform needs to be able to move freely. Within the environmental chamber there is a limited height which prevents the t-25 humidifier from standing upright during imaging. This requires the humidifier to be redesigned in order to fit within the system and humidify the inlet gas during experimental runs.

5.3.4.1 Humidifier Development

The Cell-IQ incubated area has a maximum height of 3cm. This limits the height of a humidifying system that can be accommodated into the incubation area. Previously the humidifier utilised a t-25 flask with sparger filled with water standing upright as depicted in Figure 108, named humidifier version 2.

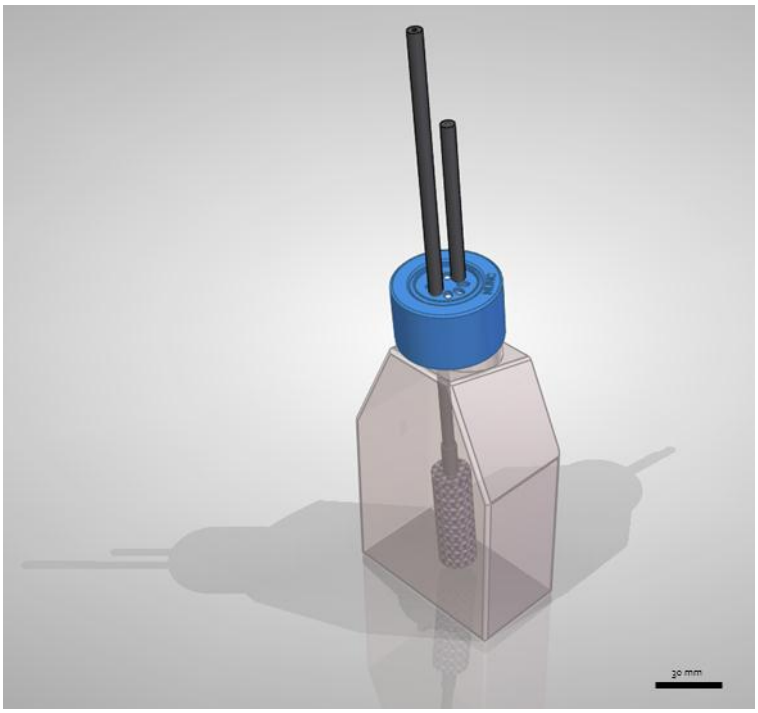

Figure 108. Humidifier Version 2. Computer Aided Design (CAD) diagram of humidifying chamber showing t-25 flask upturned with sparger inside.

This successfully humidified the inlet air, however the height restriction within the Cell-IQ during imaging requires the flask to lie flat, this was tested and the relative humidity reached a maximum of only 40%, as shown in Figure 109.

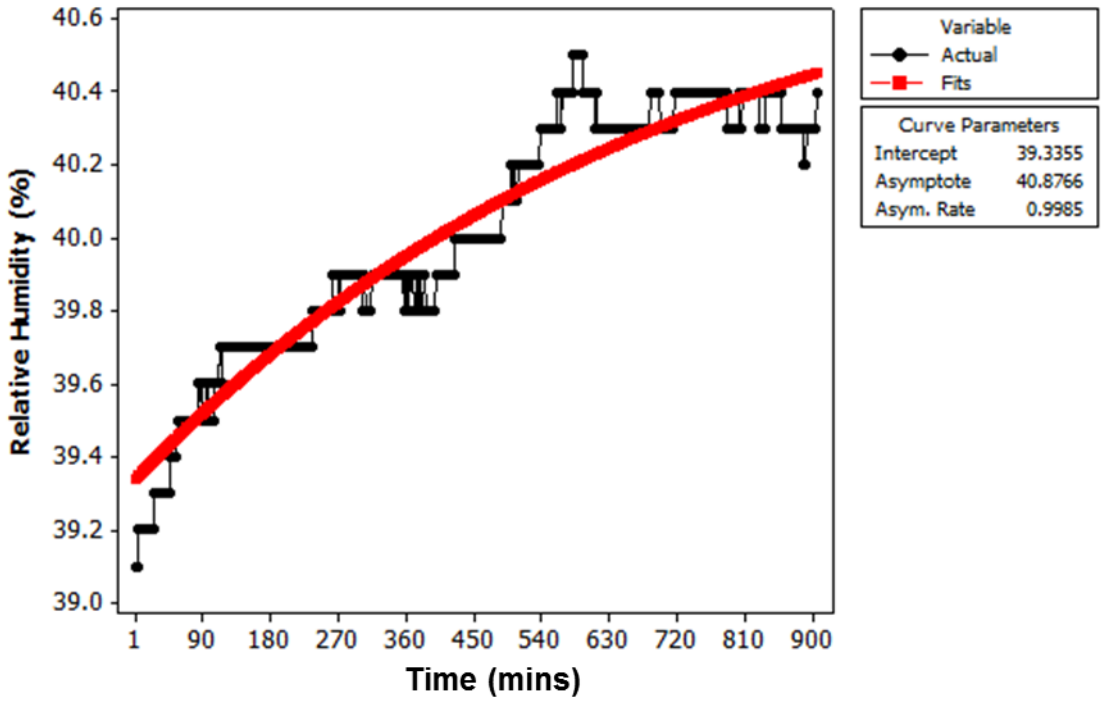

Figure 109. Humidity using the humidifier with sparger lying down at an angle. Due to the height restriction with the Cell-IQ the humidifier must be laid down during continual imaging. This reduced the depth of water with which the dry air bubbles pass though. The effect of this is a reduced humidity in the culture vessel of less than 41%.

This reduction in humidity shows that both the water depth and sparger set-up are required to maintain a high relative humidity in the culture vessel. Another option would be to place the humidifying system externally to the culture chamber, but this would require a separate incubation device to ensure the humidifier was at the same temperature as the Cell-IQ system. Without this temperature equilibrium the saturation pressure changes which can lead to condensation as the humid gas enters the culture plate or increased evaporation rate from the culture vessel if it is cooler.

A new humidifier design was required which mimicked the properties of humidifier version 2 in its upright position, this data provided the necessary information in order to build a suitable replacement that fits within the space limitations. The key points are detailed below in Table 17.

Table 17. Humidifier's necessary properties A list of key properties to include in new humidifier design in order to achieve humidity in the Cell-IQ representative of that found in a standard incubator.

Required Property	Information
Accommodate Sparger	The 20µm sparger suitable atomises the inlet gas forming small bubbles that can pick-up moisture
40mL reservoir	This water amount remains at a constant temperature despite the variation in inlet gas temperature
3cm column height	The water height impacts on the level of humidity reached, using the 20m sparger a column height of more than 3cm is required
Easy to sterilise	It is important to be able to maintain sterility both prior to use and during use
Prevent water entering the gas lines	It is important that water cannot enter the inlet gas line when it is turned off, and also no water enters the culture plate.
Size restriction	The humidifying cannot be larger than a standard culture plate () and must be less than ……in height

Given these required properties, humidifier version 3 was developed to fulfil all the requirements. Humidifier version 3 is shown in Figure 110.

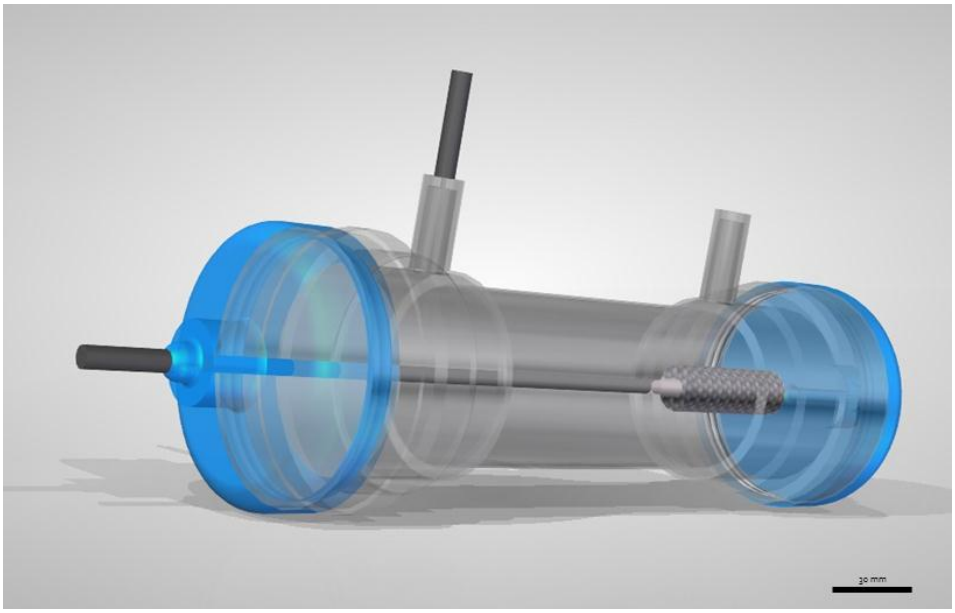

Figure 110. Humidifier Version 3. The new design of humidifier that fulfils the attributes in Table 17 drawn in CAD showing a long tube shape with sparger present inside. Once filled with water there is a small headspace near the outlet to take humidified air into the culture vessel.

Humidifier version 3 utilises a cylinder to increase the distance the bubbles travel through liquid to ensure a high humidity is reached. This shape also allows the cylinder to be laid at a slight angle to ensure it fits within the height restricted Cell-IQ culture system. This reduces the water depth slightly from humidifier version 2, but maintains a liquid volume of greater than 40 mL to accommodate for evaporation and slight temperature variations. After ensuring that the platform could freely move with humidifier version 3 installed, the humidity within a culture vessel was measured. This is shown in Figure 111.

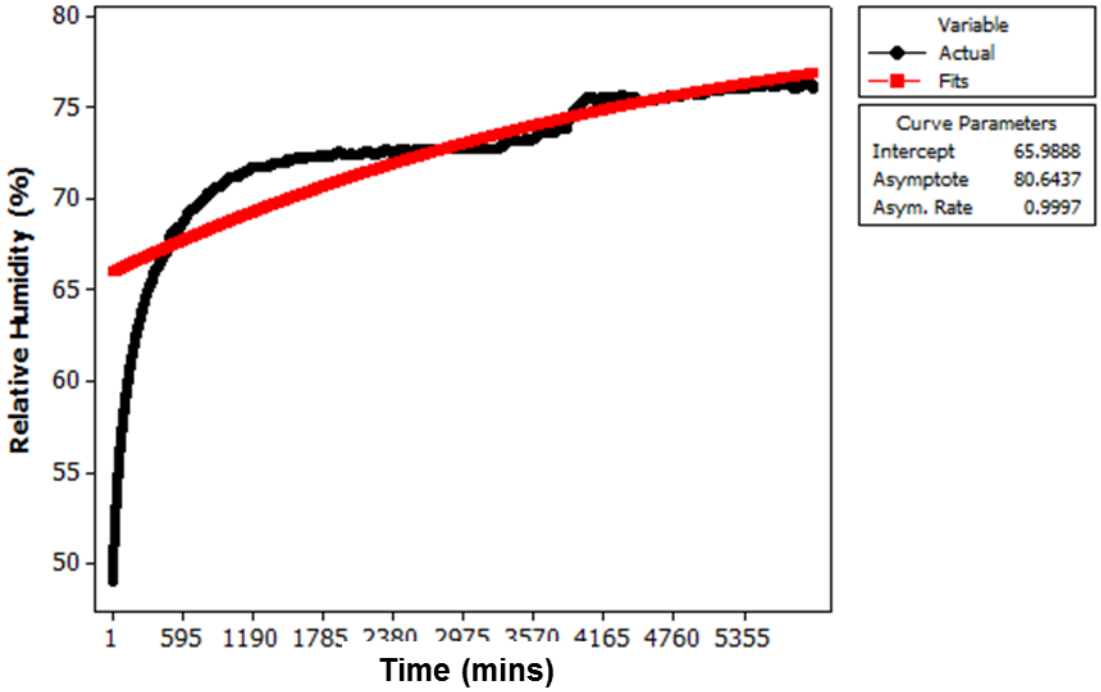

Figure 111. Humidity of culture vessel using humidifier version 3. Using the new design of humidifier (Humidifier version 2) continual imaging can take place and the humidity in the culture vessel is above 75%.

Using a Pearl-Reed logistic fit an asymptote can be predicted. This is not possible using a quadratic model, and the significant information to gain from Figure 111 is the asymptotic value. As predicted by reducing the water depth the asymptote predicted humidity has slight dropped to 80%. This is slightly less than a standard incubator but much improved on the dry gas inlet. The next series of experiments were to test the evaporation rate from the culture vessel using humidifier version 3 in comparison to the previous set-up without a humidifier.

5.3.5 Assessing the evaporation rates using water droplets within the Cell-IQ

Previous work has shown that during the CFU assay the gels rapidly dry out due to the Cell-IQ's mechanism of dry air gassing. By adding a humidifying step prior to feeding the gas into the culture vessel holding the CFU assay this evaporation can be reduced. In order to determine the rate of evaporation droplets are placed within the culture vessel and continually imaged to show the decrease in size and therefore evaporation of water over time. Using the Threshold method

explained earlier in Section 3.3.2 the droplet size can be continually monitored to show the evaporation over time. An example is shown in Figure 112.

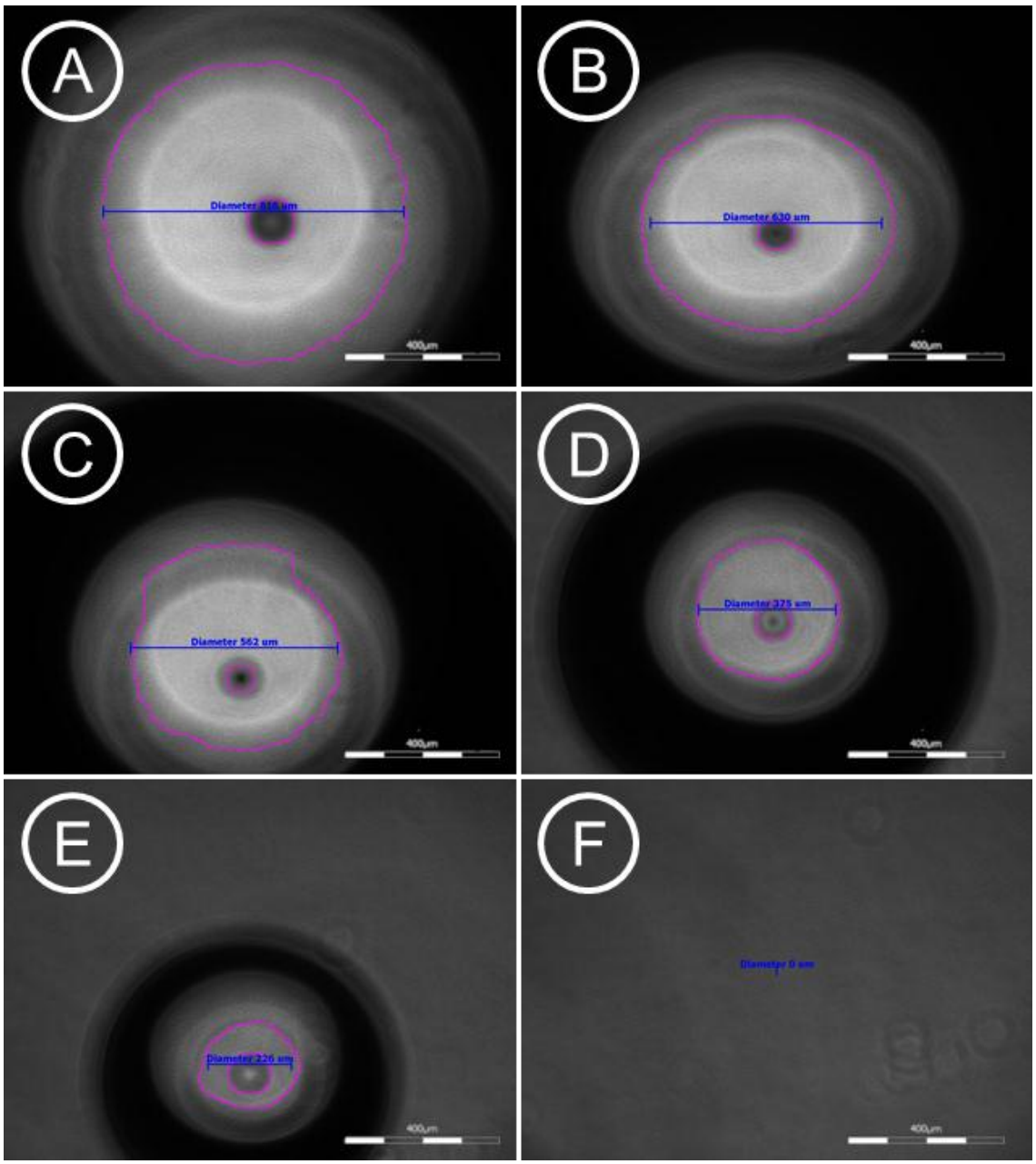

Figure 112. Example of droplet size reduction analysis. By measuring the central diameter of the droplet, the reduction in droplet size can be measured over time as seen by A)-F) taking at 1 hour intervals using a flow rate of 20 mL/min with 5 minutes on 20 minutes off.

Figure 113 shows the rate of droplet size decrease using gas flow rate of 20 mL/min of dry gas cycling through 5 minutes on and 20 minutes off. This was the set-up used initially according to the manufacturer's recommendation.

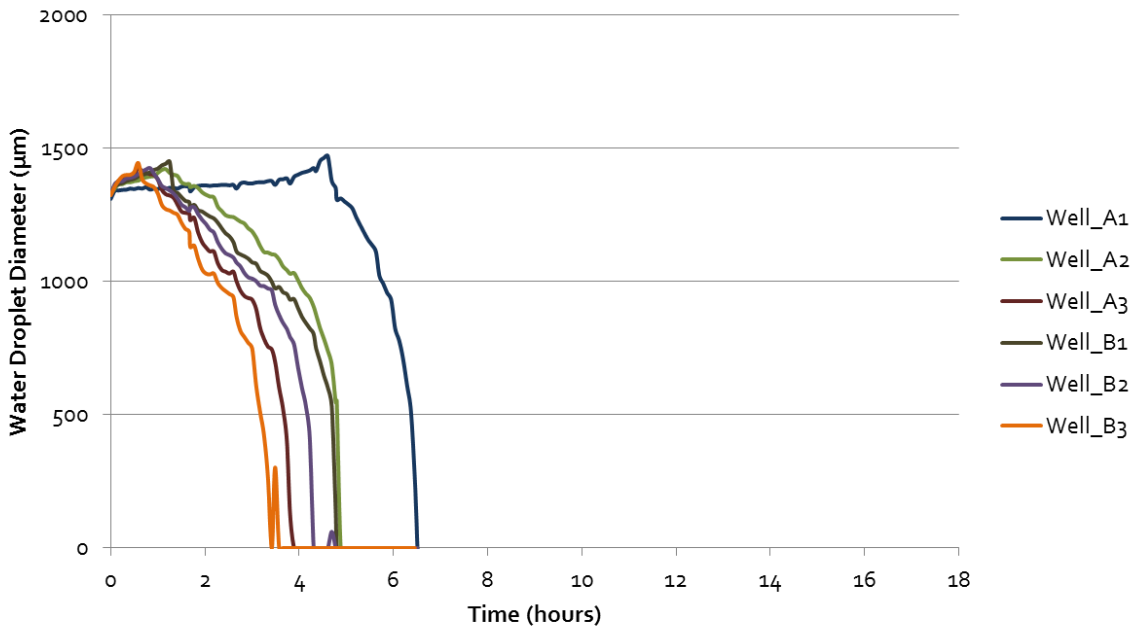

Figure 113. Water droplet evaporation from image analysis without humidifier. Using 30 mL/min gas cycling on for 5 minutes off for 20 minutes with no humidifier 20 µL water droplet diameters decreases over time. The decrease in droplet size corresponds to evaporation, it can be seen that complete evaporation occurs by 7 hours, but the different wells have various evaporation rates.

The 20 µL droplets rapidly evaporate when there is no humidification of the gas inlet, starting with those closest to the gas inlet (Wells A3 and B3), with all droplets evaporated prior to 7 hours elapsed. This data equates to 2.88 mL of moisture evaporating from the culture plate during the 14 day assay period (14 days = 168 hours, with 120µL evaporating every 7 hours). Although slightly less than the ideal gas law calculations in Section 5.3.1, this is still a significant volume to evaporate during the assay. Previously it was shown that through the addition of a humidifier the inlet gas can be humidified to 80% using humidifier version 3 along with a constant gassing regime. This would therefore reduce the evaporation rate, showing an increase in the time it takes to fully evaporate the droplets, a result shown in Figure 114.

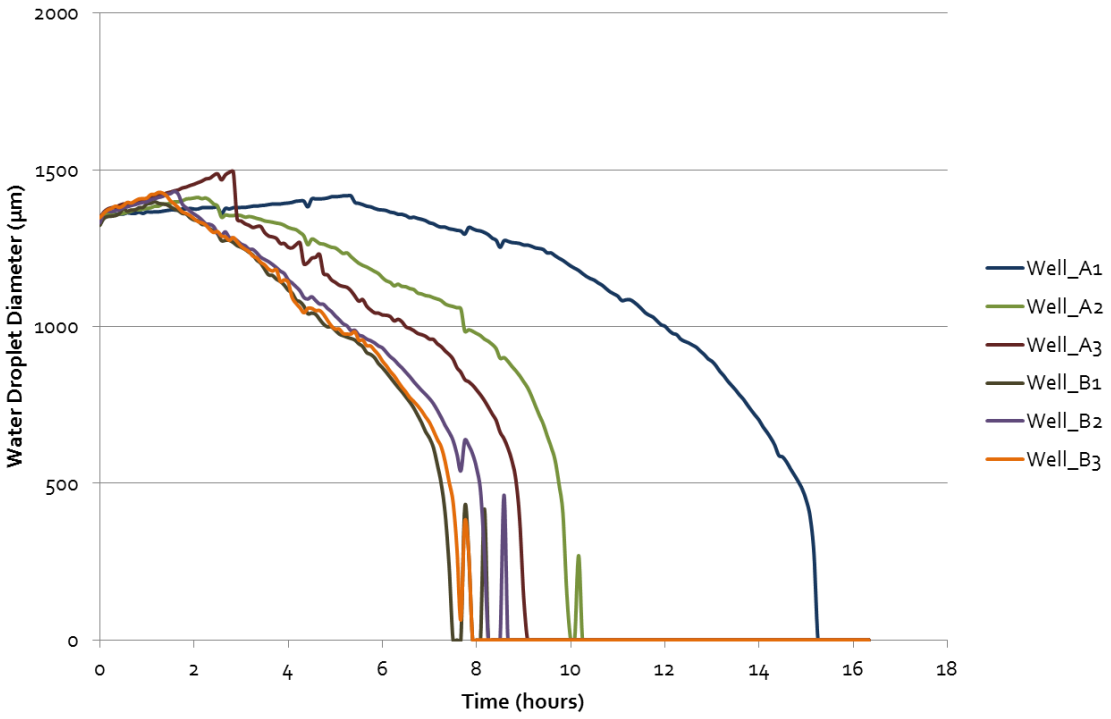

Figure 114. Water droplet evaporation from image analysis with humidifier version 3. Using a constant gas regime at 20 mL/min with humidifier version 3 the 20 µL water droplet diameters in each well decrease over time. This increases the time for complete evaporation from using no humidifier at 7 hours to 15 hours.

The evaporation rate is reduced by pre-humidifying the gas to 80%. By increasing the time for complete evaporation from 7 hours to 15 hours, the evaporation volume is more than halved to 1.26 mL during the 14 day assay period.

This work has also demonstrated that the wells closes to the gas inlet evaporate quicker than those near the outlet. As the gas flows over the wells near the inlet moisture will be taken up, so that by the time the gas reaches the wells near the exit the gas will already have been humidified. Therefore by filling these wells with water the evaporation from the MethoCult filled wells is hypothesised to significantly reduce, this is shown in Figure 115.

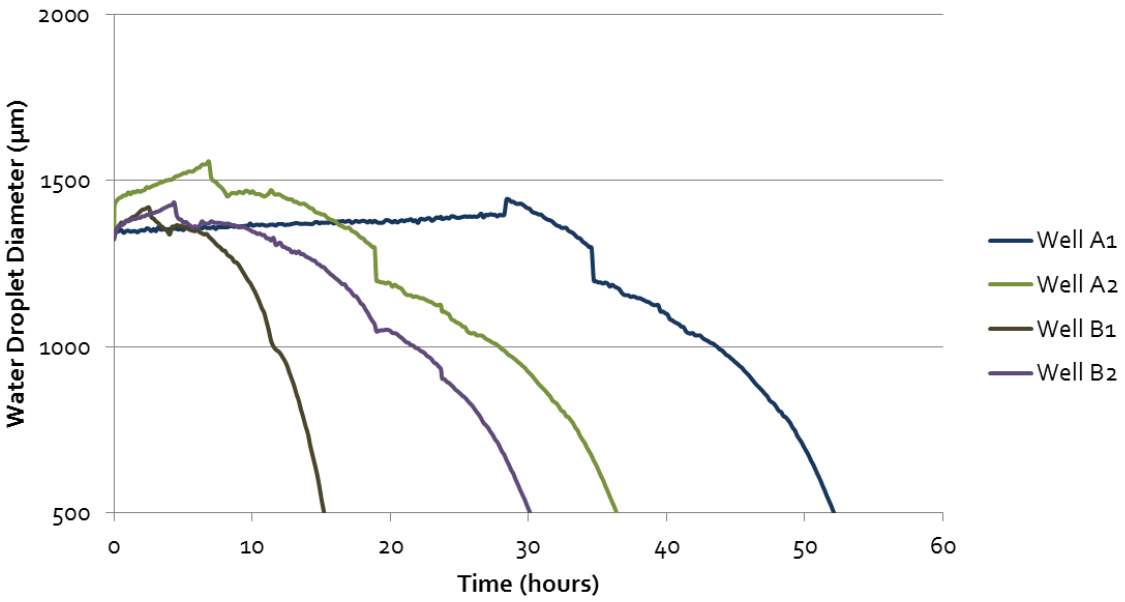

Figure 115. Water droplet evaporation with humidifier version 3 with water in wells A3 and B3. Using 20 mL/min gas constantly on with humidifier version 3 and 20 µL water droplet diameters decreases over time (as measured from image analysis)and there is little increase in time until complete evaporation compared to no humidifier in Figure 113.

As was seen previously the liquid in the wells closest to the gas inlet evaporate first, by filling these wells with water the evaporation rate in the other wells is reduced. This is shown in Figure 115, as hypothesised the liquid evaporates in these inlet wells reducing the evaporation rate in the remaining wells. This increases the time for complete evaporation from the wells to 50 hours, compared to the 15 seen previously in Figure 114. This provides promising data that the environment in the Cell-IQ is equal to that of a standard incubator, and evaporation will not have a significant effect on the assay development.

5.3.6 Computation Fluid Dynamics

In order to confirm the results seen it is also possible to use computation fluid dynamics (CFD) to predict the gas flow seen within the plate. This involves building a model of the culture vessel, then using the given flow rates a simulation can be run to model the fluid movement. In order to model the culture vessel a number of assumptions were made to simplify the model. These includes neglecting any loses from the vessel other than the outlet, and modelling the fluid as a uniform flow. The previous data highlighting the well order of drying out, suggests that the angle of the inlet provides a slightly skewed flow rate. With these key assumptions the following model can be built as shown in Figure 116 using a flow velocity of 0.3 m/s as calculated in Section 5.3.

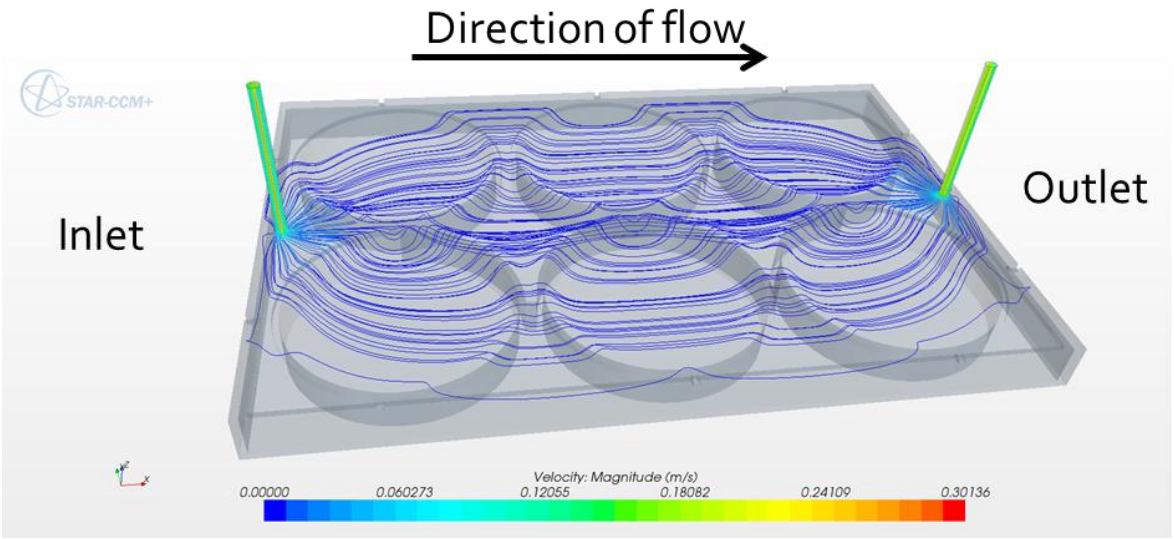

Figure 116. CFD model showing velocity streamlines within the culture vessel. The CFD shows high flow rate at the inlet and outlet where the pipes narrow, shown by red/green streamlines. As the flow enters the culture vessel the velocity drops as the pressure drops due to the expansion from the pipe diameter, shown as blue streamlines.

By assessing the streamlines it is possible to conclude that there is a sudden pressure drop shown by a decrease in velocity past the inlet. As seen from the evaporation of droplets the air enters the wells nearest the inlet first prior to moving onto the next line of wells. As expected the majority of the flow goes straight down the centre, the shortest route to the outlet where the pressure is much lower. Another way to depict this information is using the velocity vectors; this is shown in Figure 117

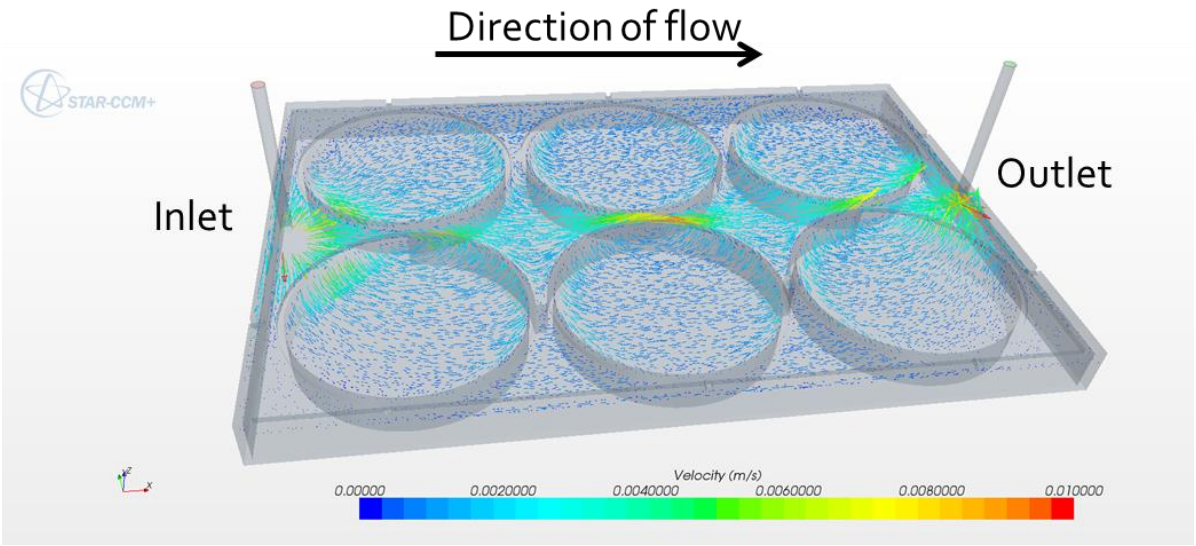

Figure 117. CFD model showing velocity vectors within the culture vessel. The CFD shows high flow rate at down the shortest path to the exit. As the flow enters the culture vessel the velocity drops as the pressure drops due to the expansion from the pipe diameter, shown as light blue vectors.

Figure 117 has a different scale to Figure 116 to focus on the flow change within the culture vessel. Therefore no vectors are shown on the inlet and outlet pipes. Again this diagram highlights the low velocity within each well with increased velocity as the air moves between wells. Similarly as before the air first enters the two wells nearest the inlet before moving down the plate towards the outlet, with the highest velocity noted through the centre and near the inlet and outlet pipes. This data shows how CFD modelling can be used to describe the flow regime within culture vessels. Although a simplified model is utilised here, further work could build on this and accurately model the flow patterns within the vessel. By placing water in the wells closest to the inlet the incoming air can be further humidified before passing over the wells containing MethoCult.

5.3.7 Comparison of Cell-IQ to Standard Incubator on the CFU Assay

Following the successful development of a humidifier to increase the water content of the inlet gas, the next stage was to compare the 14 day assay in a standard incubator to that in the Cell-IQ. By placing CFU assay samples from the same starting population it is possible to measure as an end point the number (Figure 118) and phenotype of the colonies (Appendix 8.3).

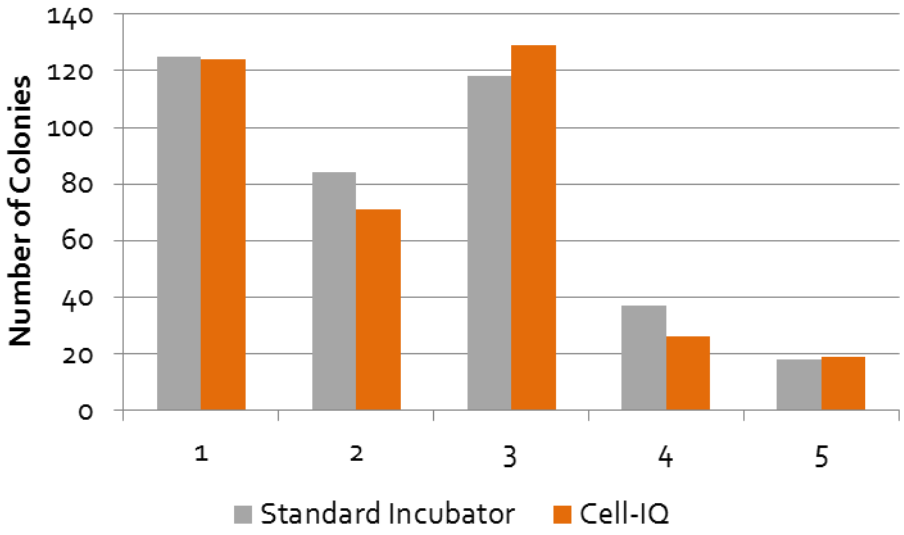

Figure 118. Total colony counts from standard incubator and Cell-IQ. The colony counts performed on day 14 of 5 samples held both in a standard incubator and in the Cell-IQ. Each sample represents a MethoCult filled well, with different volumes of cell population. n=5

Taking 5 samples from the cell population and placing those in MethoCult the CFU assay can be completed in both a standard incubator, shown in grey, and the Cell-IQ, shown in orange. The 5 samples in each place were completed with various volumes of the starting population to ensure neither system had growth saturation, or influenced the total number of colonies. From user verification, as is the standard, the colonies could be counted and categorised (data not shown). Both incubator systems show very similar data suggesting that the environmental factors, highlighted earlier, are now at equilibrium. The total colony number shown in Figure 118 were a mixture of CFU-GM, CFU-GEMM and BFU-E identified colonies, the ratios of each were also maintained in both systems (data not shown). This final experiment has shown that using humidifier version 3 within the Cell-IQ provides comparable end point results to a standard incubator and therefore suggests that using the Cell-IQ to continually monitor colony development whilst not affecting their growth characteristics.

5.3.8 Conclusions

Initially the environments within the Cell-IQ and a standard incubator were different, largely due to the Cell-IQ passing dry air over the substrate to maintain pH and oxygen levels. As described by the manufacturer this would cause large variation within the CFU assay. It therefore was important to match the conditions found within a standard incubator to that in the culture vessel of the Cell-IQ. This was accomplished by pre-humidifying the gas inlet, to prevent the methylcellulose gel from rapidly drying. Through testing it has been possible to develop a humidifier which fits within the Cell-IQ imaging area and is therefore held at the same temperature as the culture vessel. In addition the use of a 20 µm sparger further increased the humidity, along with tailoring the gas flow rate in terms of flow rate and cyclic behaviour. All this development has allowed for the conditions in the Cell-IQ to match those found in a standard incubator, this allows for the CFU assay to be continually monitored without introducing unknown variation to the culture procedure. This has been shown by end point analysis of cultures in the Cell-IQ and in a standard incubator to be of similar colony phenotype and numeration. The next stage is to identify individual cells that make up a colony and any metrics which can be non-invasively measured to make informed decisions on colony phenotype.

5.4 Colony Identification

After plating purified CD_{34}+ cells in methylcellulose gel into culture vessels the development of colonies is followed through continual imaging. This creates a continuum of images following colony formation over time. From these images it is possible, through the use of machine vision from the Cell-IQ analyser package, to successfully identify single cells from within a colony. This is completed by 'teaching' the Cell-IQ the image of a single cell, which is depicted as a group of pixels. This pattern of pixels can then be searched for throughout the image to identify further cells. A

technique similar to that employed previously in identifying coverage areas of various morphologies in Section 3.4.2.2.

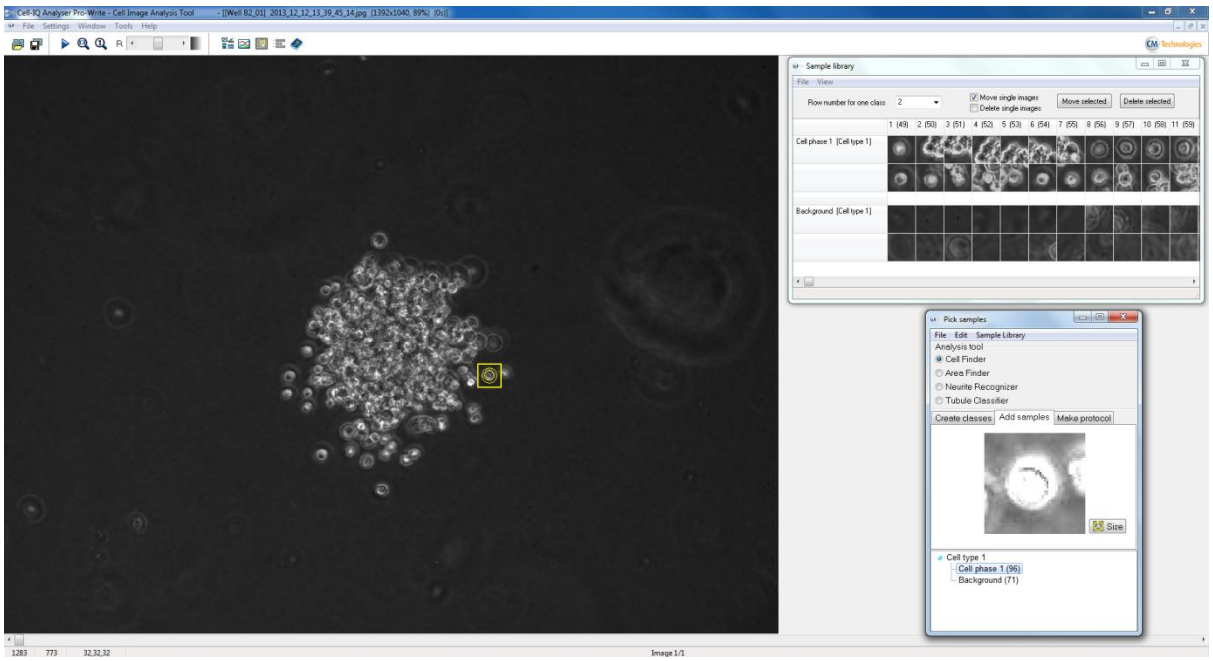

Figure 119. Count/Classify protocol for identifying individual cells. By selecting individual cells shown by the yellow boxed circle, the picked samples shown in the bottom right are added to the population library shown in the top right.

Figure 119 shows the protocol for selecting exemplar images of individual cells using the yellow circle and box. Having built a library of exemplar images showing the background/debris and cells this protocol is then used to identify single cells in a colony as shown in Figure 120. Once again library sizes of 200 images as used for the accuracy describe in Section 3.4.2.3. Identified cells are marked by a red dot, with cells that are slightly out of focus marked by a green dot.

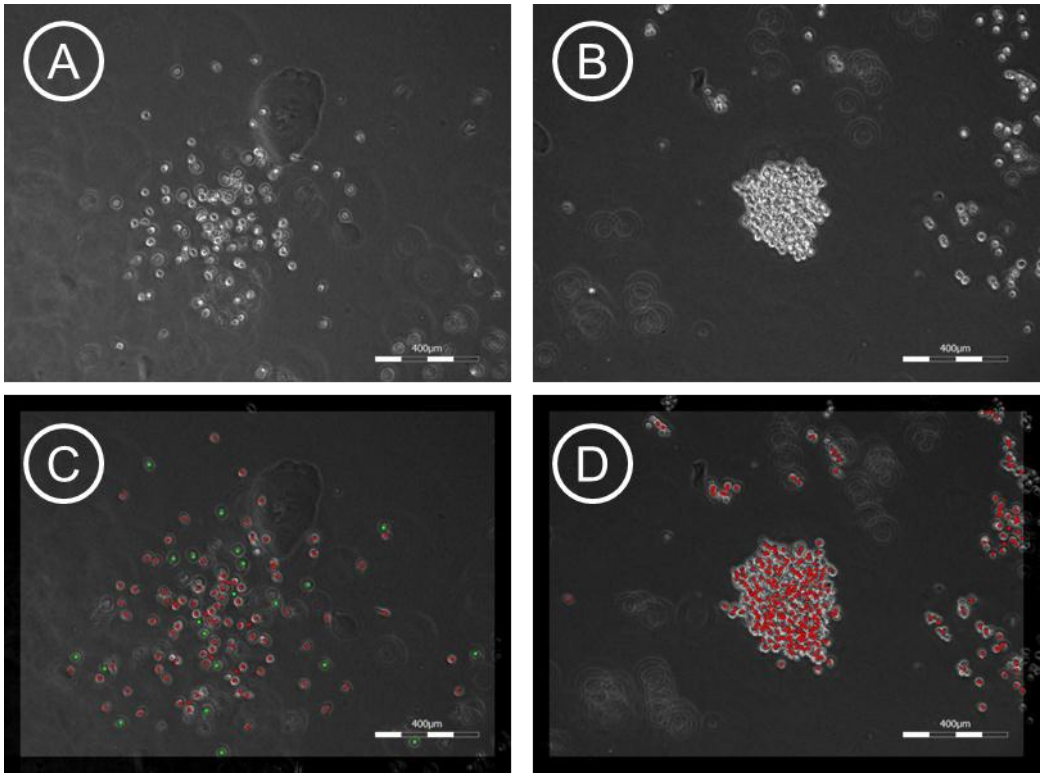

Figure 120. Raw and analysed images of a BFU-E and CFU-GM colony from the Cell-IQ at one time point during development. A GM colony is shown in A) with the respective analysed image shown in C). A BFU-E is shown in B) with its analysed image in D). The red dots show where the analysis identifies a cell, whereas the green dots represent out of focus cells.

Figure 120 has shown that it is possible to identify single cells during colony formation with images of both GM and BFU-E colonies used as examples. This successful identification then allows quantitative metrics to be determined during colony growth within the Cell-IQ system. From assessing captured images of colony development it is possible to identify possible metrics which may be characteristic of the originating cell. These are listed in Table 18.

Table 18.HSC Identification Metrics. A list of potential metrics that could be used to classify colonies rather than the current user defined morphology identification.

Characteristic	Metric	Abbreviation	Evidence
Growth	Cell Number over time	d#C/dt	Varied colony size by day 14, suggestive of variable growth
Distance between cells	Voronoi Triangulation	V	Colony morphology is the core identifier of colony phenotype
Distance Cells Move	Tracking of Cells	D	Related to morphology, the varied morphology is attributed to a difference in cell migration
Speed of cell movement	Tracking of cells over time	S	Distance cells move normalised for time variation

Each of these metrics can then be tested using a sample of colonies imaged over 200 hours, to test if they are predictive of colony phenotype. Purified $CD34^+$ cells are added to MethoCult and left in a standard incubator for 72 hours as described in Section 2.13. This allows gelation to occur and the cells to begin proliferation. Following this 72 hour lag period the culture vessels are placed into the Cell-IQ to begin imaging. Colonies are then imaged continually for 200 hours before the captured images are analysed. After analysis the data is colour coded based on colony phenotype which is assessed through user verification on day 14 of the assay, as is standard practice. All times are based from when the cells are first placed into the Cell-IQ as t=0, as opposed to when they begin culture which is 72 hours previous.

Following analysis of these metrics it is possible to analyse the population distribution to evaluate the most useful metric, or combination to achieve colony phenotype categorisation.

5.4.1 Colony Growth

After analysing all the images captured following colony development the number of cells present in each image can be plotted against time. 65 colonies from 5 separate experiments, each which have been imaged for 200 hours, are shown in Figure 121.

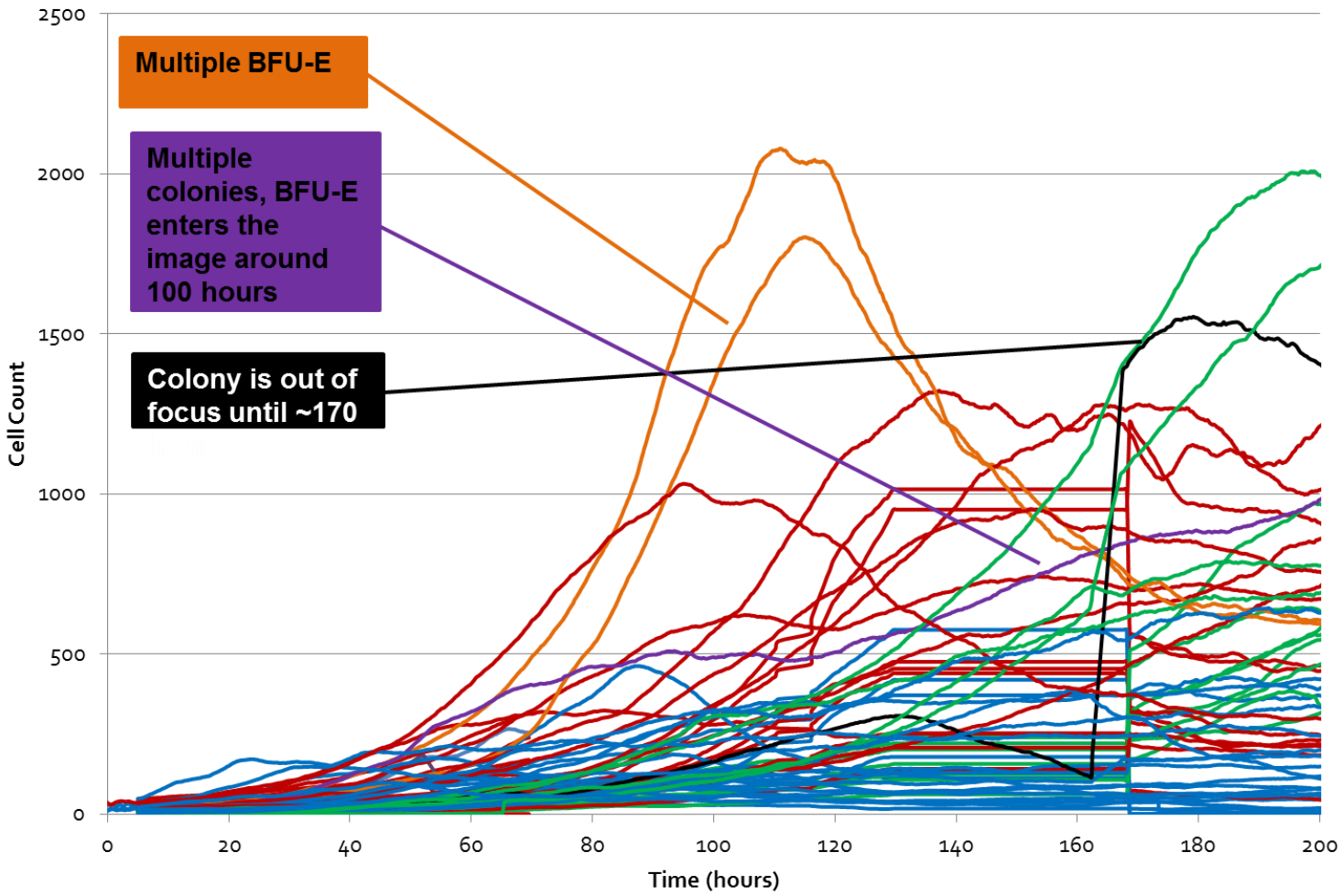

Figure 121. Haematopoietic progenitor Colony growth based on cell number. Number of cells within a colony over time as determined by Cell-IQ Analyser program using machine vision technology. The red lines represent BFU-E, the blue GM and the green GEMM, all determined by post processing user defined assessment. Also highlighted are 4 colonies that have a different growth pattern to that expected. Post processing assessment drew conclusions noted in the coloured boxes that identified reasons for these colonies having properties that were outlying form the others. (Smoothed over 5 hour data sets, n=65)

In Figure 121 the red lines depict burst forming unit - erythroid (BFU-E) colonies, the blue lines are colony forming unit - granulocyte, macrophages (CFU-GM) colonies and the green are colony forming unit - granulocyte, erythrocyte, macrophages and megakaryocyte (CFU-GEMM) colonies, all which have been user-categorised at the end point of the assay. This user identification is currently the standard for CFU assay evaluation by reference to categorised colonies from CFU assay manufacturers. These are the three colony phenotypes that are most commonly categorised due to their value in determining the biological properties of the seeding population (183). The data shows that the number of identified cells increases faster and reaches a higher value for BFU-E colonies suggesting an increased proliferation over CFU-GM and CFU-GEMM colonies. It is important to note that the cells forming a CFU-GM colony are more motile then the tight ball of cells constructing a BFU-E colony, and therefore as the CFU-GM colony expands often cells will move out of both focus and the imaged area. This is especially noted as the cell count of CFU-GM colonies plateau out after 100 hours, which from evaluating the raw images is when the cells begin to occupy the entire image window; further proliferation occurs but due to the increased motility cells migrate out of the image window. This causes the cells to remain a set distance apart, therefore preventing a measured increase in cell number within the imaged area, (distance is another metric analysed later). This data suggests there is a continuous spectrum of colony growth rates, although growth rates are broadly grouped by colony type, there remains a variability of growth rates observed within a given colony type. It is inferred that this distribution of growth rates relates to the maturity level of the seeded cell; with the fastest growing representing the least mature, and the slowest the most mature (194) . Some research groups also classify colony forming unit – erythroid (CFU-E) as another phenotype arising from a more mature BFU-E, with a similar morphology but typically less than 100 cells (195,196). This data suggests that the clarity between BFU-E and CFU-E becomes blurred, signifying there is a continuum through the classifications. Current methods for analysing hematopoietic progenitor cells categorise colonies into 3 or 4 species. This analysis allows these categories to be subdivided based on growth rates, and provides

evidence of growth kinetics which could be related to population maturity. Further work could aim to measure this maturity based on gene expression from single colony picking.

The BFU-E population also tends to decline as the assay progresses past 100 hours. In a standard growth curve this would represent cell death. In this image analysis this is due to the change in morphology of the colonies. As BFU-E colonies develop and mature there is a red colouring that develops which is seen as a dark area on a monochrome phase contrast image. Once this has occurred the image analysis loses the ability to identify single cells, and therefore a drop in cell number is recorded. An example of this is shown in Figure 122.

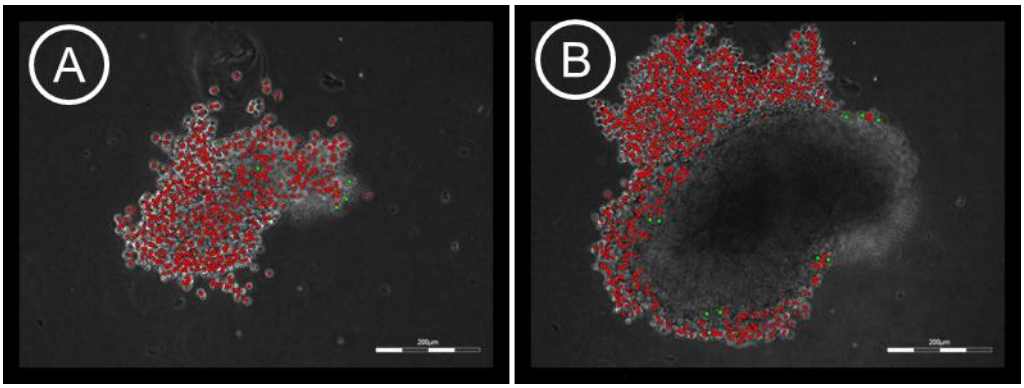

Figure 122. Example of miss-identification as BFU-E colony develops. At an early stage of development A), all cells within a colony are identified with a red dot. As the colony grows and develops, the core becomes opaque and individual cells are not identified B). On a growth curve based on image identified cell numbers this can be perceived as cell death.

The decline of BFU-E cell numbers in the growth curves in Figure 121 is due to the opaque colony cores not being identified as shown in Figure 33. It is important therefore not to see this as cell death but as a morphological change within the colony.

Assessment of the growth curve from image analysis cannot provide sufficient separation of colony type. However it provides an assessment tool which can highlight any images which have unusual growth patterns. There are colonies present in this data set which have dissimilar cell number profiles to colonies of the same phenotype, such colonies are highlighted as the orange, purple and black growth curves. The orange profiles rise much faster than the other BFU-Es. From assessing the captured images it is possible to identify that these images contain more than one BFU-E and

therefore the cell count and proliferation is doubled. It is inferred that the multiple colonies identified may have come from a single colony that has been split due to plate movement prior to imaging. The purple line shows a CFU-GM colony which past 100 hours continues to increase in cell number within the image. This occurs due to a BFU-E entering the edge of the image at 100 hours, causing the identification of its own proliferation alongside that of the more spread CFU-GM colony. The final anomaly identified from Figure 121 is the black line. This represents a BFU-E which has a sudden increase in cell number past 170 hours. This colony was out of focus for the majority of the imaging and only came into focus post 170 hours, where cells were then correctly identified. The capability of this process to identify these erroneous colonies from the population highlights the benefit and utility that these growth curves provide on a first stage of improved colony phenotype identification.

As the cells differentiate down the lineage map shown in Figure 88 the cells loose proliferation potential, shown by a reduction in growth rates, noted previously by Ogawa (194). This confirms that the growth rate or cell number is representative of cell maturity. This data confirms previous work (171,178) that there is a heterogeneous population within the CD34+ compartment of cells. However using growth rate alone the CFU-E and CFU-GM colonies cannot be distinguished successfully, due to an overlapping of growth rates. Therefore a further metric is required to improve the resolution of differentiating between colony phenotypes.

5.4.2 Distance between Cells within a Colony

Another proposed metric was the ability to measure the distance between neighbouring cells within a colony, it is hypothesised that CFU-GM colonies will have a far greater distance between cells then BFU-E due to their difference in morphologies. This was previously seen with the cell counts plateauing as the cells migrate from CFU-GM colonies out of the field of view.

The most common method for measuring distances between objects is through triangulation. In 1934, Delaunay proved that when a dual graph is drawn with straight lines it produces a planar triangulation, Delaunay triangulation, which creates a triangle with points such that no point lies within the circumcircle of a triangle (197). Delaunay triangulation is widely used in scientific computing in many diverse applications (198). The fundamental property that favours Delaunay Triangulation over other triangulation algorithms is firstly the empty circumcircle criterion, stating that each triangle contains no other points within its interior. The second property is that triangles are created using the nearest neighbour point and triangles with large internal angles are selected over ones with small internal angles (198). For its application here the nearest neighbour triangulation property is the most important to measure the distance between points or in this case cells. The Delaunay triangulation of a CFU-GM colony is shown below in Figure 123.

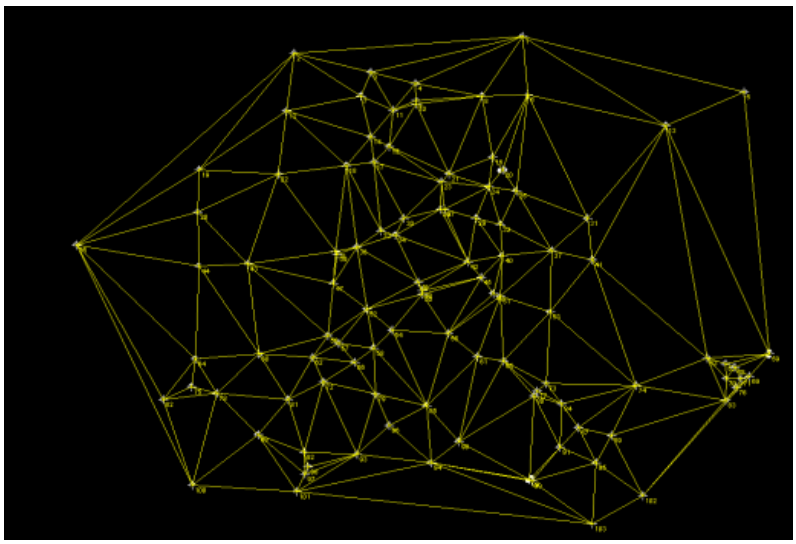

Figure 123. Delaunay Triangulation of a GM Colony. By mapping each cell with an x and y position it is possible to calculate the nearest neighbours using triangulation, shown as yellow lines linking cells together

This triangulation creates a relationship between cells allowing the nearest neighbours to be highlighted. However due to the triangulation there are 2 or more distances to the neighbours, it is therefore advantageous to get a single output for each cell. This is where the Voronoi Diagram is beneficial. Delaunay triangulation and Voronoi diagrams are dual structures of each other, that is to say they contain the same 'information' but it is represented in a different form. In Figure 124 the

Delaunay triangulation from Figure 123 with the 'equivalent' Voronoi Diagram superimposed is shown.

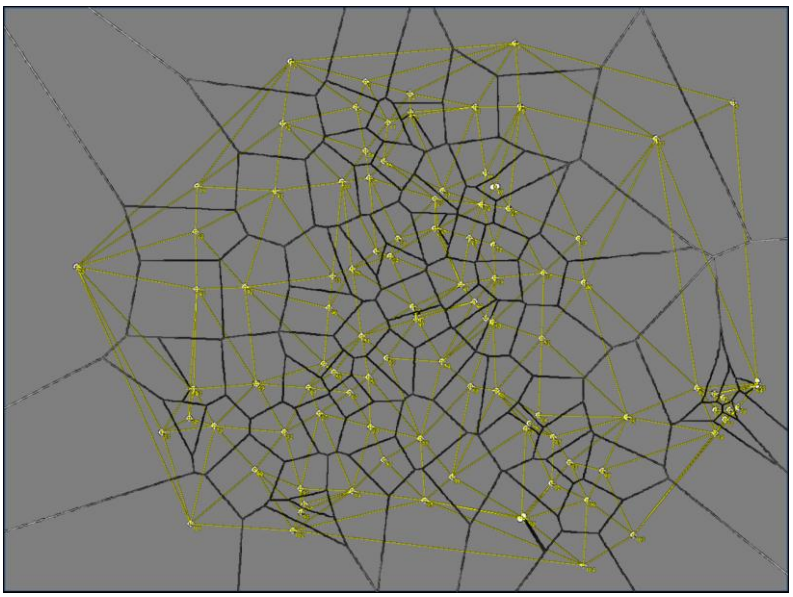

Figure 124. Voronoi diagram superimposed on Delaunay triangulation of a GM colony By taking the Delaunay triangulation from Figure 123 it is possible to divide the planes (yellow lines) into a set of areas based on the nearest neighbour measurements. This is achieved by creating an area around each cell in which no other cell lies. Delaunay triangulation and Voronoi diagrams contain the same information just represented in a different format. The Voronoi diagram creates a single area measurement for each cell, which is more useful for process control.

The Voronoi diagram divides the plane into a set of regions or areas based on the nearest neighbour notation. In this example each cell is therefore specified an area, the closer the cells are together then the smaller this area is. This allows each cell to have a single output or quantitative value assigned. This then means a population average can be deduced from the entire image. In order to create a Delaunay triangulation and in turn a Voronoi diagram a number of steps must succeed to transform the original image captured by the Cell-IQ into a binary dot image.

Firstly the cells are identified from the raw image (Figure 125 A) using the algorithm in the previous section 5.4.1. This places a dot on every cell, such as in Figure 125 B. Due to the captured images taken on a monochrome camera, and the identified cells marked with red or green dots, a colour based threshold can be used such that only the identified cells with red and green dots on are visible, Figure 125 C. This image can then be made binary, Figure 125 D. Following this the Delaunay

triangulation algorithm can be applied, creating a triangle with the nearest neighbours for every cell, as shown in Figure 125 E. The final part is to create a Voronoi Diagram from the triangulation as shown in Figure 125 F.

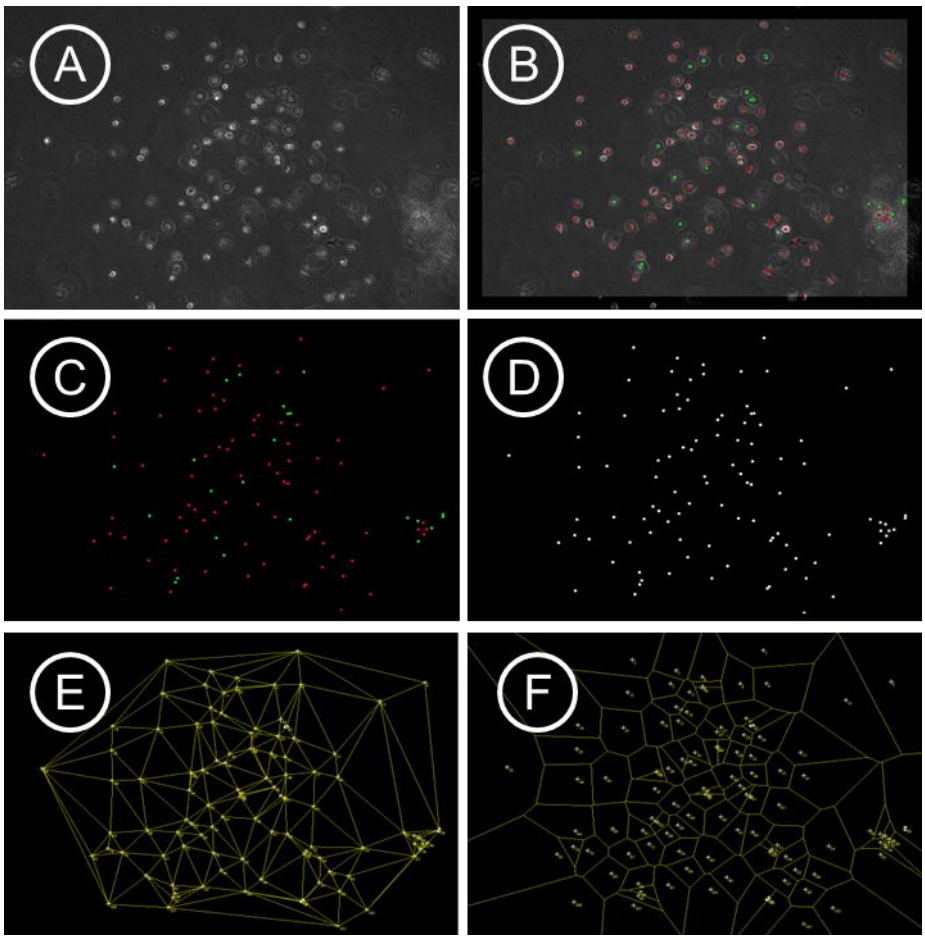

Figure 125. Creating a Voronoi Diagram of a CFU-GM Colony. By first taking the raw image (A), using Cell-IQ Analyser software each cell can be identified and marked with either a red dot(in focus) or green dot (out of focus) (B). For this analysis both red and green dots are included. The image is then threshold to only include red and green, therefore removing the background data (C). Following this the image is made binary so that each cell is now represented by a white dot on a black background (D). Using ImageJ the 'Analyse Particles' algorithm using threshold to measure all white objects, here the cells. Once this is completed each cell has an x and y position. Next the 'Delaunay Voronoi' algorithm is used to create images (E) and (F) where a triangulation around the white dots is created and then an area for each cell with which no other cell lies can be drawn.

Completing this Voronoi analysis on colony development over time allows the mean distance between all the cells within a colony to be calculated at each time point of image capture. Completing this for a number of images shows how the distance between cells within a colony changes during colony growth. The macro written in ImageJ software is shown in Appendix 8.3. The same data as used in Section 5.4.1 is utilised here, with the same colour coding for anomalies.

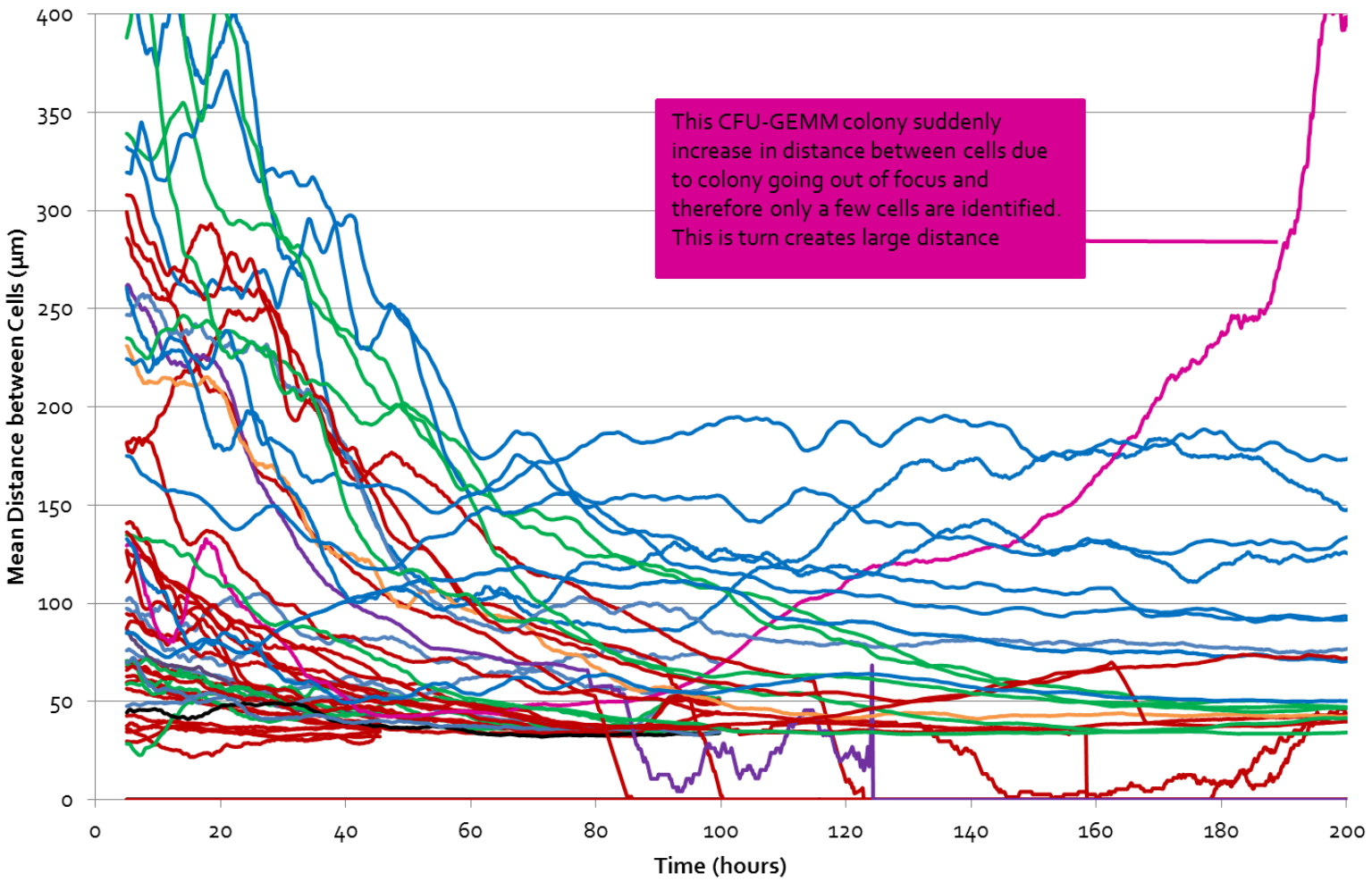

Figure 126. Mean distance between cells within a colony By using the Delaunay triangulation the mean distance between each cell can be calculated. By completing this on every image of a colony a variation in distance between cells over time can be drawn. From this figure it is possible to see that BFU-E colonies, shown in red, over time get much closer together, forming the ball structure. GM colonies in blue however seem to keep separated. GEMM colonies, shown in green, initially behave as a BFU-E before suddenly bursting at around 100 hours. (Smoothed over 5 hour data sets, n=65)

The anomalies once again are highlighted here by using orange, purple and black. The orange line signifies the very high growth rate which related to two BFU-E colonies in the same image. For the distance between cells this has little effect, so does not appear as an anomaly. The purple line depicts a CFU-GM colony which is invaded with a BFU-E after about 80 hours, this is shown by the fluctuating line after this time period. The black line identifies a BFU-E that goes out of focus, due to the low cell count, this drops to zero and is cannot be distinguished in Figure 126. This drop to zero is a current limitation of using the current Voronoi identification coding. If no cells are measured then the distance between cells goes to zero and forces the algorithm to stop measuring the remaining images in the series. This can be seen at the 100 hour mark, where previously it was seen in the growth curve that a computer malfunction caused no measurements to be taken, this malfunction registers zero cells and prevents further image processing. A new detected anomaly is shown by the pink line in Figure 126. This represents a CFU-GEMM colony that past 100 hours quickly increases the distance between cells. This increase in distance is due to the colony going out of focus, and therefore less cells are identified, increasing the distance between them. Similarly to the cell counts the Voronoi diagram also offers a useful tool for the identification of anomalies, where the image capture and analysis are at fault rather than the colony development.

On top of anomaly identification the data collected here provides us with evidence of how Voronoi triangulation can be used. The first 100 hours begins with a large distance between cells that reduces as time increases for all colonies. This is expected as at t=0 there are only a few cells forming each colony and therefore there is a large distance between them. This is further exaggerated as the Voronoi diagram uses the image boundary as a point from which to create a triangulation from. An example of the large effect this can have is shown in Figure 127.

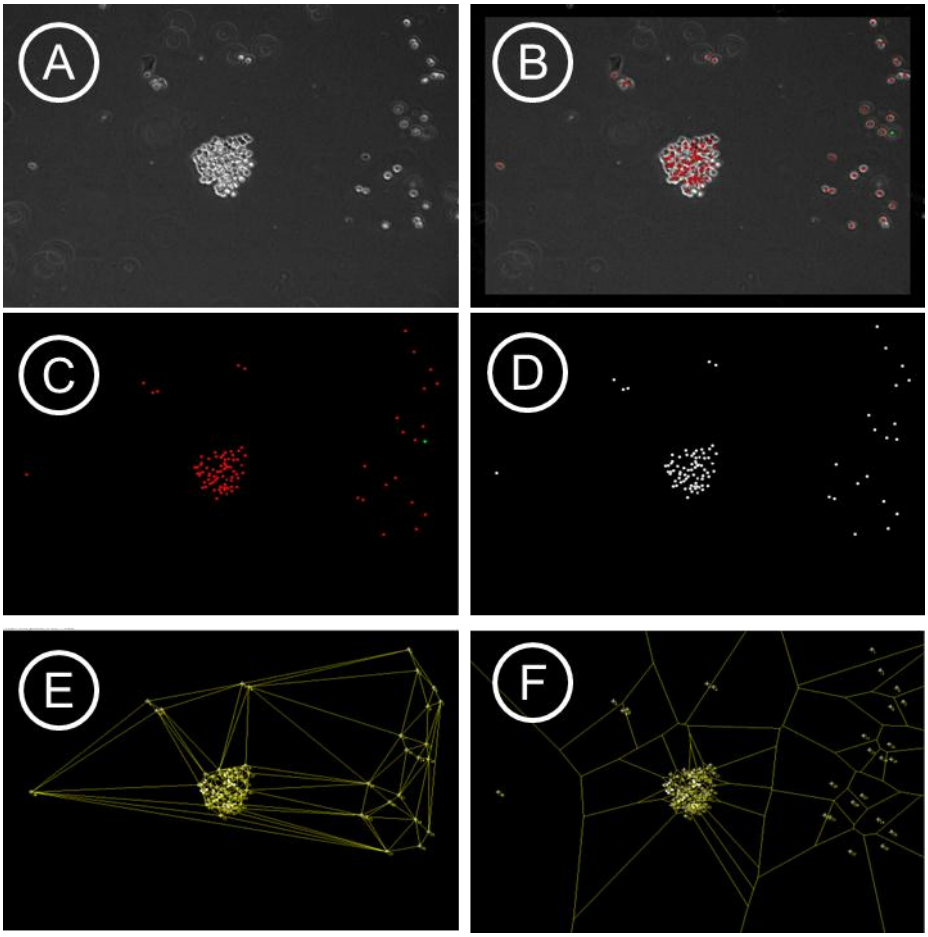

Figure 127. Voronoi diagram showing boundary being used as a position.

A developing BFU-E colony is shown in Figure 127, by creating a Voronoi triangulation in Figure 127 F) it is possible to see that the image boundary acts as another point with which to create an area with. Therefore the average of this image is far greater than the centre where the colony is developing as a tight ball. Therefore by including the entire area the mean distance between the cells is skewed. By taking a point later in time such as at 100 hours, where all the colonies have a tighter range of distance the edge effect has less of an effect due to the number of cells, this can be seen in Figure 128.

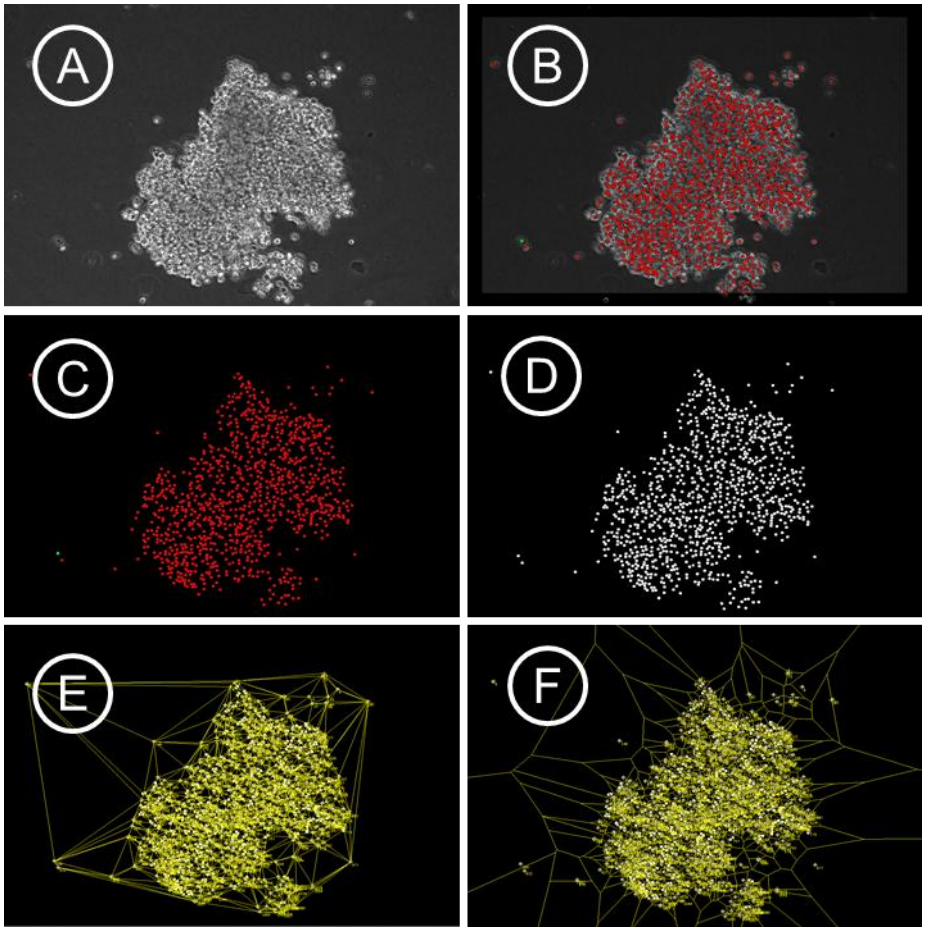

Figure 128. BFU-E colony at t=100 hours. By taking an image at 100 hours there is a large number of cells, thus the edge effect is negligible, as the mean area is only slightly skewed.

By analysing the image at 100 hours there are now lots of cells present. This therefore means that the mean distance is skewed less, and therefore a meaningful value is calculated. This allows separation between the colony species at 100 hours, whereas earlier there was not a clear separation.

Another option which would further remove the edge effect is to take a region of interest (ROI) in the centre of the image and use only that for the Voronoi triangulation. An example of this is seen in Figure 129 by taking the centre 300 by 300 pixels.

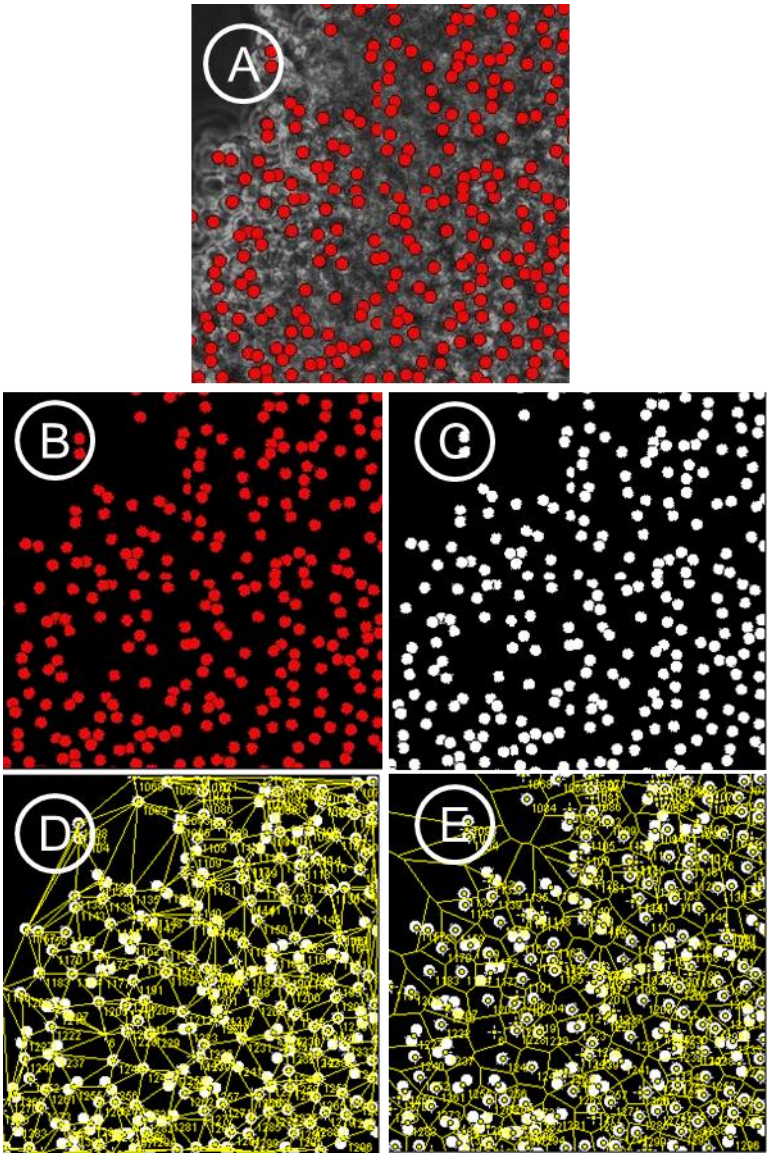

Figure 129. 300 x 300 pixel region of interest (ROI). Highlighting the effect of taking just the centre of an image, the edge effect previously noted is neglected here as the image is full of cells.

Figure 129 highlights that by taking the centre area the edge effect has very little overall effect on the mean distance between cells. However by taking a region of interest the colony must be in the centre of an image, if the colony is off-centre then the region of interest misses the colony, an example shown in Figure 130

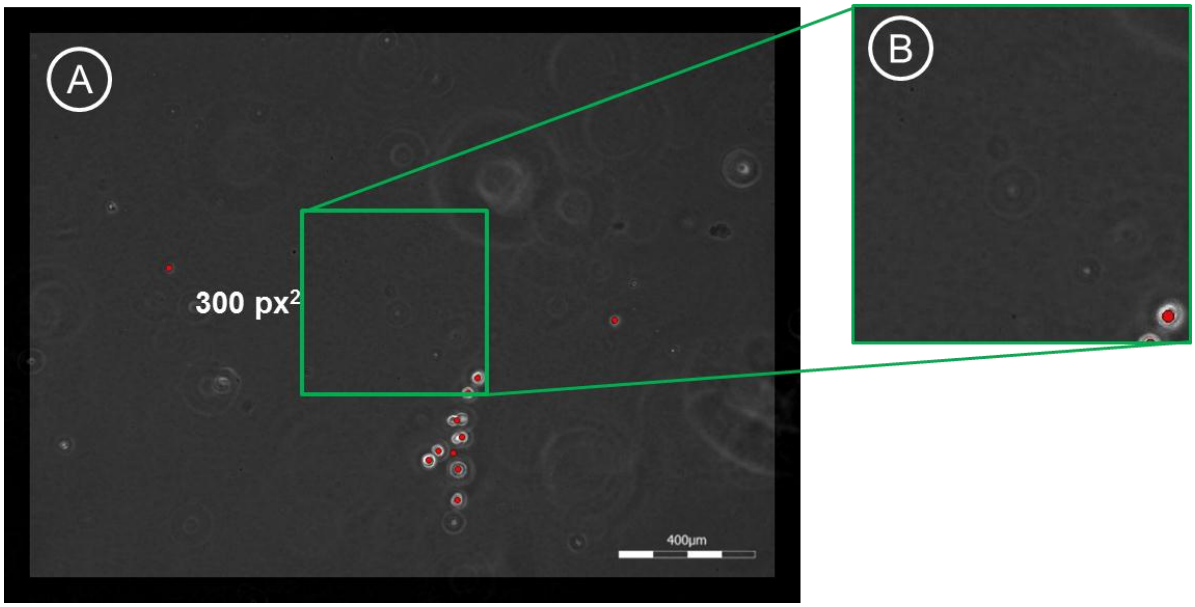

Figure 130. Example of region of interest avoiding an off-centre colony. Using the raw image A) a 300 x 300 pixels ROI can be taken shown in B). However due to the off-centre nature of the colony this is missed and therefore cannot be assessed using the Voronoi metric on a ROI.

By taking a ROI as in Figure 130 where the colony is off centre then the data cannot be used unless the colony is re-centred or the ROI can be centred around the colony. Currently both of these methods are outside the capable limits of the image capture and analysis software, although this is something that could later be implemented. This would permit the time of clear separation to be shortened as the edge has little effect. However until this is developed the full image will be used. It is still possible to separate the colonies at ~100 hour mark. The cells forming a BFU-E colony reduce this distance as the colony grows, however the CFU-GM colonies remain more spread out and by 100 hours a difference can be seen in the distance between cells in a BFU-E to that in a GM colony. The CFU-GEMM colony shown by a green line also shows a sudden increase in distance. This data provides evidence that the Voronoi metric can be used around 100 hours into the culture to categorise colony species. However similar to the growth curve there is still a large variation on the colonies, and providing a complete separation is not possible with Voronoi. The next metric to assess is cell migration, as the cells in a CFU-GM are further apart, this would suggest that they migrate further than the cells assembling BFU-E colonies.

5.4.3 Migration - Cell Tracking

Cell migration is a key biological process with a role in both physiological and pathological conditions (199). The ability to accurately analyse and quantify cell migration is important to understand development, homeostasis and disease; this includes embryonic development where exact positioning is essential for correct development in the organism. Failure for the migration of cells in such development can result in severe defects such as skull, limb abnormalities and defective wound healing for example (200).

One of the key differences between haematopoietic colonies is the morphology which for a BFU-E is represented by a tight ball of cells, and for a CFU-GM is spread out with single cells. This variation has already been detected by measuring the distance between cells in the Voronoi diagram, but in this section the migration of individual cells is assessed. From user verification individual cells that make up a BFU-E colony move little and remain within a tight ball of cells, whereas the cells making up the CFU-GM lineage colony move rapidly and spread out from each other. Often the comparison of a tight ball for a BFU-E is in contrast to firework morphology of a CFU-GM colony.

Due to the large migratory effect seen from some colonies it is important to image regularly. It has been acknowledge from user identification that imaging must occur every 10 minutes in order for the automated analysis to track the same cell. Using less frequent imaging the automated system has to guess where the cells move to and therefore is prone to large error in measuring the migration of cells. Using an increased frequency allows the algorithm for cell tracking to identify the same cell continuously.

The tracking algorithm also identifies cells in the first image and then continually monitors the same cells. This means that if there are only 3 cells in the first image then only 3 cells are monitored for the entire image sequence. In order to increase the sample size that is measured the first image used is after 24 hours of imaging. By this point there are more cells visible to track in each image. The cells are then tracked every 10 minutes for 8 days. In order to normalise for the number of cells,

the mean speed of the cells within a colony can be calculated by dividing the total cell movement by the time period that was analysed. This therefore produces a chart of average speed for each identified colony (Figure 131). For this analysis 2 time period were chosen; 24-48 hours and 90-110 hours. These were chosen to represent the initial speed of cells as the colony develops, and then a later point after which the colony is fully developed and a representative morphology is seen. These time points were judged using the cell count graph (Figure 121) and by reviewing raw images.

Tracking cells over a 24 hour period between 24 and 48 hours in the Cell-IQ allows the speed of individual cells within a colony to be measured. The speed from all cells within the same colony can then be averaged (Figure 131). This forms the first column for each colony, the second bar the represents the same average speed taken between 90 and 110 hours. This is completed using 65 colonies from 4 separate experiments. Once again there is significant variability both between colony phenotypes and between data sets. The fastest CFU-GM (blue) colony is over 80 µm and the slowest 9 µm, similarly BFU-E (red) colonies range from 50 µm to 7 µm. This range necessitates that it is not possible to separate the colonies on speed in this raw data form.

The variation between data sets suggests that there is assay variability as the cells forming this data set are all from the same donor. In order to accommodate for this variation it is possible to normalise each data set to the mean speed. This allows for a comparison of the data sets to one another, acknowledging that there is assay variation that needs to be accounted for. The normalised data is shown in Figure 132. One data set was not imaged past 60 hours, and therefore has no data for the 90-110 hour point.

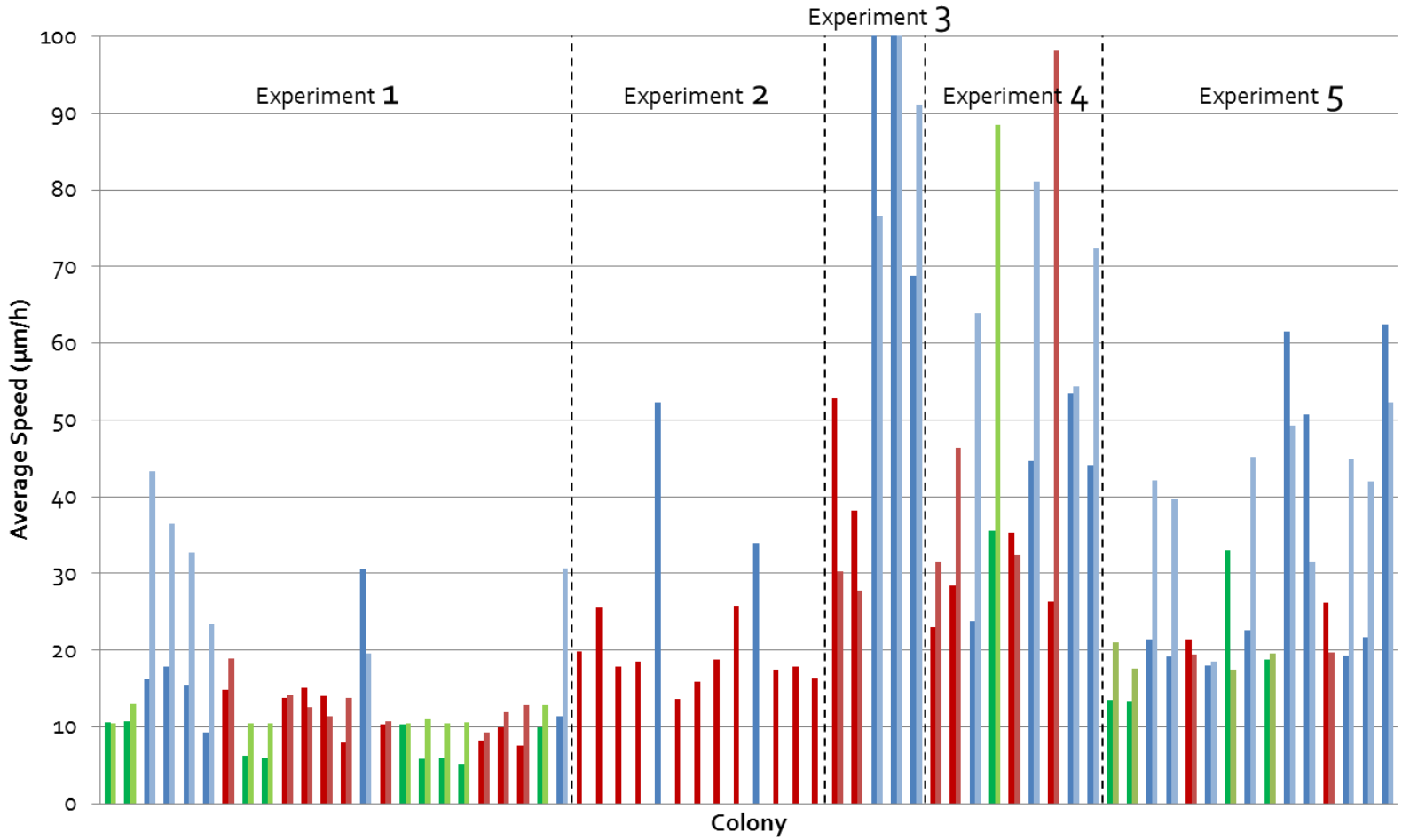

Figure 131. Average speed of cells that form a colony over a 24-48 and 90-110 hour period. After tracking the cells movement the speed that the cells move can be calculated by distance over time. The colonies are coloured based on end point user identification, red=BFU-E, blue=CFU-GM, green=CFU-GEMM. The first column of each colony is based on 24 hour period between 24 and 48 hours, the second column between 90 and 110 hours in culture. This data suggests that the cells that form a GM colony shown in blue are more mobile than those making a BFU-E colony, shown in red (Smoothed over 5 hour data sets, n=65 from 5 experiments; separated by dotted vertical lines)

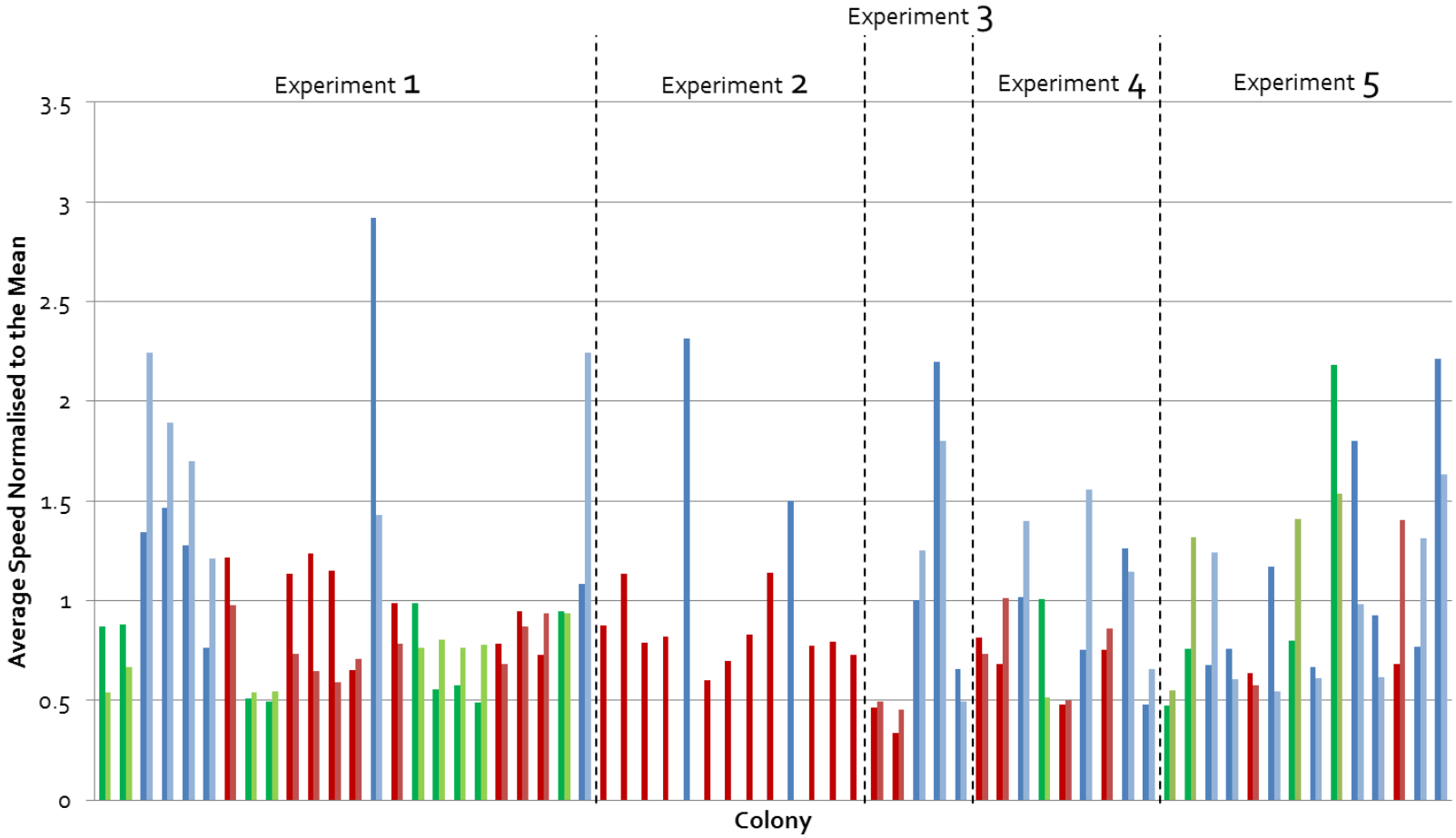

Figure 132. Normalised average speed of over a 24-48 and 90-110 hour period. After tracking the cells movement the speed that the cells move can be calculated by distance over time. The colonies are coloured based on end point user identification, red=BFU-E, blue=CFU-GM, green=CFU-GEMM. The first column of each colony is based on 24 hour period between 24 and 48 hours, the second column between 90 and 110 hours in culture. Due to assay variation each data set is then normalised to its mean, allowing a non-biased comparison between data sets. This data suggests that the cells that form a GM colony shown in blue are more mobile than those making a BFU-E colony, shown in red (Smoothed over 5 hour data sets, n=65 from 5 experiments; separated by dotted vertical lines)

Having normalised the data, a comparison between data sets is now acceptable. From this data there is a distinct increase in speed for CFU-GM (blue) compared to both CFU-GEMM (green) and BFU-E (red). This was hypothesised as from watching the colonies develop it is possible to see the rapid dispersion of CFU-GM colonies, and therefore the greater movement these cell exhibited. By assessing captured images it is possible to see that the firework action happens at different time periods, likely due to micro environmental conditions or maturity levels. This therefore influences if there is a greater speed, and at which time point this is seen. Once this initial burst has occurred the cells appear to slow their movement as they proliferate. It is therefore important to capture the time period when this burst occurs. Although as mentioned this is different for each colony which makes the time point critical for an accurate categorisation. This further suggests that a single time point measurement can be improved by assessing development over a time period such as seen here with each metric continually analysed. Distributions of the colonies are drawn to allow comparison of the phenotype categorisation resolution of each metric.

5.4.4 Colony Distributions based on Identified Metrics

Three metrics have been utilised to follow the development of haematopoietic colonies with the ambition to categorise the colonies. By plotting the distribution of each colony phenotype based on its metrics it is possible to decipher which metric is the most powerful at resolving the colony phenotypes. Figure 133 shows each normal distribution plot for the metrics of count at 110 hours, distance between cells at 100 hours, speed of cells at 24-48 hours, and speed of cells at 90-110 hours. Each of these time points represent when the greatest difference is observed, as verified by user identification.

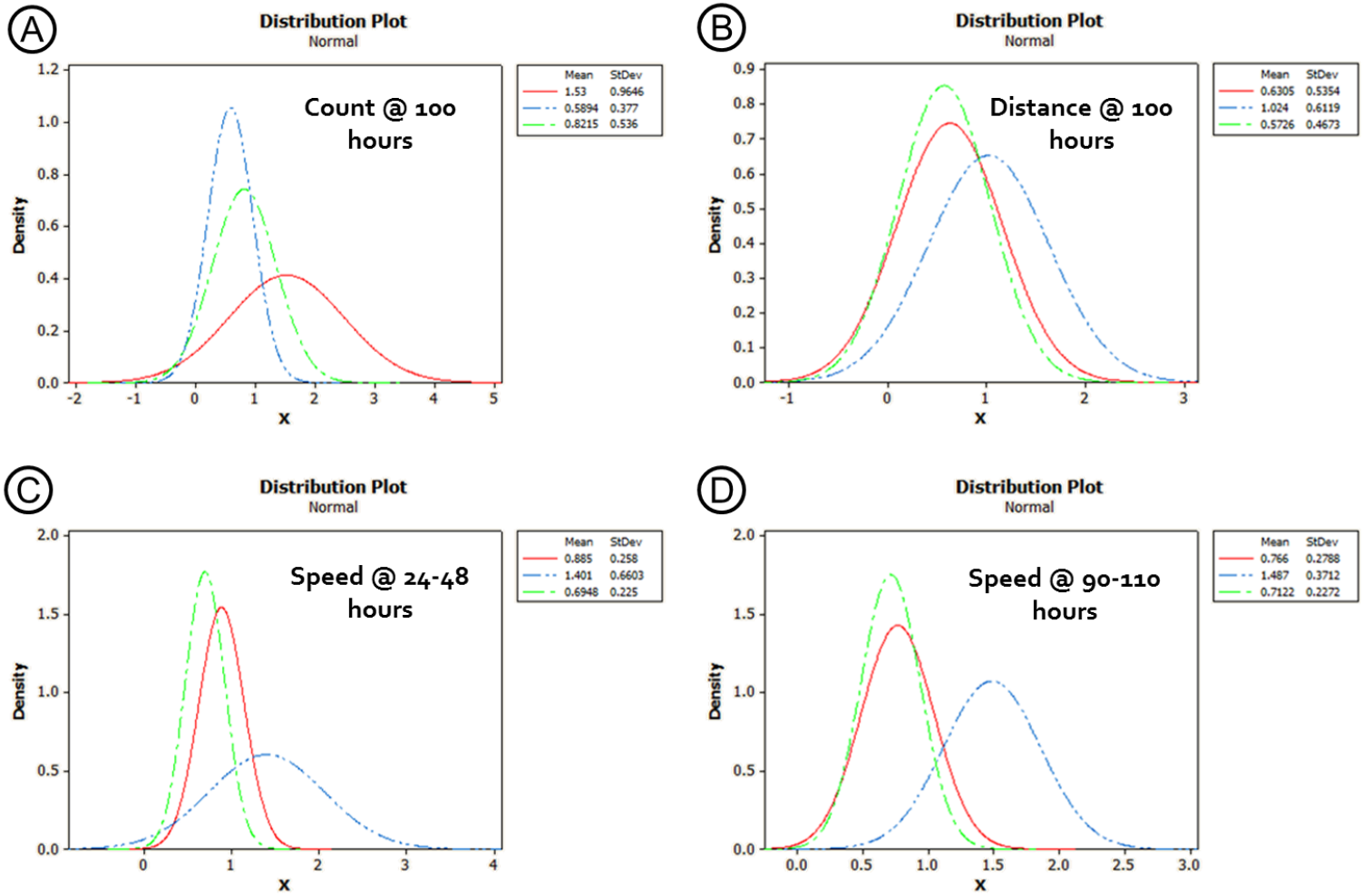

Figure 133. Distribution plots of colony phenotype based on 3 metrics. Identifying colony phenotype using cell count of colonies at 100 hours A), distance between cells within a colony at 100 hours B), speed of cell movement within a colony between 24 and 48 hours C) and 90-110 hours D). The distributions are coloured based on colony type, BFU-E – red, CFU-GM – blue, CFU-GEMM – green. n=65

Figure 133 shows the distributions of each individual metric which are colour coded based on user verification, with red for BFU-E's, blue for CFU-GMs and green for CFU-GEMMs. As predicted previously both the count at 100 hours and distance between cells taken from Voronoi diagram at 100 hours have overlaps of each colony phenotype, known as a mixed population. The clearest separation between colony phenotypes is seen using the speed measurement between 90 and 110 hours, which shows distinction between CFU-GEMM and BFU-E to CFU-GMs. By taking the point of intersection in Figure 133 D) between BFU-E and CFU-GM (red and blue) it is possible to calculate the confidence interval for the identification of a single colony to fall within the correct category. This intersection occurs at 1.11442 as shown in Figure 134.

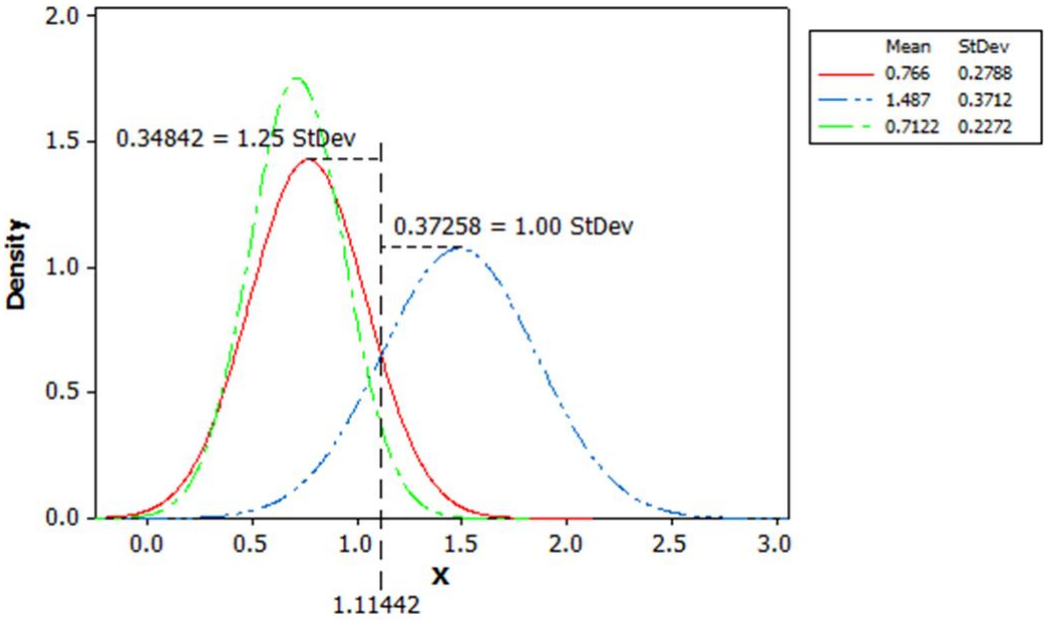

Figure 134. Distribution plot of speed between 90-110 hours, with intersection and standard deviation markings. Marking the intersection of BFU-E (red) and CFU-GM (blue) the confidence of correct classification can be calculated.

From Figure 134 the intersection lies 1 standard deviation away from the mean of CFU-GM distribution. Therefore a confidence interval of ~82% (50% one side and 32% of the overlapping side) is defined. Given the difference in standard deviation and therefore shape of the distribution for BFU-E, this is 1.25 standard deviations from the mean to the intersection, relating to a 90% confidence interval for the correct categorisation of a BFU-E. Both of these confidence intervals

represent a high degree of classification however this is ignoring the overlap of about 23% as calculated from the overlapping coefficient (201) shown in Appendix 8.5. This overlap represents a large potential error which must be accounted for to use the distributions for colony identification. The statistic required to calculate the confidence interval for a mixture of Gaussian distributions is known as the 'Bootstrap Algorithm for Mixture Models' (202). This requires extensive computer simulations to produce an accurate estimate and falls outside the scope and knowledge for this thesis. However it does form an interesting further work section to be able to provide a confidence interval for any given colony to fall within the correct categorisation. This will be discussed later in Section 6.2

Using this distribution it is possible to measure the speed of cells within any colony and distinguish between BFU-E and CFU-GM colonies. This method does not provide a separation of the CFU-GEMM phenotype, although as stated previously for the majority only BFU-E and CFU-GM colonies are often categorised. However the BFU-E population would also contain GEMM, and therefore the total number of categorised BFU-Es would be exaggerated. From Figure 133 it's possible to appreciate that using counts at 100 hours provides the best separation of BFU-E to GEMM. Therefore using the same method (bootstrap algorithm) as shown previously and the data in Figure 135, the confidence intervals can be calculated.

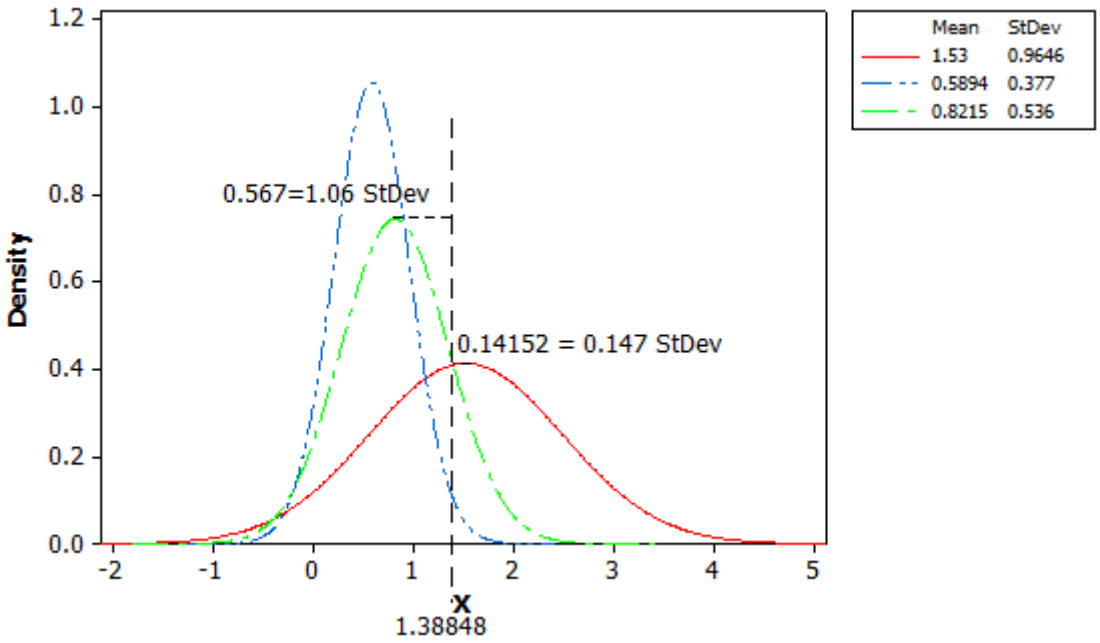

Figure 135. Distribution plot of count at 100 hours, with intersection and standard deviation markings. Marking the intersection of BFU-E (red) and CFU-GEMM (green) it is then possible to calculate the confidence interval for a single measured colony to fall into the correct category.

These two examples identify an opportunity to use the image derived metrics to conclude the colony phenotype after 110 hours. It is important to remember that this 100 hours is from the point of imaging, rather than culture which occurs 3 days prior. Therefore in total the image derived metrics method of colony identification can be applied 182 hours into the culture. This is half the current time for the CFU assay, with the benefit of automated analysis and calculated confidence.

5.5 Conclusions

The first aim of this chapter was to evaluate and improve, if required, the environment found within the Cell-IQ imaging platform to that of a standard incubator. Initially it was found that due to the gassing mechanism within the Cell-IQ, the cultures were continually exposed to a very low humidity, causing significant drying of the methylcellulose gel assay. This rapid drying had major growth characteristic consequences that prohibited the use of the Cell-IQ for CFU assay monitoring.

In order to accommodate for this humidity issue, a humidifier was developed, improved and ultimately tested in order to ensure the humidity within a standard incubator was comparable. By passing the dry inlet air from the Cell-IQ through a 20 µm pore size atomiser in a 3 cm head of water the humidity in the culture vessels could be increased to 80%. This was further enhanced using water in the culture wells where the pre-humidified gas entered. This was seen to vastly reduce the drying time of 20 µl droplets that were used as a test mechanism.

Following the successful pre-humidification of the inlet gas, it was seen that a comparable colony number and phenotype were noted within a standard incubator to the Cell-IQ samples 14 days after CFU assay. This allowed for continual imaging and monitoring of the growth of colonies within the Cell-IQ and led to the finding of measurable image metrics. 3 metrics of cell number, distance between cells and cell migration within individual colonies were noted to be informative and measurable within the system. Following colony development over time allowed time points were colony behaviour was dependent on phenotype. This was seen by correlating back user identified colonies to the image derived metrics. Taking the cell count at 100 hours, distance between cells at 100 hours, and the migration of cells between 24-48 and 90-110 hours were deemed to be the most informative. By plotting distribution plots of each metric after categorisation of phenotype allows for the confidence in separation between phenotype to be measured. Due to the lack of clear separation this involves the use of computer algorithms using the bootstrap method to measure the probability of correct colony identification. There are mathematical methods available to address these issues which can be progressed as further work.

6. CONCLUSIONS AND FURTHER WORK

6 Conclusions and Further Work

6.1 Conclusions

Regenerative medicine represents a promising enabling technology to revolutionize healthcare. This has been highlighted through numerous publications (203–205), with regenerative medicine being highlighted as one of the UK's Eight Great technologies (204) due to its potential for technological advancement and economic benefits. Further proof of regenerative medicines current momentum is expressed with John Gurdon of Cambridge and Shinya Yamanka from Japan recently being awarded a joint Nobel Prize for their work revealing the re-programming of mature cells to immature, pluripotent cells in 2012 (206). Also the establishment of the Cell Therapy Catapult in 2012 as a centre of excellence in innovation (207) further shows the significant capital being invested into regenerative medicine. This said there are still major gaps between the commercial promise and the reality of the cell therapy sector of regenerative medicine (208). There is a common consensus to '*develop high through-put and automated technologies for safety assessment of cells, for pre-clinical work, and for the manufacture of clinical regenerative medicine products*' (3,4,204).

Imaging has been quoted to have the capacity to contribute to this technological gap for cell therapies by the FDA's Critical Path to New Medical Products (47) as well as the British Standards Institution (BSI) in PAS93:2011 (29). Furthermore imaging is particularly attractive to provide non-destructive monitoring with high spatial and temporal resolution (48).

With that in mind this thesis was aimed at developing and testing a novel imaging platform to aid the ability to monitor cell cultures during manufacturing. The work utilised an automated, non-invasive phase contrast imaging platform to measure, analyse and ultimately quantify image derived metrics for 2 cell types, colonies of human embryonic stem cells and human haematopoietic stem cells.

This work has shown that image analysis has the ability to improve the precision of current evaluation methods, namely cell counting, with the best tested automated capable of a CV of 7% (Cedex, Roche) whilst manual counting is reported to have a CV of 11% (111). Non-invasive image analysis has the key benefit of being able to tailor the CV through sampling frequency. The initial work showed that for embryonic colonies taking 50 systematically sampled images produced a CV of less than 5%. Further sample increases the precision of this measurement tool.

Using the 50 image sample set it was concluded that total colony coverage created a poor correlation to cell counts, which was deemed neither an error in the image analysis or cell counting. This gave grounding that there was heterogeneity within the culture which ensured that the cell/area varied across and between cultures. This was the core reason for why coverage and counts did not accurately correlate and therefore a measure of this heterogeneity was required. By assessing captured images overtime further image derived metrics were identified which separated total colony coverage into 3 separate regions; dark colony, core periphery and edge cell coverage. Using both thresholding and machine vision identification technology these areas could accurately be recognised by the software, as verified through user identification. Machine vision is the term given to duplicating the effect of human vision by electronically perceiving and understanding an image (83), this therefore permits the separation and measurement of each of these 3 'taught' areas. These new metrics provided a measure of the heterogeneity prominent across cell populations, but often not measured. This is especially noted in cell counts, where a viability assay distinguishes viable to non-viable cells, but provides no further information with regard to the culture. Using regression of the triple metrics provided an improvement to the correlation of image metrics to cell counts, however immunostaining highlighted that these morphological distinct areas were representative of variation in markers. Predominantly the edge cell coverage was negative for Oct-3/4 a marker of pluripotency. This provided conclusive evidence that edge cell coverage was a measureable culture attribute which could be used to predict the culture state or quality.

Building on the emergence of image derived metrics to inform culture state, the behaviour of these metrics were assessed over time. It was hypothesised that a variation in these attributes would provide a timely method to determine population changes. This has been shown initially through varying the feed regime, which in turn changes the metric growth curves, and correlates to a median change in pluripotent markers. As a decrease in the pluripotent markers were seen over the population it was then theorised that these metrics could also be used for measuring the controlled differentiation of cells. The addition of chemical cues in the form of a growth factor cocktail of BMP4, VEGF, FGF and Activin A stimulated a morphological response around the periphery of adhered colonies detected as a change in the edge cell coverage metric. This ability to discriminate between culture conditions of embryonic colonies using non-invasive imaging permits the use of such a novel tool for in-process monitoring.

After successfully developing such a tool the next phase was to prove the utility within a process. Initially this was completed by comparing embryonic culture which used a single vessel to predict the cell numbers in similarly seeded flasks to the Cell-IQ as a imaging platform. It was shown that the Cell-IQ increased the precision whilst maintaining non-invasiveness and therefore no flasks were required to be sacrificed at great cost to a manufacturing process. The advantage of providing a non-invasive tool permits real-time measurements to be continually gathered. By measuring the diameter of embryonic colonies it was possible to provide the afore mentioned differentiation stimuli at a timely point of culture. An example of this use was presented where monitoring the colony size, and acting on that information, has delivered differing differentiation yields. By exposing smaller colonies (<350 μm diameter) to the differentiation a more homogeneous differentiation occurs, whereas the larger colonies (>800 μm diameter) maintain a core of pluripotent morphology alongside the periphery of differentiated cells. These differentiated cells were shown to be $HAND1^{+}$ through immunostaining.

The work on embryonic stem cell colonies has provided strong evidence that image derived metrics can successfully be implemented into process development. Non-invasive imaging provides a

fantastic opportunity to create bespoke sampling frequencies to achieve desired precision for manufacturing cell therapies. Human embryonic stem cells formed one cell type of interest in this thesis due to their ability to differentiate into all 3 germ layers, along with their self-renewal potential (35,93). These properties make hESCs very attractive for the regenerative medicine industry, although any clinical use is still many years away. A cell type already used for regenerative capacity is the haematopoietic stem cell (HSC).

The ability to restore haematopoietic activity in patients who have undergone chemotherapy or irradiation forms many of the 60,000 clinical uses each year (159). However there is still a need for an in-vitro method of assessing haematopoietic quality. Current methods include total nucleated cell count, $CD34^+$ percentage and the colony forming unit (CFU) assay. All of these remain with limitations, with the CFU assay regarded to be the best predictor of engraftment (160–162). One of the key limitations of the CFU assay is the user defined end point analysis which incorporates large variation into the readout measurements. This thesis has aimed to enhance the CFU assay by measuring image derived metrics of the developing haematopoietic colonies which are predictive of colony phenotype and ultimately population quality. Prior to imaging such attributes the environmental conditions within the Cell-IQ and a standard incubator required balancing. This involved increasing the humidity within the culture vessel placed into the Cell-IQ due to its unique gassing mechanism. By directly pumping dry air into the culture plate, the Cell-IQ caused the viscous gel of the CFU assay to dry and prevent colony development. In order to maintain a constant environment to that of a standard incubator a humidification step of the gas was required prior to entering the culture vessel. This was completed by passing the gas through a fermentation sparger submerged in a 4cm depth of water. Computational fluid dynamics (CFD) along with droplet evaporation confirmed the presence and improvement of this humidity issue, and aided in the development of a solution. Following the successful humidification it was possible to continually image colony development within the Cell-IQ and identify possible attributes of the colonies to enable identification. Cell number, distance between cells and cell migration within individual

colonies were noted to be both informative and measurable within the imaging system. By following the behaviour of each of these metrics specified time points or periods were identified that provided a degree of colony phenotype separation. Although the distance between cells was hypothesised to be the best separator due to the firework and tight ball morphologies of CFU-GM and BFU-E respectively, measuring the speed of cell movement between 90 and 110 hours provided the greatest separation. With a 23% overlap coefficient for the Gaussian distributions, this provided encouraging data to suggest that such image derived metrics could be utilised to make informed colony categorisation 7 days prior to the current standard and more importantly in an automated fashion. Quantitative, novel, image derived metrics have been identified that improve the current recognition by improving reliability through computer automation, cost by removing user verification and time by reducing the assay time from 14 days to 7 days.

6.2 Further Work

This work has demonstrated the ability of using such an imaging platform as the Cell-IQ to automate the analysis and measurement of culture state. However to be fully functional and validated for manufacturing use further work is required. A number of proposed activities are outlined below.

Concentrating initially on the in-process use for pluripotent manufacture further image derived metrics could be recognised. It was mentioned that dark colony coverage utilises a single threshold value, and further resolution could be aided by segmenting the dark colony into further categories. Initially work would be required to identify the benefit of further classification especially as only small coverage amounts were observed in this thesis. Potentially the threshold value for dark colony was too high, only capturing the very dark colony, whereas a reduced threshold may hold further benefit.

One of the key attributes of the Cell-IQ is to provide live cell imaging whilst maintaining environmental conditions. This work utilised this in measuring the behaviour of the image derived metrics over time and therefore detect morphological responses immediately as they occurred. It was shown that single time points could be misperceived especially when using the colony periphery roughness as a measure of differentiation, as this was seen to be cyclic. This does highlight how live cell imaging can be used in conjunction with image derived metrics to measure the response to stimuli. This thesis showed the effect of adding differentiation stimuli in the form of chemical cues, and also effect from feeding regime. Other stimuli that also warrant attention are mechanical stimulants to induce differentiation (209), migratory response to stimuli (210) and microparticles uptake (211). The Cell-IQ permits the behaviour of cell response to any stimuli and therefore is an important tool for measuring characteristic changes in a population.

The measurement of edge cell coverage in a differentiating population was shown to be useful for measuring the yield and therefore optimisation of a protocol. This therefore allows a comparison of stimulant, be it chemical, environmental or/and mechanical. With embryonic stem cells becoming less favoured with the development and characterisation of induced pluripotent stem cells (iPSCs), it is also possible to utilise the same metrics unearthed in this thesis. The morphology of iPSCs is very similar to that of the ESCs, both with pluripotent colonies surrounded with a periphery of differentiating cells in a poor culture state. One of the interesting points to iPSC generation is the current inefficiency of producing such cells from differentiated adult cells (212). Although this harbours vast therapeutic implications if successfully achieved current poor generation leads to mixed reviews regarding their future (213). Image analysis could therefore be utilised in measuring the emergence of pluripotent morphology colony rather than measuring the emergence of differentiation as shown in this thesis. By observing the iPSC production timely process actions could be used to improve and direct improvements to the current procedure.

All the measurements carried out overtime also require media exchange to occur. It was seen that this required accurate autofocus capabilities to ensure that peaks and troughs were not measured

due to out-of-focus images. This thesis used 50 µm auto-focus stacks to improve the time it took to find the focal point, although further improvement of the autofocus feature was shown to be required if colonies were more than 50 µm out-of-focus following an intervention. There is also a possibility to remove a period of time of data following these interventions, however if the measured metric immediately changes then this transformation would be missed.

Within the haematopoietic culture further assessment is required to separate phenotypes using automated colony detection. The bootstrap method for measuring the confidence intervals of a mixed Gaussian distribution will provide a level of assurance. But the inherent inconsistency within the assay needs further investigation to assess where this variability comes from. Is it patient specific, due to inhomogeneity within the assay materials, Cell-IQ environment, or a combination of these factors? There is also an unanswered question regarding the maturity levels of colonies. It was stated that the slower growing colonies, although morphologically similar, were deemed more mature. BY following the growth and selecting colonies of similar morphology but growing at different rates would allow further characterisation with techniques such as gene expression using PCR. This may be able to sub-divide the populations and correlate these back to the observed growth rates.

Again mentioned is the environment within the Cell-IQ. By pre-humidifying the inlet gas the conditions were made comparable to a standard incubator, but a measured difference in humidity still occurs. Through improved CFD modelling and humidification of the inlet gas this difference could be eradicated which may improve the CFU assays reliability. Following from the discovery that the humidity within the culture vessel is dependent on evaporation form the culture medium, further work is also required to assess the effect of this. Overtime evaporation of liquid from the culture medium would cause an increase in the media supplement concentrations along with any waste products produced from the cells. As stated for embryonic culture it was declared that due to the 24 hour feeding regime this effect would be negligible and was not seen to effect the culture behaviour. However in cell phenotypes where less frequent feeding is required, this effect could

become more dominant, especially of note would be mesenchymal stem cells, with fast proliferation and a media exchange occurring every 3 days. The environment for cell culture is often neglected with standard incubators trusted for maintaining humidity, temperature and CO_2 concentrations and therefore pH levels. The use of methylcellulose gel highlights the evaporation that occurs and the knock-on effect within the growth dynamics. The Cell IQ allows the growth kinetics to be monitored whilst also measuring any change in environment through the use of probes.

Image automation has been instrumental in this work for the timely analysis. There is a wide consensus that automation reduces variability in measurement and often can increase productivity. The batch metric measurements have shown how automated analysis can be utilised to accelerate measured outcomes. Further to this work other, currently non-automated, image analysis uses can be developed. Such examples include the CFU assay from mesenchymal stem cells. Currently this is an end point, user based assessment, but further knowledge then number of colonies can be established from live cell imaging such as proliferation rates, migration and overall size of colony.

Finally there is the capacity to repeat and gather further data to improve the confidence in this work. This is especially noted when using a single vessel as a predictor of further vessels. It was shown that image analysis improved on the error of this method, and could be utilised non-invasively. A repeat with more samples, over a great confluency range would improve the reliability and credibility of image derived metrics to replace current identification tools.

The culminating objective will be to get these tools into product manufacture, so the most promising methods need to be taken forward to be validated and have data sets collated that would be suitable for regulatory submissions to a make a real impact on product delivery and quality within the regenerative medicine industry.

7. REFERENCES

7 References

1. Winston, Lord. Regenerative medicine. 2013;(July).

2. Lee MH, Arcidiacono J a, Bilek AM, Wille JJ, Hamill C a, Wonnacott KM, et al. Considerations for tissue-engineered and regenerative medicine product development prior to clinical trials in the United States. Tissue Eng Part B Rev [Internet]. 2010 Mar;16(1):41–54. Available from: http://www.ncbi.nlm.nih.gov/pubmed/19728784

3. Williams DJ, Thomas RJ, Hourd PC, Chandra A, Ratcliffe E, Liu Y, et al. Precision manufacturing for clinical-quality regenerative medicines. Philos Trans A Math Phys Eng Sci [Internet]. 2012 Aug 28 [cited 2012 Sep 27];370(1973):3924–49. Available from: http://www.ncbi.nlm.nih.gov/pubmed/22802496

4. Archer R, Williams DJ. Why tissue engineering needs process engineering. Nat Biotechnol [Internet]. 2005 Nov;23(11):1353–5. Available from: http://www.ncbi.nlm.nih.gov/pubmed/16273058

5. Huttunen TT, Sundberg M, Pihlajamäki H, Suuronen R, Skottman H, Äänismaa R, et al. An automated continuous monitoring system: a useful tool for monitoring neuronal differentiation of human embryonic stem cells. Stem Cell Stud [Internet]. 2011 Feb 24 [cited 2012 Sep 27];1(1). Available from: http://www.pagepress.org/journals/index.php/scs/article/view/2636

6. Kretzmer G. Industrial processes with animal cells. Appl Microbiol Biotechnol [Internet]. 2002 Jul [cited 2014 Jun 17];59(2-3):135–42. Available from: http://www.ncbi.nlm.nih.gov/pubmed/12111138

7. life: definition of life in Oxford dictionary (British & World English) [Internet]. [cited 2014 Jun 23]. Available from: http://www.oxforddictionaries.com/definition/english/life?q=life

8. Koshland DE. The seven pillars of life. Science (80-) [Internet]. 2002 [cited 2012 Dec 24];64–5. Available from: http://www.sciencemag.org/content/295/5563/2215.short

9. Cochran DM, Fukumura D, Ancukiewicz M, Carmeliet P, Jain RK. Evolution of oxygen and glucose concentration profiles in a tissue-mimetic culture system of embryonic stem cells. Ann Biomed Eng [Internet]. 2006 Aug [cited 2014 Apr 2];34(8):1247–58. Available from: http://www.ncbi.nlm.nih.gov/pubmed/16832606

10. Kagami H, Agata H, Kato R. Fundamental Technological Developments Required for Increased Availability of Tissue Engineering. 1984;

11. Rathore AS, Winkle H. Quality by design for biopharmaceuticals. Nat Biotechnol. 2009;27(1):26–34.

12. FDA. Providing Regulatory Submissions to the Center for Biologics Evaluation and Research (CBER) in Electronic Format — Biologics Marketing Applications [Biologics License Application (BLA), Product License Application (PLA)/Establishment License Application [Internet]. [cited 2012 Feb 14]. Available from:

http://www.fda.gov/downloads/BiologicsBloodVaccines/GuidanceComplianceRegulatoryInformation/Guidances/General/UCM192413.pdf

13. Research C for DE and. Guidances (Drugs) - Demonstration of Comparability of Human Biological Products, Including Therapeutic Biotechnology-derived Products [Internet]. Center for Drug Evaluation and Research; Available from: http://www.fda.gov/Drugs/GuidanceComplianceRegulatoryInformation/Guidances/ucm122879.htm

14. FDA. Pharmaceutical CGMPs for the 21st Century - A Risk-Based Approach. 2004.

15. ICH. Q8(R2) - Pharmaceutical Development. Current. 2009;8(August).

16. Vogt FG, Kord AS. Development of Quality-By-Design Analytical Methods. J Pharm Sci. 2011;100(3):797–812.

17. ICH. Q10 - Pharmaceutical Quality System. Risk Management. 2008.

18. MBI Training - Quality by Design for Effective Bioprocess Characterisation and Validation. Quality by Design for Effective Bioprocess Characterisation and Validation. 2010.

19. Chassin M. Is Health Care Ready for Six Sigma Quality? A J Public Heal Heal Care Policy [Internet]. 1998 [cited 2012 Feb 14];76(4). Available from: http://www.milbank.org/quarterly/764featchas.html

20. Haury JF. Implementation of Quality by Design Implementation of Quality by Design. Philadelphia: DIA; 2006. Available from: http://www.fda.gov/ohrms/dockets/ac/06/briefing/2006-4241B1-02-22-FDA-QbD OBP2 304_Haury.pdf

21. The Quality Portal. Six Sigma : Overview [Internet]. [cited 2012 Feb 14]. Available from: http://thequalityportal.com/q_6sigma.htm

22. Shetty U. Quality by Design : For Beginners. 2012 [cited 2014 Jun 23]. p. 1–133. Available from: http://www.slideshare.net/shettyuc/qbd-for-beginners-design-space

23. Roy S. Quality by design : A holistic concept of building quality in pharmaceuticals. 2012;3(2):100–8.

24. ICH. Q8 Pharmaceutical Development [Internet]. 2006. Available from: http://www.bcg-usa.com/regulatory/docs/2006/ICHQ8.pdf

25. ICH. Q11 - Development and Manufacture of Drug Substances (Chemicals Entities and Biotechnological/Biological Entities). Strategy. 2011.

26. FDA. Guidance for Industry PAT — A Framework for Innovative Pharmaceutical Development, Manufacturing and Quality Assurance. Qual Assur. 2004;(September).

27. Suzaki K. New Manufacturing Challenge: Techniques for Continuous Improvement [Internet]. Simon and Schuster; 1987 [cited 2014 Jun 23]. Available from: http://books.google.com/books?hl=en&lr=&id=6EHtJE8NHDoC&pgis=1

28. Mason C, Hoare M. Regenerative medicine bioprocessing: building a conceptual framework based on early studies. Tissue Eng [Internet]. 2007 Feb [cited 2013 Jun 3];13(2):301–11. Available from: http://www.ncbi.nlm.nih.gov/pubmed/17518564

29. BSI. Characterization of human cells for clinical applications Guide. 2011;

30. U.S. Department of Health and Human Services F and DA. Guidance for Industry - Current Good Tissue Practice (CGTP) and Additional Requirements for Manufacturers of Human Cells, Tissues, and Cellular and Issue-Based Products (HCT/Ps). 2011;(December).

31. CFR - Code of Federal Regulations Title 21. [cited 2014 Feb 5]; Available from: http://www.accessdata.fda.gov/scripts/cdrh/cfdocs/cfcfr/CFRSearch.cfm?CFRPart=1271&showFR=1

32. Gefen A. Computational Modeling in Tissue Engineering [Internet]. 10th ed. Liege, Belgium: Springer; 2011 [cited 2014 Aug 19]. Available from: http://scholar.google.com/scholar?hl=en&btnG=Search&q=intitle:Studies+in+Mechanobiology+,+Tissue+Engineering+and+Biomaterials#3

33. Shahdadfar A, Frønsdal K, Haug T, Reinholt FP, Brinchmann JE. In vitro expansion of human mesenchymal stem cells: choice of serum is a determinant of cell proliferation, differentiation, gene expression, and transcriptome stability. Stem Cells [Internet]. 2005 Oct [cited 2014 Mar 19];23(9):1357–66. Available from: http://www.ncbi.nlm.nih.gov/pubmed/16081661

34. Thomas RJ, Anderson D, Chandra A, Smith NM, Young LE, Williams D, et al. Automated, scalable culture of human embryonic stem cells in feeder-free conditions. Biotechnol Bioeng [Internet]. 2009 Apr 15 [cited 2012 Aug 3];102(6):1636–44. Available from: http://www.ncbi.nlm.nih.gov/pubmed/19062183

35. Narkilahti S, Rajala K, Pihlajamäki H, Suuronen R, Hovatta O, Skottman H. Monitoring and analysis of dynamic growth of human embryonic stem cells: comparison of automated instrumentation and conventional culturing methods. Biomed Eng Online [Internet]. 2007 Jan [cited 2012 Feb 9];6:11. Available from: http://www.pubmedcentral.nih.gov/articlerender.fcgi?artid=1854905&tool=pmcentrez&rendertype=abstract

36. Materials S. Standard Test Method for Automated Colony Forming Unit (CFU) Assays — Image Acquisition and Analysis Method for Enumerating and Characterizing Cells and Colonies in Culture 1. 2012;1–11.

37. Chan J, Lieu D, Huser T, Li R. Label-free separation of human embryonic stem cells and their cardiac derivatives using Raman spectroscopy. Anal Chem [Internet]. 2009 [cited 2014 Mar 6];81(4):1324–31. Available from: http://pubs.acs.org/doi/abs/10.1021/ac801665m

38. Pascut FC, Goh HT, George V, Denning C, Notingher I. Toward label-free Raman-activated cell sorting of cardiomyocytes derived from human embryonic stem cells. J Biomed Opt [Internet]. 2011 Apr [cited 2012 Nov 6];16(4):045002. Available from: http://www.ncbi.nlm.nih.gov/pubmed/21529069

39. Puppels GJ, de Mul FF, Otto C, Greve J, Robert-Nicoud M, Arndt-Jovin DJ, et al. Studying single living cells and chromosomes by confocal Raman microspectroscopy. Nature [Internet]. 1990 Sep 20 [cited 2014 Mar 6];347(6290):301–3. Available from: http://dx.doi.org/10.1038/347301a0

40. Pascut FC, Goh HT, Welch N, Buttery LD, Denning C, Notingher I. Noninvasive detection and imaging of molecular markers in live cardiomyocytes derived from human embryonic stem cells. Biophys J [Internet]. Biophysical Society; 2011 Jan 5 [cited 2012 Nov 6];100(1):251–9. Available from: http://www.pubmedcentral.nih.gov/articlerender.fcgi?artid=3010010&tool=pmcentrez&rendertype=abstract

41. Jr CHC, Lee YJ, Heddleston JM, Hartshorn CM, Walker ARH, Rich JN, et al. High-Speed Coherent Raman Fingerprint Imaging of Biological Tissues. 1990;20–3.

42. Räty JK, Liimatainen T, Unelma Kaikkonen M, Gröhn O, Airenne KJ, Jumani Airenne K, et al. Non-invasive Imaging in Gene Therapy. Mol Ther [Internet]. 2007 Sep [cited 2014 Mar 6];15(9):1579–86. Available from: http://www.ncbi.nlm.nih.gov/pubmed/17579578

43. Werth CJ, Zhang C, Brusseau ML, Oostrom M, Baumann T. A review of non-invasive imaging methods and applications in contaminant hydrogeology research. J Contam Hydrol [Internet]. Elsevier B.V.; 2010 Apr 1 [cited 2014 Jan 21];113(1-4):1–24. Available from: http://www.pubmedcentral.nih.gov/articlerender.fcgi?artid=3864598&tool=pmcentrez&rendertype=abstract

44. Shapiro EM, Skrtic S, Sharer K, Hill JM, Dunbar CE, Koretsky AP. MRI detection of single particles for cellular imaging. Proc Natl Acad Sci U S A [Internet]. 2004 Jul 27;101(30):10901–6. Available from: http://www.pubmedcentral.nih.gov/articlerender.fcgi?artid=503717&tool=pmcentrez&rendertype=abstract

45. Moore A, Josephson L, Bhorade RM, Basilion JP, Weissleder R. Human transferrin receptor gene as a marker gene for MR imaging. Radiology [Internet]. Radiological Society of North America; 2001 Oct 3 [cited 2014 Mar 6];221(1):244–50. Available from: http://pubs.rsna.org/doi/full/10.1148/radiol.2211001784

46. Weiss P, Garber B. Shape and Movement of Mesenchymal Cells as Functions od the Physical Structure of the Medium. Contributions to a Quantitative Morphology. Zoology. 1952;3:264–80.

47. Commissioner O of the. Critical Path Opportunities Reports - Challenges and Opportunities Report - March 2004 [Internet]. Office of the Commissioner; [cited 2013 Jul 29]. Available from: http://www.fda.gov/ScienceResearch/SpecialTopics/CriticalPathInitiative/CriticalPathOpportunitiesReports/ucm077262.htm#char

48. Freed LE, Guilak F, Guo XE, Gray ML, Tranquillo R, Holmes JW, et al. Advanced Tools for Tissue Engineering : Scaffolds ,. 2006;12(12).

49. Ramesh A, Upadhyay A, Thomas B. Microsurgery-Periodontics magnified!!.. J Soc Periodontists Implantol Kerala. 2013;7(1):33–8.

50. Rosenthal C. The Beginning. Nat Cell Biol. 2009;2009.

51. Microscope History [Internet]. [cited 2012 Feb 14]. Available from: http://inventors.about.com/od/mstartinventions/a/microscope.htm

52. Who invented the microscope - History of the microscope [Internet]. [cited 2012 Feb 14]. Available from: http://www.microscope-microscope.org/basic/microscope-history.htm

53. Borel W, Jansen H. Milestones. Nat Rev Mol Cell Biol. 2009;6–22.

54. Houtermans FG. Frits Zernike. Phys Today [Internet]. 1966 [cited 2012 Feb 9];19(4):126. Available from: http://link.aip.org/link/PHTOAD/v19/i4/p126/s1&Agg=doi

55. Nikon MicroscopyU | Phase Contrast Microscopy | Introduction [Internet]. [cited 2012 Feb 14]. Available from: http://www.microscopyu.com/articles/phasecontrast/phasemicroscopy.html

56. Olympus Microscopy Resource Center | Phase Contrast Microscopy - Introduction [Internet]. [cited 2012 Feb 14]. Available from: http://www.olympusmicro.com/primer/techniques/phasecontrast/phase.html

57. Egelberg P. Phase contrast microscopy | Phase Holographic Imaging [Internet]. [cited 2014 Jun 23]. Available from: http://www.phiab.se/technology/phase-contrast-microscopy

58. Gao P, Yao B, Harder I, Lindlein N, Torcal-Milla FJ. Phase-shifting Zernike phase contrast microscopy for quantitative phase measurement. Opt Lett [Internet]. 2011 Nov 1;36(21):4305–7. Available from: http://www.ncbi.nlm.nih.gov/pubmed/22048399

59. Stephens DJ, Allan VJ. Light microscopy techniques for live cell imaging. Science [Internet]. 2003 Apr 4 [cited 2011 Jun 29];300(5616):82–6. Available from: http://www.ncbi.nlm.nih.gov/pubmed/12677057

60. Rieder CL, Khodjakov A. Mitosis through the microscope: advances in seeing inside live dividing cells. Science [Internet]. 2003 May 4 [cited 2014 Mar 31];300(5616):91–6. Available from: http://www.ncbi.nlm.nih.gov/pubmed/12677059

61. Isherwood B, Timpson P, McGhee EJ, Anderson KI, Canel M, Serrels A, et al. Live Cell in Vitro and in Vivo Imaging Applications: Accelerating Drug Discovery. Pharmaceutics [Internet]. 2011 Apr 4 [cited 2012 Mar 8];3(2):141–70. Available from: http://www.mdpi.com/1999-4923/3/2/141/

62. Foster PL. Stress-induced mutagenesis in bacteria. Crit Rev Biochem Mol Biol [Internet]. 2007 [cited 2014 Jun 23];42(5):373–97. Available from: http://www.sciencemag.org/content/300/5624/1404.short

63. Frigault MM, Lacoste J, Swift JL, Brown CM. Live-cell microscopy - tips and tools. J Cell Sci [Internet]. 2009 Mar 15 [cited 2013 Mar 5];122(Pt 6):753–67. Available from: http://www.ncbi.nlm.nih.gov/pubmed/19261845

64. Eilken HM, Nishikawa S-I, Schroeder T. Continuous single-cell imaging of blood generation from haemogenic endothelium. Nature [Internet]. Nature Publishing Group; 2009 Feb 12

[cited 2011 Jul 22];457(7231):896–900. Available from: http://www.ncbi.nlm.nih.gov/pubmed/19212410

65. Sung M-H. A checklist for successful quantitative live cell imaging in systems biology. Cells [Internet]. 2013 Jan [cited 2014 Jun 23];2(2):284–93. Available from: http://www.pubmedcentral.nih.gov/articlerender.fcgi?artid=3972678&tool=pmcentrez&rendertype=abstract

66. Tokai Hit. Stage Top Incubators. Shizuoka-ken, Japan; 2011;

67. Delta T Open Dish System [Internet]. [cited 2014 Feb 6]. Available from: http://www.bioptechs.com/Products/Delta_T/delta_t.html

68. Montreal-Biotech-JuLI Smart fluorescent cell analyzer [Internet]. [cited 2012 Feb 15]. Available from: http://www.montreal-biotech.com/Products/?link=JuLI+Smart+fluorescent+cell+analyzer

69. Essen Instruments IncuCyte Live Cell Imaging System [Internet]. [cited 2012 Feb 15]. Available from: http://www.usedlabequipment.com/lab_equipment/Essen+Instruments+IncuCyte+Live+Cell+Imaging+System_18228.php

70. Chipmantech [Internet]. [cited 2012 Feb 15]. Available from: http://www.chipmantech.com/Cell_IQ.asp?ID=17&Level1ID=13

71. Chen H, Bai C, Wang X. Application of Probes in Live Cell Imaging. 2010;40–8.

72. Bolton D, Gall K. Nanoparticles & Nanotubes - Toxicity studies using live cell imaging and label free analysis. Nanobio Europe. 2010. p. 23.

73. Microscope Imaging Software captures images and measurement data., Carl Zeiss Micro [Internet]. [cited 2012 Feb 15]. Available from: http://news.thomasnet.com/fullstory/Microscope-Imaging-Software-captures-images-and-measurement-data-561671

74. Cells L. Microscopy from Carl Zeiss The Systems Approach for Imaging Living Cells. Cell. 1–28.

75. Nikon. BioStation CT.

76. Healthcare GE, Sciences L. IN Cell Analyzer 2200.

77. GE Healthcare. IN Cell Analyzer 2200 Imaging System [Internet]. [cited 2014 Feb 10]. Available from: http://www.gelifesciences.com/webapp/wcs/stores/servlet/catalog/en/GELifeSciences-uk/products/AlternativeProductStructure_12997/29027886

78. StemCell Technologies. Maintenance of Human Pluripotent Stem Cells in mTeSR1 and TeSR.

79. Roche. Cedex HiRes - Image-Based High Resolution Cell Analysis. Mannheim; 2011.

80. Chemometec. Mammalian cell counter, the NC-100 - The standard in cell counting [Internet]. [cited 2014 Aug 19]. Available from: http://chemometec.com/products/nc-100-family/nucleocounter-nc-100/

81. Merck Millipore. Guava ViaCount Assay - Data Sheet [Internet]. [cited 2014 Aug 19]. Available from: file:///C:/Users/cgds3/Downloads/ds0125en00 (1).pdf

82. Life Technologies. Countess® Automated Cell Counter. [cited 2014 Aug 19]; Available from: http://www.lifetechnologies.com/uk/en/home/brands/product-brand/countess-automated-cell-counter.html

83. Sonka M, Vaclav H, Boyle R. Image Processing, Analysis, and Machine Vision [Internet]. Fourth Edi. Cengage Learning; 4 edition; 2014 [cited 2014 Jul 29]. Available from: http://www.amazon.co.uk/Image-Processing-Analysis-Machine-Vision/dp/1133593607/ref=dp_ob_title_bk

84. Pera MF, Reubinoff B, Trounson a. Human embryonic stem cells. J Cell Sci [Internet]. 2000 Jan;113 (Pt 1:5–10. Available from: http://www.ncbi.nlm.nih.gov/pubmed/11574514

85. Ringe J, Kaps C, Burmester G-R, Sittinger M. Stem cells for regenerative medicine: advances in the engineering of tissues and organs. Naturwissenschaften [Internet]. 2002 Aug [cited 2014 Mar 10];89(8):338–51. Available from: http://www.ncbi.nlm.nih.gov/pubmed/12435034

86. Wert G De, Mummery C. Human embryonic stem cells: research, ethics and policy. 2003;18(4).

87. Horikawa M, Fox a S. Culture of Embryonic Cells of Drosophila Melanogaster in Vitro. Science [Internet]. 1964 Sep 25;145(3639):1437–9. Available from: http://www.ncbi.nlm.nih.gov/pubmed/807670

88. Adewumi O, Aflatoonian B, Ahrlund-Richter L, Amit M, Andrews PW, Beighton G, et al. Characterization of human embryonic stem cell lines by the International Stem Cell Initiative. Nat Biotechnol [Internet]. 2007 Jul [cited 2012 Jul 13];25(7):803–16. Available from: http://www.ncbi.nlm.nih.gov/pubmed/17572666

89. Evans M, Kaufman M. Establishment in culture of pluripotential cells from mouse embryos. Nature [Internet]. 1981 [cited 2012 Nov 18]; Available from: http://download.bioon.com.cn/upload/month_0911/20091124_1dd267377e5b7eaca806j5u1icjkiTpk.attach.pdf

90. Martin GR. Isolation of a pluripotent cell line from early mouse embryos cultured in medium conditioned by teratocarcinoma stem cells Developmental Biology : 1981;78(12):7634–8.

91. Thomson J a. Embryonic Stem Cell Lines Derived from Human Blastocysts. Science (80-) [Internet]. 1998 Nov 6 [cited 2012 Nov 2];282(5391):1145–7. Available from: http://www.sciencemag.org/cgi/doi/10.1126/science.282.5391.1145

92. Oh SKW, Choo ABH. Advances and perspectives in human and mouse embryonic stem cell bioprocessing. Drug Discov Today Technol [Internet]. Elsevier Ltd; 2008 Dec [cited 2012 Sep 27];5(4):e125–e130. Available from: http://linkinghub.elsevier.com/retrieve/pii/S1740674908000048

93. Oh SKW, Choo ABH. Human embryonic stem cell technology: large scale cell amplification and differentiation. Cytotechnology [Internet]. 2006 Mar [cited 2012 Sep 27];50(1-3):181–90. Available from: http://www.ncbi.nlm.nih.gov/pubmed/19003078

94. Li L, Baroja M, Majumdar A. Human embryonic stem cells possess immune-privileged properties. Stem ... [Internet]. 2004 [cited 2013 Apr 23];(22):448–56. Available from: http://onlinelibrary.wiley.com/doi/10.1634/stemcells.22-4-448/full

95. Kino-oka M, Taya M. Recent developments in processing systems for cell and tissue cultures toward therapeutic application. J Biosci Bioeng [Internet]. Elsevier B.V.; 2009 Oct [cited 2014 Mar 10];108(4):267–76. Available from: http://www.ncbi.nlm.nih.gov/pubmed/19716513

96. Bhatia S, Pilquil C, Roth-Albin I, Draper JS. Demarcation of Stable Subpopulations within the Pluripotent hESC Compartment. PLoS One [Internet]. 2013 Jan [cited 2013 Feb 28];8(2):e57276. Available from: http://www.ncbi.nlm.nih.gov/pubmed/23437358

97. Zipori D. The stem state: plasticity is essential, whereas self-renewal and hierarchy are optional. Stem Cells [Internet]. 2005 [cited 2014 Mar 5];23(6):719–26. Available from: http://www.ncbi.nlm.nih.gov/pubmed/15917468

98. Guo G, Huss M, Tong GQ, Wang C, Li Sun L, Clarke ND, et al. Resolution of cell fate decisions revealed by single-cell gene expression analysis from zygote to blastocyst. Dev Cell [Internet]. Elsevier Ltd; 2010 Apr 20 [cited 2013 Feb 28];18(4):675–85. Available from: http://www.ncbi.nlm.nih.gov/pubmed/20412781

99. Takahashi K, Yamanaka S. Induction of pluripotent stem cells from mouse embryonic and adult fibroblast cultures by defined factors. Cell [Internet]. 2006 Aug 25 [cited 2014 Feb 19];126(4):663–76. Available from: http://www.ncbi.nlm.nih.gov/pubmed/16904174

100. Blum B, Benvenisty N. The tumorigenicity of human embryonic stem cells. Adv Cancer Res [Internet]. 2008 Jan [cited 2014 Mar 4];100:133–58. Available from: http://www.sciencedirect.com/science/article/pii/S0065230X08000055

101. Lee M-O, Moon SH, Jeong H-C, Yi J-Y, Lee T-H, Shim SH, et al. Inhibition of pluripotent stem cell-derived teratoma formation by small molecules. Proc Natl Acad Sci U S A [Internet]. 2013 Aug 27 [cited 2014 Mar 6];110(35):E3281–90. Available from: http://www.pubmedcentral.nih.gov/articlerender.fcgi?artid=3761568&tool=pmcentrez&rendertype=abstract

102. Geron: Investor Relations: Press Release [Internet]. [cited 2014 Mar 10]. Available from: http://ir.geron.com/phoenix.zhtml?c=67323&p=irol-newsArticle&ID=1636192&highlight

103. Geron: Investor Relations: Press Release [Internet]. [cited 2014 Mar 10]. Available from: http://ir.geron.com/phoenix.zhtml?c=67323&p=irol-newsArticle_Print&ID=1636192&highlight

104. Fertilisation TH, Authority E. Human Fertilisation and Embryology Act 2008. 2008;

105. Waldby C. Stem Cells, Tissue Cultures and the Production of Biovalue. Health: [Internet]. 2002 Jul 1 [cited 2014 Feb 25];6(3):305–23. Available from: http://hea.sagepub.com/cgi/doi/10.1177/136345930200600304

106. HTA. Regulation of stem cell lines FAQs. HTA; [cited 2014 Mar 11]; Available from: http://www.hta.gov.uk/licensingandinspections/sectorspecificinformation/tissueandcellsforpatienttreatment/regulationofstemcelllinesfaqs.cfm

107. Xu-van Opstal WY, Ranger C, Lejeune O, Forgez P, Boudin H, Bisconte JC, et al. Automated image analyzing system for the quantitative study of living cells in culture. Microsc Res Tech [Internet]. 1994 Aug 1;28(5):440–7. Available from: http://www.ncbi.nlm.nih.gov/pubmed/7919532

108. Topman G, Sharabani-yosef O, Gefen A. M icroscopy M icroanalysis A Method for Quick , Low-Cost Automated Confluency Measurements. 2011;915–22.

109. Rubin H. Effect of Magnesium Content on Density-dependent Regulation of the Onset of DNA Synthesis in Transformed 3T3 Cells Effect of Magnesium Content on Density-dependent Regulation of the Onset of DMA Synthesis in Transformed 3T3 Cells1. 1982;1761–8.

110. Sahoo P., Soltani S, Wong AK. A survey of thresholding techniques. Comput Vision, Graph Image Process [Internet]. 1988 Feb [cited 2014 May 24];41(2):233–60. Available from: http://www.sciencedirect.com/science/article/pii/0734189X88900229

111. Jaccard N, Griffin LD, Keser A, Macown RJ, Super A, Veraitch FS, et al. Automated method for the rapid and precise estimation of adherent cell culture characteristics from phase contrast microscopy images. Biotechnol Bioeng [Internet]. 2014 Mar [cited 2014 Mar 28];111(3):504–17. Available from: http://www.ncbi.nlm.nih.gov/pubmed/24037521

112. Ji L, LaPointe VLS, Evans ND, Stevens MM. Changes in embryonic stem cell colony morphology and early differentiation markers driven by colloidal crystal topographical cues. Eur Cell Mater [Internet]. 2012 Jan;23:135–46. Available from: http://www.ncbi.nlm.nih.gov/pubmed/22370796

113. Turksen K. Human embryonic stem cell protocols [Internet]. 2006 [cited 2014 Apr 4]. Available from: http://link.springer.com/content/pdf/10.1007/978-1-60761-369-5.pdf

114. Reubinoff BE, Pera MF, Fong CY, Trounson a, Bongso a. Embryonic stem cell lines from human blastocysts: somatic differentiation in vitro. Nat Biotechnol [Internet]. 2000 Apr;18(4):399–404. Available from: http://www.ncbi.nlm.nih.gov/pubmed/10748519

115. Turksen K. Human Embryonic Stem Cell Protocols (Google eBook) [Internet]. Springer; 2006 [cited 2013 Nov 22]. Available from: http://books.google.com/books?id=VA7xDeozZQAC&pgis=1

116. Moogk DR. Live cell imaging , cell tracking and lineage analysis as a tool to investigate dynamic culture processes in heterogeneous cell systems by. 2009;

117. Das P, Ezashi T, Schulz LC, Westfall SD, Livingston K a, Roberts RM. Effects of fgf2 and oxygen in the bmp4-driven differentiation of trophoblast from human embryonic stem cells. Stem Cell Res [Internet]. 2007 Oct [cited 2014 Apr 3];1(1):61–74. Available from: http://www.pubmedcentral.nih.gov/articlerender.fcgi?artid=2634289&tool=pmcentrez&rendertype=abstract

118. Moogk D, Stewart M, Gamble D, Bhatia M, Jervis E. Human ESC colony formation is dependent on interplay between self-renewing hESCs and unique precursors responsible for niche generation. Cytometry A [Internet]. 2010 Apr [cited 2012 Aug 6];77(4):321–7. Available from: http://www.ncbi.nlm.nih.gov/pubmed/20217858

119. Hayashi K, Lopes SMCDS, Tang F, Surani MA. Dynamic equilibrium and heterogeneity of mouse pluripotent stem cells with distinct functional and epigenetic states. Cell Stem Cell [Internet]. 2008 Oct 9 [cited 2014 Mar 19];3(4):391–401. Available from: http://www.pubmedcentral.nih.gov/articlerender.fcgi?artid=3847852&tool=pmcentrez&rendertype=abstract

120. Monod J. The growth of bacterial cultures. Annu Rev Microbiol [Internet]. 1949 [cited 2014 Apr 9];(x). Available from: http://www.annualreviews.org/doi/pdf/10.1146/annurev.mi.03.100149.002103

121. Ami D, Neri T, Natalello A, Mereghetti P, Doglia SM, Zanoni M, et al. Embryonic stem cell differentiation studied by FT-IR spectroscopy. Biochim Biophys Acta [Internet]. 2008 Jan [cited 2014 Mar 18];1783(1):98–106. Available from: http://www.ncbi.nlm.nih.gov/pubmed/17916392

122. Richards M, Fong C-Y, Chan W-K, Wong P-C, Bongso A. Human feeders support prolonged undifferentiated growth of human inner cell masses and embryonic stem cells. Nat Biotechnol [Internet]. 2002 Sep [cited 2014 Mar 18];20(9):933–6. Available from: http://www.ncbi.nlm.nih.gov/pubmed/12161760

123. Li YJ, Chung EH, Rodriguez RT, Firpo MT, Healy KE. Hydrogels as artificial matrices for human embryonic stem cell self-renewal. 2006;1–5.

124. Heng BC, Liu H, Rufaihah AJ, Cao T. Human embryonic stem cell (hES) colonies display a higher degree of spontaneous differentiation when passaged at lower densities. In Vitro Cell Dev Biol Anim [Internet]. 2006;42(3-4):54–7. Available from: http://www.ncbi.nlm.nih.gov/pubmed/16759148

125. Itskovitz-Eldor J, Schuldiner M, Karsenti D, Eden a, Yanuka O, Amit M, et al. Differentiation of human embryonic stem cells into embryoid bodies compromising the three embryonic germ layers. Mol Med [Internet]. 2000 Feb;6(2):88–95. Available from: http://www.pubmedcentral.nih.gov/articlerender.fcgi?artid=1949933&tool=pmcentrez&rendertype=abstract

126. Almeida PA, Bolton VN. The effect of temperature fluctuations on the cytoskeletal organisation and chromosomal constitution of the human oocyte. Zygote [Internet]. 1995 Nov [cited 2014 Apr 9];3(4):357–65. Available from: http://www.ncbi.nlm.nih.gov/pubmed/8730901

127. Ratcliffe A, Niklason L. Bioreactors and bioprocessing for tissue engineering. Ann New York Acad ... [Internet]. 2002 [cited 2014 Jun 27];215:210–5. Available from: http://onlinelibrary.wiley.com/doi/10.1111/j.1749-6632.2002.tb03087.x/full

128. Kino-Oka M, Ogawa N, Umegaki R, Taya M. Bioreactor design for successive culture of anchorage-dependent cells operated in an automated manner. Tissue Eng [Internet]. 2005;11(3-4):535–45. Available from: http://www.ncbi.nlm.nih.gov/pubmed/15869432

129. Balis UJ, Yarmush ML, Toner M. Bioartificial liver process monitoring and control systems with integrated systems capability. Tissue Eng [Internet]. 2002 Jul;8(3):483–98. Available from: http://www.ncbi.nlm.nih.gov/pubmed/12167233

130. Amabile G, Meissner A. Induced pluripotent stem cells: current progress and potential for regenerative medicine. Trends Mol Med [Internet]. 2009 Feb [cited 2013 May 25];15(2):59–68. Available from: http://www.ncbi.nlm.nih.gov/pubmed/19162546

131. Dos Santos F, Campbell A, Fernandes-Platzgummer A, Andrade PZ, Gimble JM, Wen Y, et al. A xenogeneic-free bioreactor system for the clinical-scale expansion of human mesenchymal stem/stromal cells. Biotechnol Bioeng [Internet]. 2014 Jan 14 [cited 2014 Mar 24];9999(xxx):1–12. Available from: http://www.ncbi.nlm.nih.gov/pubmed/24420557

132. Eibes G, dos Santos F, Andrade PZ, Boura JS, Abecasis MM a, da Silva CL, et al. Maximizing the ex vivo expansion of human mesenchymal stem cells using a microcarrier-based stirred culture system. J Biotechnol [Internet]. 2010 Apr 15 [cited 2014 Jun 12];146(4):194–7. Available from: http://www.ncbi.nlm.nih.gov/pubmed/20188771

133. Chan L, Yim E, Choo A. Normalized Median Fluorescence: An Alternative Flow Cytometry Analysis Method for Tracking Human Embryonic Stem Cell States During Differentiation. ... Eng Part C Methods [Internet]. 2012 [cited 2014 Aug 11];19(2):156–65. Available from: http://online.liebertpub.com/doi/abs/10.1089/ten.TEC.2012.0150

134. Williams L a, Davis-Dusenbery BN, Eggan KC. SnapShot: directed differentiation of pluripotent stem cells. Cell [Internet]. Elsevier; 2012 May 25 [cited 2013 May 29];149(5):1174–1174.e1. Available from: http://www.ncbi.nlm.nih.gov/pubmed/22632979

135. Odorico JS, Kaufman DS, Thomson J a. Multilineage differentiation from human embryonic stem cell lines. Stem Cells [Internet]. 2001 Jan;19(3):193–204. Available from: http://www.ncbi.nlm.nih.gov/pubmed/11359944

136. Hay ED. An overview of epithelio-mesenchymal transformation. Acta Anat (Basel) [Internet]. 1995 Jan [cited 2014 Jun 6];154(1):8–20. Available from: http://www.ncbi.nlm.nih.gov/pubmed/8714286

137. Evseenko D, Zhu Y, Schenke-layland K, Kuo J, Latour B, Ge S, et al. Mapping the first stages of mesoderm commitment during differentiation of human embryonic stem cells. 2010;

138. Pedersen RA. Mechanisms of Mesoderm Differentiation in Pluripotent Mammalian Stem Cells Both mouse & human embryonic stem. 2012;

139. Melichar H, Li O, Ross J, Haber H, Cado D, Nolla H, et al. Comparative study of hematopoietic differentiation between human embryonic stem cell lines. PLoS One [Internet]. 2011 Jan [cited 2013 May 12];6(5):e19854. Available from: http://www.pubmedcentral.nih.gov/articlerender.fcgi?artid=3095633&tool=pmcentrez&rendertype=abstract

140. Bauwens CL, Peerani R, Niebruegge S, Woodhouse K a, Kumacheva E, Husain M, et al. Control of human embryonic stem cell colony and aggregate size heterogeneity influences differentiation trajectories. Stem Cells [Internet]. 2008 Sep [cited 2014 Feb 20];26(9):2300–10. Available from: http://www.ncbi.nlm.nih.gov/pubmed/18583540

141. Peerani R, Rao BM, Bauwens C, Yin T, Wood GA, Nagy A, et al. Niche-mediated control of human embryonic stem cell self-renewal and differentiation. EMBO J [Internet]. 2007 Nov 14 [cited 2012 Jul 27];26(22):4744–55. Available from: http://www.pubmedcentral.nih.gov/articlerender.fcgi?artid=2080799&tool=pmcentrez&rendertype=abstract

142. Watanabe K, Ueno M, Kamiya D, Nishiyama A, Matsumura M, Wataya T, et al. A ROCK inhibitor permits survival of dissociated human embryonic stem cells. Nat Biotechnol [Internet]. 2007 Jun [cited 2013 Nov 12];25(6):681–6. Available from: http://www.ncbi.nlm.nih.gov/pubmed/17529971

143. No C. StemPro ® EZPassage ™ Disposable Stem Cell Passaging Tool. 2007;(23181).

144. StemCell Technologies. ReLeSR. 2014 p. 1–2.

145. Abraham E, Campbell A, Brandwein H, Oh S. Meeting Lot-Size Challenges of Manufacturing Adherent Cells for Therapy.

146. Chang C-W, Hwang Y, Brafman D, Hagan T, Phung C, Varghese S. Engineering cell–material interfaces for long-term expansion of human pluripotent stem cells. Biomaterials [Internet]. Elsevier Ltd; 2012 Nov [cited 2012 Nov 6];1–10. Available from: http://linkinghub.elsevier.com/retrieve/pii/S0142961212011416

147. Bendall SC, Stewart MH, Bhatia M. Human embryonic stem cells: lessons from stem cell niches in vivo. Regen Med [Internet]. 2008 May;3(3):365–76. Available from: http://www.ncbi.nlm.nih.gov/pubmed/18462059

148. Xu C, Inokuma MS, Denham J, Golds K, Kundu P, Gold JD, et al. Feeder-free growth of undifferentiated human embryonic stem cells. Nat Biotechnol [Internet]. 2001 Oct;19(10):971–4. Available from: http://www.pubmedcentral.nih.gov/articlerender.fcgi?artid=2958897&tool=pmcentrez&rendertype=abstract

149. Oh SKW, Chua P, Foon KL, Ng E, Chin A, Choo ABH, et al. Quantitative identification of teratoma tissues formed by human embryonic stem cells with TeratomEye. Biotechnol Lett [Internet]. 2009 May [cited 2012 Sep 27];31(5):653–8. Available from: http://www.ncbi.nlm.nih.gov/pubmed/19169887

150. Orkin SH, Zon LI. Hematopoiesis: an evolving paradigm for stem cell biology. Cell [Internet]. 2008 Feb 22 [cited 2013 Mar 1];132(4):631–44. Available from: http://www.pubmedcentral.nih.gov/articlerender.fcgi?artid=2628169&tool=pmcentrez&rendertype=abstract

151. Orkin SH. Diversification of haematopoietic stem cells to specific lineages. Nat Rev Genet [Internet]. Nature Publishing Group; 2000 Oct 1 [cited 2014 Mar 21];1(1):57–64. Available from: http://www.nature.com/nrg/journal/v1/n1/pdf/nrg1000_057a.pdf

152. Huang S, Wang J, Liu S, Li Y, Hu J, Kou Z, et al. Differentiation of reprogrammed somatic cells into functional hematopoietic cells. Differentiation [Internet]. Elsevier; 2009 [cited 2013 Aug 7];78(2-3):151–8. Available from: http://www.ncbi.nlm.nih.gov/pubmed/19640630

153. Jollie WP. Development, morphology, and function of the yolk-sac placenta of laboratory rodents. Teratology [Internet]. 1990 Apr [cited 2014 Mar 21];41(4):361–81. Available from: http://www.ncbi.nlm.nih.gov/pubmed/2187257

154. Orkin SH, Zon LI. SnapShot: hematopoiesis. Cell [Internet]. 2008 Feb 22 [cited 2012 Oct 26];132(4):712. Available from: http://www.ncbi.nlm.nih.gov/pubmed/18295585

155. Akashi K, Traver D, Miyamoto T, Weissman IL. A clonogenic common myeloid progenitor that gives rise to all myeloid lineages. Nature [Internet]. 2000 Mar 9;404(6774):193–7. Available from: http://www.ncbi.nlm.nih.gov/pubmed/10724173

156. Ceredig R, Rolink AG, Brown G. Models of haematopoiesis: seeing the wood for the trees. Nat Rev Immunol [Internet]. 2009 Apr;9(4):293–300. Available from: http://www.ncbi.nlm.nih.gov/pubmed/19282853

157. National Institutes of Health (NIH). 5. Hematopoietic Stem Cells [Stem Cell Information] [Internet]. 2001. Available from: http://stemcells.nih.gov/info/scireport/pages/chapter5.aspx

158. Marks-Bluth J, Pimanda JE. Cell signalling pathways that mediate haematopoietic stem cell specification. Int J Biochem Cell Biol [Internet]. Elsevier Ltd; 2012 Sep 17 [cited 2012 Sep 24];1–10. Available from: http://www.ncbi.nlm.nih.gov/pubmed/22995476

159. Shirvaikar N, Marquez-Curtis L a, Janowska-Wieczorek A. Hematopoietic Stem Cell Mobilization and Homing after Transplantation: The Role of MMP-2, MMP-9, and MT1-MMP. Biochem Res Int [Internet]. 2012 Jan [cited 2013 Dec 10];2012:685267. Available from: http://www.pubmedcentral.nih.gov/articlerender.fcgi?artid=3310200&tool=pmcentrez&rendertype=abstract

160. Douay L, Gorin NC, Mary JY, Lemarie E, Lopez M, Najman A, et al. Recovery of CFU-GM from cryopreserved marrow and in vivo evaluation after autologous bone marrow transplantation are predictive of engraftment. Exp Hematol [Internet]. 1986 Jun [cited 2013 Dec 11];14(5):358–65. Available from: http://www.ncbi.nlm.nih.gov/pubmed/3519263

161. Page KM, Zhang L, Mendizabal A, Wease S, Carter S, Gentry T, et al. Total colony-forming units are a strong, independent predictor of neutrophil and platelet engraftment after unrelated umbilical cord blood transplantation: a single-center analysis of 435 cord blood transplants. Biol Blood Marrow Transplant [Internet]. Elsevier Ltd; 2011 Sep [cited 2013 Apr 30];17(9):1362–74. Available from: http://www.ncbi.nlm.nih.gov/pubmed/21277377

162. Rowley SD, Zuehlsdorf M, Braine HG, Colvin OM, Davis J, Jones RJ, et al. CFU-GM content of bone marrow graft correlates with time to hematologic reconstitution following autologous bone marrow transplantation with 4-hydroperoxycyclophosphamide-purged bone marrow. Blood [Internet]. 1987 Jul;70(1):271–5. Available from: http://www.ncbi.nlm.nih.gov/pubmed/3297203

163. McLeod DL, Shreeve MM, Axelrad a a. Improved plasma culture system for production of erythrocytic colonies in vitro: quantitative assay method for CFU-E. Blood [Internet]. 1974 Oct;44(4):517–34. Available from: http://www.ncbi.nlm.nih.gov/pubmed/4137721

164. Yoo KH, Lee SH, Kim H-J, Sung KW, Jung HL, Cho EJ, et al. The impact of post-thaw colony-forming units-granulocyte/macrophage on engraftment following unrelated cord blood

transplantation in pediatric recipients. Bone Marrow Transplant [Internet]. 2007 May [cited 2013 Mar 27];39(9):515–21. Available from: http://www.ncbi.nlm.nih.gov/pubmed/17334379

165. Crosta GF, Fumarola L, Malerba I, Gribaldo L. Scoring CFU-GM colonies in vitro by data fusion: a first account. Exp Hematol [Internet]. 2007 Jan [cited 2013 Mar 18];35(1):1–12. Available from: http://www.ncbi.nlm.nih.gov/pubmed/17198868

166. Sarang S, Group RM, Ambani D, Sciences L, Road T, Life A, et al. Functional assessment of cord blood units using two different assays. 2012;6(3):20–6.

167. World Health Organisation. Global database on blood safety [Internet]. Summary Report. Geneva; 2001 p. 1–30. Available from: http://scholar.google.com/scholar?hl=en&btnG=Search&q=intitle:Global+Database+on+Blood+Safety#0

168. Lapillonne H, Kobari L, Mazurier C, Tropel P, Giarratana M-C, Zanella-Cleon I, et al. Red blood cell generation from human induced pluripotent stem cells: perspectives for transfusion medicine. Haematologica [Internet]. 2010 Oct [cited 2011 Jun 10];95(10):1651–9. Available from: http://www.pubmedcentral.nih.gov/articlerender.fcgi?artid=2948089&tool=pmcentrez&rendertype=abstract

169. Wattendorf D. Blood Pharming [Internet]. [cited 2013 May 8]. Available from: http://www.darpa.mil/Our_Work/DSO/Programs/Blood_Pharming.aspx

170. Red blood cell production from human embryonic stem cells in a scalable suspension format [Internet]. [cited 2014 Mar 21]. Available from: http://www.epsrc-regen-med.org/research/epsrc-centre-projects/red-blood-cell-production-from-human-embryonic-stem-cells-in-a-scalable-suspension-format/

171. Arber C, Halter J, Stern M, Rovó a, Gratwohl a, Tichelli a. Graft source determines human hematopoietic progenitor distribution pattern within the CD34(+) compartment. Bone Marrow Transplant [Internet]. 2011 May [cited 2012 Nov 22];46(5):650–8. Available from: http://www.ncbi.nlm.nih.gov/pubmed/20711241

172. Perey L, Peters R, Pampallona S, Schneider P, Gross N, Leyvraz S. Extensive phenotypic analysis of CD34 subsets in successive collections of mobilized peripheral blood progenitors. Br J Haematol [Internet]. 1998 Dec;103(3):618–29. Available from: http://www.ncbi.nlm.nih.gov/pubmed/9858209

173. Baum CM, Weissman IL, Tsukamoto a S, Buckle a M, Peault B. Isolation of a candidate human hematopoietic stem-cell population. Proc Natl Acad Sci U S A [Internet]. 1992 Apr 1;89(7):2804–8. Available from: http://www.pubmedcentral.nih.gov/articlerender.fcgi?artid=48751&tool=pmcentrez&rendertype=abstract

174. Wang JC, Doedens M, Dick JE. Primitive human hematopoietic cells are enriched in cord blood compared with adult bone marrow or mobilized peripheral blood as measured by the quantitative in vivo SCID-repopulating cell assay. Blood [Internet]. 1997 Jun 1;89(11):3919–24. Available from: http://www.ncbi.nlm.nih.gov/pubmed/9166828

175. Lindsey S, Papoutsakis ET. Ex Vivo. 2011;

176. Coulombel L. Identification of hematopoietic stem/progenitor cells: strength and drawbacks of functional assays. Oncogene [Internet]. 2004 Sep 20 [cited 2013 Dec 4];23(43):7210–22. Available from: http://www.ncbi.nlm.nih.gov/pubmed/15378081

177. ColonyGEL - Methylcellulose-Based Media for Colony-Forming Cell Assays [Internet]. [cited 2014 May 8]. Available from: http://www.colonygel.com/index.htm

178. Prasad VK, Mendizabal A, Parikh SH, Szabolcs P, Driscoll T a, Page K, et al. Unrelated donor umbilical cord blood transplantation for inherited metabolic disorders in 159 pediatric patients from a single center: influence of cellular composition of the graft on transplantation outcomes. Blood [Internet]. 2008 Oct 1 [cited 2013 Apr 30];112(7):2979–89. Available from: http://www.pubmedcentral.nih.gov/articlerender.fcgi?artid=2556628&tool=pmcentrez&rendertype=abstract

179. Optimization and Standardization of the Colony Forming Unit (CFU) Assay [Internet]. [cited 2013 Apr 30]. Available from: http://www.youtube.com/watch?v=fU71K-BY1sE

180. Cber FDA. Guidance for Industry Potency Tests for Cellular and Gene. 1800;(October 2008).

181. Netcord & FACT. International Standards For Cord Blood Collection, Banking, And Release For Administration. 2012;

182. FACT & JACIE. International Standards For Cellular Therapy Product Collection, Processing, and Administration. 2011;(March).

183. Pamphilon D, Selogie E, McKenna D, Cancelas-Peres J a, Szczepiorkowski ZM, Sacher R, et al. Current practices and prospects for standardization of the hematopoietic colony-forming unit assay: a report by the cellular therapy team of the Biomedical Excellence for Safer Transfusion (BEST) Collaborative. Cytotherapy [Internet]. 2013 Mar [cited 2013 Jun 4];15(3):255–62. Available from: http://www.ncbi.nlm.nih.gov/pubmed/23579058

184. Ballen K, Broxmeyer HE, McCullough J, Piaciabello W, Rebulla P, Verfaillie CM, et al. Current status of cord blood banking and transplantation in the United States and Europe. Biol Blood Marrow Transplant [Internet]. 2001 Jan;7(12):635–45. Available from: http://www.ncbi.nlm.nih.gov/pubmed/11787526

185. Van Epps DE, Bender J, Lee W, Schilling M, Smith A, Smith S, et al. Harvesting, characterization, and culture of CD34+ cells from human bone marrow, peripheral blood, and cord blood. Blood Cells [Internet]. 1994 Jan [cited 2014 May 15];20(2-3):411–23. Available from: http://www.ncbi.nlm.nih.gov/pubmed/7538347

186. Nimgaonkar MT, Roscoe RA, Persichetti J, Rybka WB, Winkelstein A, Ball ED. A unique population of CD34+ cells in cord blood. Stem Cells [Internet]. 1995 Mar [cited 2014 Apr 25];13(2):158–66. Available from: http://www.ncbi.nlm.nih.gov/pubmed/7540469

187. Arena GD, Musto P, Cascavilla N, Giorgio G Di, Zendoli F, Carotenuto M. HETEROGENEITY OF CD34 + HEMATOPOIETIC PROGENITOR CELLS ta. 1996;404–9.

188. Melnik K, Nakamura M, Comella K, Lasky LC, Zborowski M, Chalmers JJ. Evaluation of eluents from separations of CD34+ cells from human cord blood using a commercial, immunomagnetic cell separation system. Biotechnol Prog [Internet]. 2001;17(5):907–16. Available from: http://www.ncbi.nlm.nih.gov/pubmed/11587583

189. De Wynter EA, Coutinho LH, Pei X, Marsh JC, Hows J, Luft T, et al. Comparison of purity and enrichment of CD34+ cells from bone marrow, umbilical cord and peripheral blood (primed for apheresis) using five separation systems. Stem Cells [Internet]. 1995 Sep [cited 2014 Aug 20];13(5):524–32. Available from: http://www.ncbi.nlm.nih.gov/pubmed/8528102

190. Handgretinger R, Lang P, Schumm M, Taylor G, Neu S, Koscielnak E, et al. Isolation and transplantation of autologous peripheral CD34+ progenitor cells highly purified by magnetic-activated cell sorting. Bone Marrow Transplant [Internet]. 1998 May;21(10):987–93. Available from: http://www.ncbi.nlm.nih.gov/pubmed/9632271

191. Stachowiak MK, Tzanakakis ES, editors. Stem Cells: From Mechanisms to Technologies [Internet]. World Scientific Publishing Company; 1 edition; 2011 [cited 2014 Jun 16]. Available from: http://www.amazon.com/Stem-Cells-From-Mechanisms-Technologies/dp/9814317705

192. Doran PM. Bioprocess Engineering Principles. Elsevier; 1995.

193. Coulson JM, Richardson JF. Coulson & Richardson's Chemical Engienering Volume 1. Sixth Edit. Oxford: Butterworth-Heinemann; 1999.

194. Ogawa M. Differentiation and proliferation of hematopoietic stem cells. Blood [Internet]. 1993 Jun 1;81(11):2844–53. Available from: http://www.ncbi.nlm.nih.gov/pubmed/8499622

195. Gregory C, Eaves A. Human marrow cells capable of erythropoietic differentiation in vitro: definition of three erythroid colony responses. Blood [Internet]. 1977 [cited 2014 Jul 25];49(6):855–64. Available from: http://bloodjournal.hematologylibrary.org/content/49/6/855.short

196. Stephenson JR, Axelrad AA, Mcleod DL, Shreeve MM. Hemoglobin-Synthesizing Erythropoietin. 1971;68(7):1542–6.

197. Aurenhammer F. Voronoi diagrams---a survey of a fundamental geometric data structure. ACM Comput Surv [Internet]. 1991 Sep 1;23(3):345–405. Available from: http://portal.acm.org/citation.cfm?doid=116873.116880

198. Delaunay Triangulation - MATLAB & Simulink - MathWorks United Kingdom [Internet]. Available from: http://www.mathworks.co.uk/help/matlab/math/delaunay-triangulation.html

199. Cordelières FP, Petit V, Kumasaka M, Debeir O, Letort V, Gallagher SJ, et al. Automated cell tracking and analysis in phase-contrast videos (iTrack4U): development of Java software based on combined mean-shift processes. PLoS One [Internet]. 2013 Jan [cited 2014 Feb 19];8(11):e81266. Available from: http://www.pubmedcentral.nih.gov/articlerender.fcgi?artid=3842324&tool=pmcentrez&rendertype=abstract

200. Vicente-Manzanares M, Webb DJ, Horwitz a R. Cell migration at a glance. J Cell Sci [Internet]. 2005 Nov 1 [cited 2014 Jan 22];118(Pt 21):4917–9. Available from: http://www.ncbi.nlm.nih.gov/pubmed/16254237

201. Linacre J. Overlapping normal distributions. Rasch Meas Trans [Internet]. 1996 [cited 2014 Aug 12]; Available from: http://scholar.google.co.uk/scholar?q=Overlapping+normal+distributions.+Linacre+JM&btnG=&hl=en&as_sdt=0,5#0

202. Efron B. Bootstrap methods: another look at the jackknife. Ann Stat [Internet]. 1979 [cited 2014 Aug 13]; Available from: http://www.jstor.org/stable/2958830

203. For O, Sciences L. Taking Stock of Regenerative Medicine in the United Kingdom. 2011;(July).

204. Willetts D. Eight Great Technologies.

205. MRC. A Strategy for UK Regenerative Medicine.

206. Nobel Media AB. The Nobel Prize in Physiology or Medicine 2012 [Internet]. 2014 [cited 2014 Aug 12]. Available from: http://www.nobelprize.org/nobel_prizes/medicine/laureates/2012/

207. Cell Therapy Catapult. Who we are [Internet]. 2014 [cited 2014 Aug 1]. Available from: https://ct.catapult.org.uk/who-we-are

208. Buckler R. Opportunities in regenerative medicine. BioProcess Int 9 (Suppl 1) 14 [Internet]. 2011 [cited 2014 Aug 12]; Available from: http://www.bioprocessintl.com/multimedia/archive/00124/BPI_A_110901SUPAR04_124785a.pdf

209. Mauney JR, Sjostorm S, Blumberg J, Horan R, O'Leary JP, Vunjak-Novakovic G, et al. Mechanical stimulation promotes osteogenic differentiation of human bone marrow stromal cells on 3-D partially demineralized bone scaffolds in vitro. Calcif Tissue Int [Internet]. 2004 May [cited 2014 Aug 14];74(5):458–68. Available from: http://www.ncbi.nlm.nih.gov/pubmed/14961210

210. Ridley AJ, Schwartz M a, Burridge K, Firtel R a, Ginsberg MH, Borisy G, et al. Cell migration: integrating signals from front to back. Science [Internet]. 2003 Dec 5 [cited 2014 Jul 10];302(5651):1704–9. Available from: http://www.ncbi.nlm.nih.gov/pubmed/14657486

211. Desai M, Labhasetwar V, Walter E. The mechanism of uptake of biodegradable microparticles in Caco-2 cells is size dependent. Pharm … [Internet]. 1997 [cited 2014 Aug 19]; Available from: http://link.springer.com/article/10.1023/A:1012126301290

212. Maherali N, Hochedlinger K. Guidelines and techniques for the generation of induced pluripotent stem cells. Cell Stem Cell [Internet]. Elsevier Inc.; 2008 Dec 4 [cited 2014 Jul 11];3(6):595–605. Available from: http://www.ncbi.nlm.nih.gov/pubmed/19041776

213. Hochedlinger K, Jaenisch R. Nuclear reprogramming and pluripotency. Nature [Internet]. 2006 Jun 29 [cited 2014 Aug 19];441(7097):1061–7. Available from: http://www.ncbi.nlm.nih.gov/pubmed/16810240

214. Rogers GFC. Thermodynamic and Transport Properties of Fluids [Internet]. Wiley; 1995 [cited 2014 May 8]. Available from: http://books.google.co.uk/books/about/Thermodynamic_and_Transport_Properties_0.html?id=kH__ngEACAAJ&pgis=1

215. Abulencia JP, Theodore L. Fluid Flow for the Practicing Chemical Engineer. Hoboken, NJ, USA: John Wiley & Sons, Inc.; 2009.

216. Medical Gas Data Sheet (MGDS) 5 % carbon dioxide / air medical gas mixture BOC : Living healthcare. :2–5.

8. APPENDIX

8 Appendix

8.1 Saturation pressure of water vapour

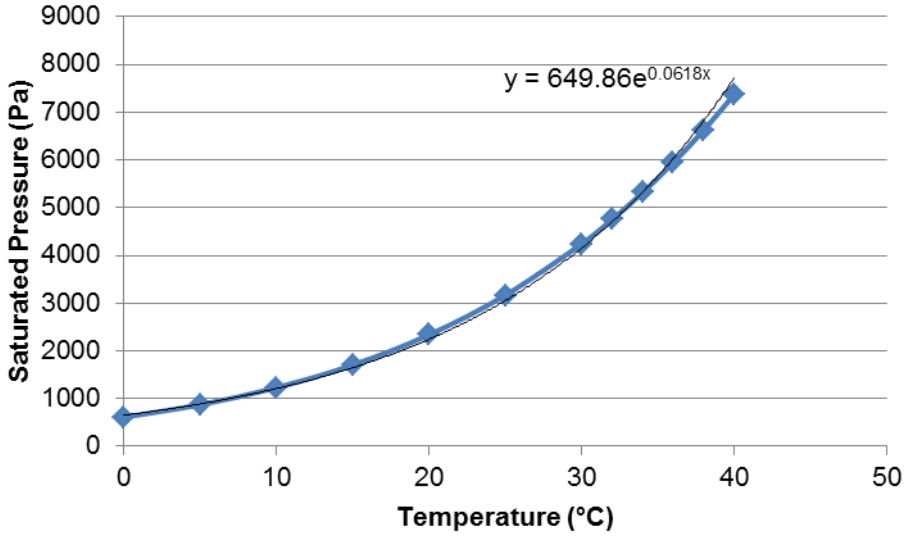

Figure 136. Saturated Pressure of water vapour at different temperatures (214).

When x=37

$$y = 649.86e^{0.0618\times37} = 6396\ Pa = Satuaration\ pressure\ of\ water\ vapour\ at\ 37°C$$

8.2 Mass of Water in 150 mL of Air at 90% Humidity

- p_s = 6396 Pa (saturation pressure of water vapour at 37°C)
- φ = 90% = 0.9 (relative humidity)
- V = 150 mL = 0.00015m^3 (gas flow rate of 30mL/min, gas on for 5 minutes)
- R = 8.314472 Pa m^3 / mol K (ideal gas constant)
- T = 37°C =312.25 K (culture conditions)
- M = 18 g/mol (Molar mass of water)

Ideal Gas Law (215)

$$PV = nRT$$

$$\varphi \cdot (p_s) \cdot V = nRT$$

$$n = \frac{p_s \cdot V}{RT} \cdot \varphi = \left(\frac{6396 \cdot 0.00015}{8.314472 \cdot 312.25}\right) 0.9 = 0.00594\ g = 5.94\ mg$$

Assumptions:

- The inlet gas is air (21% oxygen, 78% nitrogen, 1% argon and trace elements, (216))
- The dry gas reaches 90% relative humidity in the culture system
- The inlet gas is at 37°C
- The system is sealed with no losses other than the gas inlet and outlet
- There is a maintained reservoir of water
- Atmospheric pressure throughout the system

5.94 mg of water evaporates for every 150 mL of gas. 150 mL every 25 minutes, in 14 days there are 50400 minutes.

$$\frac{50400\ mins}{25\ mins} = 2016$$

$$2016 \times 150\ mL = 302400\ mL$$

302400 mL or 3.024 m^3 of gas enters the culture vessel over the entire assay. Using this volume of gas in the previous equation gives:

$$n = \frac{p_s \cdot V}{RT} \cdot \varphi = \frac{6396 \cdot 3.024}{8.314472 \cdot 312.25} \cdot 0.9 = 6.70\ g$$

So over the entire culture period 6.70 g (~6.70 mL) of water will evaporate.

8.3 Colony Phenotype Comparison between Standard Incubator and Cell-IQ

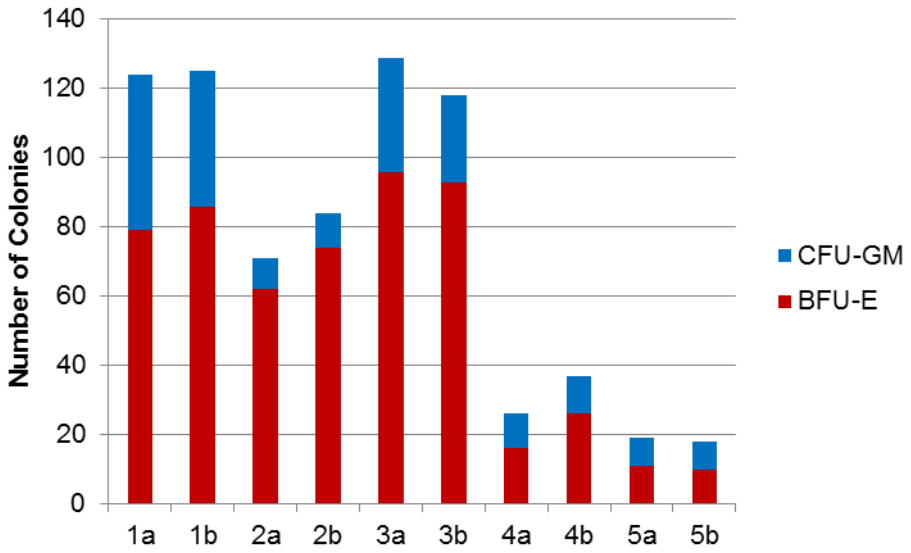

Figure 137. Colony phenotypes from Figure 118. Splitting the total number of colonies into CFU-GM (blue) or BFU-E (red) stacked columns. The x-axis values show the sample, with the letter a) denoting those in a standard incubator, and b) in the Cell-IQ. This figure shows comparison of both total number and phenotype of colonies.

8.4 Voronoi Macro

```
//run("Threshold...");
//run("Threshold...");
// Color Thresholder 1.48f
// Autogenerated macro, single images only!
min=newArray(3);
max=newArray(3);
filter=newArray(3);
a=getTitle();
run("HSB Stack");
run("Convert Stack to Images");
selectWindow("Hue");
rename("0");
selectWindow("Saturation");
rename("1");
selectWindow("Brightness");
rename("2");
min[0]=0;
max[0]=255;
filter[0]="pass";
min[1]=0;
max[1]=160;
filter[1]="pass";
min[2]=0;
max[2]=255;
filter[2]="pass";
for (i=0;i<3;i++){
  selectWindow(""+i);
  setThreshold(min[i], max[i]);
  run("Convert to Mask");
  if (filter[i]=="stop")  run("Invert");
}
imageCalculator("AND create", "0","1");
imageCalculator("AND create", "Result of 0","2");
for (i=0;i<3;i++){
  selectWindow(""+i);
  close();
}
selectWindow("Result of 0");
close();
selectWindow("Result of Result of 0");
rename(a);
// Colour Thresholding----------
run("Make Binary");
run("Analyze Particles...", "size=25-Infinity circularity=0.00-1.00 show=Nothing
clear");
run("Delaunay Voronoi", "mode=Delaunay make showmeandistance
inferselectionfromparticles");
saveAs("Results", "/C:/Users/cgds3/Desktop/Image J/B2_11/Voronoi-" + getTitle() +
".txt");
```

8.5 Overlapping Coefficient for Normal Distributions

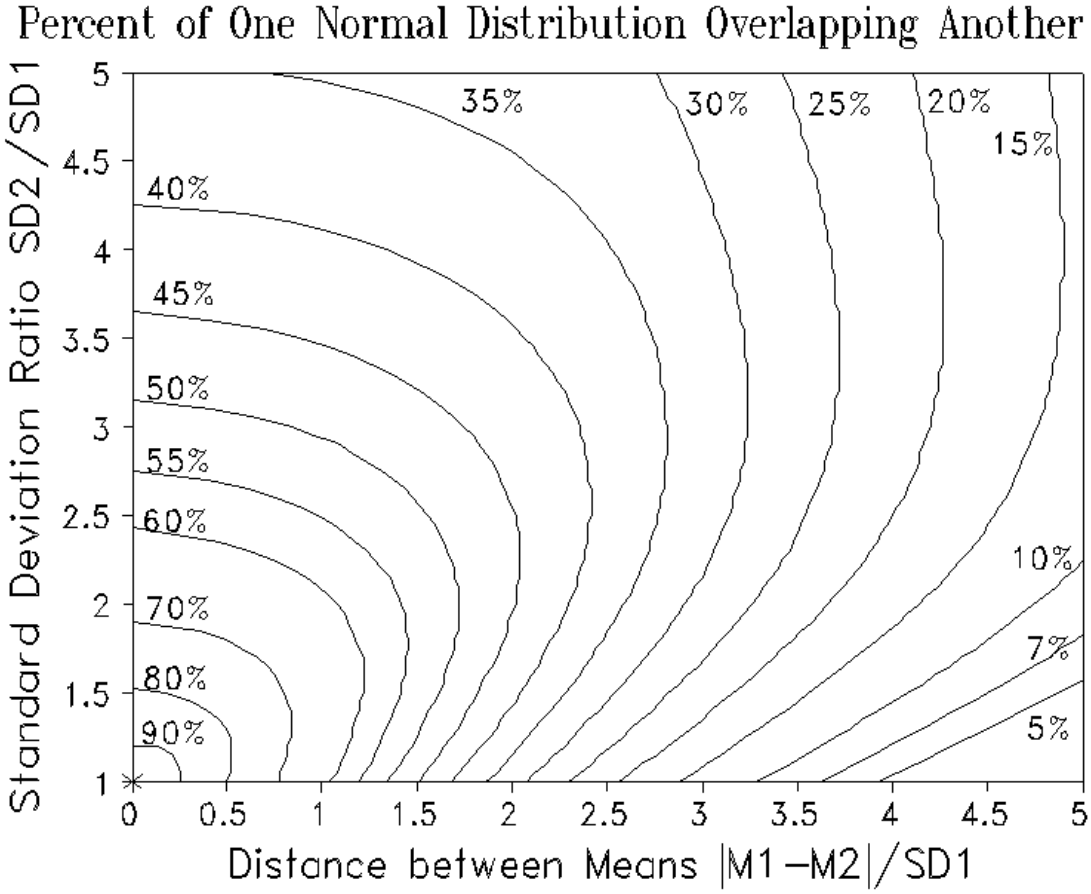

Figure 138. Nomogram of percentage overlapping of normal distributions (201)

BFU-E Mean = 0.766 = M1

BFU-E Standard Deviation = 0.2788 = SD1

CFU-GM Mean = 1.487 = M2

CFU-GM Standard Deviation = 0.3712 = SD2

$$\frac{SD2}{SD1} = \frac{0.3712}{0.2788} = 1.33$$

$$\frac{|M1 - M2|}{SD1} = \frac{0.766 - 1.487}{0.2788} = 2.59$$

Using 1.33 (y-axis) and 2.59 (x-axis) the percentage of overlap is interpolated by eye as 23%.